People's Democratic Republic of Algeria
Ministry of Higher Education and Scientific Research
University of Larbi Ben M'hidi – Oum El Bouaghi

Faculty of Exact Sciences and Natural and Life Sciences
Department of Mathematics
Laboratory of Dynamical systems and control

Doctoral Thesis

Presented by :

Debbouche Nadjate

titled by :

A Study of Some Fractional-Order Chaotic Systems

Specialty: Applied Mathematics

In front of the jury:

Mr. Oussaeif Taki eddine	**MCA**	Univ. Larbi Ben M'hidi d'Oum El Bouaghi	President
Mr. Zehrour Okba	**Prof.**	Univ. Larbi Ben M'hidi d'Oum El Bouaghi	Supervisor
Mr. Ouannas Adel	**Prof.**	Univ. Larbi Ben M'hidi d'Oum El Bouaghi	Assistant Supervisor
Mr. Dhiliss Sofiane	**MCA**	Univ. Larbi Ben M'hidi d'Oum El Bouaghi	Examiner
Mr. Saoudi Khaled	**Prof.**	Univ. Abbas Leghrour de Khenchela	Examiner

JUIN 2022


بسم الله الرحمن الرحيم

ACKNOWLEDGEMENTS

بداية و قبل كل شيء، إن الحمد لله نحمده و نستعينه و نستغفره، والشكر لله على توفيقه لي لهذا العمل، قال تعالى:

"وَمَا تَوْفِيقِي إِلَّا بِاللَّهِ عَلَيْهِ تَوَكَّلْتُ وَإِلَيْهِ أُنِيبُ (88) " - هود –

" (88) And my success is not but through Allah. Upon him I have relied, and to Him I return." -Hud-

I would like to express my great thanks to my supervisor **Professor Okba Zehrour** for his guidance, throughout the realization of this work.

I would like also to express my great thanks and gratitude to my second supervisor **Professor Adel Ouannas** for his guidance and his steady faith in me, throughout the realization of this work.

I am thankful to **Doctor Taki eddine Oussaeif** for the honor he made me, of having kindly agreed to chair my thesis commitee.

I wish also to express all my gratitude to **Doctor Sofiane Dhiliss** and to **Professor Khaled Saoudi** for their willingness to read and examine my thesis, and for their help during the realization of this work.

I am also thankful to **my family** for their everyday patience, understanding, love and support.

Dedicated to my parents.

CONTENTS

General Introduction **8**

I Fractional-Order Chaotic Systems 12

1 Fractional-order systems (FOS) **13**
1.1 Special functions . . . 13
1.1.1 Gamma function . . . 13
1.1.2 Mittag-Leffler function . . . 14
1.2 Fractional calculus . . . 16
1.2.1 Fractional integrals . . . 16
1.2.2 Fractional derivatives . . . 17
1.2.3 Properties . . . 18
1.3 Stability of fractional-order systems (FOS) . . . 19
1.3.1 Asymptotic stability of linear FOS . . . 19
1.3.2 Asymptotic stability of nonlinear FOS . . . 20
1.4 Fractional numerical methods . . . 22
1.4.1 Numerical method according Caputo's definition . . . 22
1.4.2 Numerical method according Grünwald Letnikov's definition . . . 23

2 Fractional chaos **25**
2.1 Preliminaries . . . 25
2.1.1 Definition of dynamical system . . . 25
2.1.2 Classification . . . 25
2.1.3 Phase space . . . 27
2.1.4 Flow . . . 27
2.1.5 Invariant set . . . 28
2.1.6 Poincaré section . . . 28
2.1.7 Attractor . . . 28
2.2 General theory of chaos . . . 30
2.2.1 Presentation . . . 30
2.2.2 Bref history . . . 31
2.2.3 Examples of chaos in FONDS . . . 31
2.3 Chaos in fractional systems . . . 34
2.3.1 Sensitivity to initial conditions . . . 35
2.3.2 Lyapunov exponents . . . 35
2.3.3 Fractal dimension . . . 38
2.3.4 Hopf Bifurcation . . . 40
2.3.5 Basin of attraction . . . 42
2.3.6 Strange attractors . . . 42

II Applications 45

3 Chaos in fractional-order biological systems 46
3.1 Chaotic dynamics in a novel COVID-19 pandemic model described by commensurate and incommensurate fractional-order derivatives . . . 46
3.1.1 Introduction . . . 46
3.1.2 Mathematical model . . . 48
3.1.3 Dynamic analysis of model . . . 48
3.1.4 Discussion . . . 57
3.1.5 Conclusion . . . 58
3.2 Chaos and coexisting attractors in glucose-insulin regulatory system with incommensurate fractional-order derivatives . . . 61
3.2.1 Introduction . . . 61
3.2.2 FoGIRM with incommensurate-orders . . . 62
3.2.3 Dynamics of the system . . . 66
3.2.4 Conclusion . . . 78
3.3 Fractional-order biological system: chaos, multistability and coexisting attractors . . . 81
3.3.1 Introduction . . . 81
3.3.2 Mathematical Model . . . 82
3.3.3 Dynamics of FIONBS . . . 85
3.3.4 Symmetry, Multistability and Coexisting attractors . . . 86
3.3.5 Conclusions . . . 93
3.4 Chaos in cancer tumour growth model with commensurate and incommensurate fractional-order derivatives . . . 98
3.4.1 Introduction . . . 98
3.4.2 Fractional-order cancer model and its equilibrium points . . . 98
3.4.3 Dynamics of the commensurate fractional-order cancer model . . . 102
3.4.4 Dynamics of the incommensurate fractional-order cancer model . . . 108
3.4.5 conclusion . . . 114

4 Chaos in fractional-order physical systems 115
4.1 Chaos in fractional system with extreme events . . . 115
4.1.1 Introduction . . . 115
4.1.2 Fractional oscillator . . . 116
4.1.3 Extreme events in fractional oscillator . . . 118
4.1.4 Conclusion . . . 138
4.2 Chaotic Behavior Analysis of a New Incommensurate Fractional-Order Hopfield Neural Network System . . . 140
4.2.1 Introduction . . . 140
4.2.2 Mathematical model . . . 141
4.2.3 Dynamics of incommensurate fractional-order model . . . 142
4.2.4 Variable-boostable attractors of incommensurate fractional-order model . . . 149
4.2.5 Conclusion . . . 152
4.3 Secure Multiple-Input Multiple-Output Communications Based on F-M Synchronization of FOCS with Non-Identical Dimensions and Orders . . . 153
4.3.1 Introduction . . . 153
4.3.2 Problem Formulation . . . 154
4.3.3 F-M Synchronization . . . 155
4.3.4 Numerical Example . . . 157
4.3.5 Conclusion . . . 161

5 Chaos in fractional-order general systems 163
5.1 Dynamics of fractional-order chaotic and hyper-chaotic systems . . . 163
5.1.1 Introduction . . . 163
5.1.2 Fractional-order 3D autonomous chaotic system . . . 163
5.1.3 Fractional-order 4D autonomous chaotic system . . . 166

5.2 Generating multidirectional variable hidden attractors via newly commensurate and incommensurate non equilibrium fractional-order chaotic systems 175
5.2.1 Introduction 175
5.2.2 A non-equilibrium FoS 176
5.2.3 The commensurate FoS 177
5.2.4 Incommensurate FoS 185
5.2.5 Variable-boostable hidden attractors of commensurate and incommensurate FoS 191
5.2.6 Conclusion 194

General Conclusion **196**

Glossary **197**

Bibliography **198**

Abstract **212**

Résumé **213**

Arabic abstract **214**

GENERAL INTRODUCTION

The fractional calculus is a name for the theory of integrals and derivatives of arbitrary order, which unify and generalize the notions of integer-order differentiation and n-fold integration [1]. The concept of differentiation and integration to noninteger order is by no means new. We mention the most important stages in the development of this concept [2]:

- **In 1695:** L'Hôpital sent a letter to Leibniz, in his letter, a question about the order the derivatives emerged: what meaning could be ascribed to derivative of order n if n was a fraction? In a forecast answer, Leibniz predicted the beginning of the area that today is named fractional calculus (FC).
- **In 1738:** Euler observed the problem for a derivative of noninteger order, he noted that the result of the evaluation of a derivative of a power function has a meaning for noninteger orders [3].
- **In 1812:** Laplace suggested the idea of differentiation of noninteger order for functions representable by an integral [3].
- **In 1822:** Fourier proposed an integral representation in order to define the derivative, this version is considered the first definition for the derivative of fractional (positive) order [4].
- **In 1826:** Abel applied the fractional calculus in the solution of an integral equation that arises in the formulation of the tautochrone problem, which is considered to be the first application of FC [5].
- **In 1832:** Liouville suggested a definition based on the formula for differentiating the exponential function, which is known as his first definition [6]. The second definition given by Liouville is presented in terms of an integral which is the integration of noninteger order [7].
- **In 1868, 1867:** It was Grünwald and Letnikov who first unified the results of Liouville and Riemann, they develop a method to noninteger order derivatives in terms of a convergent series.
- **It was not until 1900:** that the theory about FC has a great interest, and in an attempt to formulate particular problems, other definitions were proposed that gave a point of departure for the development of this area.
- **In 1967:** Caputo proposed a definition to discuss problems involving a fractional differential equation with initial conditions [7]. The definition given by Caputo inverts the position of integral and derivative operators with the noninteger order derivative in relation to Riemann-Liouville definition [8].

- **In 1974:** The first conference devoted to the topic of fractional calculus took place in New Haven, USA. Circumstances have changed considerably since then.

Despite a long history, the doubts that fractional-order (FO) derivatives have no clear geometrical interpretations (see [9]), was one of the several reasons that fractional calculus was not used in physics or engineering. However, during the last more than ten years, fractional calculus has started to attract increasing attention. There are nowadays more and more works on FO systems and their related applications. Some particular characteristics for using FC are [10]:

- Fractional derivatives provide an excellent instrument for the description of memory and hereditary properties of various materials and processes. This is the main advantage of fractional models in comparison with classical integer-order models, in which such effects are in fact neglected.
- Engineers and scientists have developed new models that involve fractional differential equations in mechanics (theory of viscoelasticity and viscoplasticity), bio-chemistry (modelling of polymers and proteins), electrical engineering (transmission of ultrasound waves), medicine (modelling of human tissue under mechanical loads), etc.
- The development of fractional-order algorithms allowed to use of FC in the applications.

Chaos theory is an interdisciplinary scientific theory and branch of mathematics, it has become applicable to a variety of other situations. One of the important applications of FC is the chaos applications in different disciplines such as: electrical engineering, information processing, secure communications, biology, medicine, economics, finance, meteorology, physics, etc...
Therefore, new fractional chaotic systems are crucial to enhance the performance of several integer-order chaos-based applications. One of the main objectives of this work is found that chaotic behavior in fractional-order countinous systems.

Thesis organization

The thesis is organized into two parts as follows:

- 1^{st} part: is devoted to the fractional systems and it contains two chapters:
  - Chapter 1: contains some preliminaries about fractional-order system (FOS) including special functions (the Gamma and the Mittag-Leffler function), defintions of three fractional integer and derivatives (Riemann-Liouville, Caputo and Grüunwald-Letnikov approaches), the generalization of the notions of fractional derivation and integration in Fractional systems and at the end of this chapter, some numerical methods of solving FOS are introduced including matlab programs.
  - Chapter 2: contains a generalization of notion of fractional-order chaotic systems (FOCS) including basic concepts of continuous dynamical systems, chaos theory, some methods to detecting chaos in FODS and at the end of this chapter, two theorems for studing the asymptotic stability for commensurate and incommensurate FOS. it is shown that all most classical criterion and tools for the study of dynamical systems have been reformulated in a general sitting and used for the study of fractional-order dynamical systems.
- 2^{nd} part: presents an applications of the mathematical tools introduced in the previous chapters. This chapter has been the subject of ten publications [11, 12, 13, 14, 15, 16, 17, 18, 19, 20], and it contains three chapters:

- Chapter 3: applications of chaos in FO biological systems.
- Chapter 4: applications of chaos in FO Physical systems.
- Chapter 5: applications of chaos in FO general systems.

At the end, our thesis will be concluded with a general conclusion followed by a rich bibliography, containing several references concerning chaos theory in Fractional-order countinious dynamical systems.

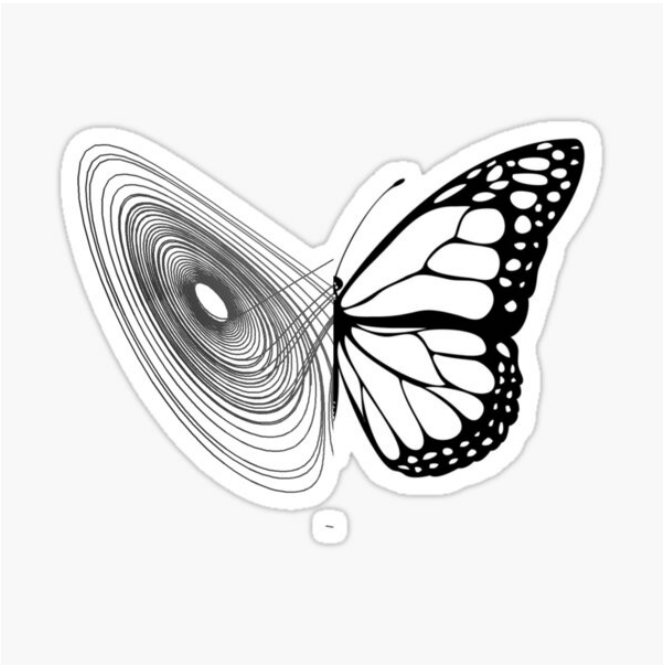

Part I

Fractional-Order Chaotic Systems

CHAPTER 1

FRACTIONAL-ORDER SYSTEMS (FOS)

Starting from fundamentals definitions of fractional calculus until a numerical method for solving fractional order differential equations, this chapter is a review of necessary concepts.

1.1 Special functions

There are many special functions used in fractional calculus such as the Gamma and the Beta functions, the Mittag-Leffler functions and the Wright function; these functions play the most important role in the theory of differentiation of arbitrary order and in the theory of fractional differential equations. In this section, we should mention some basic information of two of them (Gamma and Mittag-Leffler functions) which are used later in this work.

1.1.1 Gamma function

The Euler's Gamma function is a generalization of the factorial function $n!$ which allows n to take also non-integer and even complex values. The Gamma function $\Gamma(z)$ is one of the important basic functions of fractional calculus [1].

Definition 1.1.1. For all $z \in \mathbb{C}$, such as $\Re e(z) > 0$

$$\Gamma(z) = \int_0^\infty t^{z-1} e^{-t} dt, \tag{1.1.1}$$

this integral converges in the right half of the complex plane.
An important property of $\Gamma(z)$ is the following reccurence relation:

$$\Gamma(z+1) = z\Gamma(z), \tag{1.1.2}$$

that it can be demonstrated by an integration by parts:

$$\Gamma(z+1) = \int_0^\infty t^z e^{-t} dt = [-t^{-z} e^{-t}]_0^\infty + z \int_0^\infty t^{z-1} e^{-t} dt = z\Gamma(z).$$

And specially:

- $\Gamma(1) = \int_0^\infty t^{1-1} e^{-t} dt = \int_0^\infty e^{-t} dt = 1.$

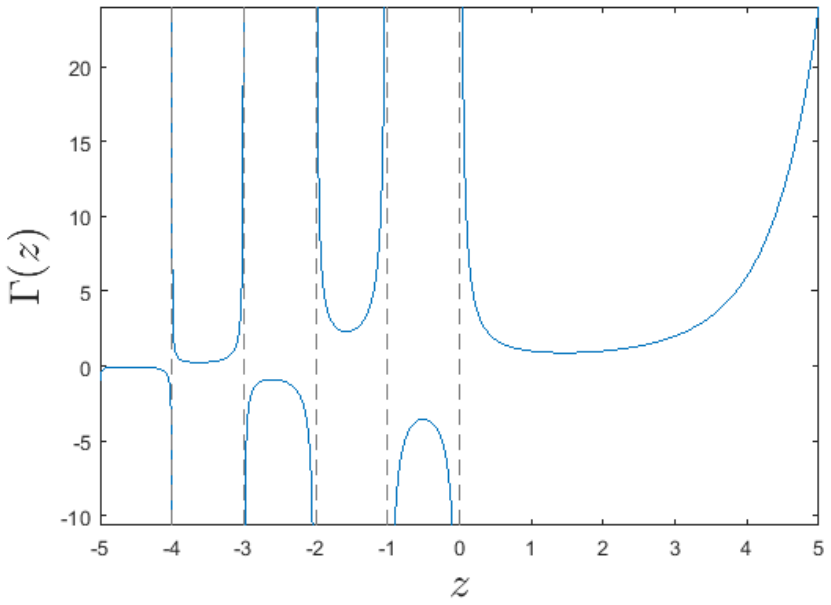

Figure 1.1: The graph of Gamma function

- $\forall n \in \mathbb{N}^* : \Gamma(n+1) = n!$.
- For $z = \frac{1}{2}, \Gamma(\frac{1}{2}) = \sqrt{\pi}$.

Graphical representation of Gamma function is presented in Figure 1.1.

1.1.2 Mittag-Leffler function

The Mittag-Leffler function is a generalization of the exponential function. The Mittag-Leffler function is an important function that is found widely used in fractional calculus and plays an analogous role in the solution of the fractional derivative equations.

Definition 1.1.2. For $z \in \mathbb{C}$, the Mittag Leffler function is defined by [1]:

$$E_\alpha(z) = \sum_{k=0}^{\infty} \frac{z^k}{\Gamma(\alpha k + 1)}, \quad \alpha > 0. \tag{1.1.3}$$

In particular:

- If $\alpha = 1$, $E_1(z) = e^z$ (the exponential function).
- If $\alpha = 2$, $E_2(z) = cosh(\sqrt{z})$.

A two parameter Mittag-Leffler function is given by:

$$E_{\alpha,\beta}(z) = \sum_{k=0}^{\infty} \frac{z^k}{\Gamma(\alpha k + \beta)}, \quad \alpha > 0, \beta > 0; z \in \mathbb{C}. \tag{1.1.4}$$

For special choices of the values of the parameters α and β, we can get from the definition (1.1.4) that [1]:

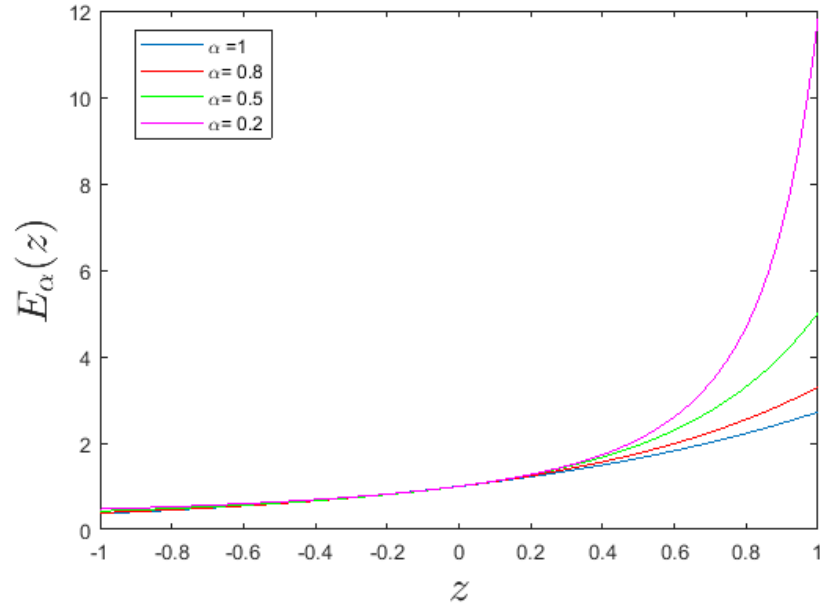

(a)

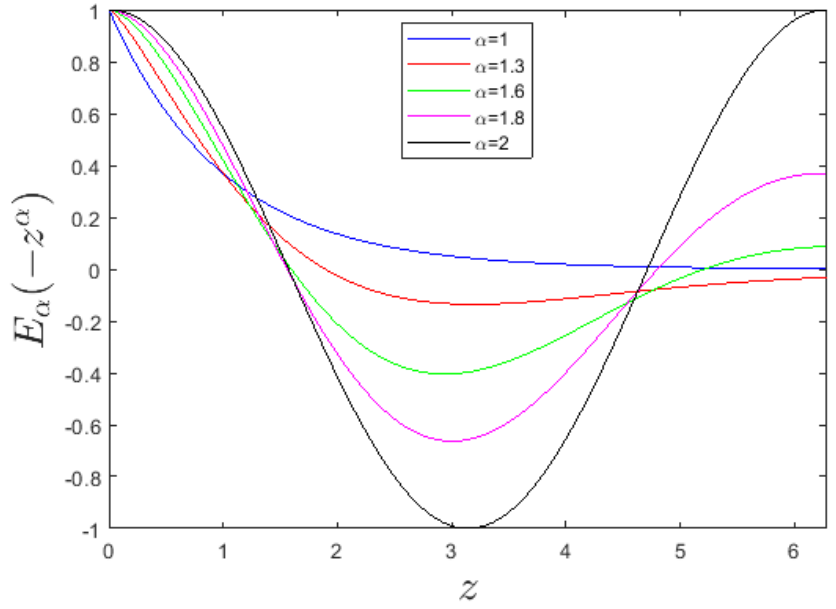

(b)

Figure 1.2: The graphs of one parameter Mittag-Leffler function for parameters: (a)$E_\alpha(z)$, where $z \in [-1,1]$, (b)$E_\alpha(-z^\alpha)$, where $z \in [0,2\pi]$.

- If $\alpha = 1, \beta = 1, E_{1,1}(z) = e^z$.
- If $\alpha = 1, \beta = 2, E_{1,2}(z) = \frac{e^z - 1}{z}$.
- If $\alpha = 2, \beta = 1, E_{2,1}(z^2) = cosh(z)$.
- If $\alpha = 2, \beta = 2, E_{2,2}(z^2) = \frac{sinh(z)}{z}$.
- If $\alpha = 1/2, \beta = 1, E_{1/2,1}(\sqrt{z}) = \frac{2}{\sqrt{\pi}} e^{-z} erfc(-\sqrt{z})$, (where $erfc$ is the error function defined by $erfc(z) = \frac{2}{\sqrt{\pi}} \int_z^{\infty} e^{-t^2} dt$).

For $\beta = 1$ we obtain the Mittag-Leffler function in one parameter:

$$E_{\alpha,1}(z) = \sum_{k=0}^{\infty} \frac{z^k}{\Gamma(\alpha k + 1)} = E_{\alpha}(z).$$

The graphs of of one parameter Mittag-Leffler function for some values of α are presented in Figure 1.2 (a) and Figure 1.2 (b) .

1.2 Fractional calculus

In this work we will mention the three most frequently used definitions for the general fractional calculus [1, 4, 21]: the Riemann-Liouville (RL), the Caputo definitions and the Grünwald-Letnikov (GL) definition, the three best known definitions are equivalent under some conditions [1].

1.2.1 Fractional integrals

Rimann-Liouville fractional integral

The Rimann-Liouville fractional integral is a generalization of the Cauchy's formula of n-fold integral wich defined as [1]:

$$\begin{aligned} I_a^n f(x) &= {}_aD_x^{-n} f(x) \\ &= \int_a^x dx_1 \int_a^{x_1} dx_2 ... \int_a^{x_{n-1}} f(t)dt \\ &= \frac{1}{(n-1)!} \int_a^x (x-t)^{n-1} f(t)dt, \quad x > a, n \in \mathbb{N}^*. \end{aligned}$$

Using the Gamma function in this formula and replacing the integer n by a real positive number α, we have obtain the Riemann-Liouville fractional integral of order $\alpha > 0$ as follows:

$$ {}_a^{RL}D_x^{-\alpha} f(x) = \frac{1}{\Gamma(\alpha)} \int_a^x (x-t)^{\alpha-1} f(t)dt, \quad x > a, \alpha > 0. \tag{1.2.1}$$

Grünwald-Letnikov Fractional integral

The Grünwald-Letnikov fractional-order integral of order $\alpha < 0$ is given by [22]:

$$ {}_a^{GL}D_t^{-\alpha} f(t) = lim_{h \to 0} h^{\alpha} \sum_{j=0}^{[\frac{t-a}{h}]} (_j^{-\alpha}) f(t - jh), \tag{1.2.2}$$

where$[\frac{t-a}{h}]$ means the integer part.
For binomial coefficients calculation $\binom{-\alpha}{j}$, it is not defined using factorials. We have:

$$\binom{-\alpha}{j} = (-1)^j \frac{\Gamma(\alpha+j)}{\Gamma(j+1)\Gamma(\alpha)}.$$

1.2.2 Fractional derivatives

Rimann-Liouville fractional derivative

Now, we recall the following identity:

$$D^n = D^m I^{m-n} f$$

where the function f has a continuous n^{th} derivative on interval $[a,b]$, $n,m \in \mathbb{N}$, such that $m > n$.
The Rimann-Liouville fractional derivative is obtained by remplacing the integer n by a positive real number α and taking $m = \lceil \alpha \rceil$ (the smallest integer that exceeds α) in th previous identity, we have found [1]:

$$ {}_a^{RL}D_t^{\alpha} = D^m I^{m-\alpha} f, \quad \alpha \in \mathbb{R}_+, m = \lceil \alpha \rceil. \tag{1.2.3}$$

The identity 1.2.3 is equivalent to:

$$ {}_a^{RL}D_t^{\alpha} = \begin{cases} \dfrac{1}{\Gamma(m-\alpha)} \dfrac{d^m}{dt^m} \displaystyle\int_a^t (t-s)^{m-\alpha-1} f(s) ds, & m-1 < \alpha < m, \\ \dfrac{d^m}{dt^m} f(t), & \alpha = m. \end{cases}$$

Caputo fractional derivative

The definition of Caputo fractional derivative is given by [1]:

$$ {}_a^{c}D_t^{\alpha} f(t) = \frac{1}{\Gamma(m-\alpha)} \int_a^t (t-s)^{m-\alpha-1} f^{(m)}(s) ds, \quad m-1 < \alpha < m \tag{1.2.4}$$

with $\alpha \geq 0, m = \lceil \alpha \rceil$ and $f \in C^n[a,b]$.
Caputo's definition is almost used in Applied maths because of their advantages such as: the initial conditions for the fractional-order differential equations with the Caputo derivatives are in the same form as for the integer-order differential equations. It is an advantage because applied problems require definitions of fractional derivatives, where there are clear interpretations of initial conditions, which contain $f(a)$, $f'(a)$, $f''(a)$,...
Moreover, it has the benefit of possessing a value of zero when it is applied to a constant.

Grünwald-Letnikov Fractional derivative

The Grünwald-Letnikov fractional-order derivative of order $\alpha > 0$ is given by [22]:

$$ {}_a^{GL}D_t^{\alpha} f(t) = lim_{h \to 0} \frac{1}{h^{\alpha}} \sum_{j=0}^{[\frac{t-a}{h}]} (-1)^j \binom{\alpha}{j} f(t-jh), \tag{1.2.5}$$

where$[\frac{t-a}{h}]$ means the integer part.
For binomial coefficients calculation $\binom{\alpha}{j}$ we can use the relation between Euler's Gamma function and factorial,

defined as:

$$\binom{\alpha}{j} = \frac{\alpha!}{j!(\alpha-j)!} = \frac{\Gamma(\alpha+1)}{\Gamma(j+1)\Gamma(\alpha-j+1)}$$

for $\binom{\alpha}{0} = 1$.

1.2.3 Properties

The main properties of fractional derivatives/integrals are as follows [21] :

- If $f(t)$ is an analytical function of t, then its fractional derivative ${}_0D_t^\alpha f(t)$ is an analytical function of t, α.
- For $\alpha = n$, where n is integer, the operation ${}_0D_t^\alpha f(t)$ gives the same result as classical differentiation of integer order n.
- For $\alpha = 0$ the operation ${}_0D_t^\alpha f(t)$ is the identity operator:

$${}_0D_t^0 f(t) = f(t).$$

- Fractional differentiation and fractional integration are linear operations:

$${}_aD_t^\alpha f(\lambda f(t) + \mu g(t)) = \lambda {}_aD_t^\alpha f(t) + \mu {}_aD_t^\alpha g(t)$$

- The additive index law (semigroup property)

$${}_0D_t^\alpha \ {}_0D_t^\beta f(t) = {}_0D_t^\beta \ {}_0D_t^\alpha f(t) = {}_0D_t^{\alpha+\beta} f(t)$$

  holds under some reasonable constraints on the function $f(t)$.

  The fractional-order derivative commutes with integer-order derivative

$$\frac{d^n}{dt^n}\Big({}_aD_t^r f(t)\Big) = {}_aD_t^r\Big(\frac{d^n f(t)}{dt^n}\Big) = {}_aD_t^{r+n} f(t),$$

  under the condition $t = a$ we have $f^{(k)}(a) = 0, (k = 0, 1, 2, ..., n-1)$. The relationship above says the operators $\frac{d^n}{dt^n}$ and ${}_aD_t^r$ commute.
- Geometric and physical interpretation of fractional integration and fractional differentiation was clearly explained in Podlubny's work [9].

1.3 Stability of fractional-order systems (FOS)

"The fractional-order system" is a system which is described by fractional differential equations which are an equations that contain one or more fractional derivatives.
Consider the following Fractional-order system:

$$\begin{cases} {}_0^C D_t^{\alpha_i} x_i(t) = f_i(x_1(t), x_2(t), ..., x_n(t), t), \\ x_i(0) = c_i, \qquad i = 1, 2, ..., n, \end{cases} \tag{1.3.1}$$

where c_i are initial conditions. The vector representation of (1.3.1) is:

$$D^{\alpha} \boldsymbol{x} = \boldsymbol{f}(\boldsymbol{x}), \tag{1.3.2}$$

where $\boldsymbol{\alpha} = [\alpha_1, \alpha_2, ..., \alpha_n]$ for $0 < \alpha_i < 1, (i = 1, 2, ..., n)$ and $\boldsymbol{x} \in \mathbb{R}^n$.
The system (1.3.2) is called a commensurate order system when $\alpha_1 = \alpha_2 = ... = \alpha_n$, otherwise it is an incommensurate order system. The system (1.3.2) is called non-autonomous system if If $\boldsymbol{f}$ depends explicitly on t otherwise it is called autonomous system. The equilibrium points of system (1.3.2) are calculated via solving the following equation:

$$\boldsymbol{f}(\boldsymbol{x}) = 0. \tag{1.3.3}$$

The solution $x(t) = 0$ of the system (1.3.2) is said to be:

- stable if: for any $\epsilon > 0$ there exists some $\delta > 0$ such that the solution of the initial value problem consisting of (1.3.2) and the initial condition $x(0) = x_0$ satisfies $x(t) < \epsilon$ for all $t \geq 0$ whenever $\|x_0 < \delta\|$.
- asymptotically stable if: it is stable and there exists some $\gamma > 0$ such that $\lim_{t \to \inf} x(t) = 0$ whenever $\|x_0\| < \gamma$.
- locally exponentially stable if there exist two real constants $\alpha, \lambda > 0$ such that

  $$\|x(t)\| \leq \alpha \|x(t_0)\| e^{-\lambda t} \quad \text{for all} t > t_0, \tag{1.3.4}$$

  whenever $||x(t_0)|| < \delta$. It is said to be globally exponentially stable if (1.3.4) holds for any $x(t_0) \in \mathbb{R}^n$.
- Mittag-Leffler stable if

  $$\|x(t)\| \leq \{m[x(t_0)] E_{\alpha}(\lambda (t - t_0)^{\alpha})\}^b,$$

  where t_0 is the initial time, $\alpha \in (0, 1)$ the fractional order, $\lambda \geq 0, b > 0, m(0) = 0, m(x \geq 0)$ and $m(x)$ is locally Lipschitz on $x \in \boldsymbol{B} \subset \mathbb{R}$ with constant Lipschitz m_0.

Remark 1.3.1. As mentioned in [23], exponential stability cannot be used to characterize asymptotic stability of fractional-order systems. A new definition was introduced [24].

Definition 1.3.1 (Power law stability $t^{-\beta}$). The trajectory $x(t) = 0$ of the system (1.3.5) is $t^{-\beta}$asymptotically stable if there is a positive real β such that:

$$\forall \|x(t)\| \quad \text{with} \quad t \leq t_0, \exists N(x(t)), \quad \text{such that} \quad \forall t \geq t_0, \|x(t)\| \leq N t^{-\beta}.$$

1.3.1 Asymptotic stability of linear FOS

In this section, we discuss the asymptotic stability of both commensurate and incommensurate linear FOS.

Commensurate case

Theorem 1.3.1. *Consider the n-dimensional linear differential system with fractional commensurate order α [23]:*

$$ {}_0^C D_t^{\alpha} X = AX, \tag{1.3.5}$$

where A is an arbitrary constant $n \times n$ matrix.
The system (1.3.5) is asymptotically stable if and only if $|\arg(spec(A))| > \alpha\pi/2$.

Proof. See [10]. □

Incommensurate case

Theorem 1.3.2. *Consider the n-dimensional linear differential system with fractional incommensurate order α_i [25]:*

$$ {}_0^C D_t^{\alpha_i} X = AX, \tag{1.3.6}$$

where A is an arbitrary constant $n \times n$ matrix.
Suppose that $\alpha_1 \neq \alpha_2 \neq ... \neq \alpha_n$ and all α_i's are rational numbers between 0 and 1, and suppose that m is the lowest common multiple of the denominators u_i of $\alpha_i, (i = 1, ..., n)$ where $\alpha_i = \frac{v_i}{u_i}, v_i, u_i \in \mathbb{Z}^+$ for $i = 1, ..., n$, and setting $\gamma = \frac{1}{m}$ then system (1.3.6) is asymptotically stable if:

$$ |\arg(\lambda)| > \gamma \frac{\pi}{2}, \tag{1.3.7}$$

for all roots λ of the following characteristic equation

$$ \det(diag([\lambda^{m\alpha_1}, ..., \lambda m\alpha_n]) - A) = 0. \tag{1.3.8}$$

Proof. See [10]. □

1.3.2 Asymptotic stability of nonlinear FOS

Stability of the fractional-order nonlinear system is very complex and is different from the fractional-order linear system. The main difference is that for a nonlinear system it is necessary to investigate steady states having two types: equilibrium point and limit cycle. Nonlinear systems may have several equlibrium points.
In this section, we discuss the asymptotic stability of both commensurate and incommensurate nonlinear FOS.

Commensurate case

Theorem 1.3.3. *consider the following commensurate fractional order system [26]:*

$$ \frac{d^{\alpha}}{dt^{\alpha}} x = f(x), \tag{1.3.9}$$

where $0 < \alpha < 1$ and $x \in R^n$. The equilibrium points of system (1.3.9) are locally asymptotically stable if all eigenvalues λ_i of the Jacobian martrix $J = \frac{\partial f}{\partial x}$ evaluated at the equilibrium points satisfy:

$$ |arg(\lambda_i)| > \alpha\pi/2. $$

Incommensurate case

Consider the incommensurate fractional ordered dynamical system [26]:

$$D^{\alpha_i} x_i = f_i(x_1, x_2, x_3), \qquad 1 \le i \le 3, \tag{1.3.10}$$

where $0 < \alpha_i < 1, \alpha_i = v_i/u_i, (u_i, v_i) = 1, u_i, v_i$ are positive integer. Define M to be the least common multiple of u_i's. Let $p \equiv (x_1^*, x_2^*, x_3^*)$ be an equilibrium point of the system (1.3.10) and $\xi_i = x_i - x_i^*, 1 \le i \le 3$ a small perturbation from a fixed point. Then

=

$$\begin{aligned} D^{\alpha_i}\xi_i &= D^{\alpha_i} x_i, \\ &= f_i(x_1, x_2, x_3) = f_i(\xi_1 + x_1^*, \xi_2 + x_2^*, \xi_3 + x_3^*) \\ &= f_i(x_1^*, x_2^*, x_3^*) + \xi_1 \frac{\partial f_i(p)}{\partial x_1} + \xi_2 \frac{\partial f_i(p)}{\partial x_2} + \xi_3 \frac{\partial f_i(p)}{\partial x_3} + \text{higher ordered terms} \\ &\approx \xi_1 \frac{\partial f_i(p)}{\partial x_1} + \xi_2 \frac{\partial f_i(p)}{\partial x_2} + \xi_3 \frac{\partial f_i(p)}{\partial x_3}. \end{aligned}$$

We obtained

$$D^{\alpha_i}\xi_i \approx \xi_1 \frac{\partial f_i(p)}{\partial x_1} + \xi_2 \frac{\partial f_i(p)}{\partial x_2} + \xi_3 \frac{\partial f_i(p)}{\partial x_3}. \tag{1.3.11}$$

System (1.3.11) is equivalent to

$$\begin{pmatrix} D^{\alpha_1}\xi_1 \\ D^{\alpha_2}\xi_2 \\ D^{\alpha_3}\xi_3 \end{pmatrix} = J \begin{pmatrix} \xi_1 \\ \xi_2 \\ \xi_3 \end{pmatrix}, \tag{1.3.12}$$

where J is the Jacobian matrix evaluated at point p defined as

$$J = \begin{pmatrix} \partial_1 f_1(p) & \partial_2 f_1(p) & \partial_3 f_1(p) \\ \partial_1 f_2(p) & \partial_2 f_2(p) & \partial_3 f_2(p) \\ \partial_1 f_3(p) & \partial_2 f_3(p) & \partial_3 f_3(p) \end{pmatrix}$$

Define

$$\Delta(\lambda) = diag([\lambda^{M\alpha_1} \lambda^{M\alpha_2} \lambda^{M\alpha_3}]) - J. \tag{1.3.13}$$

Then the solution of the linear system (1.3.12) is asymptotically stable if all the roots of the equation $det(\Delta(\lambda)) = 0$ satisfy the condition $|arg(\lambda)| > \pi/(2M)$ [27]. This condition is equivalent to the following inequality

$$\frac{\pi}{2M} - min_i\{|arg(\lambda_i)|\} < 0. \tag{1.3.14}$$

Thus an equilibrium point p of the system (1.3.10) is asymptotically stable if the condition (1.3.14) is satisfied. The term $\frac{\pi}{2M} - min_i\{|arg(\lambda_i)|\}$ is called the instability measure for equilibrium points in fractional order systems (IMFOS). Hence, a necessary condition for fractional order system (1.3.10) to exhibit a chaotic attractor is [26]

$$IMFOS \ge 0. \tag{1.3.15}$$

Remark 1.3.2. Daftardar-Gejji was demonstrated in [28] that the condition (1.3.15) is not sufficient for chaos to exist.

Remark 1.3.3. An interesting difference between stable integer-order system and a stable fractional-order system is that the last one may have roots in right half of the complex plane (see Figure 1.3).

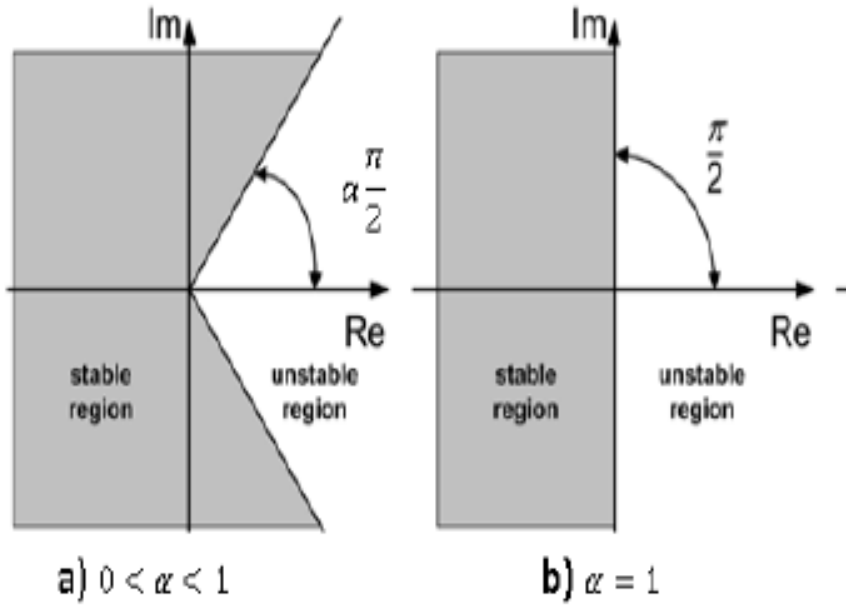

Figure 1.3: Stability regions of FOS.

1.4 Fractional numerical methods

Various numerical methods exist in the literature for solving fractional-order systems, predictor-corrector type methods such as Fractional Adams Method (FAM) or New Predictor Corrector Method (NPCM) are more suitable and are extensively used in the literature. In this section, we discuss two numerical alghorithms according Caputo's definition and Grünwald Letnikov's definition.

1.4.1 Numerical method according Caputo's definition

To approximate the fractional-order system using the ABM and PECE numerical approximation method consider [29]:

$$D^q x = f(t,x), \tag{1.4.1}$$

where q is the fractional-order, $0 \le t \le T$ with initial values $x^k(0) = x_0^k$ for $k \in [0, n-1]$. Equation (1.4.1) can be solved using the Volterra integral equation (VIE) given by:

$$x(t) = \sum_{k=0}^{n-1} x_0^k \frac{t^k}{k!} + \frac{1}{\Gamma(q)} \int_0^t \frac{f(\tau,x)}{(t-\tau)^{1-q}} d\tau \tag{1.4.2}$$

The numerical approximation form of (1.4.2) can be defined as:

$$x_h(t_{n+1}) = \sum_{k=0}^{n-1} x_0^{(k)} \frac{t_n^{k+1}}{k!} + \frac{h^q}{\Gamma(q+2)} f(t_{n+1}, x_h^p(t_{n+1}))$$

$$+ \frac{h^q}{\Gamma(q+2)} \sum a_{j,n+1} f(t_{n+1}, x_h^p(t_{n+1})) \tag{1.4.3}$$

where

$$\begin{cases} a_{j,n+1} = \begin{cases} n^{q+1} - (n-q)(n+q)^{q+1}, & j = 0, \\ -2(n-j+1)^{q+1}, & 1 \le j \le n, \\ 1, & j = n+1, \end{cases} \\ x_h^p(t_{n+1}) = \sum_{k=0}^{n-1} x_0^{(k)} \frac{t_n^{k+1}}{k!} + \frac{h^q}{\Gamma(2)} \sum_{j=0}^{n} b_{j,n+1}(t_j x_h(t_j)), \\ b_{j,n+1} = \frac{h^q}{q}((n-j+1)^q - (n-j)^q), \end{cases} \tag{1.4.4}$$

$h = T/N$, and $t_n = nh$ with $h \in [0, N]$ The error for this method can be estimated as $e_{max} = max|x(t_j) - x_h(t_j)| = 0(h^p)$, where $i = 0, 1, ..., N$ and $p = min(2, 1+q)$.

Matlab program

Matlab code of this method is given:

- in [30] for commensurate FOS.
- in [31] for incommensurate FOS.

1.4.2 Numerical method according Grünwald Letnikov's definition

For numerical calculation of fractional-order derivatives we can use the relation(1.4.5) derived from the GL definition (1.2.5). The relation to the explicit numerical approximation of q-th derivative at the points $kh, (k = 1, 2, ...)$ has the following form [1],[32], [33]:

$$_{k-L_m/h}D_{t_k}^q f(t) \approx h^{-q} \sum_{j=0}^{k} (-1)^j \binom{q}{j} f(t_{k-j}), \tag{1.4.5}$$

where L_m is the "memory length", $tk = kh$, h is the time step of calculation and$(-1)^j\binom{q}{j}$are binomial coefficients $c_j^k (j = 0, 1, ...)$.
For their calculation we can use the following expression [32]:

$$c_0^{(q)} = 1, \quad c_j^{(q)} = \left(1 - \frac{1+q}{j}\right) c_{j-1}^{(q)} \tag{1.4.6}$$

Then, general numerical solution of the fractional differential equation

$$_aD_t^q y(t) = f(y(t), t),$$

can be expressed as

$$y(t_k) = f((y(t_k), t_k)h^q - \sum_{j=v}^{k} c_j^{(q)} y(t_{k-j}). \tag{1.4.7}$$

For the memory term expressed by the sum, a "short memory" principle can be used. Then the lower index of the sums in relations (1.4.7) will be $v = 1$ for $k < L_m/h$ and $v = k - L_m/h$ for $k > L_m/h$, or without using the "short memory" principle, we put $v = 1$ for all k.

Obviously, for this simplification we pay a penalty in the form of some inaccuracy. If $f(t) \leq M$, we can easily establish the following estimate for determining then memory length L_m, providing the required accuracy ε :

$$L_m \geq \left(\frac{M}{\varepsilon |\Gamma(1-q)|} \right)^{1/q}$$

An evaluation of the short memory effect and convergence relation of the error between short and long memory were clearly described and also proved in [32].

Matlab program

Matlab code of this method is given in [22]. The program here, is for both commensurate and incommensurate FOS.

CHAPTER 2

FRACTIONAL CHAOS

The fractional-order nonlinear dynamics systems (FONDS) are used to describe a vast variety of science and engineering phenomena. This chapter describes the fundamental concepts and tools that are directly related to nonlinear dynamics with fractional derivatives that are briefly review in this thesis.

2.1 Preliminaries

This section is a review of necessary concepts about fundamentals definitions of continuous dynamical systems.

2.1.1 Definition of dynamical system

Definition 2.1.1. A dynamical system is a continuous application $\Phi : \mathbb{R} \times \mathbb{R}^n \to \mathbb{R}^n$ verifying: $\phi(0, x_0) = x_0, \phi(t + s, x_0) = \phi(t, \phi(s, x_0))$, where $(t, x_0) \in \mathbb{R} \times \mathbb{R}^n, s \in \mathbb{R}$.

Such a dynamic system presents two aspects, its state and its dynamics; that is, its evolution over time [34].

2.1.2 Classification

Dynamical systems are classified into two categories:

- Discrete dynamical system.
- Continuous dynamical system.

Definition 2.1.2. A discrete dynamical system is a system of recurrent algebraic equations defined by [35, 36, 37, 38]:

$$x_{k+1} = F(x_k, \mu), \qquad k \in \mathbb{N},$$

Where $X(k) = x_k \in U \subseteq \mathbb{R}^n$ is the state vector at time t_k. $\mu \in V \subseteq \mathbb{R}^p$ is the vector of the parameters. F is the recurrence function defines the dynamics of the discrete system. If we associate with this dynamic an initial state $x_0 = X(0)$ we will be able to have a unique solution of F.

***Example* 2.1.1.** *(Logistic function) The logistic map is given by [39] :*

$$x_{n+1} = r x_n (1 - x_n), \tag{2.1.1}$$

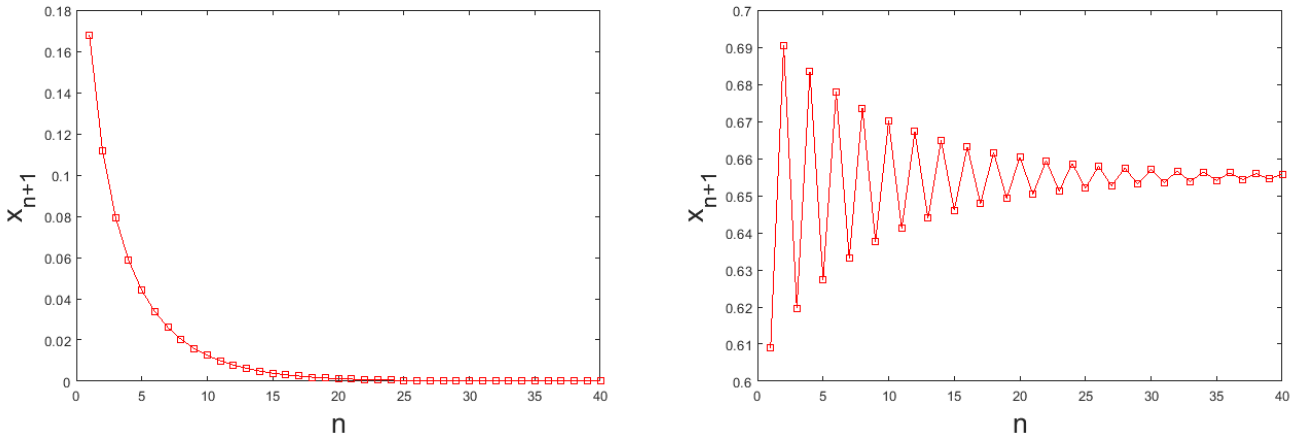

(a) (b)

Figure 2.1: Time series of logistic map for: (a) $r = 0.8$, (b) $r = 2.9$.

where $x_n \geq 0$ is dimensionless measure of population in n^{th} generation $(n = 0, 1, 2, ...)$ and $r \geq 0$ is intrinsic growth rate. Using iterations of map (2.1.1) we can find the population at any time n using the initial population x_0. Figure 2.1 shows the time series of logistic map for $r = 0.8$ in Figure 2.1(a) and for $r = 2.9$ in Figure 2.1(b).
Another examples of this type of dynamical systems was presented in [40, 41, 42, 43, 44, 45, 46, 47, 48, 49, 50].

Definition 2.1.3. A continuous dynamical system is described by a system of differential equations [51]:

$$X'(t) = G(X(t), t) \tag{2.1.2}$$

Where G of class $C^1 : \mathbb{R}^n \times \mathbb{R}^+ \to \mathbb{R}^n$ defines the dynamics of the continuous system.

Definition 2.1.4. A solution of equation (2.1.2) is a differentiable application defined on an open, non-empty interval $I \subset \mathbb{R}^+, x : I \to \mathbb{R}^n, t \to x(t)$ and verifying, for all $t \in I$,

$$(t, x(t)) \in I \times \mathbb{R}^n,$$

and

$$x'(t) = G(t, x(t)).$$

Remark 2.1.1. At each pair $(X(0), t_0)$, we can associate a unique solution of the system defined using the equation (2.1.2).

Remark 2.1.2. When G explicitly depends on time, the system (2.1.2) is said to be non-autonomous, otherwise we say that the system (2.1.2) is autonomous.

Definition 2.1.5. Let x_0 be an initial condition and $X(t, x_0)$ the solution of (2.1.2), the set of points $\{\forall t \in \mathbb{R}; X(t, x_0)\}$ is the trajectory in space of state passing to x_0 at the initial instant.

Definition 2.1.6. We call the orbit of the system (2.1.2), the set $X(t), t \in \mathbb{R}$.

Definition 2.1.7. A fixed (or critical, or singular, or stationary) point of the equation $x' = F(x)$ is a point X^* of the phase space satisfying $F(X^*) = 0$.

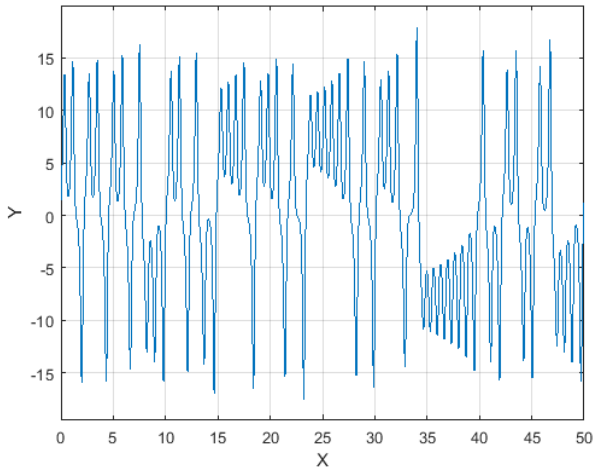

(a)

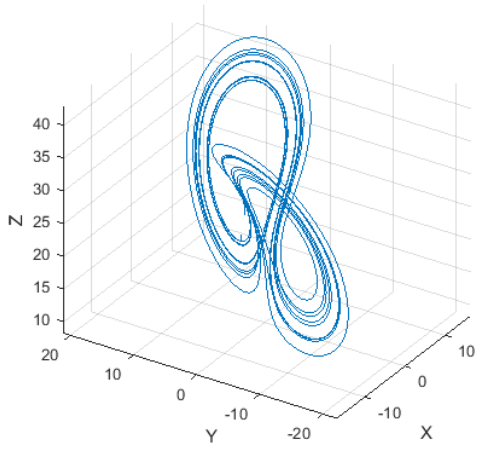

(b)

Figure 2.2: (a) Time series , (b) 3D-trajectories of Lorenz system for parameters $\sigma = 10, r = 28, b = 2.5$ and initial conditions $(x_0, y_0, z_0) = (1.5, 4.8, 19.5)$.

***Example* 2.1.2.** *(Lorenz system) The Lorenz system is defined by [52]:*

$$\begin{cases} \dot{x} = \sigma(y - x), \\ \dot{y} = rx - y - xz, \\ \dot{z} = xy - bz, \end{cases} \tag{2.1.3}$$

In this highly idealized model of a fluid, the warm fluid below rises and the cool fluid above sinks, setting up a clockwise or counterclockwise current. The Prandtl number σ, the Rayleigh (or Reynolds) number r, and b are parameters of the system. The variable x is proportional to the circulatory fluid flow velocity. If $x > 0$, the fluid circulates clockwise while $x < 0$ means counterclockwise flow. The variable y is proportional to the temperature difference between ascending and descending fluid elements, and z is proportional to the distortion of the vertical temperature profile from its equilibrium (which is linear with height) [53]. Figure 2.2(a) and Figure 2.2 (b) present the time series and 3D-trajectories of Lorenz system for parameters $\sigma = 10, r = 28, b = 2.5$ and initial conditions $(x_0, y_0, z_0) = (1.5, 4.8, 19.5)$.

2.1.3 Phase space

As soon as the n dimension of the system exceeds unity, it becomes quite difficult to "mentally" imagine how the system is evolving. The basic tool to overcome this is phase space. We consider each component x_i of X as a coordinate of a point in a space of dimension n. The following evolution t of the system then results in a displacement of the representative point in the phase space, thus drawing a phase trajectory.

2.1.4 Flow

Definition 2.1.8. A flow is a mapping

$$\varphi : X \times \mathbb{R} \to X,$$

such that, for all $x \in X$and all real numbers s and t,

$$\varphi(x, 0) = x; \qquad \varphi(\varphi(x, t), s) = \varphi(x, s + t).$$

It is customary to write $\varphi_t(x)$ instead of $\varphi(x, t)$.

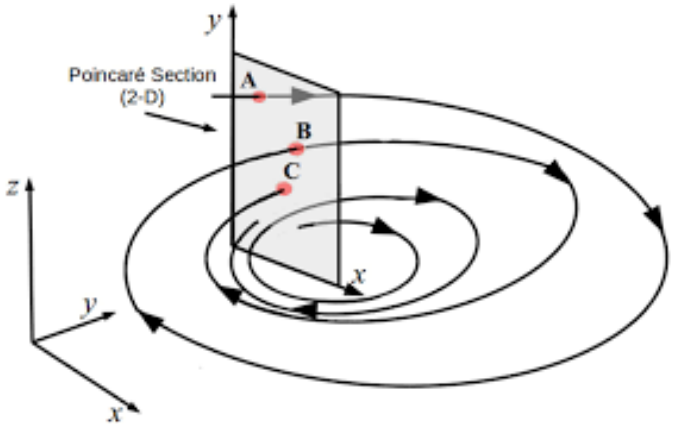

Figure 2.3: Poincaré section

2.1.5 Invariant set

Definition 2.1.9. Let A be a subset of the phase space; A is said to be invariant (resp. positively invariant) by a flows φ_t, if for all t in $\mathbb{R}$ (resp. in $[0;+\infty[$), $\varphi_t(A)$ is included in A.

2.1.6 Poincaré section

Definition 2.1.10. The Poincaré section S is defined by:

$$S = \{H \cup \varphi_t(x), t, x \in \mathbb{R}\},$$

where H is a hyperplane transverse to the flow in phase space. The Poincaré section is a very frequently used tool to study dynamic systems (in particular periodic trajectories). The principle of construction of this technique is illustrated by Figure 2.3 (the picture from the web).

2.1.7 Attractor

An attractor is a set of states toward which a system tends to evolve, for a wide variety of starting conditions of the system. System values that get close enough to the attractor values remain close even if slightly disturbed.
A mathematical definition, for an attractor, is given as follows:

Definition 2.1.11. The set A is an attractor if:

- For any neighborhood U of A, there exists a neighborhood V of A such that any solution $x(x_0, t) = \varphi_t(x_0)$ will remain in U if $x_0 \in V$,
- $\cap_{\varphi_t}(V) = A, t \geq 0$,
- There is a dense orbit in A.

There are two types of attractors: Regular attractors and strange or chaotic attractors.

Regular attractors

Regular attractors characterize the evolution of non-chaotic systems and can be of three kinds:

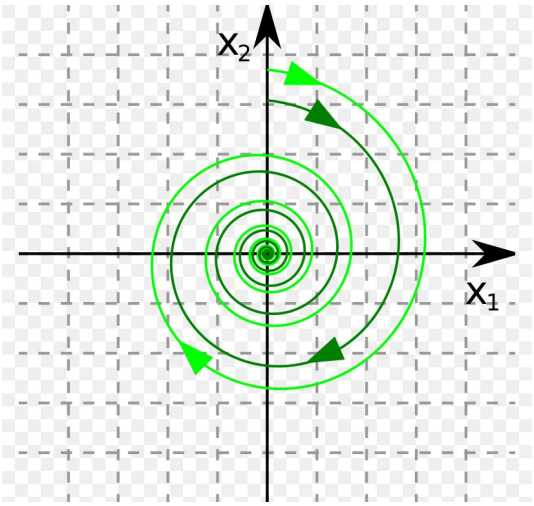

Figure 2.4: Attracting fixed point.

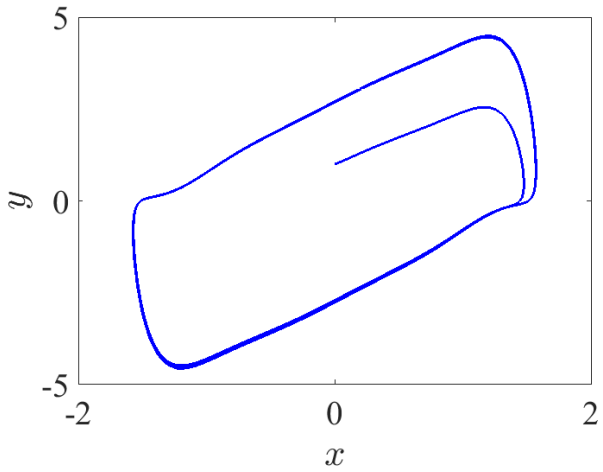

Figure 2.5: phase portrait of Van der Pol system: an attracting limit cycle

A.Fixed point

A fixed point of a function or transformation is a point that is mapped to itself by the function or transformation. If we regard the evolution of a dynamical system as a series of transformations, then there may or may not be a point which remains fixed under each transformation. The final state that a dynamical system evolves towards corresponds to an attracting fixed point of the evolution function for that system. Figure 2.4 shows an Attracting fixed point (the picture from the web).

B.Limit cycle

A limit cycle is a periodic orbit of a continuous dynamical system that is isolated. It concerns a cyclic attractor. Figure 2.5 present an example for this notion which is an attracting limit cycle for Van der Pol system (The Van der Pol system is defined at Chapter 3).

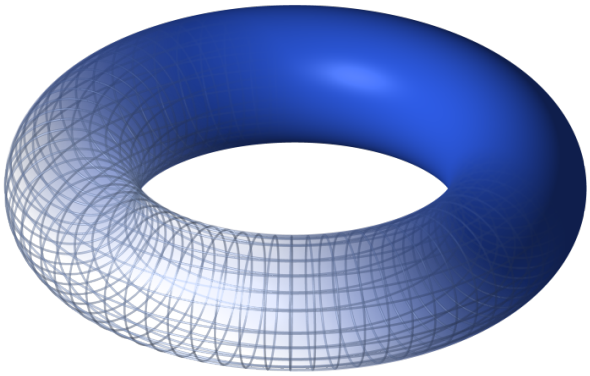

Figure 2.6: A simple torus fading out to a wireframe structure.

C.Limit torus

There may be more than one frequency in the periodic trajectory of the system through the state of a limit cycle. Figure 2.6 present a simple torus fading out to a wireframe structure (the picture from the web).

Strange attractors

The definition of this notion is given in the next section 2.3.

2.2 General theory of chaos

In this section, we present the chaos theory, it's bref history and we discuss some examples of continious FOCS.

2.2.1 Presentation

Chaos theory studies the behavior of dynamic systems which are very sensitive to initial conditions. Of small differences in initial conditions (such as those due to rounding errors in numerical computation) produce very divergent results for such dynamic systems, which makes long-term forecasting impossible in general. This happens even though these systems are deterministic, which means that their future behavior is entirely determined by their initial conditions, with no random elements involved. This behavior is known under the name of deterministic chaos, or simply chaos.
There is no definition both formal and general chaos. However, chaos is generally defined as a particular behavior of a dynamic system which includes:

- non-linearity: the irregular evolution of the behavior of a chaotic system is due to non linearities.
- determinism: a chaotic system has deterministic fundamental rules and not probabilistic.
- sensitivity: the system shows a very high sensitivity to changes in conditions.
- unpredictability: due to the sensitivity to the initial conditions, which can be known only to a finite degree of precision.
- the irregularity: the hidden order comprising an infinite number of unstable periodic models (or movements). This hidden order forms the infrastructure of chaotic systems.

2.2.2 Bref history

James Clerk Maxwell was probably the first who observed the chaos. In 1860, he studied the motion of two colliding gas particles in a box which was unpredictable for long duration. Henry Poincare (1890) was also the first person to glimpse the possibility of chaos.
The major breakthrough in Chaos Theory and Nonlinear Dynamics was after the discovery of high speed computers in 1950s. In late 1950s, the meteorologist Edward Lorenz acquired the LGP-30 computer having internal memory 16 KB. Using computer, in 1963, he discovered the chaotic motion on a strange attractor. The model studied by Lorenz [54] arising in weather prediction was consisting of autonomous system of three ordinary differential equations containing nonlinear terms. The solutions were aperiodic and sensitive to initial conditions.
A simple electronic circuit resulting chaotic attractor was given by L. Chua and T. Matsumoto [55] in 1985.
Robert May [56] in 1976 studied one dimensional maps (difference equations) modeling population dynamics. He observed that a very simple model can generate extremely complicated dynamics. This was the pioneering work in the study of chaos in maps.

2.2.3 Examples of chaos in FONDS

Chaotic fractional-order dynamical systems are obtained by replacing the derivative in the system by fractional derivative(s). Fractional-order in this case works as a chaos controller i.e. the chaotic system can be made regular by appropriate choice of fractional derivative(s).
Nowadays a lot of applications of FOCS in several disciplines such as physics, engineering, secure communication, biology, economics, meteorology, sociology, philosophy, etc, ...
Some examples of FOCS for discrete type are given in [57, 58, 59, 60, 61, 62, 63, 64, 65, 66].
Some examples of FOCS for countinuous type are given as follows:

Fractional-order Lorenz system

The FO Lorenz system is given by the following nonlinear equations [52]:

$$\begin{cases} D^q x = \sigma(y-x), \\ D^q y = x(\rho - z) - y, \\ D^q z = xy - \beta z. \end{cases} \tag{2.2.1}$$

For fractional-order $q = 0.991$, system parameters $(\rho, \sigma, \beta) = (28, 10, 8/3)$ and ICs $(x_0, y_0, z_0) = (0.1, 0.1, 0.1)$, this system exhibits a chaotic attractor which is shown in Figure 2.7.

Fractional-order Rössler system

The FO Rössler system is given by the following nonlinear equations:

$$\begin{cases} D^q x = -y - z, \\ D^q y = x + ay, \\ D^q z = bx - cz + xz. \end{cases} \tag{2.2.2}$$

For fractional-order $q = 0.98$, system parameters $(a, b, c) = (0.38, 0.3, 4.82)$ and ICs $(x_0, y_0, z_0) = (0.1, 0.1, 0.1)$, this system exhibits a chaotic attractor which is shown in Figure 2.8.

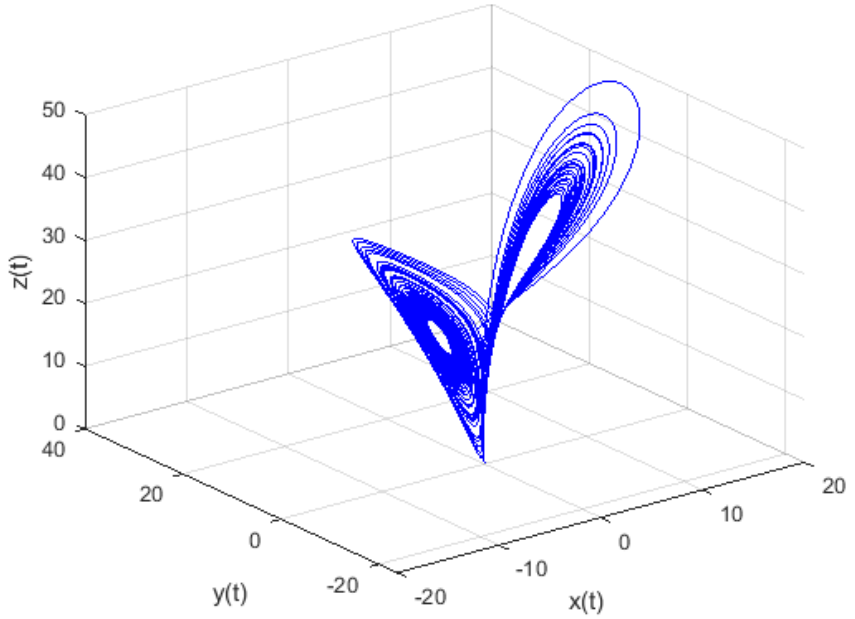

Figure 2.7: Chaotic attractor of FO Lorenz system for $q = 0.991$, $(\rho, \sigma, \beta) = (28, 10, 8/3)$ and ICs $(x_0, y_0, z_0) = (0.1, 0.1, 0.1)$.

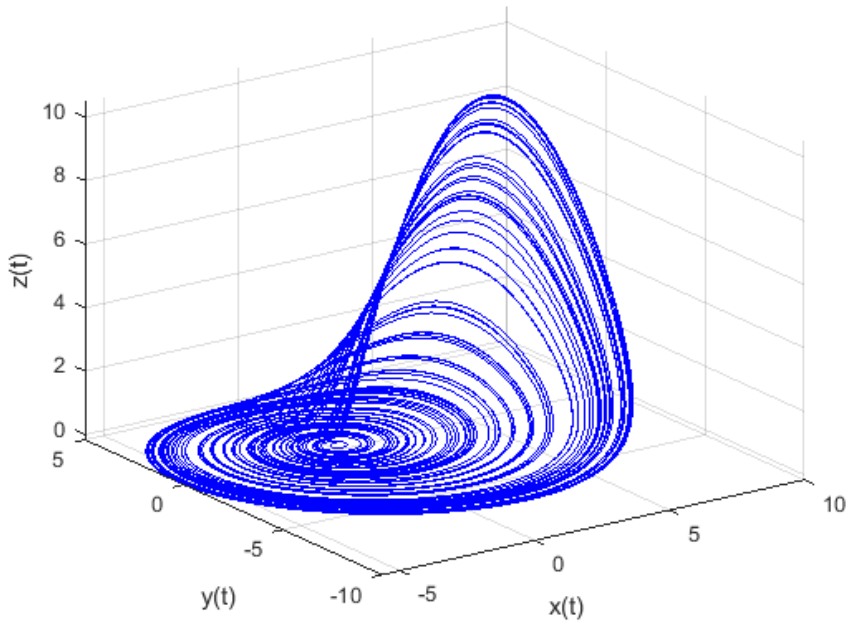

Figure 2.8: Chaotic attractor of FO Rössler system for$q = 0.98$, system parameters $(a, b, c) = (0.38, 0.3, 4.82)$ and ICs $(x_0, y_0, z_0) = (0.1, 0.1, 0.1)$.

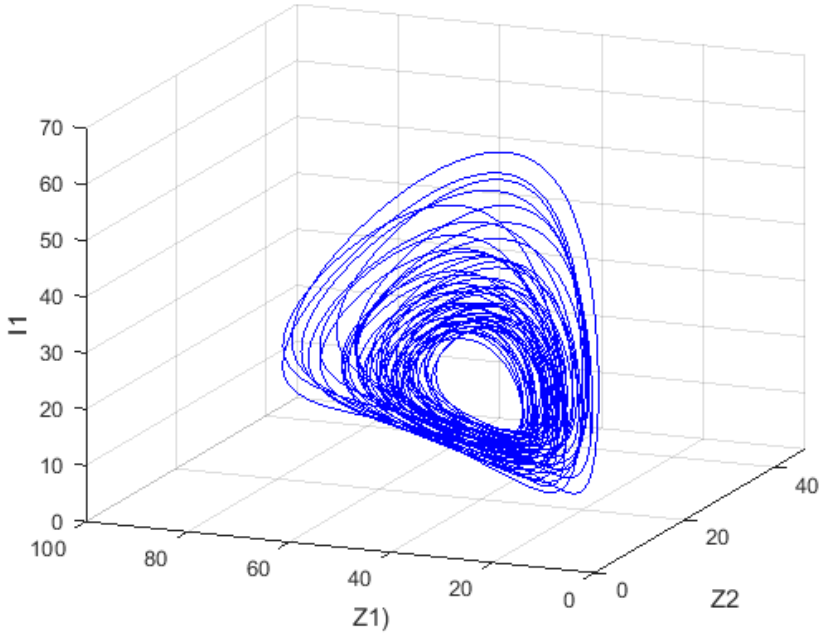

Figure 2.9: Chaotic attractor of FO HIV system for $(q_1, q_2, q_3, q_4, q_5) = (0.995, 0.995, 1, 1, 1)$, system parameters $(\lambda, b, c, a, \sigma, d, \beta_1, \beta_2) = (10, 0.8, 0.8, 0.031, 0.03, 0.02, 4 \times 10^{-4}, 2.8 \times 10^{-4})$ and ICs $(T_0, I1_0, I2_0, Z1_0, Z2_0) = (300, 19, 19, 7, 7)$.

Fractional-order HIV system

The FO HIV system is given by the following nonlinear equations [67]:

$$\begin{cases} D^{q_1} T = \lambda - dT - \beta_1 T I1 - \beta_2 T I2, \\ D^{q_2} I1 = \beta_1 T I1 - aI1 - bZ1I1/(T + I1 + I2), \\ D^{q_3} I2 = \beta_2 T I2 - a * I2 - bZ2I2/(T + I1 + I2), \\ D^{q_4} Z1 = cZ1I1/(T + I1 + I2) - \sigma Z1, \\ D^{q_5} Z2 = cZ2I2/(T + I1 + I2) - \sigma Z2. \end{cases} \tag{2.2.3}$$

For fractional-order $(q_1, q_2, q_3, q_4, q_5) = (0.995, 0.995, 1, 1, 1)$, system parameters $(\lambda, b, c, a, \sigma, d, \beta_1, \beta_2) = (10, 0.8, 0.8, 0.031, 0.03, 0.02, 4 \times 10^{-4}, 2.8 \times 10^{-4})$ and ICs $(T_0, I1_0, I2_0, Z1_0, Z2_0) = (300, 19, 19, 7, 7)$, this system exhibits a chaotic attractor which is shown in Figure 2.9.

Fractional-order economic system

The FO economic system is given by the following nonlinear equations [68]:

$$\begin{cases} D^q x = ay + bx(c - y^2), \\ D^q y = d(x + z), \\ D^q z = ex - fy. \end{cases} \tag{2.2.4}$$

For fractional-order $(q_1, q_2, q_3) = (0.99, 1, 1)$, system parameters $(a, b, c, d, e, f) = (0.05, 0.01, 1.6, 0.031847, 0.19, 0.25)$ and ICs $(x_0, y_0, z_0) = (1, 1, -1)$, this system exhibits a chaotic attractor which is shown in Figure 2.10.

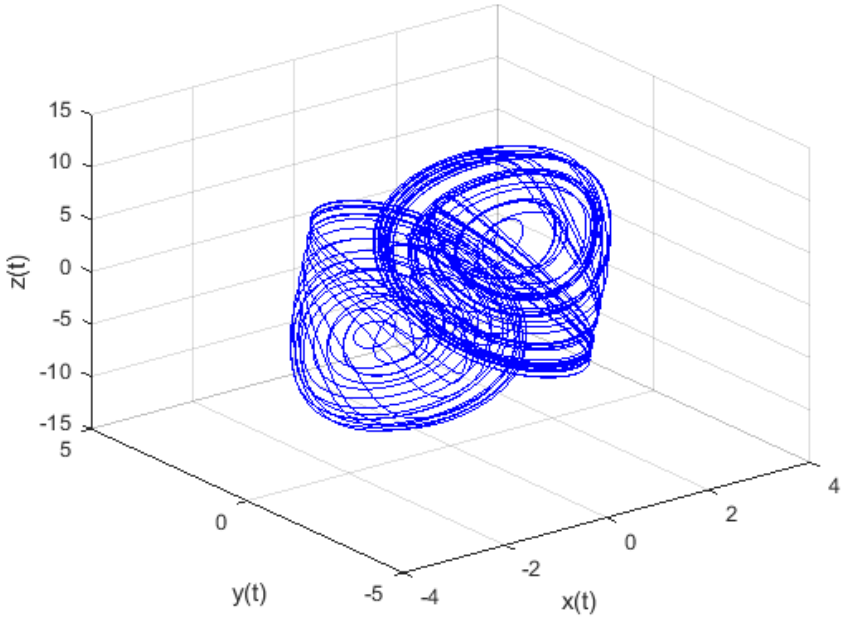

Figure 2.10: Chaotic attractor of FO economic system for $(q_1, q_2, q_3) = (0.99, 1, 1)$, system parameters $(a, b, c, d, e, f) = (0.05, 0.01, 1.6, 0.031847, 0.19, 0.25)$ and ICs $(x_0, y_0, z_0) = (1, 1, -1)$.

2.3 Chaos in fractional systems

In this section, we give a brief quantitative study on some mathematical tools for quantifying chaos. We chose an illustrative example to apply the previous knowledge represented by the fractional Vallis model for El-Niño .

A bref history about the fractional Vallis model for El-Niño

Vallis model [[69] ,[70]] is a simple continuous-time mathematical model for El Niño phenomenon defined by the following nonlinear differential equations :

$$\begin{cases} \dot{x}(t) = by - c(x + P), \\ \dot{y}(t) = -y + xz, \\ \dot{z}(t) = -z - xy + 1. \end{cases} \tag{2.3.1}$$

The integer Vallis model (2.3.1) was studied by [71] and [72].

Now, a fractional-order system is considered, where integer order derivative is replaced by a fractional one, as follows :

$$\begin{cases} D^{q_1} x(t) = by - c(x + P), \\ D^{q_2} y(t) = -y + xz, \\ D^{q_3} z(t) = -z - xy + 1, \end{cases} \tag{2.3.2}$$

where $q_i \in (0, 1), i = 1, 2, 3$.
The fractional Vallis model (2.3.2) was studied by [73] and [74]. Numerical solution of the fractional-order system (2.3.2) is realised by approximation methods with step $h = 0.005s$ (see Chapter 1.4).

Signs of LEs	Dynamic behavior	Attractor's type
$\lambda_n \leq ... \leq \lambda_1 < 0$	Asymptotically stabe to X^*	Fixed point
$\lambda_n \leq ... \leq \lambda_2 < 0, \lambda_1 = 0$	Periodic motion	Limit cycle
$\lambda_n \leq ... \leq \lambda_{k+1} < 0, \lambda_k = ... = \lambda_1 = 0$	Quasi-periodic motion	Torus
$\sum_i \lambda_i < 0, \lambda_1 > 0$	Chaotic motion	Chaotic attractor
$\sum_i \lambda_i < 0, \lambda_1 > ... > \lambda_k > 0$	Hyperchaotic motion	Hyperchaotic attractor

Table 2.1: Dynamic behavior and attractor's type according to the signs of LEs

This model is developed by treating equatorial ocean as a box of fluid characterized by temperatures in the east and west. Variable x represents current generated by the temperature gradient, co-ordinate y represents half of the difference of east-west temperatures and z represents the average of the east and west temperatures. The parameter b governs strength of air-sea interactions and the vertical temperature difference, while parameter c represents the ratio of time scales of decay of sea-surface temperature anomalies to a frictional time scale. The parameter P measures the average effect of equatorial winds on the sea [69, 74].

2.3.1 Sensitivity to initial conditions

Sensitivity to initial conditions explains the fact that, for a chaotic system, a tiny modification of the initial conditions can lead to unpredictable results in the long term. The degree of sensitivity to initial conditions quantifies the chaotic character of the system [75, 76].
Sensitivity to initial conditions is a phenomenon discovered for the first time, at the end of the nineteenth century by Poincaré, then was rediscovered in 1963 by Lorenz during his work in meteorology. This discovery led to a large number of important works, mainly in the field of mathematics.
This character also used for quantifies the chaotic motion of the fractional systems.

2.3.2 Lyapunov exponents

On October 12, 1892, Lyapunov defended a doctoral thesis at Moscow University entitled: The General Problem of the Stability of the Movement. He introduced the idea of measuring the possible divergence between two orbits resulting from neighboring initial conditions. When this divergence grows exponentially with time for almost all the initial conditions close to a given point, we have the phenomenon of sensitivity to the initial conditions, an idea to which the Lyapunov exponents are attached [77].
The Lyapunov exponents (LEs)

$$\lambda_i (i = 1, ..., n),$$

measure the average rate of divergence or convergence of orbits starting from nearby initial points. Therefore, they can be used to analyze the stability of limits sets and to check sensitive dependence on initial conditions, that is, the presence of potential chaotic attractors.
The number of Lyapunov exponents is equal to the dimension of the phase space [78, 79, 80]. Table 2.1 presents the signs of Lyapunov exponents which indicate the dynamic behavior and the attractor's type of the system.
There are two classification for computing Lyapunov exponents [81, 82, 83]:

Algorithm 1.

Input:

-ne	▶ number of equations
-x_{start}	▶ ne initial conditions of FOS
$-t_{start}, t_{end}$	▶ time span
$-h_{norm}$	▶ Normalization step-size
-q	▶ commensurate FO
$n_{it} \leftarrow (t_{end} - t_{start})/h_{norm}$	▶ iterations number
for $i \leftarrow ne+1$ to $ne(ne+1)$ do	
$\mid x(i) = 1.0$	▶ initial conditions of variational equations of FOS
end	
$t \leftarrow t_{start}$	
for $i \leftarrow 1$ to n_{it} do	
$x \leftarrow$ integration of commensurate FOS	▶ FDE12.m: solver for commensurate FDEs
$t \leftarrow t + h_{norm}$	
$zn(1),...,zn(ne) \leftarrow$ Gram-Schmidt procedure	
$s(1) \leftarrow 0$	
for $k \leftarrow 1$ to ne do	
$s(k) \leftarrow s(k) + log(zn(k))$	▶ vector magnitudes
$\mathrm{LE}(k) \leftarrow s(k)/(t - t_{start})$	▶ LEs
end	
end	

Output: LE

Table 2.2: Algorithm for LEs of commensurate FOS

- analytically: methods based on the mathematical model.
- numerically: methods based on an observed time series.

For calculating LEs on fractional systems, the numerical estimation from time series data are used, the analitical methods can't be used here because of their memory property [10]. One of the numerical estimations is the Benettin-Wolf algorithm which used for determing LEs for integer or fractional order systems [79, 81].
In this work, we use the the follmoing two studies:

- Danca and Kuznetsov was given on [84] an algorithm with the Matlab code for numerical evaluation of LEs of commensurate FOS (see 2.2).
- Danca was given on [85] an algorithm with the Matlab code for numerical evaluation of LEs of incommensurate FOS (see 2.3).

The alghorithms can be summarized in steps in Table 2.2 and Table 2.3.

Algorithm 2.

Input:

$-ne$	▶ number of equations
$-x_{start}$	▶ ne initial conditions of FOS
$-t_{start}, t_{end}$	▶ time span
$-h_{norm}$	▶ Normalization step-size
$-q = [q_1, q_2, ..., q_{ne}]$	▶ incommensurate FO
$n_{it} \leftarrow (t_{end} - t_{start})/h_{norm}$	▶ iterations number
for $i \leftarrow ne + 1$ to $ne(ne + 1)$ do	
$\mid x(i) = 1.0$	▶ initial conditions of variational equations of FOS
end	
$t \leftarrow t_{start}$	
for $i \leftarrow 1$ to n_{it} do	
$x \leftarrow$ integration of incommensurate FOS	▶ fde_pi12_pc.m: solver for noncommensurate FDEs
$t \leftarrow t + h_{norm}$	
$zn(1), ..., zn(ne) \leftarrow$ Gram-Schmidt procedure	
$s(1) \leftarrow 0$	
for $k \leftarrow 1$ to ne do	
$s(k) \leftarrow s(k) + log(zn(k))$	▶ vector magnitudes
$\mathrm{LE}(k) \leftarrow s(k)/(t - t_{start})$	▶ LEs
end	
end	

Output: LE

Table 2.3: Algorithm for LEs of incommensurate FOS

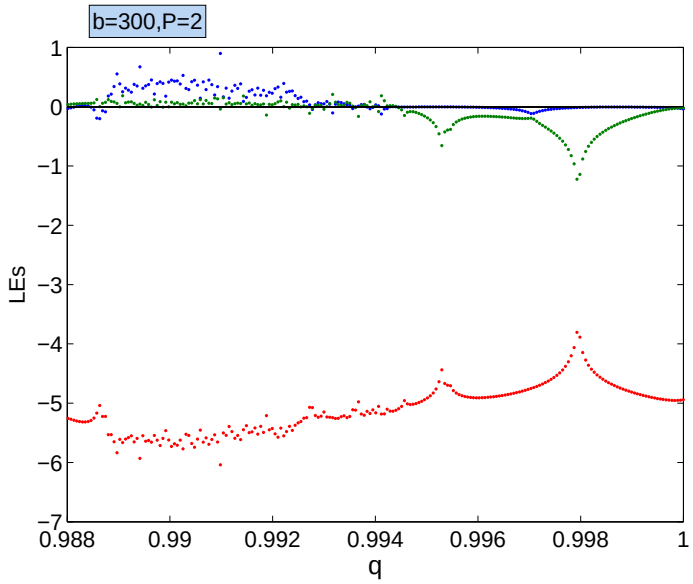

Figure 2.11: LEs of fractional Vallis model (2.3.2) as function of q for parameters $P = 2, b = 300, c = 3$ and ICs $(x_0, y_0, z_0) = (0.1, 1.2, 0.5)$.

Remark 2.3.1. The estimation of LEs in FOS presents by a function of:

- one variable:
  - as function of commensurate FO.
  - as function of incommensurate FO.
  - as function of bifurcation's parameter.
- two variables:
  - as function of FO and bifucation's parameter (presentation in surface).

***Example* 2.3.1.** *The Lyapunov exponents of fractional Vallis model (2.3.2) as function of commensurate FO q for parameters $P = 2, b = 300, c = 3$ and ICs $(x_0, y_0, z_0) = (0.1, 1.2, 0.5)$ is shown in Figure 2.11.*
The Lyapunov exponents of fractional Vallis model (2.3.2) as function of parameter p for FO $q = 0.98$, parameters $b = 400, c = 3$ and ICs $(x_0, y_0, z_0) = (0.1, 1.2, 0.5)$ is shown in Figure 2.11.
The Lyapunov exponents of Chen's system of FO represented by the function of two variables: q and parameter p. Surface S_i, for $i = 1, 2, 3$, represents $LE(q, p)$ [84] is shown in Figure 2.13.

2.3.3 Fractal dimension

This method corresponds to a measure of the dimension of the reconstructed attractor of the system studied; we can calculate the dimension of the attractor of the studied system and thus determine whether or not it is constructed in a fractal manner.
If, at the end of the calculation, we get a positive non-integer value, it means that the system has a strange attractor.
Several dimensions have been proposed, we cite a few: there is the Kolmogorov dimension, the Correlation dimension and the Lyapunov dimension, there is a slight difference between each of these dimensions, but they all characterize the attractor, strange with its fractal dimension.

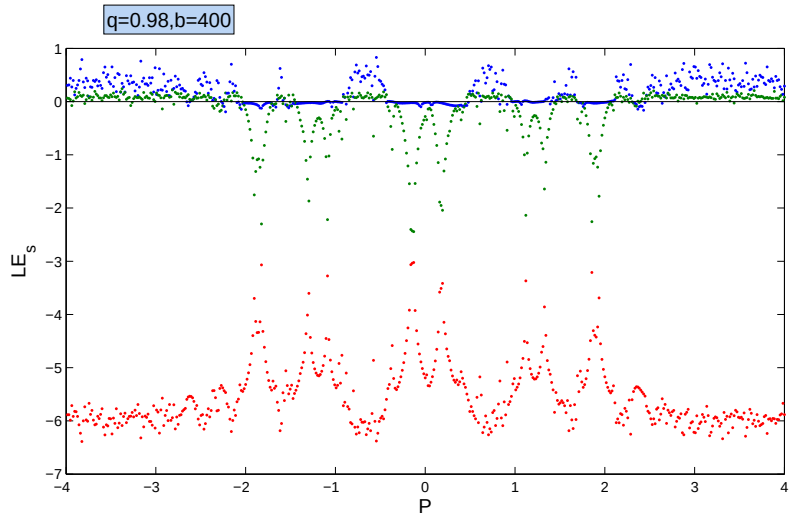

Figure 2.12: LEs of fractional Vallis model (2.3.2) as function of p for $q = 0.98$, parameters $b = 400, c = 3$ and ICs $(x_0, y_0, z_0) = (0.1, 1.2, 0.5)$.

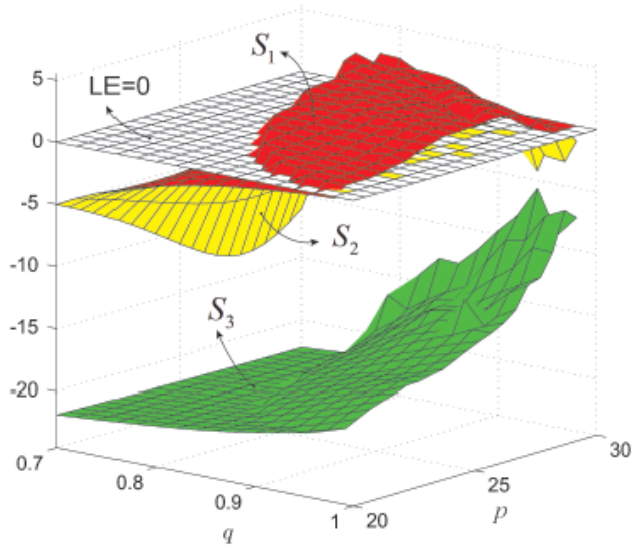

Figure 2.13: LEs of Chen's system of FO represented by the function of two variables: q and parameter p. Surface S_i, for $i = 1, 2, 3$, represents LE(q, p).

We choose to define Lyapunov dimension because this type of dimension takes into account the dynamics of the system.

Lyapunov dimension

This dimension is defined by Karlan and Yorke, and it is given by [86, 87]:

$$D_L = \frac{\sum_{i=1}^{j} \lambda_i}{|\lambda_{j+1}|} + j, \tag{2.3.3}$$

where $\lambda_n \leq ... \leq \lambda_1$ are the Lyapunov exponents of an attractor of a dynamical system, and j is the large natural integer such that: $\sum_{i=1}^{j} \lambda_i \geq 0$.

***Example* 2.3.2.** *To verify that the commensurate fractiona-order Vallis model (2.3.2) appears a complex chaotic attractor when $q = 0.985, b = 200, c = 3$, and $P = 1$, we calculate for this values the Lyapunov exponents and the fractional dimension as a function of $t \in (0, 300s)$. The three Lyapunov exponents are $LE_1 = 0.5704, LE_2 = 0$ and $LE_3 = -5.5900$. The Lyapunov dimension is calculated as : $D_L = j + \sum_{i=1}^{j} LE_i / \left|LE_{j+1}\right| = 2 + (0.5704 + 0)/|-5.5900| = 2.10 > 2$, such that $\sum_{i=1}^{j} LE_i > 0$ and $\sum_{i=1}^{j+1} LE_i < 0$. So a strange attractor is detectable in the system.*

2.3.4 Hopf Bifurcation

A dynamic system generally has one or more "control" parameters. Depending on the value of this parameter, the same initial conditions lead to qualitatively different dynamic regimes. There are several scenarios that describe the transition from fixed point to chaos. Generally speaking, the evolution from the fixed point to chaos is not gradual but marked by discontinuous changes called bifurcations. A bifurcation marks the sudden passage from one dynamic regime to another, qualitatively different.
Let be the nonlinear dynamic system of dimension n:

$$\frac{dx}{dt} = f(x, t, \beta) \tag{2.3.4}$$

with the control parameter β, and let be x^* its solution.

Definition 2.3.1. A bifurcation is a qualitative change in the solution x^* of the system (2.3.4) when modifying, and more precisely the disappearance or change of stability and the appearance of new solutions.

Definition 2.3.2. A bifurcation diagram is a portion of the parameter space on which all the bifurcation points are represented.

There are several types of bifurcation, like Saddle-node (fold) bifurcation, Transcritical bifurcation, Pitchfork bifurcation, Period-doubling (flip) bifurcation, Hopf bifurcation, Neimark-Sacker (secondary Hopf) bifurcation. In this work, we talk about Hopf bifurcation, because It's famously used detecting chaos in integer and frational-order continuous dynamical systems.
Through stability theory of equilibrium points and numerical simulations, an analyze about Hopf bifurcation of 3-dimensional fractional-order systems was given in [10] as follows:

Let consider the following three-dimensional fractional-order commensurate system:

$$D^q = f(\beta, x) \tag{2.3.5}$$

where $q \in]0,2[$, $x \in \mathbb{R}^3$, and suppose that E is an equilibrium point of this system. In the integer case (when $q = 1$) the stability of E is related to the sign of $Re(\lambda_i), i = 1,2,3$ where λ_i are the eigenvalues of the jacobian matrix $\frac{\partial f}{\partial x}|_E$. If $Re(\lambda_i) < 0$ for all $i = 1,2,3$ then E is locally asymptotically stable. If there exist i such that $Re(\lambda_i) > 0$ then E is unstable.
The conditions of system (2.3.5) with $q = 1$, to undergo a Hopf bifurcation at the equilibrium point E when $\beta = \beta^*$ are:

- The jacobian matrix has two complex-conjugate eigenvalues $\lambda_{1,2}(\beta) = \theta(\beta) \pm i\omega(\beta)$,and one real $\lambda_3(\beta)$ (this can be expressed by $D(P_E(\beta)) < 0$),
- $\theta(\beta^*) = 0$, and $\lambda_3(\beta^*), \neq 0$
- $\omega(\beta^*) \neq 0$,
- $\frac{d\theta}{d\beta}|_{\beta=\beta^*} \neq 0$.

But in the fractional case the stability of E is related to the sign of

$$m_i(q,\beta) = q\frac{\pi}{2} - |arg(\lambda_i(\beta))|, \qquad i = 1,2,3.$$

If $m_i(q,\beta) < 0$ for all $i = 1,2,3$, then E is locally asymptotically stable.
If there exist i such that $m_i(q,\beta) > 0$, then E is unstable.
So the function $m_i(q,\beta)$ has a similar effect as the real part of eigenvalue in integer systems, therefore we extend the Hopf bifurcation conditions to the fractional systems by replacing $Re(\lambda_i)$ with $m_i(q,\beta)$ as follows:

- $D(P_E(\beta)) < 0$,
- $m_{1,2}(q,\beta^*) = 0$, and $\lambda_3(\beta^*) \neq 0$,
- $\frac{\partial m}{\partial \beta}|_{\beta=\beta^*} \neq 0$.

Remark 2.3.2. The limit cycle which appear through a Hopf bifurcation is not a solution for a fractional system but it attracts a nearby solutions.

Remark 2.3.3. The bifurcation diagram in FOS presents can be plotted by a function of one variable:

- as function of commensurate FO.
- as function of incommensurate FO.
- as function of bifurcation's parameter.

Example **2.3.3.** *The bifurcation diagram as a function of commensurate FO q are plotted in Figure 2.14. It can be seen the doubling-period route to chaos when varying the fractional-order.*

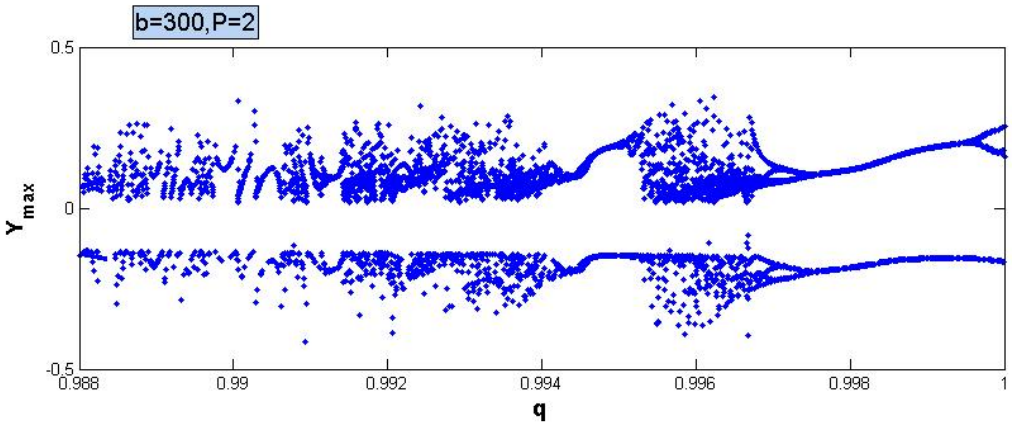

Figure 2.14: Bifurcation diagram of commensurate fractional Vallis model (2.3.2) as function of q for parameters $b = 300, p = 2, c = 3$ and ICs $(x_0, y_0, z_0) = (1.4, 0.1, 0.3)$.

2.3.5 Basin of attraction

Definition 2.3.3. The basin of attraction of an attractor is the closure of the set of initial conditions which approach the attractor as time tends to $+\infty$ [88].

***Example* 2.3.4.** *Figure 2.15 shows cross section of the basin of attraction on XY plan of fractional-order Vallis model 2.3.2 for $q = 1$, parameters $P = 1, b = 121, c = 5$. The basin has the expected symmetry about the Y-axis and an intricate fractal boundary. The blue region presents the initial conditions that converge to a chaotic attractors.*

2.3.6 Strange attractors

Strange attractors are complex geometric shapes that characterize the evolution of chaotic systems. The strange attractor is characterized by:

- Sensitivity to initial conditions (two initially neighboring attractor trajectories always end up moving away from each other, this reflects chaotic behavior).
- The dimension d of the attractor is fractal (not integers) with $2 < d < n$ (which justifies the strange adjective).
- The attractor is of zero volume in the phase space.

The term strange attractor was coined by David Ruelle and Floris Takens to describe the attractor resulting from a series of bifurcations of a system describing fluid flow [89]. It is shown that in certain types of dynamical systems it is possible to have attractors which are strange but not chaotic. [88].
Like integer systems, Strange attractors characterize also the evolution of chaotic fractional systems but in this case, the evolution is related by the varying of the fractional-order.

***Example* 2.3.5.** *Figure 2.16 presents an example of strange attractor include the Vallis attractor which is exhibited by the fractional system (2.3.2) for fractional-order $q = 0.99$, parameters $P = 1, b = 121, c = 5$ and ICs $(x_0, y_0, z_0) = (0.1, 1.2, 0.5)$.*

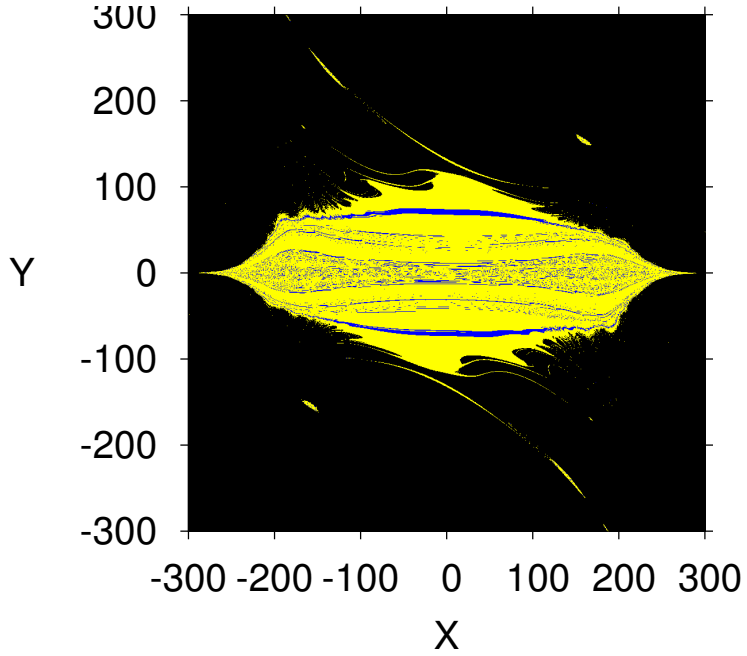

Figure 2.15: Basin of attraction offractional-order Vallis model 2.3.2 on XY plan.

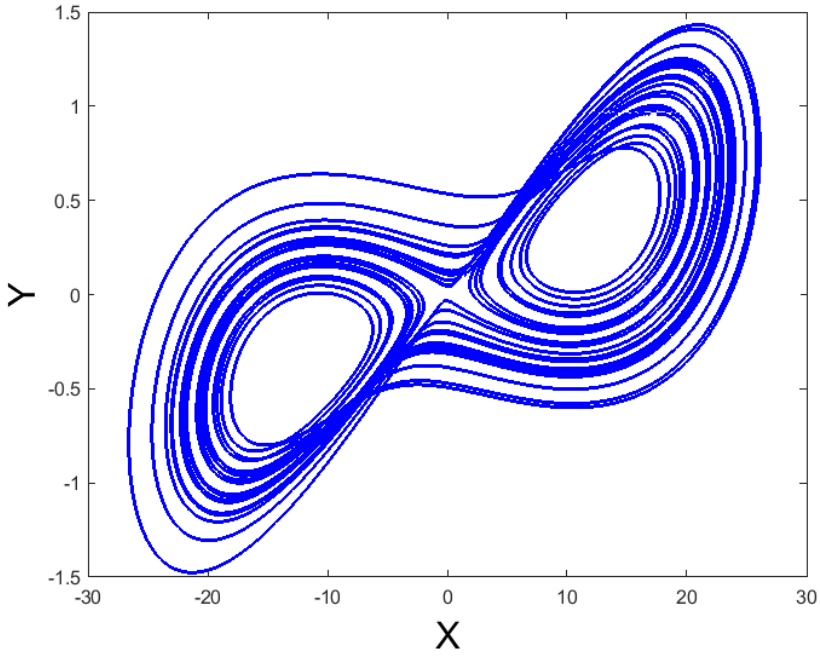

Figure 2.16: Example of strange attrator: Vallis attractor for fractional-order $q = 0.99$, parameters $P = 1, b = 121, c = 5$ and ICs $(x_0, y_0, z_0) = (0.1, 1.2, 0.5)$.

Chaotic attractor

Definition 2.3.4. A chaotic attractor is one for which typical [1] orbits on the attractor have a positive Lyapunov exponent [88].

Self-excited and hidden attractors

Definition 2.3.5. A chaotic system whose basin of attraction has an equilibrium point is called a self-excited attractor and one whose basin does not have any equilibrium point is called a hidden attractor [90, 91, 92].

[1] In the above definition we have used the idea of "typical" orbits on the attractor. That is, we assume that, for almost any initial condition in the basin of attraction of the attractor, the largest Lyapunov exponents generated by those (typical) initial conditions exist and are identical.

Part II

Applications

CHAPTER 3

CHAOS IN FRACTIONAL-ORDER BIOLOGICAL SYSTEMS

In this part, we study the chaotic behaviors in four biological models by including commensurate and incommensurate fractional-orders at this models.

3.1 Chaotic dynamics in a novel COVID-19 pandemic model described by commensurate and incommensurate fractional-order derivatives

The content of this section has been published in [11].

3.1.1 Introduction

From Wuhan in China to the whole world, COVID- 19 epidemic was first broke out in December 2019, where its biological hazards as regards of lethality and propagation were not familiar [93]. The so-called coronavirus SARS-CoV-2 is liable for such disease, which mostly causes an inflammatory storm and a viral pneumonia with certain symptomatology [94]. In the interest of assessing the epidemic tendency, controlling the COVID-19 epidemic and minimizing its harms, it is necessary to have knowledge about the behavior of this disease in terms of the speed of virus infections, the duration of its symptoms prior to diagnosis, the time of its peak and the time of its low points. One of the main aspects that can definitely help decision-makers to face such crisis is proposing suitable mathematical models, which in their turns, can offer easy, fast, and effective access to the optimum forecasts and predictions [95]. In epidemiology field, a lot of schemes have been developed to model several infectious epidemicsmathematically. The compartment models, which divide communities into certain major classes, are the most employed models. The interactions between those classes are mainly determined by certain beforehand mathematical formulas. In general, a complete model of an epidemic disease with its equations cannot be easily formulated within these formalisms due to the novelty of such disease and rapidly developing in its shape and behavior [94]. For instance, the so-called Susceptible-Exposed-Infectious-Removed model, or simply SEIR model, still cannot precisely estimate the broad range of infections resulting from COVID-19 [95]. The reader may refer to the references [96],[97] for gaining further details about such common model. In spite of all these research studies and many others, there are further complex models which have been, not long ago, proposed to describe the lightning-fast spread of several epidemic diseases around the world. More recently,Mangiarotti et al. have proposed in [94] a novel deterministic mathematical model of COVID-19 pandemic in light of the two official data sets given from two official institutions; the National Health Commission of the People's Republic of China [98] and the Johns Hudson University [99]. These data have been recently collected from these two sources by

Table 3.1: Parameter values of system (**??**).

Parameter	value	Parameter	value
α_1	-0.10530723	α_6	0.44040714
α_2	2.343×10^{-5}	α_7	0.16060376
α_3	0.15204	α_8	-0.00011493
α_4	-0.01451520	α_9	-1.215×10^{-5}
α_5	-0.20517824	α_{10}	0.2844499
α_{11}	2.38×10^{-6}		

taking into consideration the spread of this epidemic disease in each of China, South Korea, Japan and Italy, for the period from 21 January till 10-April 2020. The complete form of this model has been described by a nonlinear three-dimensional system consisting of the following states [94]:

$$\begin{cases} \dot{C} = \alpha_1 D^2 + \alpha_2 C^2 + \alpha_3 S(D + \alpha_4 C), \\ \dot{S} = \alpha_5 C + \alpha_6 S + \alpha_7 D^2, \\ \dot{D} = \alpha_8 CD + \alpha_9 CS + \alpha_{10} D + \alpha_{11} C^2, \end{cases} \tag{3.1.1}$$

where C represents the number of daily new cases of COVID-19, S represents the number of daily additional severe cases (positive or negative), D is the number of daily deaths, and where $\alpha_i, (i = 1, 2, 3, , 11)$, represent the system's parameters which are mentioned below in Table 3.1.

In fact, Mangiarotti et al. have employed the timeseries plot together with the phase portraits to prove that their proposed COVID-19 model exhibiting chaos. In particular, through comparing their obtained results with the observed real data, they have found the existence of chaos in their model (see [94]). Besides the integer-order model described in [94], some dynamical systems described by fractional-order derivatives have been recently introduced to model infectious epidemics, including the COVID-19 pandemic ([100]). For example, in [101] the analytical and computational aspects of a fractional-order COVID-19 model have been studied. The model consists of five compartments and includes a Mittag-Leffler kernel. In [102] a fractional-order COVID-19 model for examining the consequence of adaptive immune responses to the viral mutation is proposed. Specifically, in [102] three populations have been considered, i.e., the uninfected epithelial cells, the infected cells, and the SARS-CoV-2 virus. In [103] the COVID-19 pandemic is modeled via the fractional-order SIDARTHE mathematical model. In particular, in [103] the existence of a stable solution is proved and some fractional-order conditions for generating a control strategy are given. In [104] the dynamical behavior of a fractional COVID-19 model is investigated when applied to study the spread of the disease in some Brazilian cities. In [105] variable memory indexes are introduced in a SIRD epidemic model to estimate the COVID-19 pandemic. In particular, in [105] incommensurate fractional-order derivatives defined by a time-dependent function are taken into account when studying the dynamics of the model. In [106] a fractional-order SEIRD model for the spread of COVID-19 is presented. By using the real data of Italy (reported by theWorldHealth Organization), the results in [106] show that the considered fractional model provides a better prediction than the corresponding integer model. In [107] an epidemic COVID-19 model based on the fractional Caputo?Fabrizio derivative is illustrated. The existence and uniqueness of the system solution is investigated by using the Picard?Lindelöf theorem. In [108] a generalized fractional-order SEIR model is proposed. Specifically, the paper shows that, according to the real data of the USA, the considered fractional model has a good prediction ability for the epidemic trend in the next 2 weeks. In [109] numerical simulations of fractional-order modeling of COVID-19 in the case of Wuhan (China) have been

carried out. In particular, the Adams-Bashforth numerical scheme has been used in the simulations of the Caputo-Fabrizio fractional-order derivative. In [110] [N] a fractional-order SEIHDR model for COVID-19 with inter-city networked coupling effects is presented. Based on these considerations, in this work, we intend to operate the Caputo fractional-order operator on system (1) and then study and explore the resultant dynamic behaviors of its three states through using some analytical and numerical useful tools. In this work, we intend to operate the Caputo fractional-order operator on system (1) and then study and explore the resultant dynamic behaviors of its three states through using some analytical and numerical useful tools. The proposed nonlinear fractional-order COVID-19 model will be considered here in viewof the commensurate and incommensurate fractional-order cases. The stability of the equilibrium points of the proposed model will be completely analyzed by continuous varying the fractional-order derivative value, and its dynamical behaviorswill be then compared with each other. For further details about the Caputo differential operator and how could be operated on a certain mathematical model consisting of nonlinear differential equations, the reader may refer to the references [12, 20].

3.1.2 Mathematical model

In light of the above preliminaries together with the COVID-19 model (3.1.1) proposed in [94], the following nonlinear fractional-order version is established:

$$\begin{cases} D_t^{q_1} C = \alpha_1 D^2 + \alpha_2 C^2 + \alpha_3 S(D + \alpha_4 C), \\ D_t^{q_2} S = \alpha_5 C + \alpha_6 S + \alpha_7 D^2, \\ D_t^{q_3} D = \alpha_8 CD + \alpha_9 CS + \alpha_{10} D + \alpha_{11} C^2. \end{cases} \tag{3.1.2}$$

where C, S and D are the state-variables of system (3.1.1), and $D_t^{q_i}$ is the Caputo differential operator of order qi for which $0 < q_i \leq 1$ and $i = 1, 2, 3$. Observe that system (3.1.2) will be called commensurate fractional-order system if $q_1 = q_2 = q_3$, otherwise it is called incommensurate one. Actually, the predictor-corrector method (PCM), which was introduced by Diethelm as an improved version of the Adams-Bashforth-Moulton algorithm (ABMA), can be employed to provide a numerical solution to a nonlinear system consisting of a number of fractional-order differential equations formulated via Caputo operator. Furthermore, the PCM can be employed to find the Jacobian matrix of system (3.1.2), which would be here as follows:

$$J = \begin{bmatrix} 2\alpha_2 C + \alpha_3 \alpha_4 S & \alpha_3 D & 2\alpha_1 D + \alpha_3 S \\ \alpha_5 & \alpha_6 & 2\alpha_7 D \\ \alpha_8 D + \alpha_9 S + 2\alpha_{11} C & \alpha_9 C & \alpha_8 C + \alpha_{10} \end{bmatrix}$$

In view of the above result and the parameter values given in Table 3.1, one can obtain the eigenvalues of J at two equilibria of the system; the first one is the origin $E_0 = (0, 0, 0)$ which yields the eigenvalues $(\lambda_1, \lambda_2, \lambda_3) = (0.4404, 0, 0.2844)$, whereas the second one is $E_1 = (4314, 594, 62)$ which yields, in its turn, the eigenvalues $(\lambda_{1,2}, \lambda_3) = (-0.5095 \pm 1.4265i, 0.1393)$. More particularly, these two equilibrium points E_0 and E_1 can be classified according to the previous discussion as an unstable node and a saddle-focus node, respectively.

3.1.3 Dynamic analysis of model

In this part, we intend to examine the existence of a chaotic behavior of the commensurate and incommensurate fractional-order COVID-19 model which is previously proposed. Such examination will be carried out using some numerical tools such as constructing bifurcation diagrams, computing Lyapunov exponents and sketching phase portraits in 2D and 3D projections

The commensurate Model

The investigation of the stability of equilibrium points for the fractional-order COVID-19 model is considered extremely necessary for better understanding and exploring different complicated behaviors of its dynamics. From this point of view, some numerical analysis are performed below in order to determine the behavior of the system's trajectories through continuous varying the fractional-order derivative value. As we mentioned a little while ago, in view of selecting the system's parameters $\alpha_i, (i = 1, 2, 3, ..., 11)$, as previously given in Table 1, the eigenvalues $\lambda_i, i = 1, 2, 3$, of the Jacobian matrix J at the equilibrium point E_1 will be as $(\lambda_{1,2}, \lambda_3) = (-0.5095 \pm 1.4265i, 0.1393)$. Thus, if one substitutes the two previous eigenvalues λ_1 and λ_2 into the condition given in Theorem 1.3.3 in section 1.3.2, the following result will be gained: $arg(-0.5095 \pm 1.4265i) * 2/\pi \approx 0.79$, which immediately implies that system (3.1.2) will exhibit a chaotic behavior when $q > 0.80$. Such considerable result can be numerically confirmed by carrying out some numerical simulations. In particular, the bifurcation diagram of system (10) can be constructed to be as shown in Fig. 3.1(a) for $q \in (0.90, 0.98)$ according to the initial condition $(C_0, S_0, D_0) = (184, 30, 8)$. From such diagram, we can see that system (3.1.2) exhibiting asymptotic stability when $q < 0.90$, whereas it starts losing its stability and begins its behavior from a periodic motion to chaos mode when $q \in (0.90, 0.98)$. On the other hand, in light of the fact that a presence of any positive Lyapunov exponent of the fractional-order system shows a chaotic behavior for it dynamics, we observe that system (3.1.2) exhibits a chaotic behavior for $q \in (0.964, 0.98)$ as shown in Fig. 3.1(b). To further clarification, the phase portraits in CS-plan is sketched and exhibited in Fig. 3.2 according to the same system's parameters given in Table 3.1 and to the same initial condition $(C_0, S_0, D_0) = (184, 30, 8)$. It can be seen from such figure that system (3.1.2) will be asymptotically stable according to the equilibrium point E_1, when $q = 0.90$ (see Fig. 1.4.5(a)). From the other side, Fig. 3.2(b)-3.2(c) shows that the system loses its stability and then begins to construct a scroll around the point E_1 when $q = 0.92$ and $q = 0.96$. In addition, a chaotic attractor is exhibited for system (3.1.2) when $q = 0.964$ (see Fig. 3.1.2(d)), whereas another complex chaotic attractor is appeared when $q = 0.977$. For completeness, Fig. 3.3 represents a 3D projection sketch of the chaotic attractor of system (3.1.2), while Fig. 3.4 represents different 2D projection sketches for the complex chaotic attractors generated from the dynamics of the system, confirming hence the previous reported results.

The incommensurate Model

In a similar manner to the previous subsection, we intend here to study the existence of a chaotic behavior of the incommensurate fractional-order COVID- 19 model by applying the same numerical tools used before such as constructing the bifurcation diagram and sketching the phase portraits of the trajectories of system (3.1.2) in 2D and 3D projections. More particulary, we explore the behavior of the dynamics of system (3.1.2) under continuous varying of the incommensurate fractional-order value. The system?s parameters are selected here to be as given inTable 1 and the initial condition is also assumed as $(C_0, S_0, D_0) = (184, 30, 8)$. To study the stability of system (3.1.2) in its incommensurate order case, two bifurcation diagrams are plotted in Figure 3.5(a) and Figure 3.7(a) according to two corresponding cases; the first one takes the incommensurate fractional-order values as $q_2 \in (0.80, 0.97)$ and $q_1 = q_3 = 1$, while the second one takes them as $q_3 \in (0.70, 0.94)$ and $q_1 = q_2 = 1$. It can be seen from such figures that the equilibrium point is clearly asymptotically stable when $q_2 < 0.84$ and $q_3 < 0.78$. On contrary, system (3.1.2) starts losing its stability and begins its behavior from a periodic motion to chaos mode when $q_2 \in (0.84, 0.97)$ and $q_3 \in (0.78, 0.94)$. Furthermore, based on the plot of Lyapunov exponents shown in Figure 3.5(b) and Fig. **??**(b), we observe that system (3.1.2) is chaotic when $q_2 \in (0.964, 0.96)$ and $q_3 \in (0.915, 0.94)$. In connection with of the phase portraits of system (3.1.2) in its incommensurate orders, Figure 3.6 and Figure 3.8 represent the sketches of them on CS-plan according to different values of q_2 and q_3. In particular,

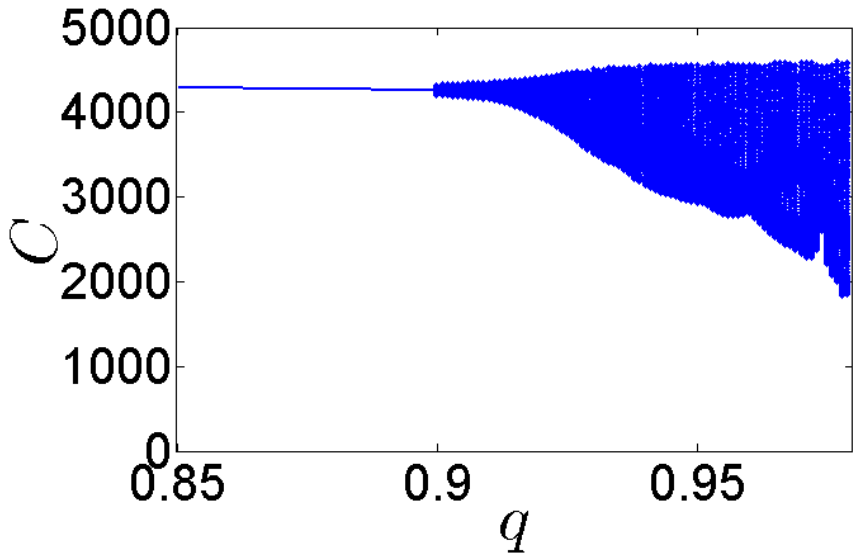

(a)

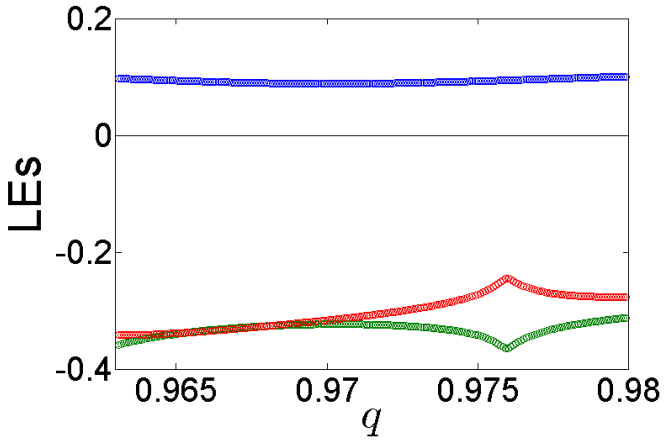

(b)

Figure 3.1: (a) Bifurcation diagram of commensurate system (3.1.2) for $q \in (0.90, 0.98)$, (b) Lyapunov exponents of commensurate system (3.1.2) for $q \in (0.964, 0.98)$ with taking system parameters selecting in Table 3.1 and initial conditions $(C_0, S_0, D_0) = (184, 30, 8)$.

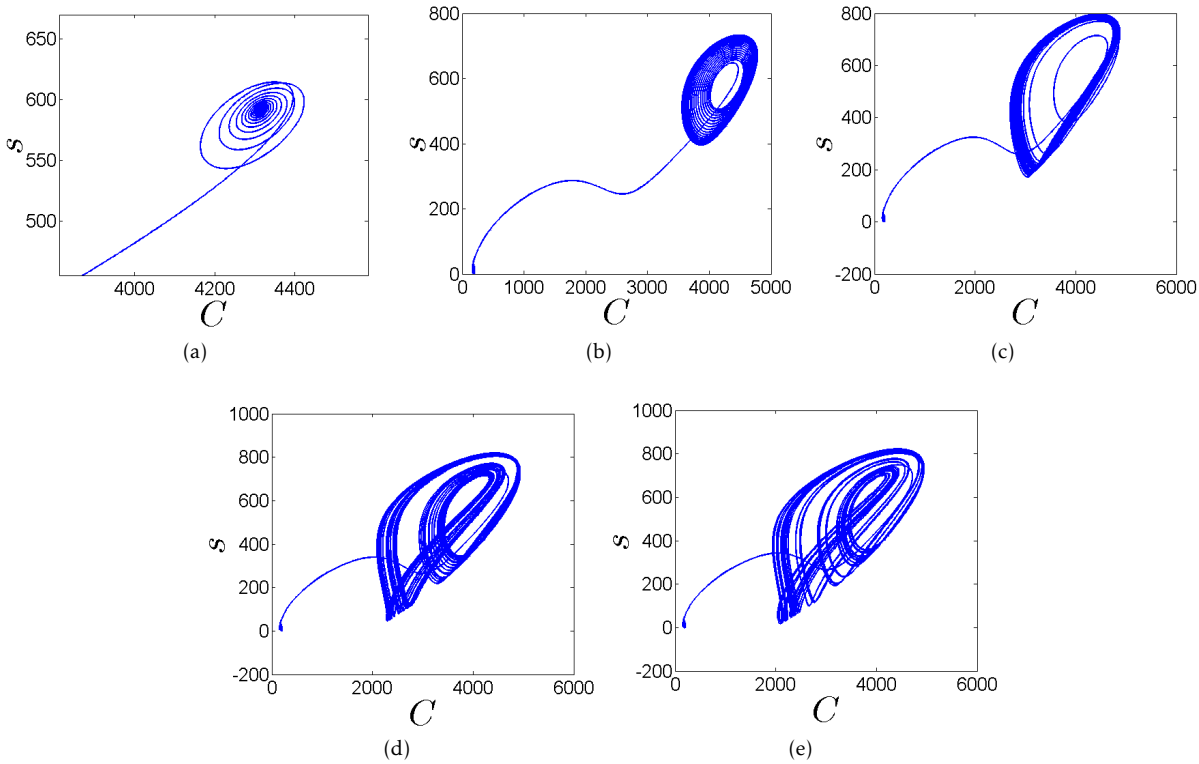

Figure 3.2: (a) Phase portraits of commensurate system (3.1.2) in $C-S$ plan with taking system parameters selecting in Table 3.1 and initial conditions $(C_0, S_0, D_0) = (184, 30, 8)$ for: (a) $q = 0.89$, (b) $q = 0.92$, (c) $q = 0.96$, (d) $q = 0.964$ and (e) $q = 0.977$.

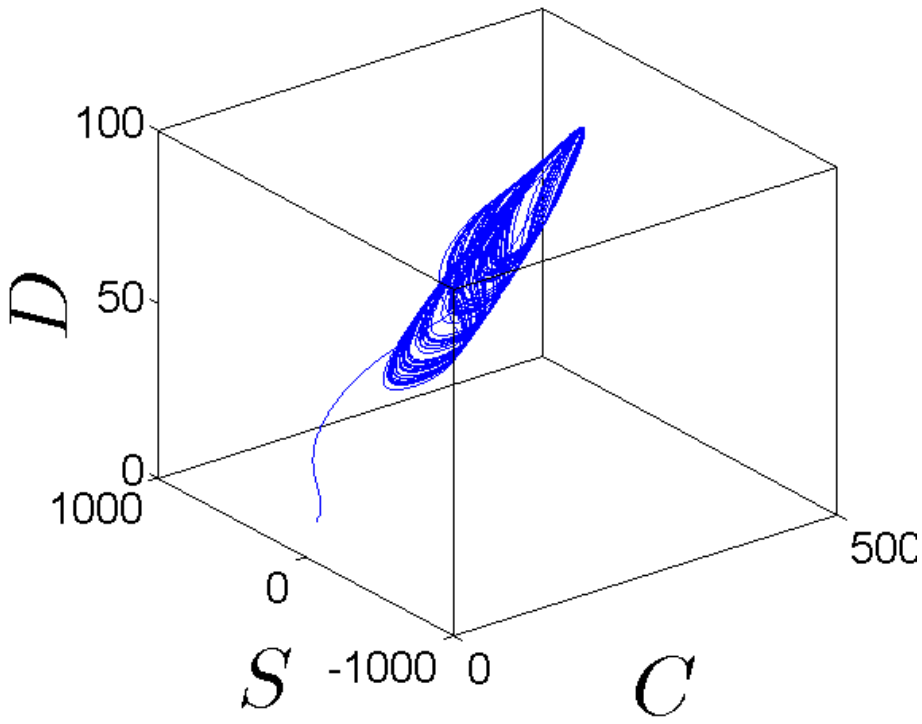

Figure 3.3: Chaotic attractor of commensurate system (3.1.2) in 3D projection for $q = 0.977$ with taking system parameters selecting in Table 3.1 and initial conditions $(C_0, S_0, D_0) = (184, 30, 8)$

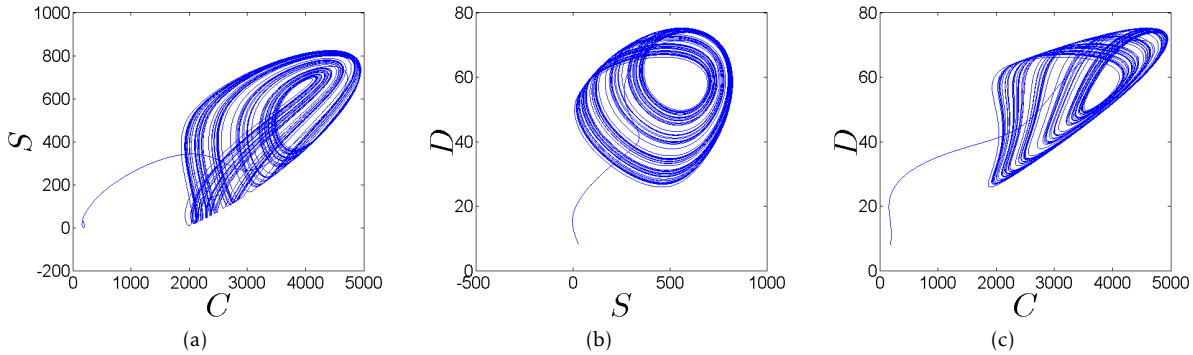

(a) (b) (c)

Figure 3.4: Chaotic attractor of commensurate system (3.1.2) in different projection for $q = 0.977$ with taking system parameters selecting in Table 3.1 and initial conditions $(C_0, S_0, D_0) = (184, 30, 8)$ for: (a) C-S plan, (b) S-D plan and (c) C-D plan

when the incommensurate fractional-order $q_2 = 0.85$, the incommensurate fractional-order system (3.1.2) will be asymptotically stable to the equilibrium point (see Figure 3.6(a). Such system will be asymptotically stable to a limit cycle when $q_2 = 0.95$ (see Figure 3.6(b)), while a chaotic attractor will be appeared when $q_2 = 0.958$ (see Figure 3.6(c)), and moreover the system under consideration will exhibit a complex chaotic attractor when $q_2 = 0.96$ (see Figure 3.6(d)). In a similar manner to the previous discussion, system (3.1.2) in its incommensurate orders will be asymptotically stable to the equilibrium point when $q_3 = 0.75$ (see Figure 3.8(a)). The same system will be asymptotically stable to a limit cyclewhen $q_3 = 0.90$ (Figure 3.8(b)), whereas a chaotic attractor will be appeared when $q_3 = 0.93$ (see Figure 3.8(c)) and it will be also exhibit a complex chaotic attractor when $q_3 = 0.94$ (see Figure 3.8(d)). In addition to these simulations which are performed according to the data given in Table 3.1 and to the initial condition $(C_0, S_0, D_0) = (184, 30, 8)$, a 3D projection sketch of the complex chaotic attractor of the incommensurate order system (3.1.2) is furthermore exhibited in Figure 3.9 by considering two cases; the first one is performed when $q_2 = 0.96$ and $q_1 = q_3 = 1$, while the second one is performed when $q_3 = 1$ and $q_1 = q_2 = 1$. For more clarification, we notice that some Lyapunov exponents are positive, particularly for the two cases: The first one occurs when $q_2 = 0.96, q_1 = q_3 = 1$ (see Figure 3.5(b)), while the second one occurs when $q_3 = 0.94, q_1 = q_2 = 1$ (see Figure 3.7(b)). From this standpoint and in view of the stability condition (1.3.15) reported in Section 1.3.2, we might take into account these two cases as follows:

* When $q_2 = 48/50, q_1 = q_3 = 1$, then the least common multiple M is become as $M = LCM(50, 1, 1) = 50$.This, consequently, implies $\Delta(\lambda) = diag(\lambda^{48}\lambda^{50}\lambda^{50}) - J(E_1)$, which yields $det(\Delta(\lambda)) = \lambda^{148} - 0.2290\lambda^{98} + 0.9508\lambda^{48} + 1.1087\lambda^{100} + 1.2018\lambda^{50} - 0.3196$. Hence, the IMFOS of system (3.1.2) would be as:

$$\text{IMFOS} = 0.0327 > 0.$$

This means that such system shows a chaotic behavior, which confirms the resultant numerical plot shown in Figure 3.9(a).

* When $q_3 = 47/50, q_1 = q_3 = 1$, we can obtain $M = LCM(50, 1, 1) = 50$, which leads to deduce $\Delta(\lambda) = diag(\lambda^{47}\lambda^{50}\lambda^{50}) - J(E_1)$. This, however, yields $det(\Delta(\lambda)) = \lambda^{147} - 0.2290\lambda^{97} + 0.9508\lambda^{47} + 1.1087\lambda^{100} + 1.2018\lambda^{50} - 0.3196$, and consequently implies the IMFOS of system (3.1.2), which would be in the form:

$$\text{IMFOS} = 0.0327 > 0.$$

Similarly, we notice that the system shows also a chaotic behavior, which confirms the numerical plot result shown in Figure 3.9(b).

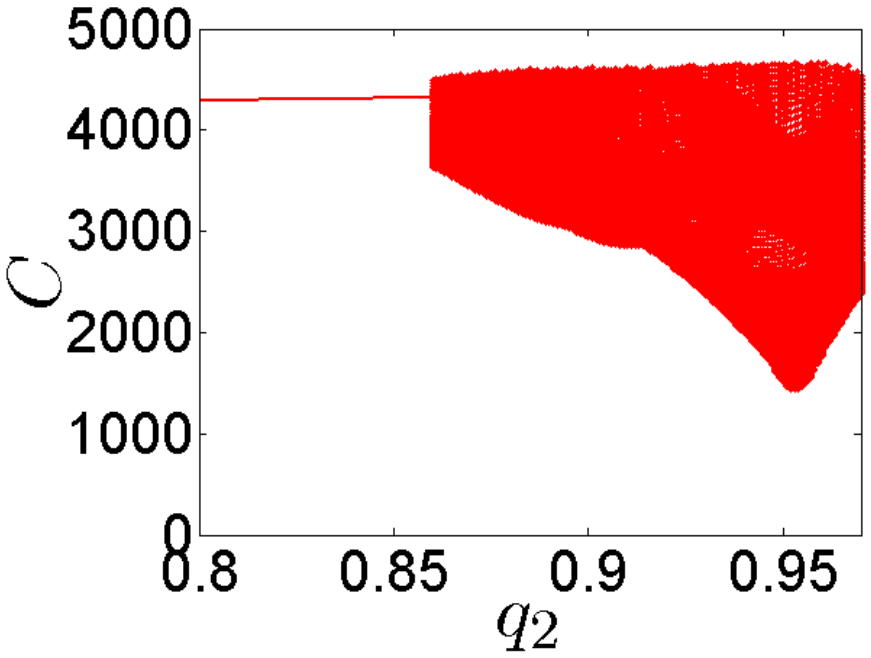

(a)

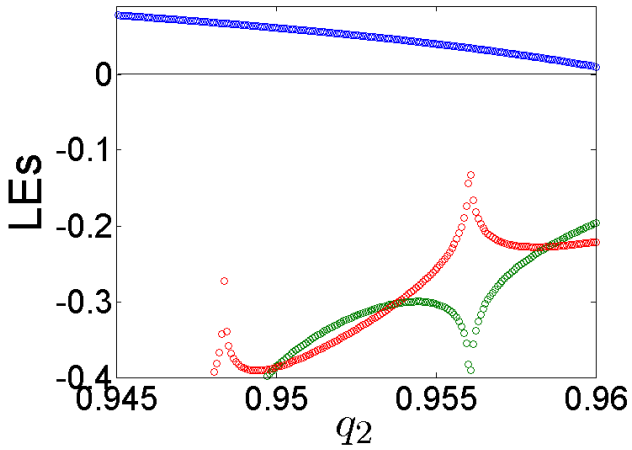

(b)

Figure 3.5: (a) Bifurcation diagram of incommensurate system (3.1.2) for $q_2 \in (0.80, 0.97), q_1 = q_3 = 1$, (b) Lyapunov exponents of incommensurate system (3.1.2) for $q_2 \in (0.945, 0.97), q_1 = q_3 = 1$ with taking system parameters selecting in Table 3.1 and initial conditions $(C_0, S_0, D_0) = (184, 30, 8)$.

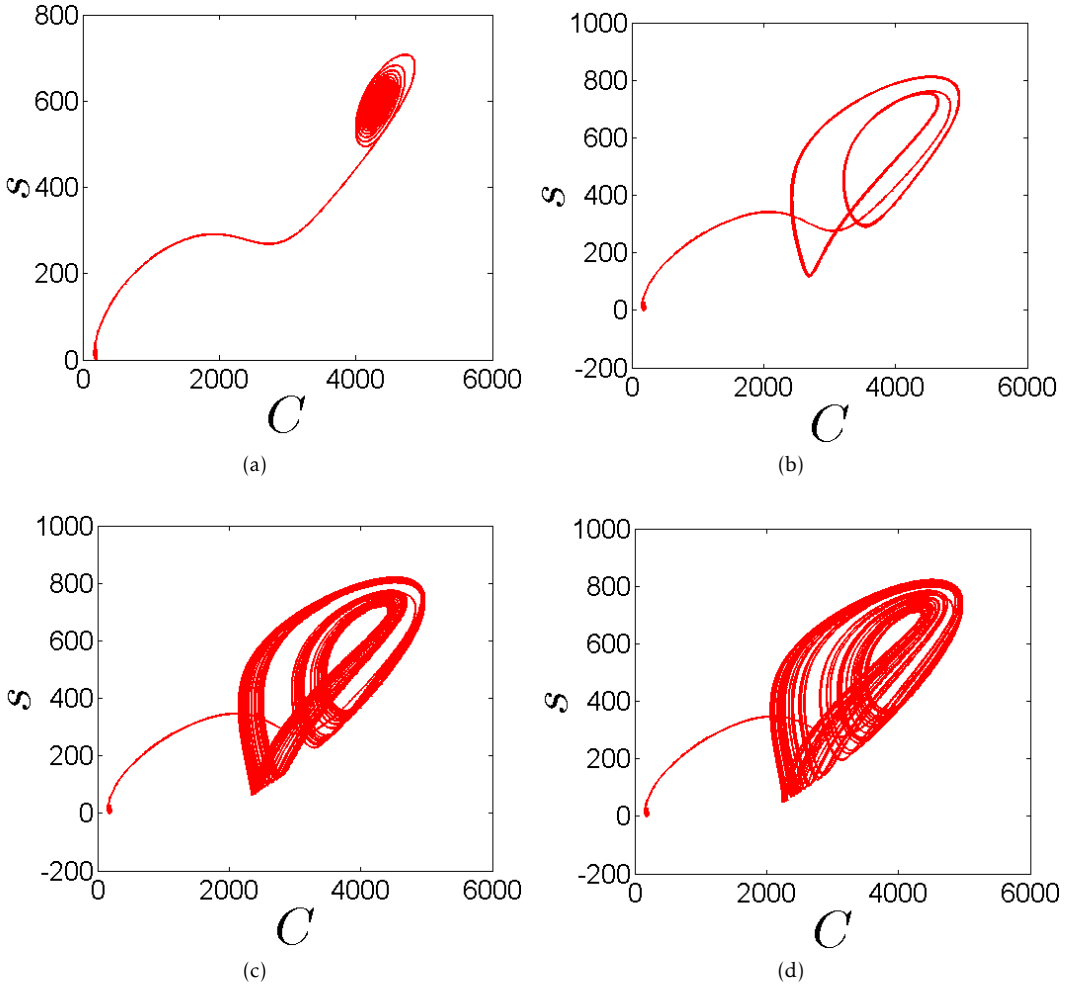

Figure 3.6: Phase portraits of incommensurate system (3.1.2) with taking system parameters selecting in Table 3.1 and initial conditions $(C_0, S_0, D_0) = (184, 30, 8)$ for: (a)$q_2 = 0.85$, (b) $q_2 = 0.95$, (c) $q_2 = 0.958$ and (d) $q_2 = 0.96$.

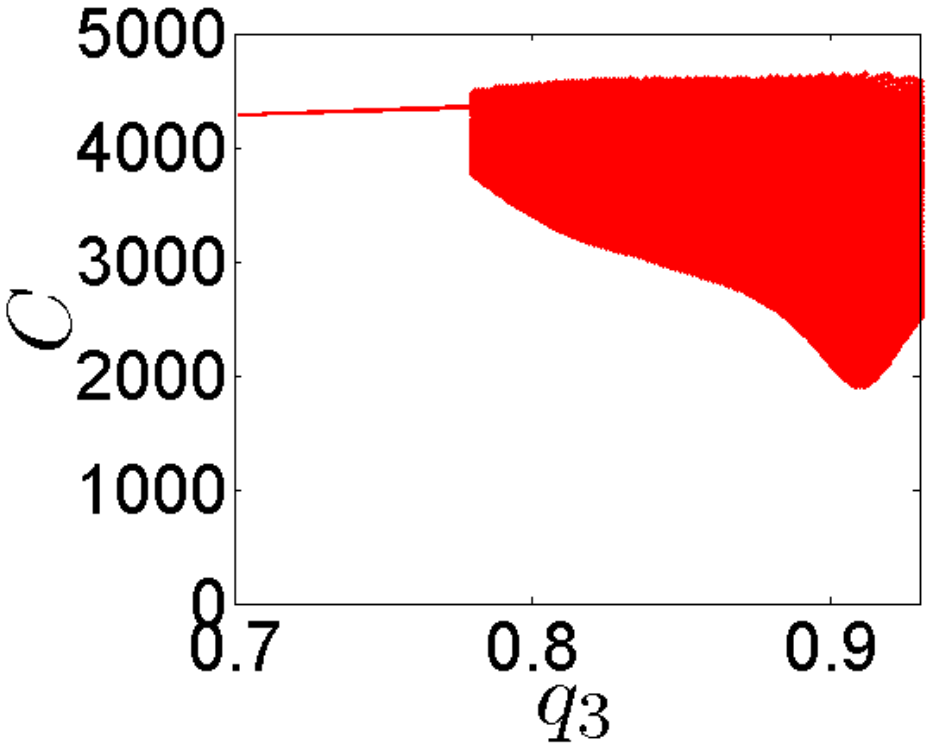

(a)

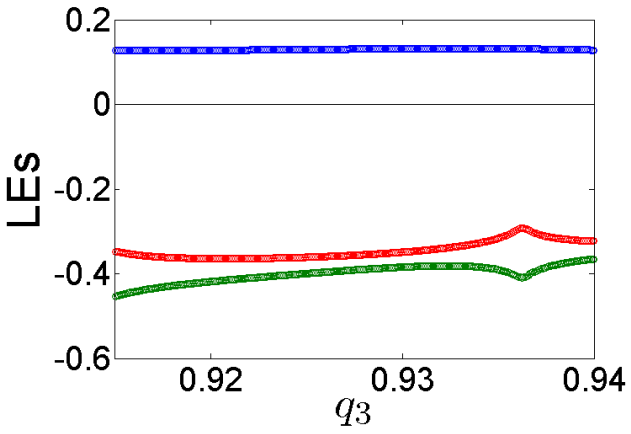

(b)

Figure 3.7: (a) Bifurcation diagram of incommensurate system (3.1.2) for $q_3 \in (0.70, 0.94), q_1 = q_2 = 1$, (b) Lyapunov exponents of incommensurate system (3.1.2) for $q_3 \in (0.915, 0.94), q_1 = q_2 = 1$ with taking system parameters selecting in Table 3.1 and initial conditions $(C_0, S_0, D_0) = (184, 30, 8)$.

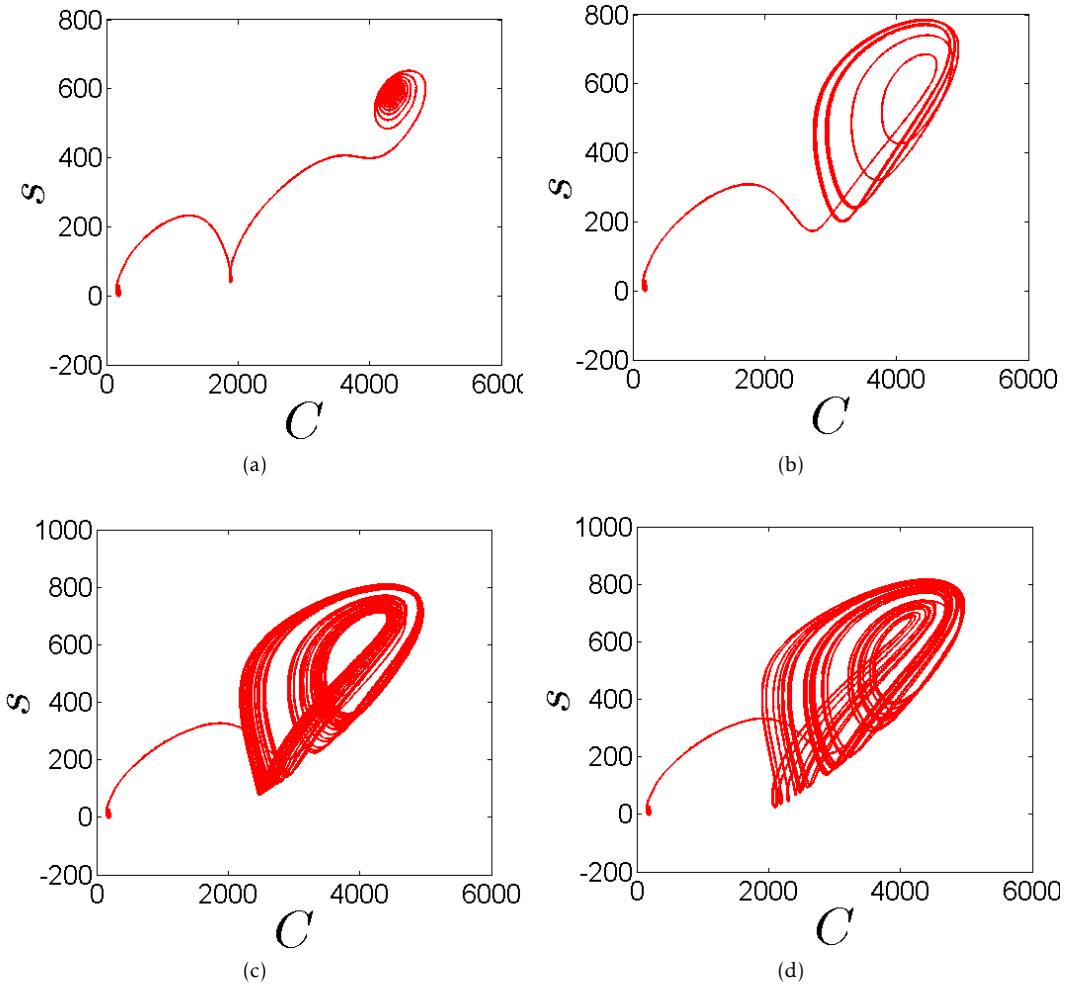

Figure 3.8: Phase portraits of incommensurate system (3.1.2) with taking system parameters selecting in Table 3.1 and initial conditions $(C_0, S_0, D_0) = (184, 30, 8)$for: (a)$q_3 = 0.75$, (b) $q_3 = 0.90$, (c) $q_3 = 0.93$ and (d) $q_3 = 0.94$.

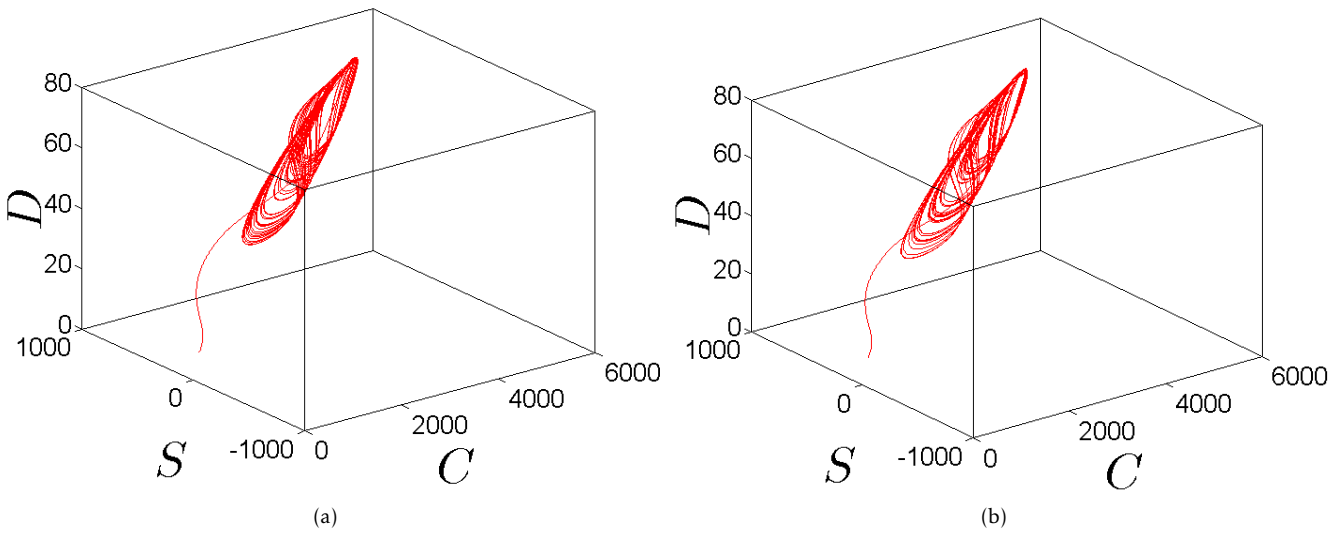

Figure 3.9: Chaotic attractor of incommensurate system (3.1.2) in 3D projection with taking system parameters selecting in Table 3.1 and initial conditions $(C_0, S_0, D_0) = (184, 30, 8)$ for: (a) $q_2 = 0.96, q_1 = q_3 = 1$ and (b) $q_3 = 0.94, q_1 = q_2 = 1$.

As a result of all previous numerical findings, we can conclude that the fractional-order version of the COVID-19 pandemic model exhibits chaotic behaviors in accordance with the two considered cases; the commensurate and the incommensurate fractional-order cases. It can be furthermore concluded that the chaotic ranges generated by system (3.1.2) in its commensurate and incommensurate orders are changed according to a change of these orders, and the minimum fractionalorder value that can exhibit a chaos for the system under consideration is $q_3 = 0.94$ which is occurred when $q_1 = q_2 = 1$.

3.1.4 Discussion

For further discussion and better understanding of the chaotic oscillations of the COVID-19 pandemic, we intend to use the time-series plot in our analysis. Here, the time used for performing some numerical comparisons is chosen from the day 21 till the day 90 because model (**??**), which was established for the outbreak of COVID-19 in China, was considered for the period that began on January 21, 2020 and ended on April 10, 2020 (see [2,14]. The time series plots of the fractional-order COVID-19 system (3.1.2) are illustrated in Figure 3.10 according to the following three cases: Daily new cases C (Figure 3.10(a)), daily additional severe cases S (Figure 3.10(b)), and daily deaths D (Figure 3.10(c)). Within these numerical comparisons, the blue, green and red lines represent the time-series plots sketched when $q_1 = q_2 = q3 = 0.977, q_2 = 0.96, q_1 = q_3 = 1$ and $q_3 = 0.94, q_1 = q_2 = 1$, respectively. In view of the above numerical results, we can continuing resume exploring the recent results obtained from the integerorder system and the observed real results given in Table 3.2 [2]. It can be observed that the maximum number of the daily new cases obtained from the fractionalorder COVID-19 system is the same maximum number obtained from the real data which is ~ 5000. Such observation confirms definitely that the use of the fractional-order system in the expectation for new cases is better than the use of the integer-order system, which it previously expected that these cases will reach to ~ 8000. On the other hand, we observe that the two integer- and fractional-order systems expect approximately the same minimum and maximum numbers of the daily severe cases and the daily death cases, which are both close to the real data. In the same vein and due to the fact that confirms the fractional-order systems can include a memory effect unlike the integer-order systems, we try next to predict the

Table 3.2: The minimum and maximum numbers of different cases

Cases	real data (min,max)	integer system (min,max)	fractional system (min,max)
Daily new cases C	(186,5000)	(186,8000)	(186,5000)
Daily additional severe cases S	(-1000,1500)	(-50,1200)	(-2,800)
Daily deaths D	(8,140)	(8,100)	(8,80)

dynamic of the fractional-order COVID-19 model through taking a wider range of time than that taken in [2]. In particular, by taking, e.g., the commensurate fractional-order values as $q_1 = q_2 = q_3 = 0.977$, the time-series plot of the three state variables C, S, and D are calculated and shown in Figure 3.11, for $t \in (0, 500)$ and $t \in (0, 1000)$. It can be seen from such figure that the chaotic oscillations still exist for the three considered cases. This means that the number of the new cases, severe cases and also death cases will continue taking a chaotic dynamical behavior and will not be decreased with the passage of time without any serious attempt to control the COVID-19 pandemic.

3.1.5 Conclusion

This study has presented a novel COVID-19 pandemic model described by commensurate and incommensurate fractional-order derivatives. By analyzing the stability of the equilibrium points and by varying the values of the fractional-order derivative, the paper has shown that the proposed model exhibits chaotic behaviors. The system dynamics have been investigated via bifurcation diagrams, Lyapunov exponents, time series and phase portraits. A comparison between integerorder and fractional-order COVID-19 pandemic models has clearly shown that the latter is more accurate in predicting the daily new cases. Simulation results have also indicated that the numbers of new cases, severe cases and deaths undertake chaotic behaviors without any useful attempt to control the disease. This would help the decision makers to better understand the epidemiological behavior of the COVID-19 disease over time. Consequently, this would also help them to select measures for effectively monitoring and controlling such pandemic.

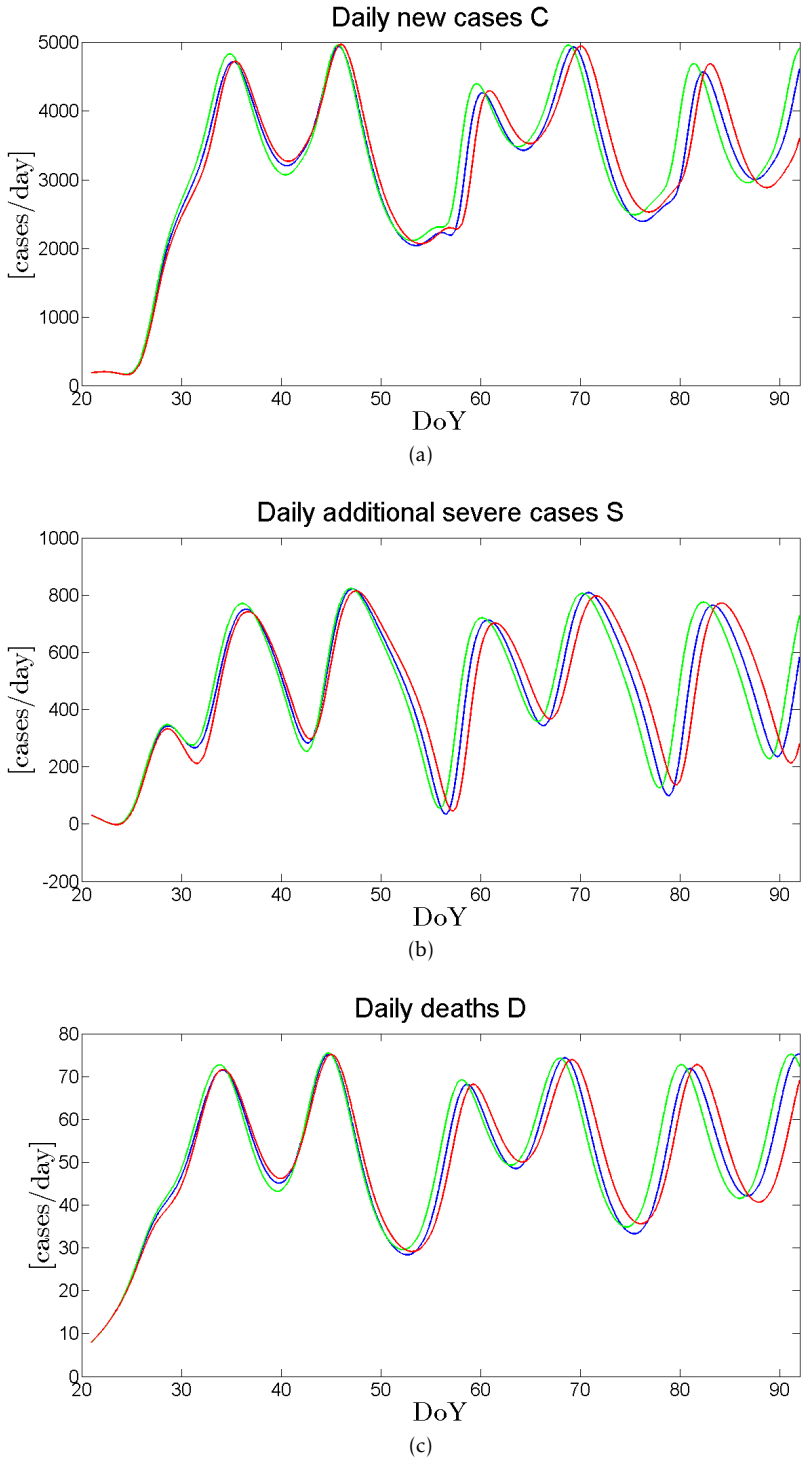

Figure 3.10: Time series of different cases of farctional-order system (3.1.2) with taking system parameters selecting in Table 3.1 and initial conditions $(C_0, S_0, D_0) = (184, 30, 8)$ for: $q = 0.977$ in blue lines, $q_2 = 0.96, q_1 = q_3 = 1$ in green lines and $q_3 = 0.94, q_1 = q_2 = 1$ in red lines.

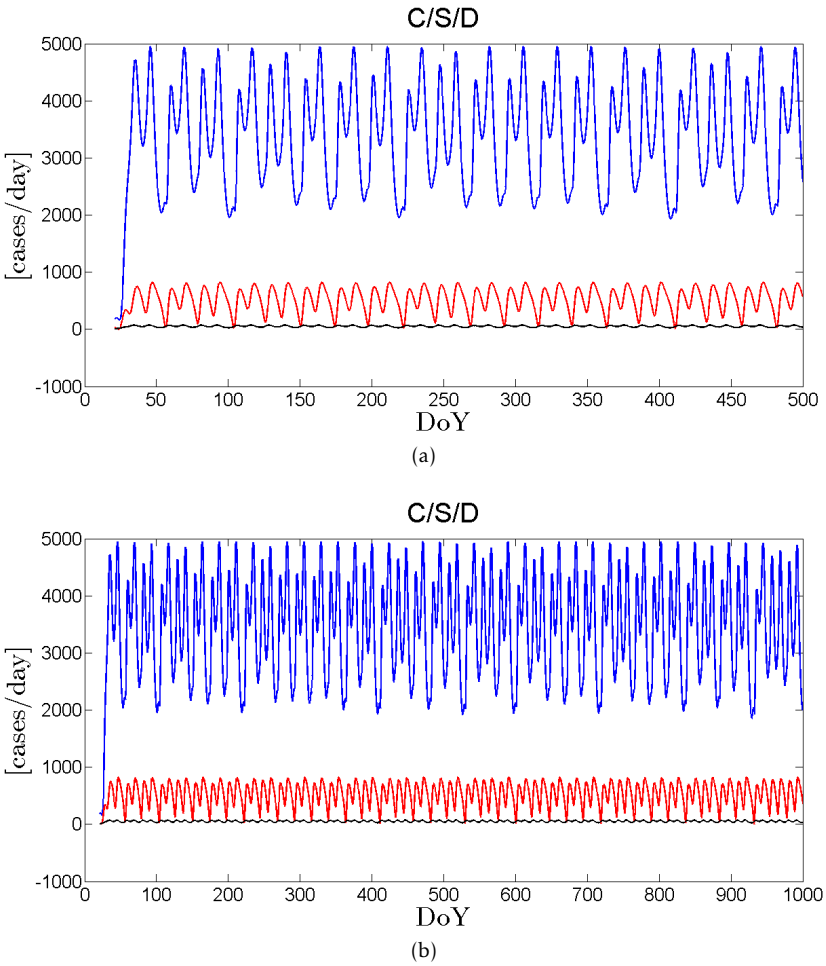

Figure 3.11: Time series of farctional-order system (3.1.2) with taking system parameters selecting in Table 3.1 and initial conditions $(C_0, S_0, D_0) = (184, 30, 8)$ when $q = 0.977$ for: (a) $t \in (0, 500)$, (b) $t \in (0, 1000)$. Blue line for daily new cases, red lines for daily severe cases and black lines for daily deaths.

3.2 Chaos and coexisting attractors in glucose-insulin regulatory system with incommensurate fractional-order derivatives

The content of this section has been published in [12].

3.2.1 Introduction

Diabetes Mellitus, which is more often than not referred to as diabetes, is one of the most widespread chronic disease that the world face nowadays. The number of subjects with diabetes in the world is increasing continuously every year. The number of people suffering from such disease, according to International Diabetes Federation (IDF), is about 463 million across the globe, which is approximately 1 to 11 of the 20-79 adult population. The figure is expected to reach 700 million people in 2045. Diabetes is resulting due to malfunctioning in the plasma glucose-insulin kinetics, leading to abnormal high plasma glucose levels known as hyperglycemia. Knowledge of this regulatory model provides a safe and efficient control algorithm of the plasma glucose level, and enhances control devices that relieve the diabetic subjects. These reasons motivated the investigation of mathematical models which may mimic this biological process. Thus, investigating the mathematical model is of great importance theoretically and practically. Both, theoretical investigation and numerical computation of the endocrine Glucose-Insulin Regulatory Model (GIRM) might enhance the medical care protocols and enrich the medical insight.

Blood glucose level is regulated through a negative feedback mechanism; where hyperglycemia triggers a rapid increase in insulin secreted from the so-called β-cell in the pancreas. An increasing in the plasma insulin level yields a further increasing in the glucose absorbing, prevents its generation by the liver, and then reduces the plasma glucose concentration level. This feedback loop mechanism keeps the glucose concentration in the human body in a limited range after fasted state (70-109 mg/dl). Besides, it is known that the range of the basal blood insulin is about (5-10 μU/ml), which it might be within a wider range reaches approximately to (10-40 μU/ml) at the whole period of the continuous feeding, while it may reach to (30-150 μU/ml) at meal ingestion and high glucose level.

Several mathematicians proposed various forms of the GIRM, (See [111]), for the purpose of exploring the connection between the elevated levels of glucose in the plasma and the insulin amount. One of the pioneer works was done in 1939 by Himsworth and his coworkers, where they proposed an initial procedure for assessing the sensitivity of insulin in organism. To test the dynamics of glucose-insulin, especially to measure the clearance of glucose, numerous mathematical models were suggested and employed. One of the first scientist in this area, and perhaps the earliest one, is Bolie who formulated a simple system involving some ordinary differential equations (ODEs). To represent the test of glucose tolerance, another model consists of two linear ODEs was suggested by Ackerman et al. [111]. Bergman and his coworkers presented the general form of the minimal system, which is considered up to this day a fundamental milestone for modeling the GIRM. Such system is extensively utilized in physiological scientific field, especially for analyzing the metabolism of glucose. All these models are based either on some Delay Differential Equations (DDEs) or some other classical ODEs.

Due to its inherent merits, the Fractional-order Differential Equations (FoDEs) have been extensively employed in modeling several complex phenomena in applied science fields. Leibniz, Abel, L'Hôpital, Riemann and Liouville are deemed the earliest scientists who handled such FoDEs under the umbrella of fractional calculus. The overall meaning of this mathematical branch is defining a real-orders or even complex ones for the operators of differentiation and integration which are, as its known, identified well in the traditional calculus. Due to the non-locality nature of the Fractional-order Derivatives (FoDs), it can be implemented to model several complex phenomena in

wide variety of engineering and applied science fields. In addition to what Integer-order Derivatives (IoDs) have, the FoDs have a further property might be named the mean intrinsic property. This property allows to consider the dynamics of the system with more degree of freedom, especially in their characteristics locality and evolution globality. Hence, the FoDs can offer more precisely models in comparison with what the IoDs offer in describing many real complex phenomena.

It is worth noting that different systems in biological field, which have some characteristics related to hereditary or memory, could be modeled better using the FoDs rather than the IoDs [1]. Therefore, the FoDEs (Based on e.g., Caputo's [112] and Grünwald-Letnikov's (GL) [113] definitions) can enhance describing many real complex systems more precisely than the classical ODEs. Besides, these FoDs (or even for integrals) are most commonly associated to the so-called fractals [114], which are plentiful in several systems of biological field. This was a standpoint of Cho et al. in their work [115], where they proposed a fractional-order generalized form of the minimal model in order to study the rheological behavior of glucose-insulin relationship. They used the Caputo's definition with fractional-order α, where $\alpha \in (0,1]$, 1.00,0.00,0.00and they deduced a presence of inversely proportional relationship between the insulin sensitivity value S_I and the time constant of fractional-order which preserves units $\beta^{(1-\alpha)}$. Besides, they also investigated the equilibrium stability and the solution boundedness of the model. Another Fractional-order GIRM (FoGIRM) was developed by Lekdee et al. [116]. They utilized some numerical and analytical schemes to obtain its solution. In 2017, Sakulranget et al. [117] concluded that the deterministic of the proposed dynamical models in its fractional-order case could offer more accurate fits than other traditional dynamic models that formulated for subjects with type 1 diabetes. Moreover, their fractional-order dynamical models provided a physiologically plausible rate of glucose elimination from the blood into the external environment. By utilizing incommensurate-orders of Caputo's definition, the delayed FoGIRM has been recently introduced by Lekdee et al. in 2019 [118]. Such proposed model is just a generalization of the same one of 1^{st}-order GIRM. Kan et al. [119] in 2019 have analyzed the interaction of insulin and blood glucose in the organism. They have verified, using several numerical simulations for some given data, that the dynamical model in its integer-order case shows an inferior accuracy in comparison to the Bergman's minimal model which has been modified to be in its fractional-order case. Furthermore, a commensurate FoGIRM version has been discussed by Rajagopal et al. in reference [120].

In general, the fractional calculus played and still playing a significant role in describing glucose insulin regulatory feedback system, implying that the intrinsic properties of the FoDs are frequently enhancing the integer-order models. For the reason of elasticity of these derivatives in generalizing the classical models, we have found that it is necessary to deal with such importance subject. In this work, a novel dynamical model, consists of some incommensurate FoDEs, has been proposed for the purpose of modeling a system that describes the glucose-insulin homeostatic. Figure 3.12 shows the general sketchy diagram of this system that involves the main compartments of the glucose-insulin connection as well as the roles of all main biological components.

3.2.2 FoGIRM with incommensurate-orders

Shabestari et al. [121] have proposed recently a new chaotic nonlinear model to study and analyze the GIRM. This model has the form:

$$\begin{cases} \dfrac{dx}{dt} = -a_1 x + a_2 xy + a_3 y^2 + a_4 y^3 + a_5 z + a_6 z^2 + a_7 z^3 + a_{20}, \\ \dfrac{dy}{dt} = -a_8 xy - a_9 x^2 - a_{10} x^3 + a_{11} y(1-y) - a_{12} z - a_{13} z^2 - a_{14} z^3 + a_{21}, \\ \dfrac{dz}{dt} = a_{15} y + a_{16} y^2 + a_{17} y^3 - a_{18} z - a_{19} yz, \end{cases} \tag{3.2.1}$$

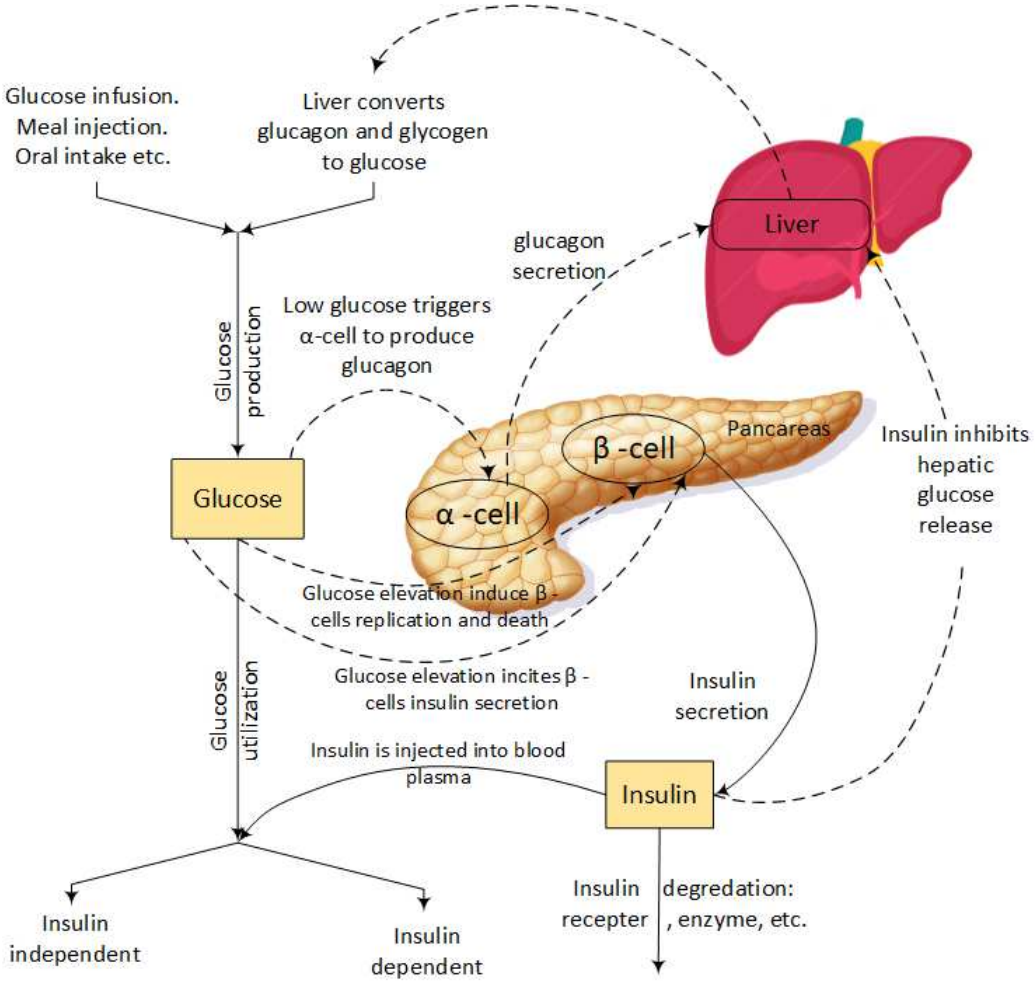

Figure 3.12: Sketchy diagram for the main components of the GIRM.

where $x(t)$, $y(t)$ and $z(t)$ indicate to the population density of insulin, glucose and β-cells, respectively. Besides, Table 1 below exhibits all parameter set used in this model.

Table 1. Summary of the parameters found in system (3.2.1).

Parameter	Meaning
$-a_1$	Indicates the normal decrease in concentration of insulin without glucose.
a_2	Indicates the rate of propagation of insulin with existence of glucose.
a_3,a_4	Indicate the rising insulin rate once the concentration of glucose is raised.
a_5 , a_6 ,a_7	Indicate the rising insulin level rate that independently excreted, from different components, by β-cells.
$-a_8$	indicates the insulin effect on glucose.
a_9,a_{10}	Indicate the rate of decrease in glucose in response to excretion of insulin.
a_{11}	Indicates the normal rising of glucose without insulin.
a_{12} , a_{13}, a_{14}	Indicate the rate of decreasing the concentration of glucose because of insulin excreted by β-cells.
a_{15}, a_{16}, a_{17}	Represent the rate of increase in β-cells caused by the increase in glucose concentration.
a_{18} ,a_{19}	Indicate the rate of decreasing β-cells because of its existing level.

The connection between the concentration of insulin and the blood glucose has been studied and dealt well by proposing some mathematical models [111]. But, unfortunately, far the most of them isolate the system from its environment by eliminating several components that could impact on the relationship between insulin and glucose. To avoid this blind spot of such models, the GIRM given in (3.2.1) can exhibit the most unusual conditions which could occur during the metabolic process. Actually, Vito Volterra proposed this model in [122] based on the so-called predator-prey model, in which prey and predator are assumed to be as glucose and insulin, respectively. From this point of view, it is thought to note that the behavior of the system will be either periodic or chaotic according to the conditions of normal metabolic process or according to the presence of faulty status in the metabolic process itself, respectively. This means that the disorder of the system will be exist if it behaves in chaotic mode [123]. To show the stability of system (3.2.1), the Jacobian matrix is employed to compute its eigenvalues at each equilibrium point. However, system (3.2.1) has the following Jacobian matrix:

$$\begin{pmatrix} -a_1 + a_2 y & a_2 x + 2a_3 y + 3a_4 y^2 & a_5 z + 2a_6 z + 3a_7 z^2 \\ -a_8 y - 2a_9 x - 3a_{10} x^2 & -a_8 x + a_{11}(1-2y) & -a_{12} - 2a_{13} z - 3a_{14} z^2 \\ 0 & a_{15} + 2a_{16} y + 3a_{17} y^2 - a_{19} z & -a_{18} - a_{19} y \end{pmatrix}$$

Based on the values given in Table 2, one might observe that system (3.2.1) has two positive equilibrium points stated in Table 3.

Table 2. Coefficients of system (3.2.1).

a_1	a_2	a_3	a_4	a_5	a_6	a_7	a_8	a_9	a_{10}	a_{11}
2.04	0.1	1.09	−1.08	0.03	−0.06	2.01	0.22	−3.48	−1.2	0.3
a_{12}	a_{13}	a_{14}	a_{15}	a_{16}	a_{17}	a_{18}	a_{19}	a_{20}	a_{21}	
1.37	−0.3	0.22	0.3	−1.35	0.5	−0.42	−0.15	−0.19	−0.56	

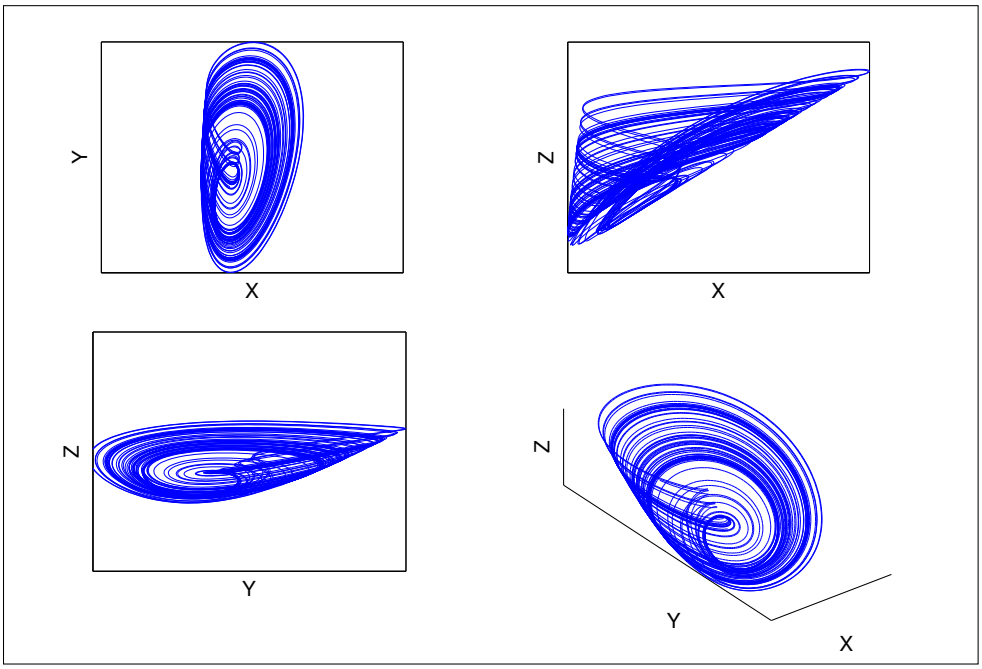

Figure 3.13: Phase portraits of chaotic system (3.2.1) for different projections, subject to $(x_0, y_0, z_0) = (0.53, 1.31, 1.03)$ and the parameters given in Table 2.

Table 3. Equilibria and eigenvalues of system (3.2.1).

Equilibria(x_0, y_0, z_0)	**Eigenvalues**
$E_1(0.654, 1.016, 0.986)$	$-3.000, 0.260 \pm 2.573i$
$E_2(0.624, 0.935, 0.877)$	$-2.837, 0.526 \pm 2.347i$

Furthermore, the condition that makes system (3.2.1) chaotic is satisfied by all eigenvalues of the system. To see this, the phase portraits for different projections of system (3.2.1) are shown in Figure 3.13. In this work, the FoGIRM is handled as a generalization of system (3.2.1) by just replacing the FoDs instead of the IoDs, as follows:

$$\begin{cases} {}_0^{GL}D^{q_1}x(t) = -a_1x + a_2xy + a_3y^2 + a_4y^3 + a_5z + a_6z^2 + a_7z^3 + a_{20}, \\ {}_0^{GL}D^{q_1}y(t) = -a_8xy - a_9x^2 - a_{10}x^3 + a_{11}y(1-y) - a_{12}z - a_{13}z^2 - a_{14}z^3 + a_{21}, \\ {}_0^{GL}D^{q_1}z(t) = a_{15}y + a_{16}y^2 + a_{17}y^3 - a_{18}z - a_{19}yz. \end{cases} \tag{3.2.2}$$

where q_i are rational numbers in the interval $(0,\ 1)$, for $i = 1, 2, 3$.

As a matter of fact, one of the major motivations of this work is to investigate the role of the incommensurate fractional-order derivatives in causing some disorders for the glucose-insulin homeostatic. More precisely, investigating the dynamics of the proposed fractional-order model given in (3.2.2) by exploring the relationship between the values of these incommensurate fractional-order derivatives and the chaotic behavior of the model, allows specialists to determine the classification of the glucose-insulin connection whether it is a disorder connection or not. Knowledge of this matter would be especially valuable in enhancing some medical treatment protocols as well as some other medical insights, especially given the fact that a presence of chaotic behavior of the model generates a disorder in the glucose-insulin connection. On the contrary, knowledge that such connection is regular would offer an efficient control scheme of the plasma glucose level. These explanations have motivated us to propose and explore the biological model given in (3.2.2).

3.2.3 Dynamics of the system

In this section, the dynamic behaviors of system (3.2.2) are studied according to a slightly change in the values of the fractional-orders, $q_i \in (0,1)$, $i = 1,2,3$. New results are established, like the stability of the system with incommensurate q_i, bifurcations, Lyapunov Exponents (LEs), coexisting hidden attractors, and parameter basins for periodic cycles. All numerical simulations are performed using Matlab software. System (3.2.2) has a numerical solution that can be realised using GL approach, with $h = 0.005$, as follows:

$$\begin{aligned}
x(t_k) &= (-a_1 x(t_{k-1}) + a_2 x(t_{k-1})y(t_{k-1}) + a_3 y(t_{k-1})^2 + a_4 y(t_{k-1})^3 + a_5 z(t_{k-1}) + \\
&\quad a_6 z(t_{k-1})^2 + a_7 z(t_{k-1})^3 + a_{20})h^{q_1} - \sum_{j=v}^{k} c_j^{q_1} x(t_{k-j}), \\
y(t_k) &= (-a_8 x(t_k)y(t_{k-1}) - a_9 x(t_k)^2 - a_{10} x(t_k)^3 + a_{11} y(t_{k-1})(1 - y(t_{k-1})) - \\
&\quad a_{12} z(t_{k-1}) - a_{13} z(t_{k-1})^2 - a_{14} z(t_{k-1})^3 + a_{21})h^{q_2} - \sum_{j=v}^{k} c_j^{q_2} y(t_{k-j}), \\
z(t_k) &= (a_{15} y(t_k) + a_{16} y(t_k)^2 + a_{17} y(t_k)^3 - a_{18} z(t_{k-1}) - a_{19} y(t_k) z(t_{k-1}))h^{q3} \\
&\quad - \sum_{j=v}^{k} c_j^{q_3} z(t_{k-j}),
\end{aligned}$$

where $k = 1,2,3,...,N$, $N = \left[\frac{T_{sim}}{h}\right]$, T_{sim} is the simulation time, $(x(0),\ y(0),\ z(0))$ is the Initial Condition (IC) of the system, and where $(c_j^{q_i})$ represents the binomial coefficients that can be computed according to (1.4.6).

Dynamic behaviors via varying the FoDs

In this part, the values of system's parameters, from a_1 up to a_{21}, are fixed to be as in Table 2, and the IC is selected to be as $(x_0,\ y_0,\ z_0) = (0.530,\ 1.310,\ 1.030)$. The bifurcation diagrams are plotted to show the stability of system (3.2.2) by taking several groups of typical differential order values, and implementing the so-called Benettin-Wolf algorithm that yields all LEs for this system [81].

First, fixing $q_2 = q_3 = 1$ yields the bifurcation diagram and space trajectories for $q_1 \in (0.92,1)$ which is shown in Figure 3.14a. It is shown that when $q_1 < 0.94$, system (3.2.2) will tend asymptotically stable towards the equilibrium point. But when $q_1 = 0.94$, such system will begin lose its stability. When $q_1 = 0.95$, the chaotic attractor will be appeared, especially over most of the scope q_1, where $q_1 \in (0.95,1)$. The LEs diagram of this system is shown in Figure 3.14b. This system has at least one positive LE, which implies a chaotic behavior of its mode. To see this, back to Figure 3.14b again. In particular, one could notice that the largest LE will be positive only if $q_1 > 0.94$, which implies directly that the system has a chaotic behavior for all values of q_1 in this range. On the other hand, the dynamic behaviors of system (6) can be further studied when $q_1 = q_3 = 1$ and $q_2 \in (0.75,\ 1)$. Based on Figures 3.15a-3.15b, one observes that system (3.2.2) is stable when $q_2 \in (0.75, 0.87)$ and there is a doubling periodic route when q_2, where $q_2 \in (0.87, 0.90)$. Thus; system (3.2.2) has a chaotic behaviour over most of the scope $q_2 \in [0.90,1]$. Finally, fixing $q_1 = q_2 = 1$ and taking $q_3 \in (0.96,1)$ yield a chaotic dynamic behavior of system (3.2.2) over most of the scope $q_3 \in [0.97,1]$, (see Figures 3.16a-3.16b). It has been shown that the so-called Minimum Effective Dimension (MEF) of system (3.2.2) is 2.90. Actually, this scale, which is frequently employed when handling lots of the fractional-order dynamical systems, indicates to the minimum order of a system to still remain chaotic.

Furthermore, the stability of FoGIRM was studied theorically by using the method in subsection 1.3.2. Consider the system (3.2.2). The Lyapunov exponent is positive for $q_1 \geq 0.95, q_2 = q_3 = 1$(see Figure 3.14b), for $q_2 \geq$

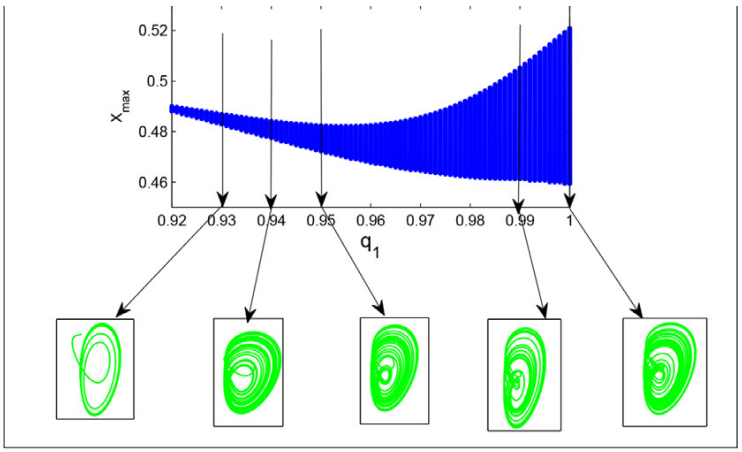

(a)

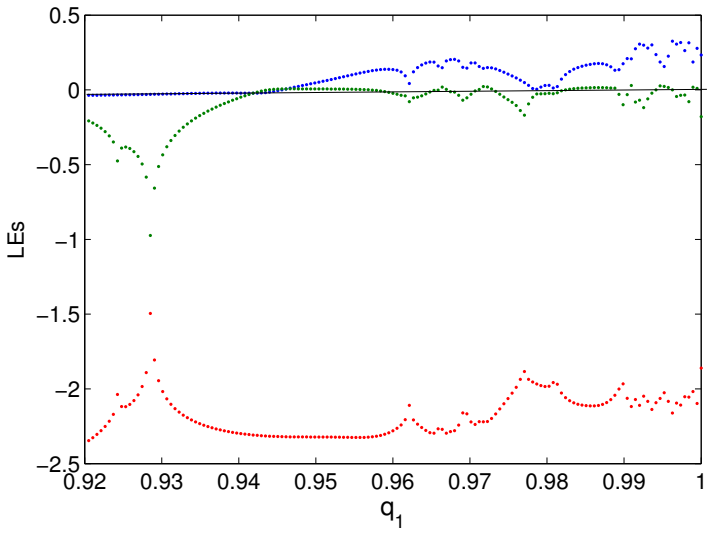

(b)

Figure 3.14: (a) Bifurcation diagram and space trajectories of incommensurate system (3.2.2) as function of $q_1 \in (0.92, 1), q_2 = q_3 = 1$. (b) LEs of incommensurate system (3.2.2) as function of $q_1 \in (0.92, 1), q_2 = q_3 = 1$.

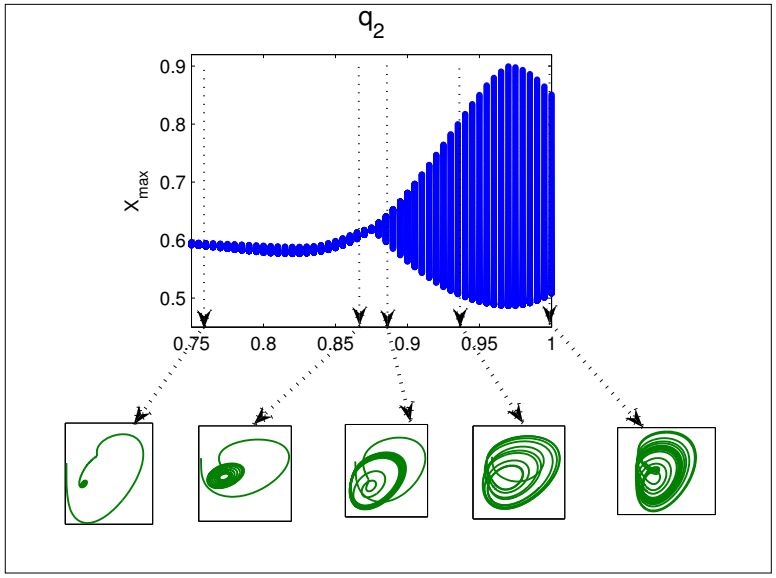

(a)

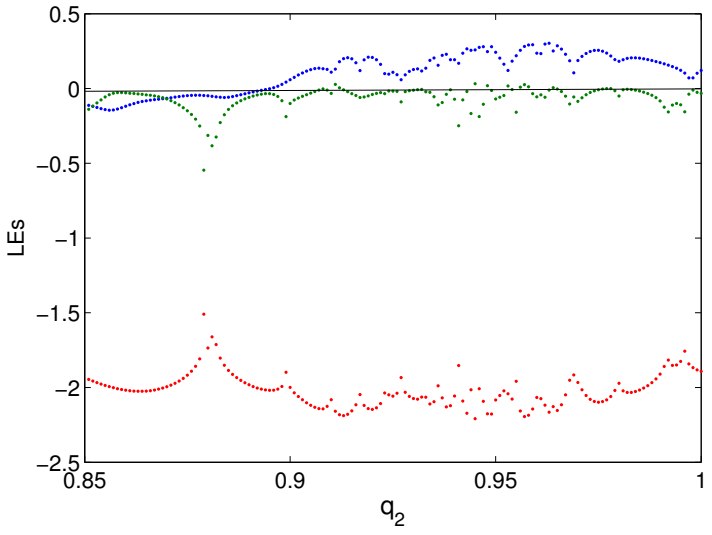

(b)

Figure 3.15: (a) Bifurcation diagram and space trajectories of incommensurate system (3.2.2) for $q_2 \in (0.75, 1), q_2 = q_3 = 1$. (b) LEs of incommensurate system (3.2.2) for $q_2 \in (0.75, 1), q_2 = q_3 = 1$.

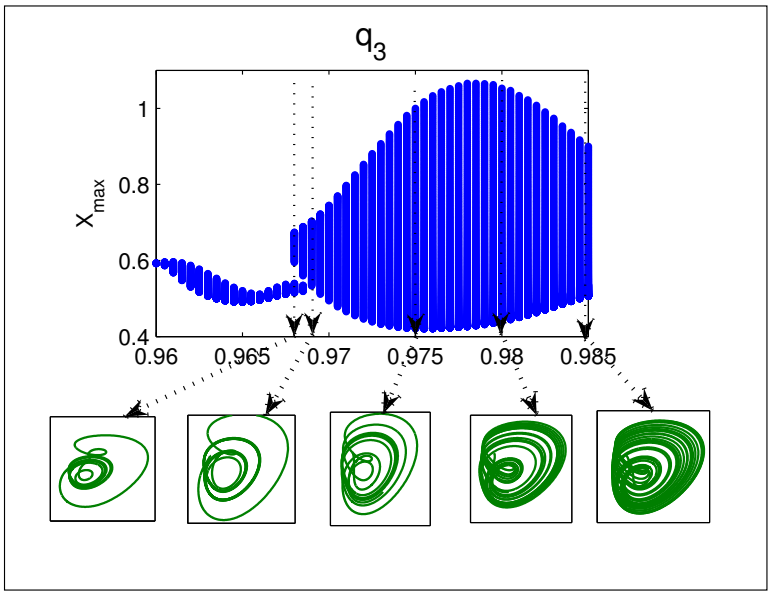

(a)

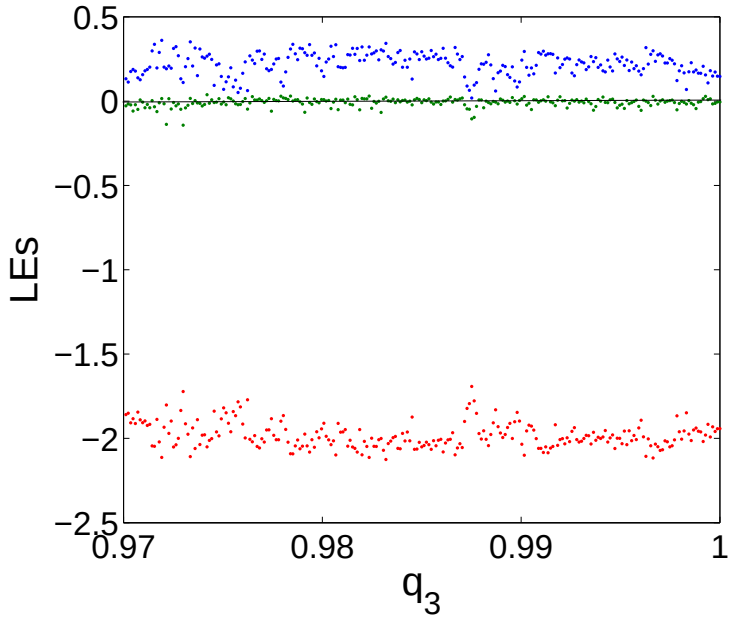

(b)

Figure 3.16: (a) Bifurcation diagram and space trajectories of incommensurate system (3.2.2) for $q_3 \in (0.96, 1), q_1 = q_2 = 1$. (b) LEs of incommensurate system (3.2.2) for $q_3 \in (0.96, 1), q_1 = q_2 = 1$.

$0.90, q_1 = q_3 = 1$(see Figure 3.15b) and for $q_3 \geq 0.97, q_1 = q_2 = 1$(see Figure 3.16b). Now consider the following cases.

* $q_1 = 47/50, q_2 = q_3 = 1$. Therfore $M = LCM(50,1,1) = 50$. Since $\Delta(\lambda) = diag(\lambda^{47}\lambda^{50}\lambda^{50}) - J(E_1)$, $det(\Delta(\lambda)) = \lambda^{147} + 1.9384\lambda^{100} - 0.1188\lambda^{97} + 6.5250\lambda^{50} - 1.3203\lambda^{47} + 20.9375$. The IMFOS of the system is $\frac{\pi}{100} - 0.0292 = 0.0022 > 0$
Though IMFOS> 0 the system shows chaotic behaviour. This is confirmed numerically in Figure 3.14b.

* $q_2 = 45/50, q_1 = q_3 = 1$. Therfore $M = LCM(50,1,1) = 50$. Since $\Delta(\lambda) = diag(\lambda^{47}\lambda^{50}\lambda^{50}) - J(E_1)$, $det(\Delta(\lambda)) = \lambda^{145} + 1.8284\lambda^{100} - 0.1278\lambda^{95} + 6.5250\lambda^{50} - 1.3153\lambda^{45} + 18.9375$. The IMFOS of the system is $\frac{\pi}{100} - 0.0297 = 0.0017 > 0$
Though IMFOS> 0 the system shows chaotic behaviour. This is confirmed numerically in Figure 3.15b.

* $q_3 = 48/50, q_1 = q_3 = 1$. Therfore $M = LCM(50,1,1) = 50$. Since $\Delta(\lambda) = diag(\lambda^{48}\lambda^{50}\lambda^{50}) - J(E_1)$, $det(\Delta(\lambda)) = \lambda^{148} + 1.9484\lambda^{100} - 0.1078\lambda^{98} + 6.5350\lambda^{50} - 1.3205\lambda^{48} + 20.941$. The IMFOS of the system is $\frac{\pi}{100} - 0.0289 = 0.0025 > 0$
Though IMFOS> 0 the system shows chaotic behaviour. This is confirmed numerically in Figure 3.16b.

On another note, by taking another set of incommensurate or- der?s values; the stability of the FoGIRM is also studied through us- ing the diagrams of Lyapunov exponents and the plots of the phase portraits of the system. Graphical comparisons between all these cases and the previous results are given in view of the following cases:

- First, Fixing $q_2 = 0.95, q_3 = 0.97$ and varing $q_1 \in (0.87, 1)$. The diagram of Lyapunov exponents and phase portraits of the system is shown in Figure 3.17(a) and 3.17(b). It can be seen from the figures that the system is stable for $q_1 < 0.94$ and it exhibits a chaotic behavior almost when $q_1 \in (0.94, 1)$. When $q_1 \in (0.97, 0.98)$, the system exhibits a periodic trajectories which is shown in Figure 3.17(b) for $q_1 = 0.975$. Here, a small difference is obtained with the previous case when varing q_1 and fixing $q_2 = q_3 = 1$ that the system exhibits a periodic trajectories when $q_1 \in (0.978, 0.983)$.

- Fixing $q_1 = 0.96, q_3 = 0.97$ and varing $q_2 \in (0.87, 1)$. It can be remarked from the diagram of Lyapunov exponents and phase portraits of the system in Figure 3.18(a) and 3.18(b) that the system is stable when $q_2 < 0.90$ and it is still appears a periodic trajectory when $q2 = 0.90$ which is shown in Figure 3.18(b), but for the previous case the system exhibits chaotic attractor for $q_2 = 0.90$ and $q_1 = q_3 = 1$. The chaotic behavior is still exits after this value i.e $q_2 = 0.90$ to $q_2 = 1$.

- Finally, Fixing $q_1 = 0.96, q_2 = 0.95$ and varing $q_3 \in (0.97, 1)$. The Figure 3.19(a)-3.19(b) shows the Lyapunov exponents and phase portraits of the system. We can see from the figures that the system exhibits chaotic behavior when q_3 increasing and this previous result is the same as the result when varing q_3 and $q_1 = q_2 = 1$.

Dynamic behaviors via varying system's parameters

In this section, various types of insulin- and glucose-related disorders are discussed through examining some of particular LE diagrams. The LE plots of the incommensurate FoGIM given in (3.2.2) are derived for various values of q_i. Besides, some graphical comparisons between some regions deduced from changing the values of system's parameters are performed to exhibit the chaotic behaviors of its mode. The parameters are chosen here to be the same as those ones in [120, 121]. This is because any slightly varying in these parameters' values (increase or decrease) yields another biological meaning. However, Table 4 states a brief description of what happens when

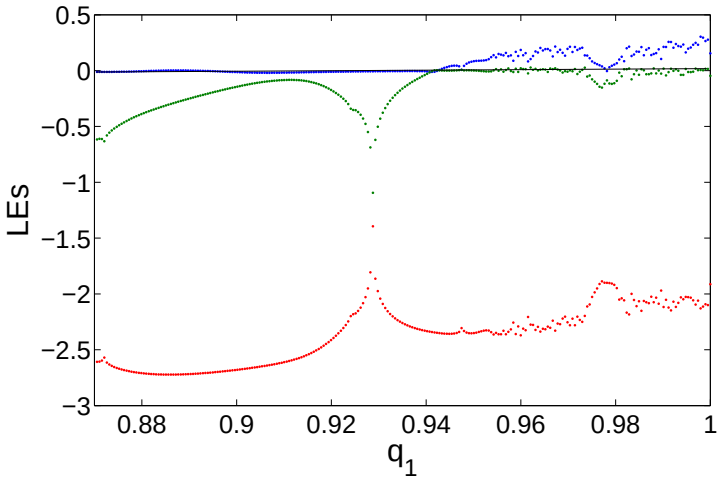

(a)

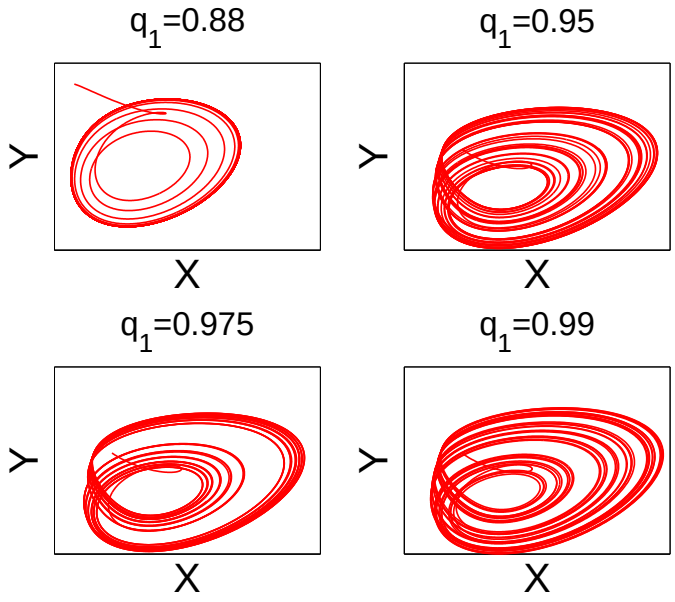

(b)

Figure 3.17: (a) Lyapunov exponents of incommensurate system (3.2.2) for $q_1 \in (0.87, 1), q_2 = 0.95, q_3 = 0.97$. (b) Phase portraits of incommensurate system (3.2.2) for different values of q_1, $q_2 = 0.95$ and $q_3 = 0.97$.

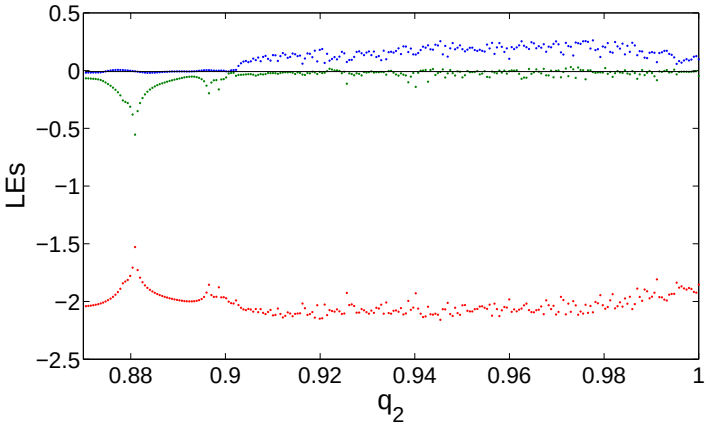

(a)

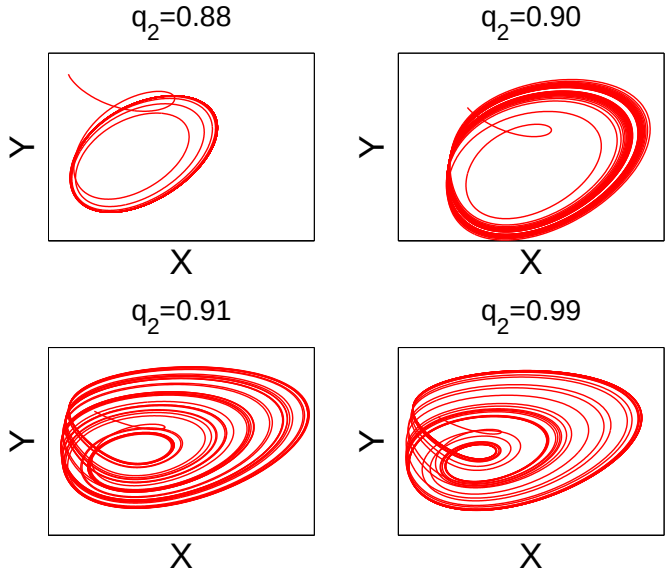

(b)

Figure 3.18: (a) Lyapunov exponents of incommensurate system (3.2.2) for $q_2 \in (0.87, 1), q_1 = 0.96, q_3 = 0.97$. (b) Phase portraits of incommensurate system (3.2.2) for different values of q_2, $q_1 = 0.96$ and $q_3 = 0.97$.

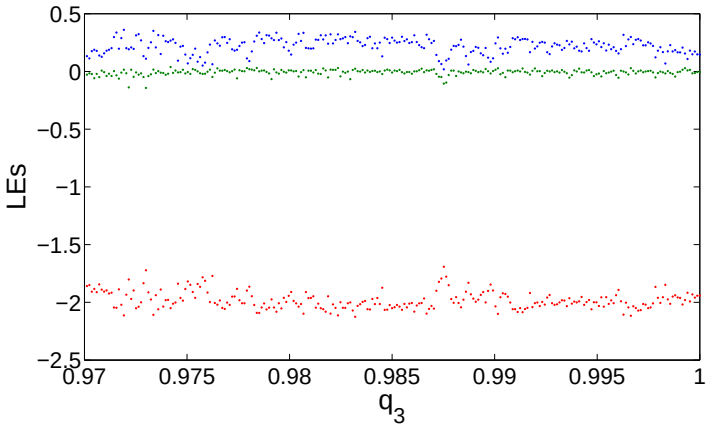

(a)

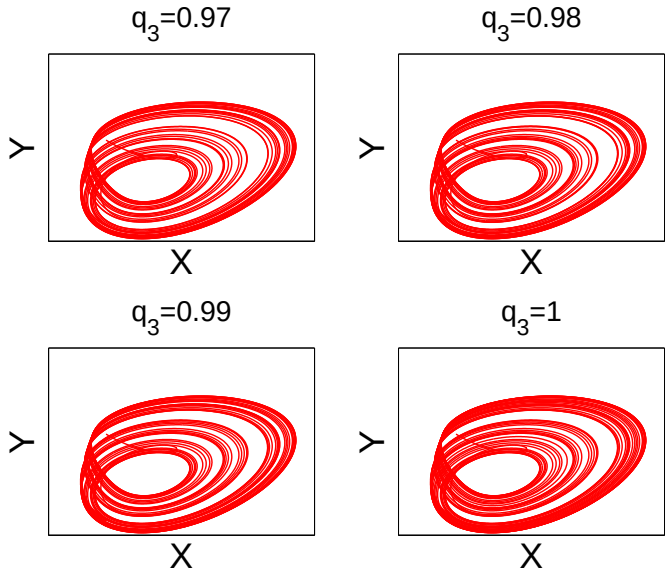

(b)

Figure 3.19: (a) Lyapunov exponents of incommensurate system (3.2.2) for $q_3 \in (0.97, 1), q_1 = 0.96, q_2 = 0.95$. (b) Phase portraits of incommensurate system (3.2.2) for different values of q_3, $q_1 = 0.96$ and $q_2 = 0.95$.

these values are changed. For plotting Figure 3.20, we consider the following three cases of the incommensurate-orders: $[q_1,\ q_2,\ q_3] = [0.97,\ 1,\ 1]$, $[q_1,\ q_2,\ q_3] = [1,\ 0.97,\ 1]$, and $[q_1,\ q_2,\ q_3] = [1,\ 1,\ 0.97]$. Based on such figure, one can observe that the chaotic regions change when the incommensurate-orders are changed. If one compares these results with another results obtained by handling a commensurate fractional-order system, like e.g. the system given in [120], some important remarks related to the orders q_2 and q_3 will be deduced. For example, when a slightly varying of q_2 is occurred, the chaotic regions will be similar to those ones obtained to the system given in that reference, while when another slightly varying of q_3 is occurred, new wider chaotic regions will be exhibited than the previous regions. Such new results would lead many specialists to deduce that the connection between the glucose and insulin can be disordered and lapped, which would consequently change some medical treatment protocols.

Table 4 Biological meaning of varying parameter's values [120].

The variety of Parameter's value	*Biological meaning*
Decrease of a_8	**Diabetes of Type 2**: Causes a disorder because of the increase in the level of glucose in the blood.
Decrease of a_1	**Hypoglycemia:** Causes an extreme excretion of insulin in the blood.
Increase of a_7	**Hyperinsulinemia:** Causes a constant over-stimulation for the resultant insulin out of pancreas's β-cells.
Decrease of a_{15}	**Diabetes of Type 1:** Causes a reduction of population density of pancreas's β-cells.

Parameter basins for periodic cycles plots

This subsection offer further discussions about the parameter basins for the periodic cycles plots. Figure 3.21, however, shows those plots when $q = 1$. Several colors in a 2D parameter space to stable cycles of various periods, are assigned using the parameter basin plot. Based on such Figure, one should know that the black color represents the unbounded region of parameter's value that leads to periodic cycles (shown in different colors), and this yields a chaotic region shown in yellow color. Actually, this verifies that system (3.2.2) has indeed a chaotic behavior, which implies an existed disorder in the glucose-insulin connection.

Coexisting hidden attractors

A new categorization of nonlinear dynamical systems have increasingly lured several researchers. This categorization includes two different types of attractors; the hidden and the self-excited ones. Earlier researches have shown that the second type of such two attractors (i.e. the self-excited one) has a basin of attraction that is connected with or excited from unstable equilibria, while the attractor will be hidden in the opposite case [124]. It has been shown via the basin of attraction plot that the attractors of the proposed model formulated in [121]were exactly categorized as hidden ones. Regarding to system (3.2.2), Figure 3.22 shows the basin of attractions when $q = 1$. In particular, Figure 3.22a exhibits its cross section at $z = 1.03$ in XY-plane, and it also illustrates some regions referred to various dynamic behaviors of the system according to the values of the given parameters in Table 2. Furthermore, the yellow and blue areas of the IC $(x_0, y_0, z_0) = (0.530, 1.310, 1.030)$ indicate to the unbounded orbits and a strange attractor, respectively. Again, based on values given in Table 2, the cross section of two different basins is sketched in XY-plane at $z = 1.03$, as shown in Figure 3.22b. In such Figure, the ICs

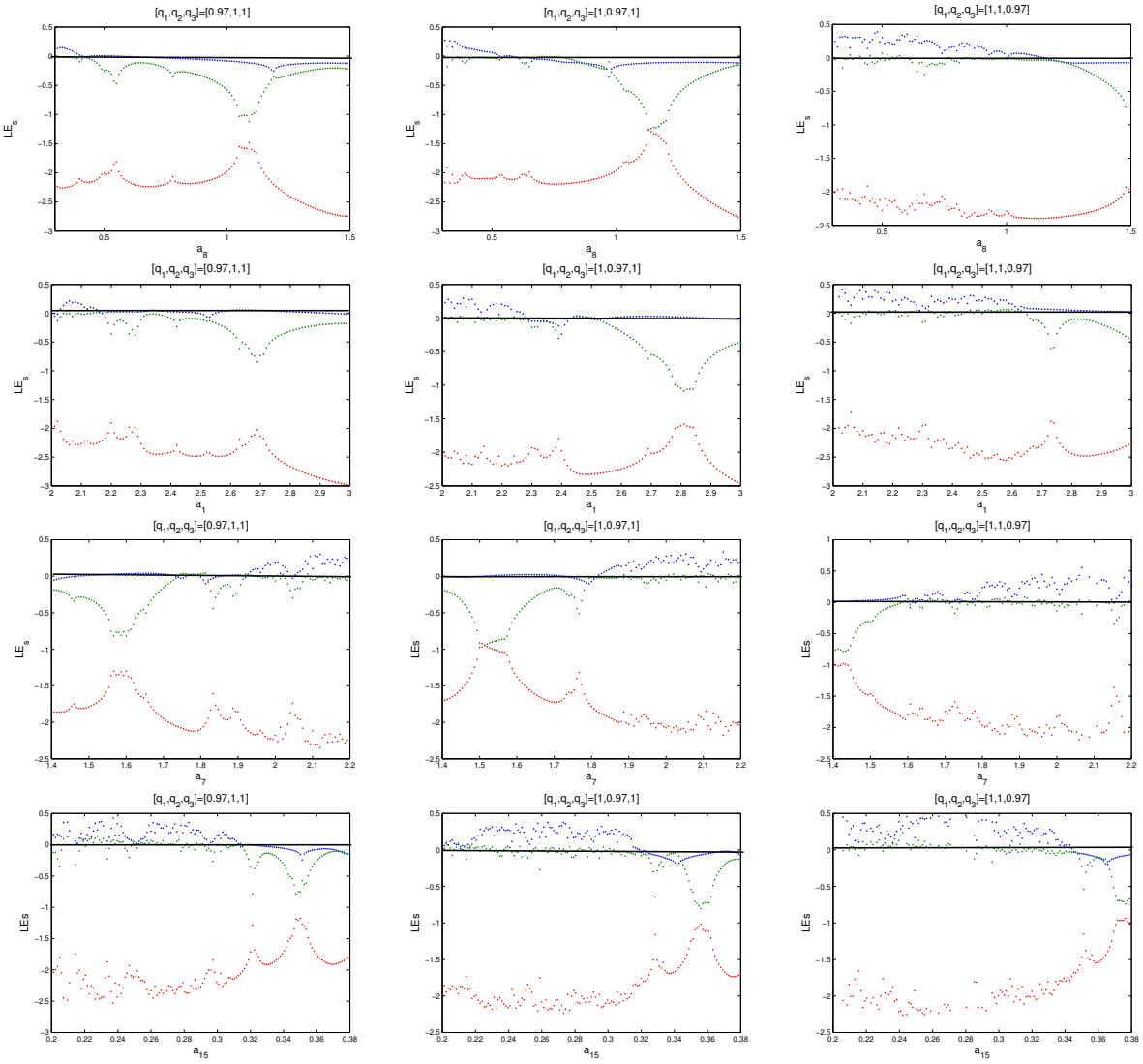

Figure 3.20: LEs of incommensurate fractional-order system (3.2.2) for different parameters.

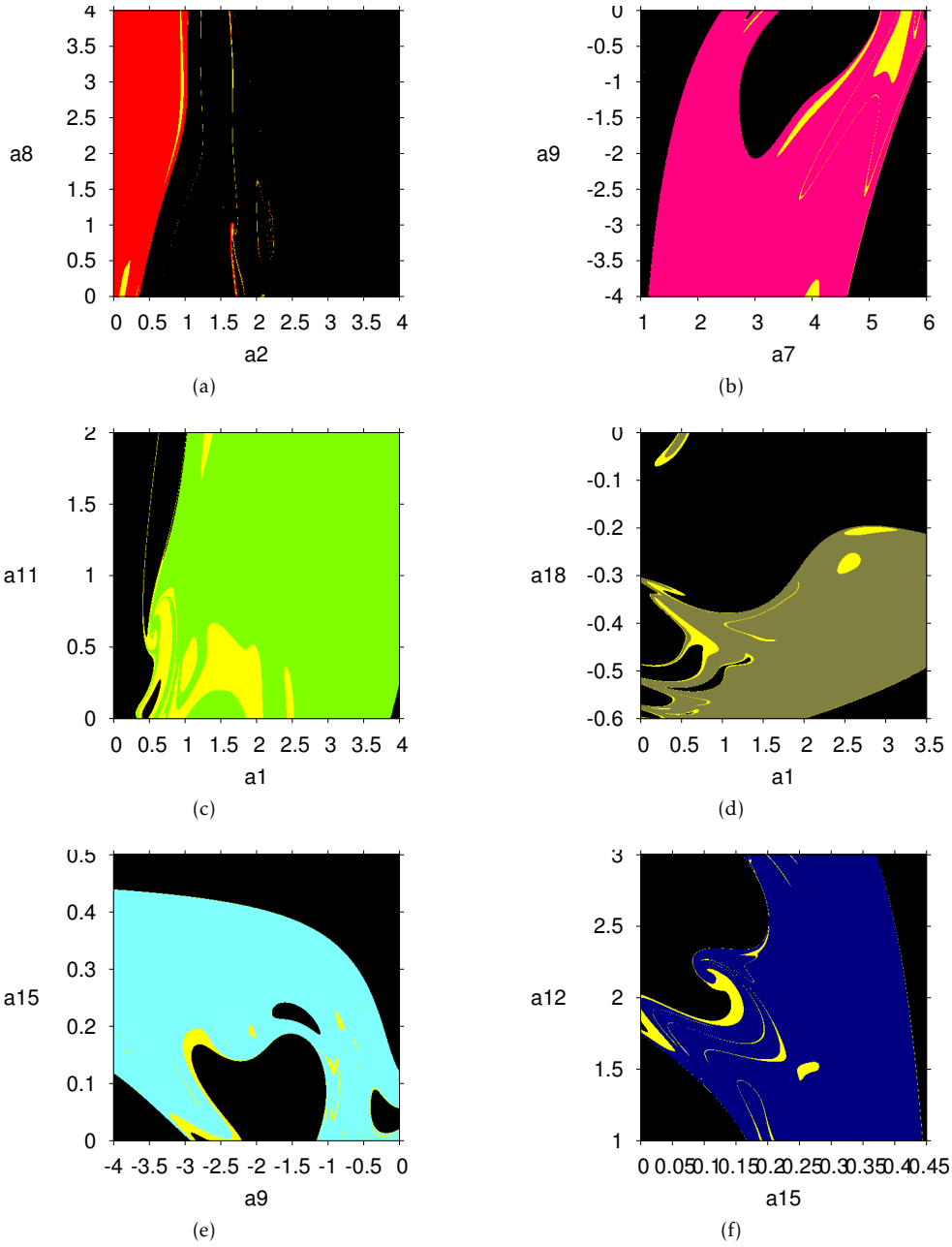

Figure 3.21: The parameter basins for periodic cycles for (a) a_2 and a_8, (b) a_7 and a_9, (c) a_1 and a_{11}, (d) a_1 and a_{18}, (e) a_9 and a_{15}, (f) a_{12} and a_{15}.

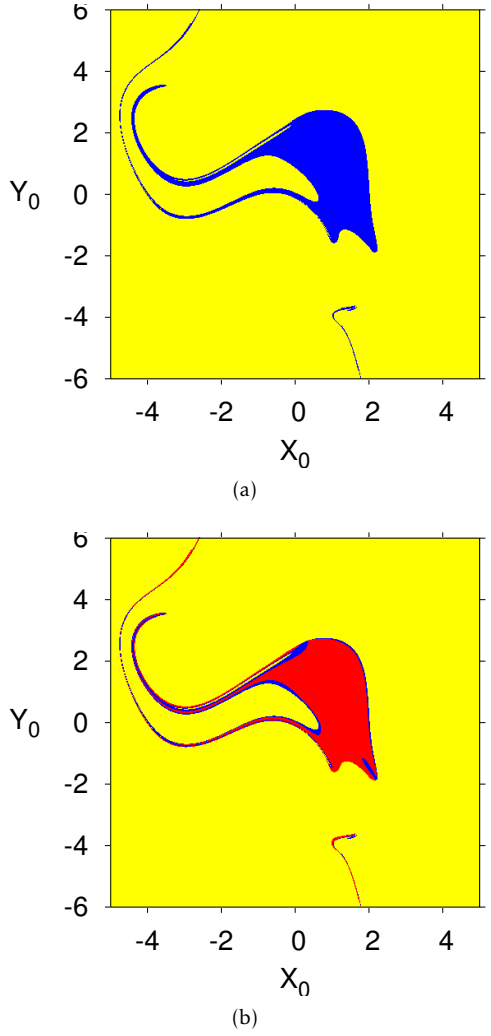

Figure 3.22: Cross section of basin of attraction for parameter set of Table 2.

($(x_0,\ y_0,\ z_0) = (0.530,\ 1.310,\ 1.03)$ and $(x_0,\ y_0,\ z_0) = (0.5,\ 1.31,\ 1.03)$) shown in yellow area indicates to the unbounded orbits, while those ones which are shown in red and blue areas indicate to two other strange attractors. One more thing, the handled system has no fixed point according to the chosen values of its parameters, which implies that such system has two-coexisting chaotic hidden attractors.

For showing the bistability of system (3.2.2), the bifurcation diagrams of the two solutions are plotted in Figure 3.23a by varying the values of q_1 in the range $q_1 \in (0.92, 1)$ and fixing $q_2 = q_3 = 1$ with two ICs; $(x_0,\ y_0,\ z_0) = (0.530,\ 1.310,\ 1.030)$ for the blue plot and $(x_0,\ y_0,\ , z_0) = (0.50,\ 1.310,\ 1.030)$ for the red plot. From this Figure, we deduce that there are two coexisting solutions of system (3.2.2). This would make the system to still remain in chaotic modes according to the two aforesaid ICs when $0.94 < q_1 < 1$, and also make the coexisting hidden attractors to be appeared when $q_1 = 0.95$, (see Figure 3.23 b). For the other cases, when q_2 and q_3 are varying, two coexisting hidden attractors will be appeared as shown in Figure 3.24.

3.2.4 Conclusion

From the standpoint that proposing a precise Glucose-Insulin Regulatory Model (GIRM) will serve specialists to describe the glucose-insulin homeostatic, this work proposes and investigates a general form of the GIRM itself by considering the role of its incommensurate fractional-order derivatives in causing disorders, for the glucose-insulin connection. It has been shown, after exploring the dynamics of the proposed fractional-order model, that such model emerges wide chaotic regions once the values of these incommensurate-orders are changed. In particular, this model has displayed periodic cycles and chaos in its dynamic behavior, especially when the coexisting hidden attractors for incommensurate fractional-orders have been shown. In the light of the rich dynamic properties of such biological model, some medical treatment protocols as well as medical insights can be enhanced and improved, especially given the fact that a presence of chaotic behavior of the model generates a disorder in the glucose-insulin connection. Exploring this fact based on converting the proposed model to its equivalent discrete form will be, however, left to future considerations.

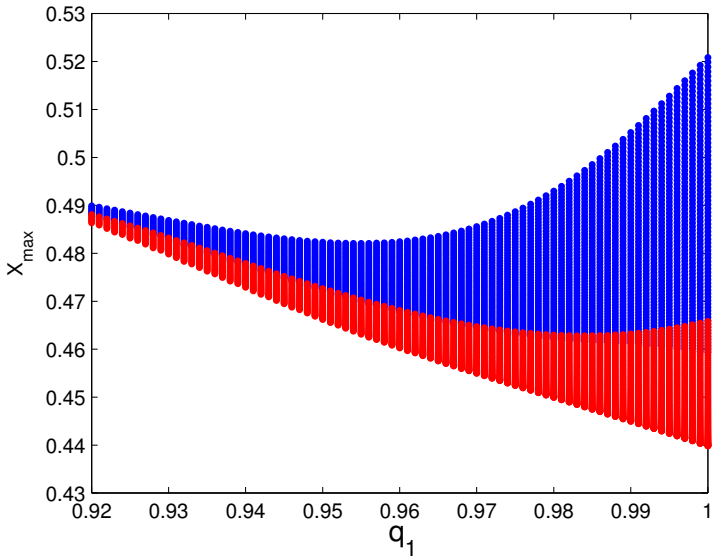

(a)

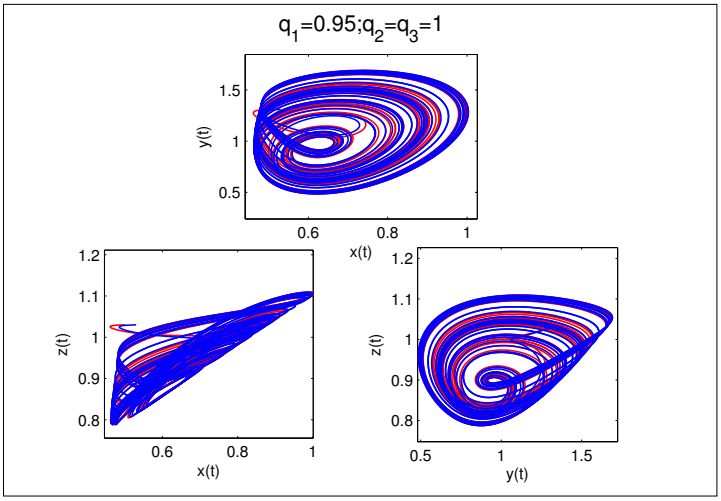

(b)

Figure 3.23: (a) Bifurcation diagrams of the coexisting solutions of system (6) for $q_1 \in (0.92, 1), q_2 = q_3 = 1$ and with $(x_0; y_0; z_0) = (0.53; 1.31; 1.03)$ for blue plot; $(x_0; y_0; z_0) = (0.5; 1.31; 1.03)$ for red plot. (b) Coexisting hidden attractors for incommensurate fractional-order q_1.

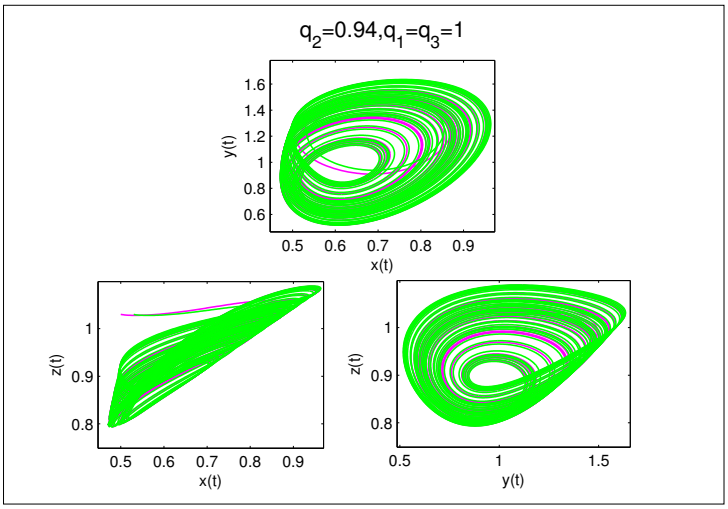

(a)

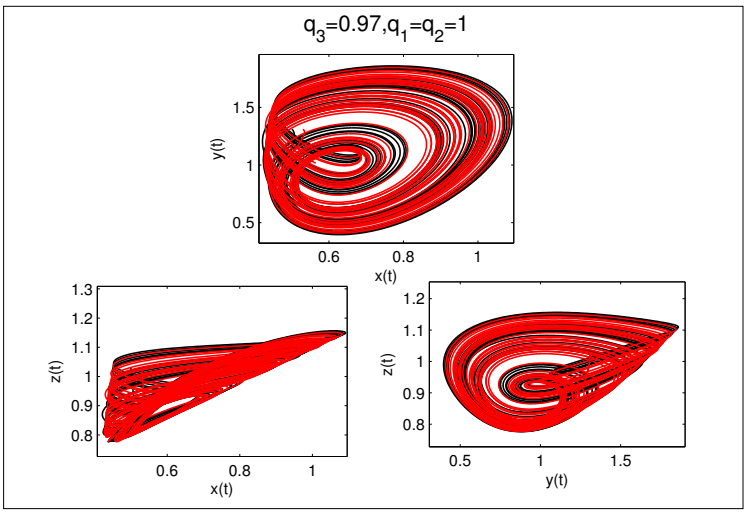

(b)

Figure 3.24: Coexisting hidden attractors for incommensurate fractional-orders (a) q_2, and (b) q_3

3.3 Fractional-order biological system: chaos, multistability and coexisting attractors

The content of this section has been published in [13].

3.3.1 Introduction

After decades of intensive research, it can be fully asserted that the study of nonlinear dynamics is extremely important for understanding natural phenomena. Various dynamical behaviors such as periodic, quasi-periodic, weak chaotic, strong chaotic and intermittent dynamics play a fundamental role in explaining complex phenomena arising in quite different domains of science and engineering. For example, nonlinear dynamics have been discovered in systems from physics, chemistry, electrical engineering, medicine, hydrology, finance and biology.
Until a few years ago, most of these systems were modeled by means of ordinary differential equations with integer order, and most of the nonlinear phenomena were discovered by applying techniques of the integer order calculus [1]. Nowadays, the great role of fractional calculus in describing nonlinear phenomena is undeniable. Although the mathematical concepts underlying fractional calculus were settled long ago by the eminent mathematicians Leibniz, Liouville and Riemann, only in recent years it has been shown that fractional order models effectively describe phenomena that occur in natural science and engineering problems. Specifically, fractional calculus enables to consider non-local, long-range memory and hereditary properties of many biological systems, which cannot be accurately described by using integer order calculus.
In this framework, researchers have proposed and intensively studied both integer and fractional order systems able to accurately model a lot of biological phenomena [125]. Among these systems, the nonautonomous Van der Pol oscillator turn out to be a paradigm for describing smoothly oscillating limit cycle and relaxation oscillations which may occur in biological systems [126]. In particular, different interesting phenomena are founded because of the existence of an external periodic excitation on this model including harmonic, sub-harmonic and superharmonic oscillations, frequency entrainment, chaotic behavior [127].
In 1920, the integer order Van der Pol oscillator was proposed by the Dutch electrical engineer Balthasar Van der Pol in his studies of electric circuits with vacuum tubes [128]. In 1961 and 1962, Fitzhugh [129] and Nagumo [130] proposed the first biological model of action potentials of neurons based on the Van der Pol equations. Several years later, in 1997, Venkatesan et al. have shown that the generalization of the classical integer order Van der Pol oscillator with a cubic nonlinear term (also known as Van der Pol-Duffing oscillator) exhibits chaotic motion between two types of regular motion, namely periodic and quasiperiodic oscillations in the principal resonance region [131]. In 2007, Kadji et al. have shown that the multi-limit cycles integer order Van der Pol oscillator describes the ferroelectric behavior of enzymes-substrates reactions in brain waves [126]. In particular, the authors pointed out that the autonomous form of the oscillator displays the phenomenon of birhythmicity; on the contrary the non-autonomous form of the oscillator displays harmonic oscillations with their corresponding stability boundaries [126]. In 2007, Barbosa et al. performed one of the first studies, in time and frequency domain, of the unforced and forced version of the fractional Van der Pol oscillator [132]. In 2009, Tavazoei et al. numerically showed that the dynamics of the fractional order Van der Pol oscillator have major differences with those of its integer order counterpart [133]. In 2014, Hammouch et al. investigated the dynamic behavior of the non-autonomous Van der Pol oscillator in the case of commensurate fractional order biological model. Moreover, the authors studied chaos synchronization of two identical fractional order Van der Pol oscillators by using the active control synchronization method and the phase-locked-loop analogy [125]. In 2019, Chen et al. studied the stability conditions and the occurrence of the Hopf bifurcation considering a commensurate fractional-order van

der Pol oscillator with time-delayed feedback [134].
To the best of authors' knowledge, the dynamic behavior of the non-autonomous Van der Pol oscillator in the case of incommensurate fractional order model has not been reported in literature yet.
Inspired by the previous investigations, in order to discover new and interesting nonlinear dynamics for possible application in the field of biology and biomedicine, in this paper the authors discuss numerically the effect of an incommensurate fractional order time derivative introduced in the Van der Pol non-autonomous equations. The stability of the proposed incommensurate system is analyzed performing several numerical simulations whose results are reported by means of bifurcation diagrams, computation of the largest Lyapunov exponent, phase portraits in 2D and 3D projections. The analysis reveals that the system can exhibit chaotic dynamics and oscillations, but also striking phenomena such as symmetry, multi-stability and coexistence of attractors.

3.3.2 Mathematical Model

A non-autonuomous biological system was studied in [125, 126] which was described by the mathematical model as follows:

$$\begin{cases} \dot{x} = y, \\ \dot{y} = m(1 - x^2 + ax^4 - bx^6)y - x + e\cos(\omega t), \end{cases} \tag{3.3.1}$$

where m is the parameter of nonlinearity, the parameters a and b are positives, the external excitation has amplitude and frequency parameters which are e and ω respectively.
Fig. 3.25 shows the chaotic trajectory of the forced system (1) for $a = 2.55, b = 1.70$, $m = 2.001$ and periodic forcing $e = 8.27$,$\omega = 3.465$.

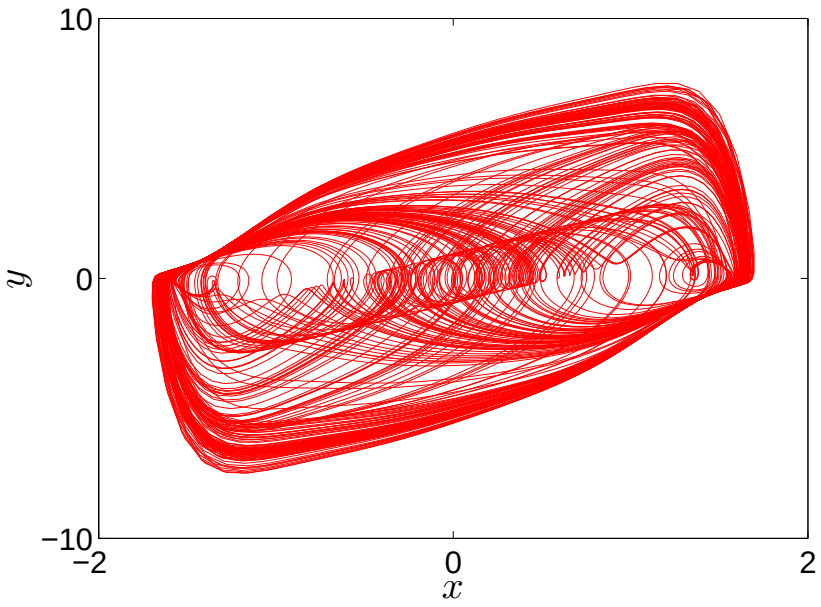

Figure 3.25: Chaotic trajectory of the forced system (1) for $a = 2.55, b = 1.70$, $m = 2.001$ and periodic forcing $e = 8.27$,$\omega = 3.465$.

In this paper, a fractional incommensurate ordered model of nonautonomous biological system (FIONBS) is considered by the following equations:

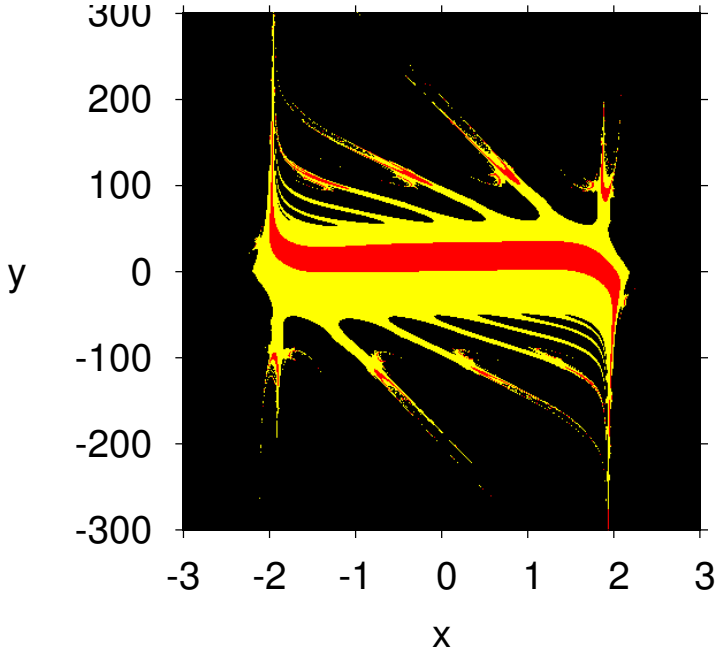

Figure 3.26: Basin of attraction of unforced system (2) for $a = 2.55, b = 1.70$ and $m = 2.001$ with $q_1 = q_2 = 1$.

(3.3.2)
$$\begin{cases} D_t^{q_1} x = y, \\ D_t^{q_2} y = m(1 - x^2 + ax^4 - bx^6)y - x + e\cos(\omega t), \end{cases}$$

Here D^q is q-order Caputo differential operator, $0 < q_i \leq 1 (i = 1, 2)$ are the derivative orders of the state variables x, y. For solving fractional differential equations numerically based on the Caputo definition, Diethelm was introduced the predictor-corrector method which is an improved version for numerical simulations of the Adams-Bashforth-Moulton algorithm.

At first the dynamics of the fractional order system (2) are discussed without external forcing. When $q_1 = q_2 = 1$, the basin of attraction of system (2) (in the unforced case, i.e.,$e = 0$) is present in Fig. 3.26 for the values $a = 2.55, b = 1.70$ and $m = 2.001$. Initial conditions from the region with black color lead to unbounded orbits in yellow region (unbounded region). The initial conditions from yellow region lead to limit cycles in the red region (bounded region). For the parameters $a = 2.55, b = 1.70$ and $m = 2.001$ and taking the incommensurate order $[q_1, q_2] = [0.95, 0.97]$, the system (2) (in the unforced case, i.e. $e = 0$) has a locally stable limit cycle that is presented in Fig. 3.27 for initial conditions $(x_0, y_0) = (0, 1)$ from the bounded (red) region.

Now, the periodic forcing is applied (the amplitude $e = 8.27$ and the frequency $\omega = 3.465$) to the autonomous system (2). For this set of parameters, the system has one equilibrium point O(0,0). Different trajectories of the forced system (2) with initial conditions $(x_0, y_0) = (0, 1)$ are plotted in Fig. 3.28 for different values of the incommensurate orders q_1 and q_2, whereas, a limit cycle in green line for $[q_1, q_2] = [0.80, 0.82]$, a periodic attractor in black line for $[q_1, q_2] = [0.92, 0.93]$ and a chaotic attractor in blue line for $[q_1, q_2] = [0.95, 0.97]$. In fact, the nonautonumous system (2) loses its stability and the stable orbits bifurcate to a chaotic orbits in blue line wich are presented with the chaotic orbits of integer-order system (1) in red line at the same figure. Fig. 3.29 present the chaotic attractor of the fractional forced system (2) for $a = 2.55, b = 1.70$, $m = 2.001$ and periodic forcing $e = 8.27, \omega = 3.465$ with $[q_1, q_2] = [0.95, 0.97]$.

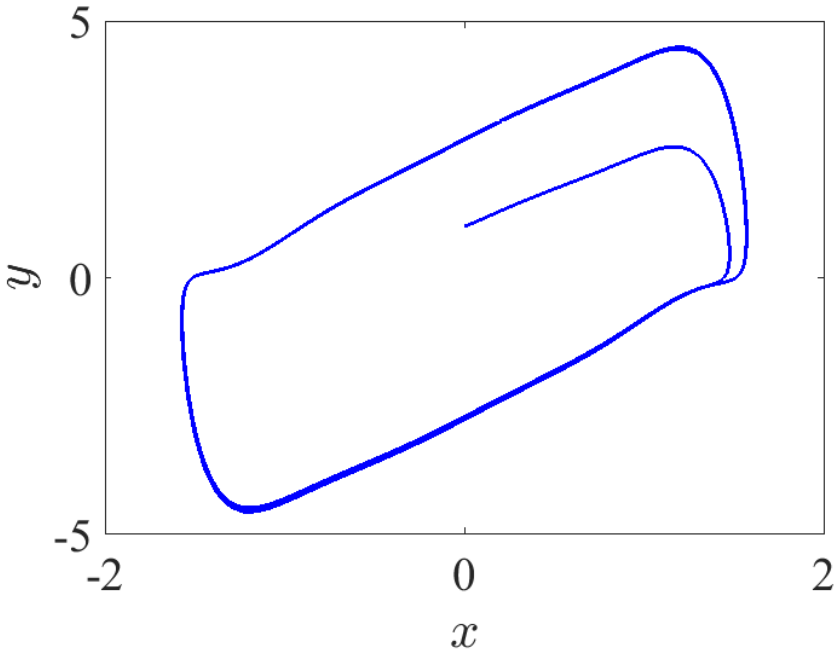

Figure 3.27: Limit cycle of unforced system (2) for $a = 2.55, b = 1.70$ and $m = 2.001$ with $[q_1, q_2] = [0.95, 0.97]$.

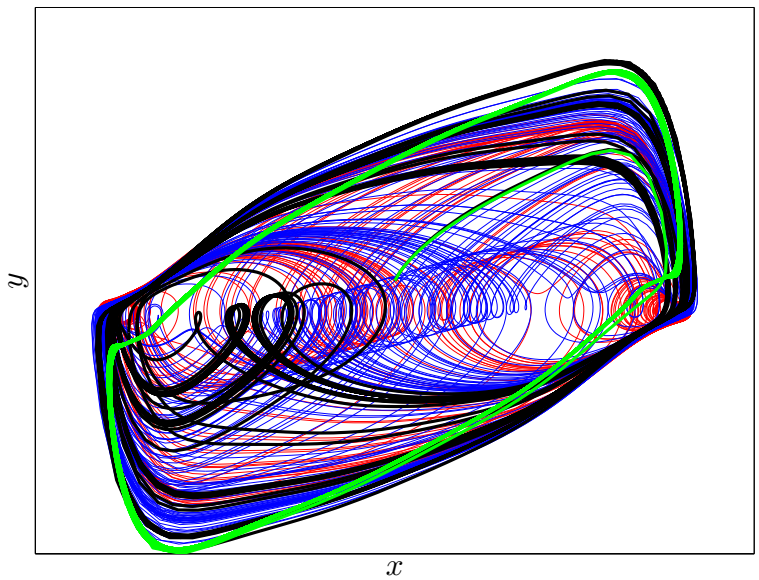

Figure 3.28: Different trajectories of the forced system (1) (red color) and (2) (other colors) with $a = 2.55, b = 1.70$, $m = 2.001$ and periodic forcing $e = 8.27, \omega = 3.465$ for certain values of q_1 and q_2; a limit cycle in green line for $[q_1, q_2] = [0.80, 0.82]$, a periodic attractor in black line for $[q_1, q_2] = [0.92, 0.93]$, a chaotic attractor in blue line for $[q_1, q_2] = [0.95, 0.97]$ and a chaotic attractor in red line for $[q_1, q_2] = [1, 1]$.

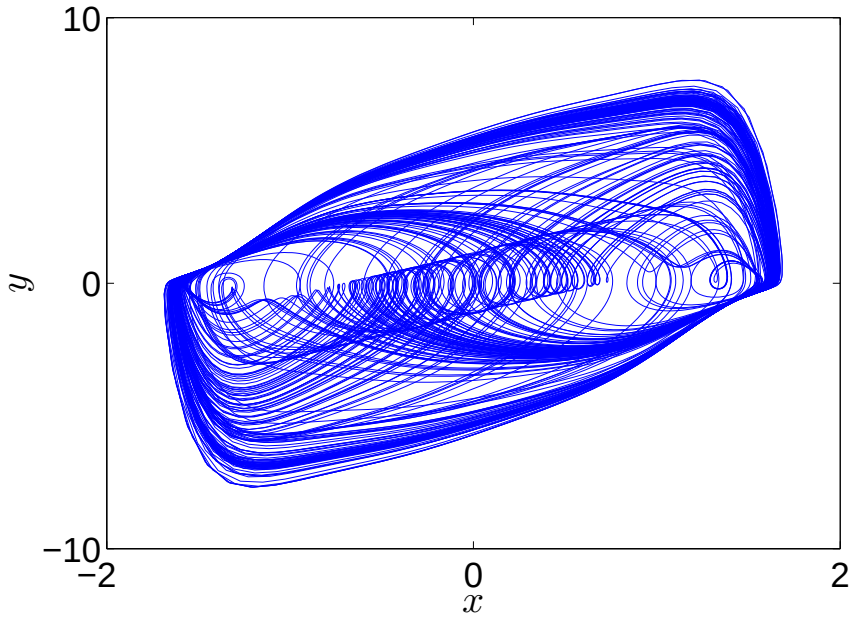

Figure 3.29: Chaotic attractor of the fractional forced system (2) for $a = 2.55, b = 1.70$, $m = 2.001$ and periodic forcing $e = 8.27$,$\omega = 3.465$ with $[q_1, q_2] = [0.95, 0.97]$.

3.3.3 Dynamics of FIONBS

In this section, different dynamical properties of FIONBS are derived for $q_1 \neq q_2$ such as bifurcation diagrams, largest Lyapunov exponents (LLE) and phase portraits on 2D-space and 3D-space. The step-size is taken $h = 2^{-6}$ for the numerical simulations.

Dynamics versus fractional-order derivatives:

Let $a = 2.55, b = 1.70, m = 2.001$, we take the amplitude $e = 8.27$, the frequency $\omega = 3.465$ and initial values $(x_0, y_0) = (0, 1)$, we study the stability of the FIONBS by varying the incommensurate orders q_1 and q_2. The bifurcation diagrams as function of $q_1 \in (0.88, 0.98), q_2 = 1$ and $q_1 = 0.95, q_2 \in (0.70, 1)$ are plotted in Figs. 3.30(a) and 3.30(c). When the order q_1 varing, the system (2) appears chaos in the range: $q_1 \in [0.902, 0.919] \cup [0.923, 0.927] \cup [0.933, 0.938] \cup [0.948, 0.957]$ and it appears a different periodic and quasiperiodic states in the other ranges (See Fig. 3.30(a)). When the order q_2 increase from 0.7 to 0.81, the fractional system (2) moves from a periodic to a quasiperiodic state. when $q_2 = 0.82$ the system exhibits a chaos. After this value, there is a transition between different dynamical states whereas the range when the system exhibits chaotic behavior is $q_2 \in [0.82, 0.832] \cup [0.965, 1]$ (see Fig. 3.30(c)). The largest Lyapunov exponents (LLE) are calculated and plotted in Figs. 3.30(b) and 3.30(d) whereas a positive value of the LLE indicates chaotic behavior in the system. The different dynamic states of the FIONBS (2) are presented in Figs. 3.31 and 3.32 on 2D projection for $q_1 \in (0.88, 0.98), q_2 = 1$ and for $q_1 = 0.95, q_2 \in (0.70, 0.97)$, respectively. In paricular, when varing q_1 the system (2) appears a limit cycle for $q_1 = 0.90$, a chaotic attractor for $q_1 = 0.91$, a complex chaotic attractor for $q_1 = 0.95$ and a periodic orbit for $q_1 = 0.97$ (see Fig. 3.31). When varing q_2 the system (2) appears a limit cycle for $q_2 = 0.70$, a quasiperiodic orbits for $q_2 = 0.75$, a chaotic attractor for $q_2 = 0.82$, and a complex chaotic attractor for $q_2 = 0.97$ (See Fig. 3.32). The fractional-order system (2) can be presented also onto 3D-space spanned by x, y and t. Figs. 3.33 show the 3D chaotic trajectories of the system with $[q_1, q_2] = [0.949, 1]$ (Fig. 3.33(a)) and $[q_1, q_2] = [0.95, 0.97]$

(Fig. 3.33(b)).

Dynamics versus system parameters:

In this part, the dynamics of the FIONBS are studied by fixing the incommensurate order $[q_1, q_2] = [0.95, 0.97]$ and taking initial values $(x_0, y_0) = (0, 1)$.
Firstly, we study the stability of the system by varying the frequency ω. Let $a = 2.55, b = 1.70, m = 2.001, e = 8.27$, the bifurcation diagram and LLE are plotted in Figs. 3.34. It can be seen from the Fig. 3.34(a) that the system (2) has a periodic route to a chaos when $\omega = 2.8$. The chaos still exists over almost in the range: $\omega \in [2.8, 3.68]$. The existence of positive LLE in this range confirms the chaotic behavior here (see Fig. 3.34(b)). When the frequency ω increase beyond this range, the system shows a quasiperiodic route to a periodic state with period-6 then a periodic state with period-2 when $\omega = 4.65$. The trajectories of the fractional system (2) are plotted in Figs. 3.35. Fig. 3.35(a) shows that the system (2) has a limit cycle when $\omega = 2.5$, Fig. 3.35(b) shows a chaotic attractor when $\omega = 3.465$. As a remark, when $\omega = 8$ and $\omega = 20$ the phase portrait shows that the system has a conservative state which still exist over the increase of the frequency ω (see Fig. 3.35(c)-(d)).
Now, we study the stability of FIONBS by varying system parameters m, a, b and e. Several dynamical states of the system (2) are presented in Figs. 3.36. The bifuraction diagrams show the ranges in which the system exhibits a periodic orbits with period-2 or period-4 or period-6 and quasiperiodic orbits. Figs. 3.36 show also the ranges when the system exhibits a chaotic behaviors which are confirmed by the existence of positive LLEs.

3.3.4 Symmetry, Multistability and Coexisting attractors

In this part, the emergence of special phenomena is studied in FIONBS including symmetry, coexisting attractors and multistability.

Coexisting symmetric strange attractors

We start with studying the first special phenomenon: coexisting of symmetric strange attractors. A symmetric dynamical systems are obtained when they often exhibit a symmetric pair of coexisting attractors. This property has attracted considerable interest [135] while Systems with a symmetry are especially vulnerable to multistability since any asymmetric attractor is guaranteed to have a twin attractor symmetric with it. However, multistability may have benefits such as allowing one to simulate and study phenomena in the real world where it also occurs [136].
In order to show the existence of this property in the system, the basin of attraction of autonumous unforced system (2) is plotted in Fig. 3.37 for two different set of initial conditions: the first is $(x_0, y_0) = (-0.1, 1)$ for blue region and the second value is $(x_0, y_0) = (-0.1, -1)$ for red region. It can be seen from the figure two bounded regions in red and blue color. These two regions are bounded and symmetric whereas the initial conditions in yellow color (from unbounded region) lead to this two symmetric regions.
Now, we consider system parameters $a = 2.55, b = 1.70, m = 2.001, e = 8.27, \omega = 3.465$ and incommensurate order $[q_1, q_2] = [0.939, 0.97]$. For two set of initial conditions $(x_0, y_0) = (-0.1, 1)$ for blue trajectory and $(x_0, y_0) = (-0.1, -1)$ for red trajectory, the forced system (2) generates a symmetric pair of coexisting chaotic attractors which are presented in Figs. 3.38. The upward attractor in blue line for $(x_0, y_0) = (-0.1, 1)$ can evolves toward the downward attractor in red line for $(x_0, y_0) = (-0.1, -1)$. We have found also this phenomenon with another set of initial conditions that is $(x_0, y_0) = (0.1, 1)$ and $(x_0, y_0) = (-0.1, -1)$ or $(x_0, y_0) = (-0.1, -1)$ and $(x_0, y_0) = (0.1, -1)$. As a remark, we have found here a new and particular chaotic trajectories (see Fig. 3.38(b)) which are different from the previous attractors.

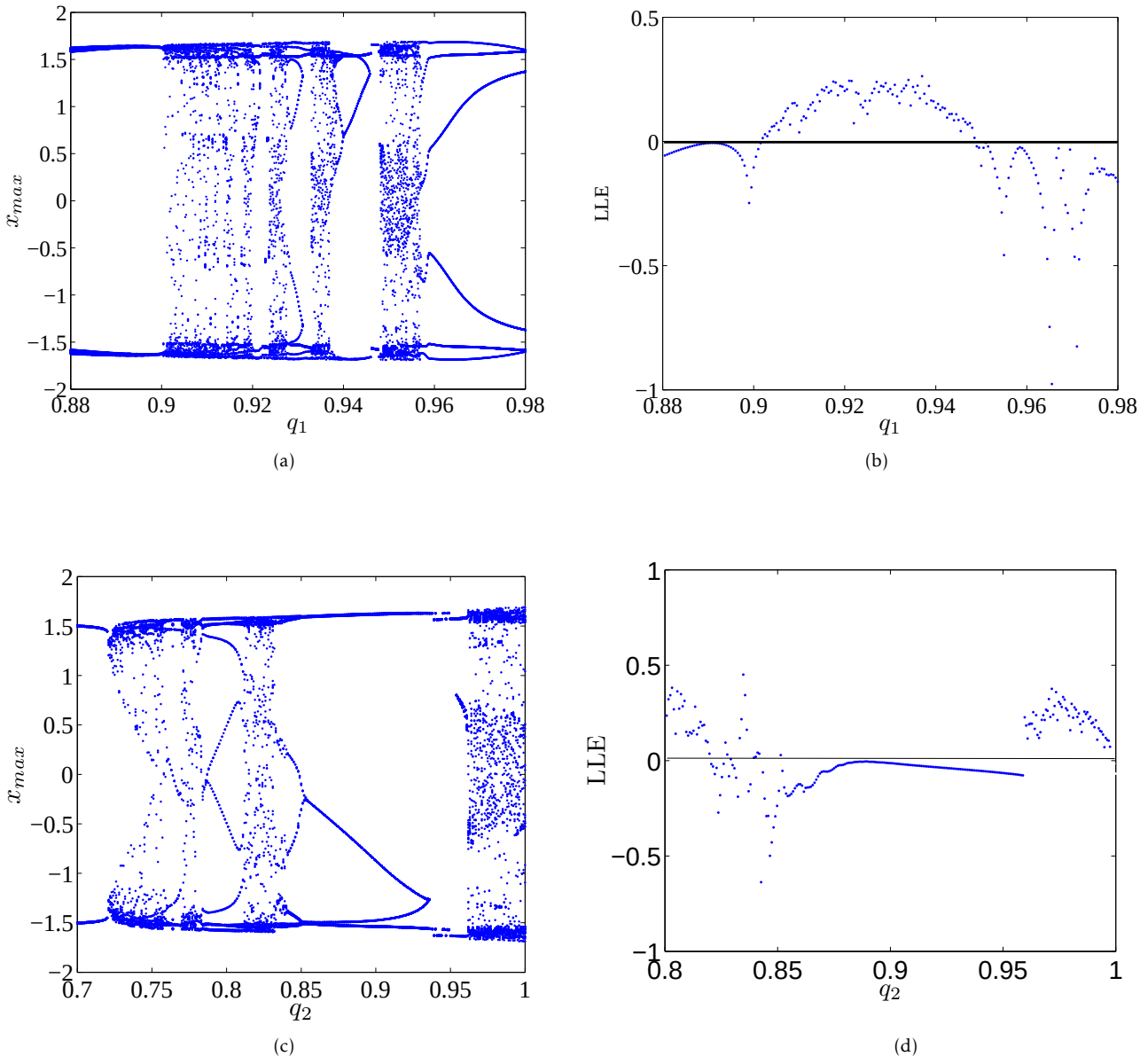

Figure 3.30: Bifurcation diagrams of fractional system (2) and their corresponding largest Lyapunov exponents (LLE) for $a = 2.55, b = 1.70, m = 2.001, e = 8.27, \omega = 3.465$, initial conditions$(x_0, y_0) = (0, 1)$ and for: (a)-(b) $q_1 \in (0.88, 0.98), q_2 = 1$; (c)-(d)$q_1 = 0.95, q_2 \in (0.70, 1)$.

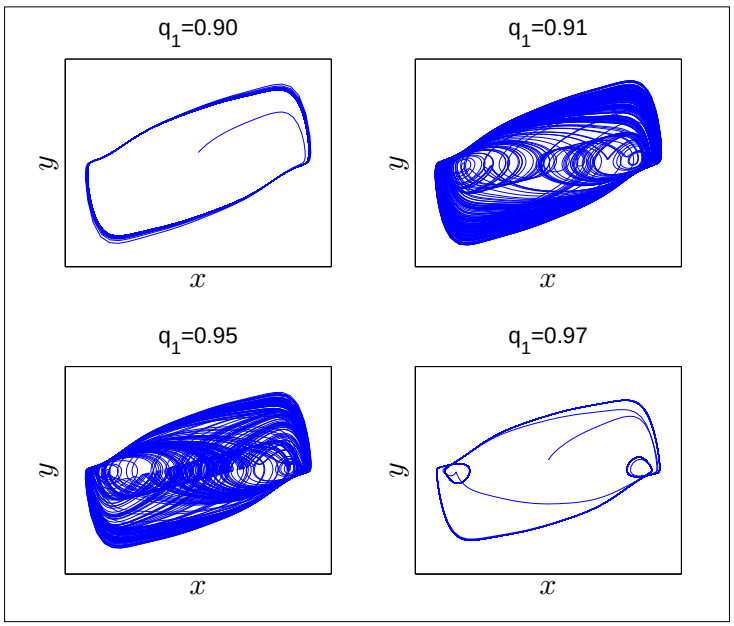

Figure 3.31: Phase portraits on 2D-space of system (2) for varing q_1 and fixing $q_2 = 1$ when system parametres $a = 2.55, b = 1.70, m = 2.001, e = 8.27, \omega = 3.465$ for initial values $(x_0, y_0) = (0, 1)$.

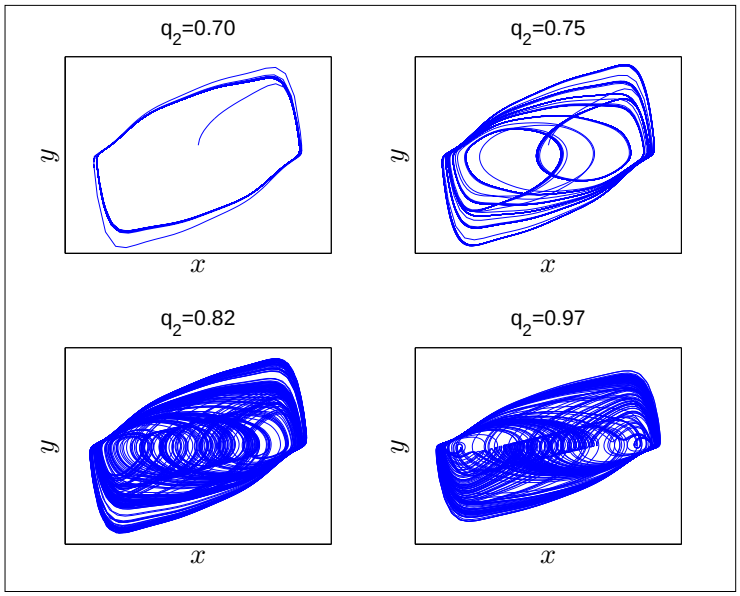

Figure 3.32: Phase portraits on 2D-space of system (2) for varing q_2 and fixing $q_1 = 0.95$ when system parametres $a = 2.55, b = 1.70, m = 2.001, e = 8.27, \omega = 3.465$ for initial values $(x_0, y_0) = (0, 1)$.

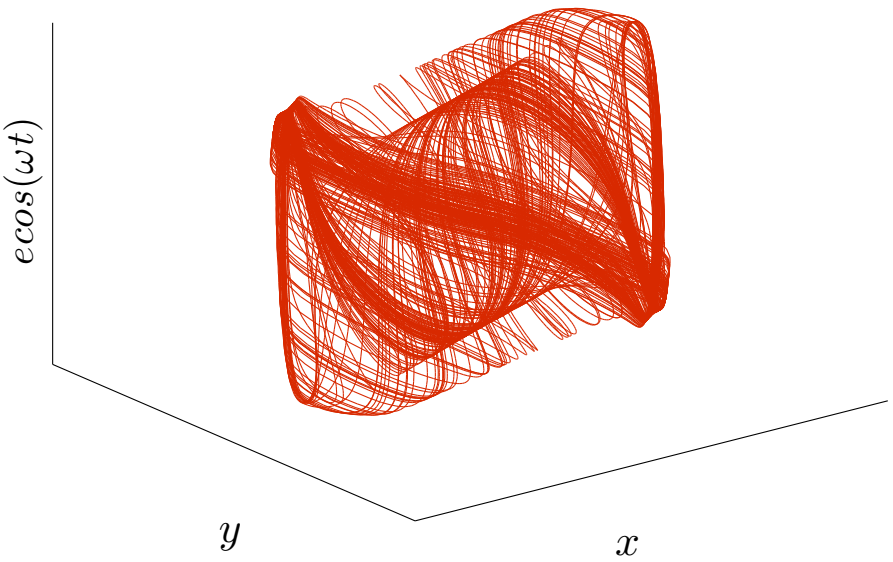

(a)

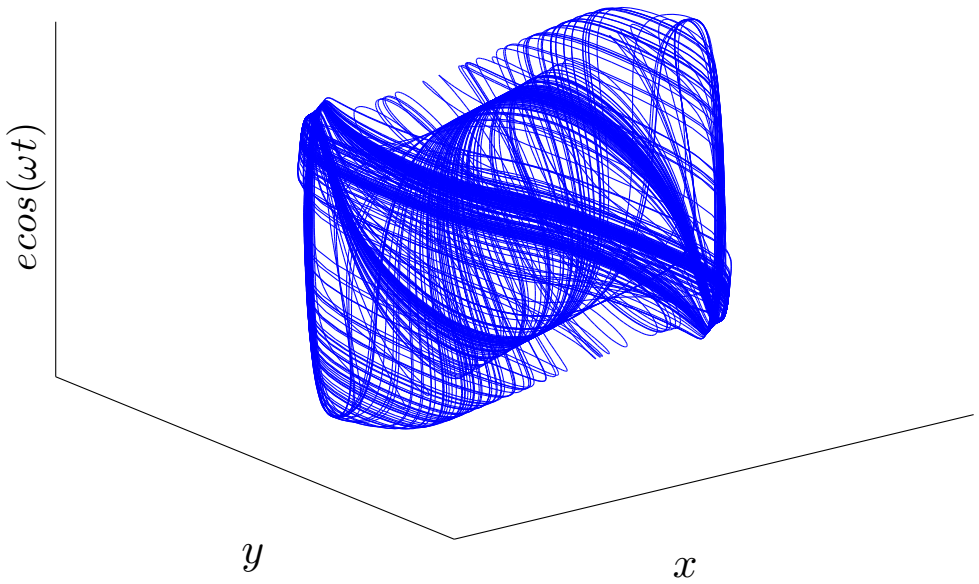

(b)

Figure 3.33: Chaotic attractor of system (2) on 3D-space for (a) $[q_1, q_2] = [0.949, 1]$, (b) $[q_1, q_2] = [0.95, 0.97]$.

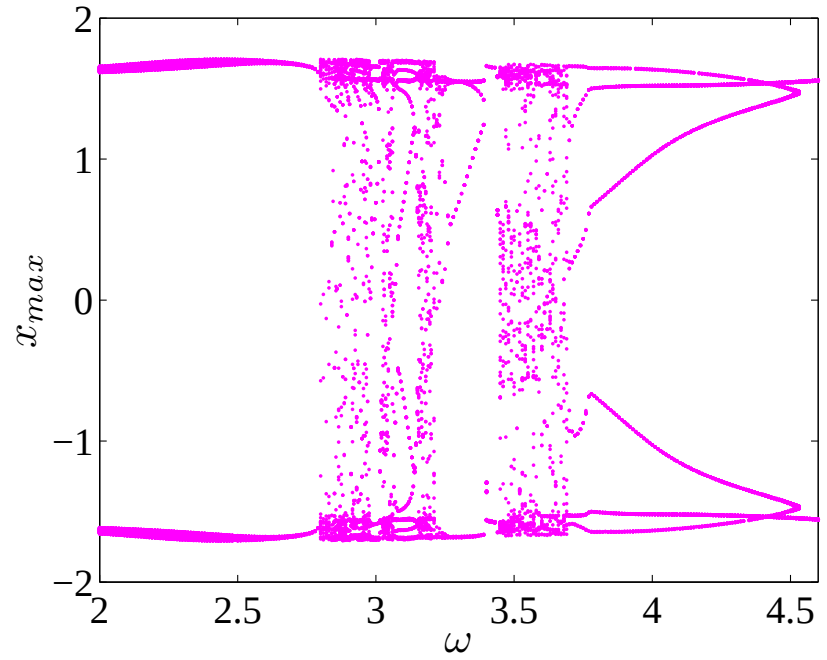

(a)

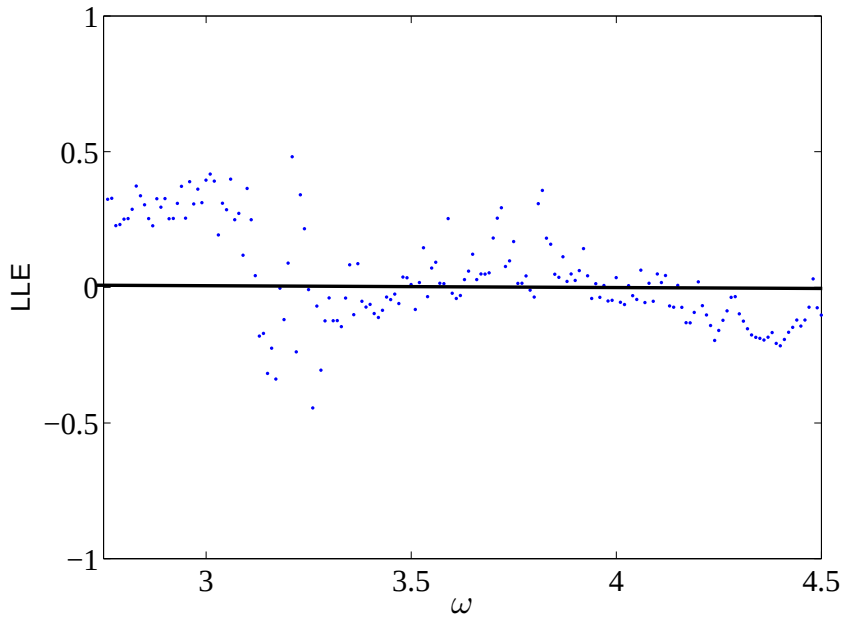

(b)

Figure 3.34: (a) Bifurcation diagram , (b) LLE of system (2) when $[q_1, q_2] = [0.95, 0.97]$, $a = 2.55, b = 1.70, m = 2.001, e = 8.27$ for initial values $(x_{0,} y_0) = (0, 1)$.

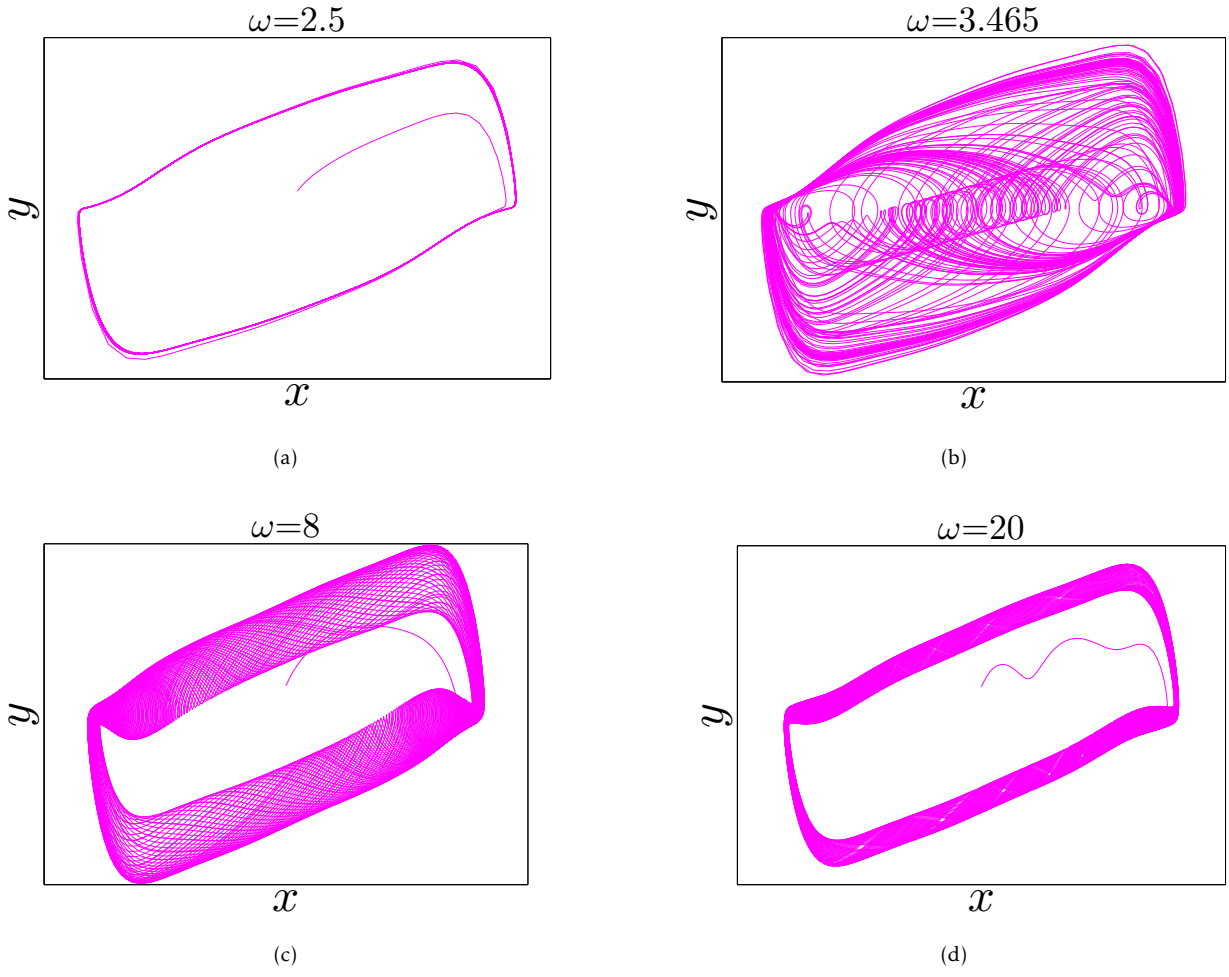

Figure 3.35: Phase portraits of system (2) with varing frequency ω when $[q_1, q_2] = [0.95, 0.97]$ and $a = 2.55, b = 1.70, m = 2.001, e = 8.27$ for initial values $(x_0, y_0) = (0, 1)$.

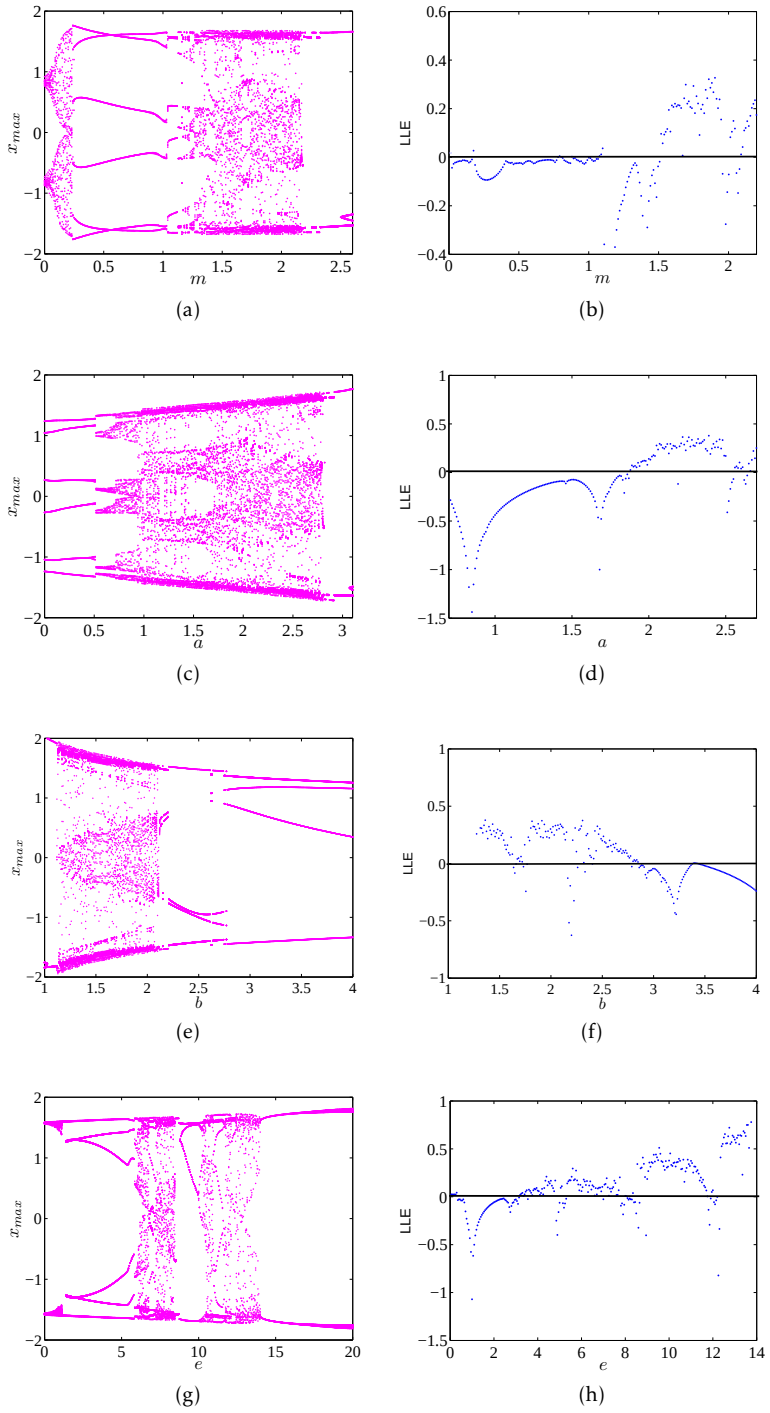

Figure 3.36: Bifurcation diagrams and LLEs of system (2) with varing system parameters m, a, b and e when $[q_1, q_2] = [0.95, 0.97]$ for initial values $(x_0, y_0) = (0, 1)$.

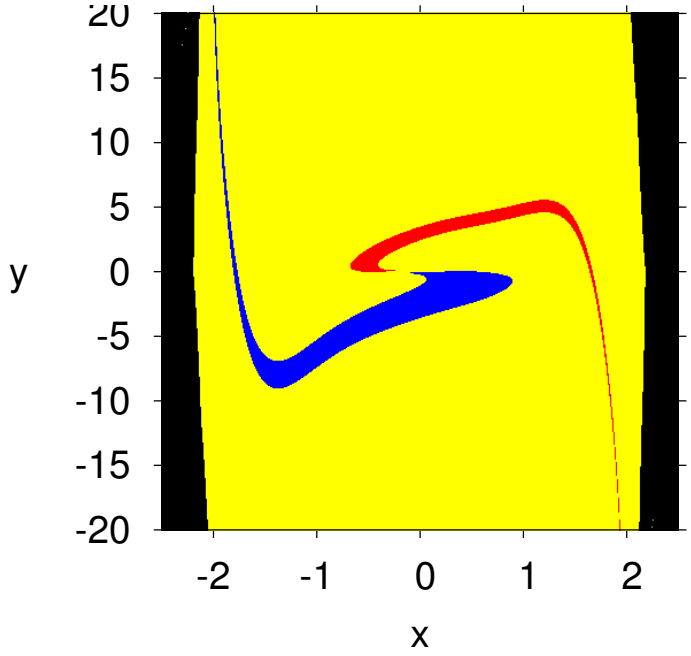

Figure 3.37: Basin of attraction of unforced system (2) with two set of initial conditions.

Multistability with coexisting attractors

Multistability is another special phenomenon which is of great interest for researchers. In order to show the multistability in the FIONBS, we plot the bifurcation diagrams for $q_1 \in (0.88, 0.98), q_2 = 1$ (Fig. 3.39(a)), and for $q_1 = 1, q_2 \in (0.92, 1)$ (Fig. 3.39(b)). Two sets of initial conditions have been considered: $(x_0, y_0) = (0, 1)$ for blue plot and $(x_0, y_0) = (1, 2)$ for red plot. The two plots show that the system exhibits bistability if the incommensurate orders q_1 and q_2 are increased. For $[q_1, q_2] = [0.95, 0.97]$, the two coexisting attractors of system (2) are plotted in Fig. 3.40(a) with $(x_0, y_0) = (0, 1)$ for blue plot and $(x_0, y_0) = (1, 2)$ for red plot. Also, the system can exhibits multiple coexisting attractors which are presented in Fig. 3.40(b) for three initial conditions: $(x_0, y_0) = (0, 1); (1, 2); (0.5, 1)$. All the reported results highlight that the proposed fractional Van der Pol forced oscillator with incommensurate order is able to exhibit not only the expected chaotic dynamics and oscillations, but also striking phenomena such as symmetry, multi-stability and coexistence of attractors. Such results, which are a direct consequence of the long term memory introduced by fractional incommensurate order derivative, confirm the rich dynamics of the proposed biological system.

3.3.5 Conclusions

Recent rigorous studies have confirmed that the differential equations with fractional orders are naturally related to systems having power-law type memory and hereditary effects which occurs in most biological systems. In this work, the fractional Van der Pol forced oscillator with incommensurate order has been considered for modelling a biological system. The stability of the proposed incommensurate system has been analyzed in detail by varying both the fractional order and system parameters. Based on the well-known Caputo fractional derivative, several numerical simulations have been reported by means of bifurcation diagrams, computation of the largest Lyapunov exponent, phase portraits in 2D and 3D projections. The analysis has highlighted that the fractional incommensurate order forced system is able to exhibit not only chaotic dynamics and oscillations, but also striking phenomena such as symmetry, multi-stability and coexistence of attractors. Moreover, as a direct consequence

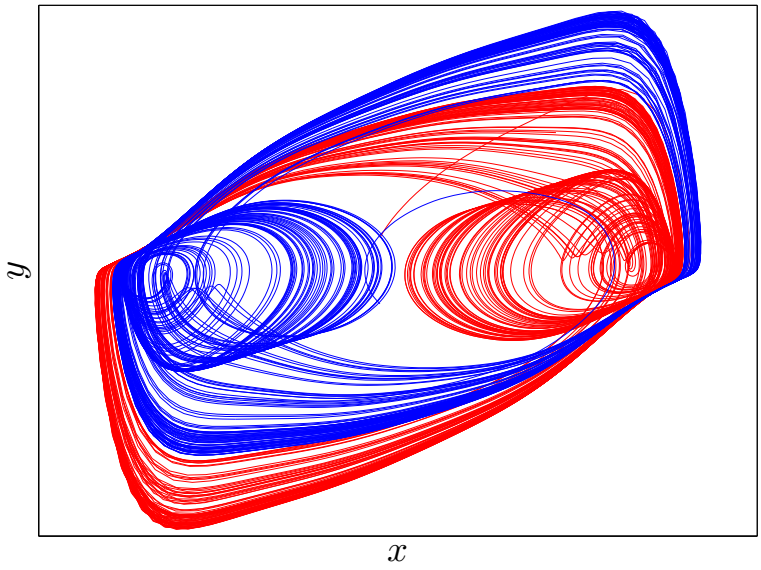

(a)

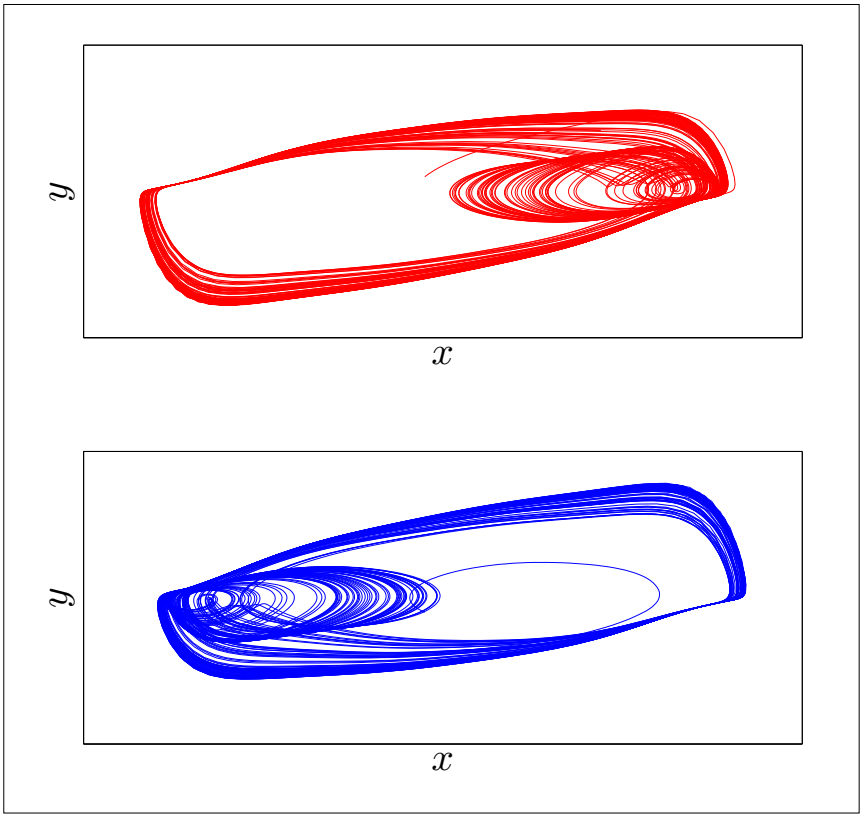

(b)

Figure 3.38: (a) Symmetric strange attractors of system (2) with incommensurate order $[q_1, q_2] = [0.939, 0.97]$, and two set of initial conditions $(x_0, y_0) = (-0.1, 1)$ for blue plot and $(x_0, y_0) = (-0.1, -1)$ for red plot. (b) The upward attractor in blue plot and the downward attractor in red plot.

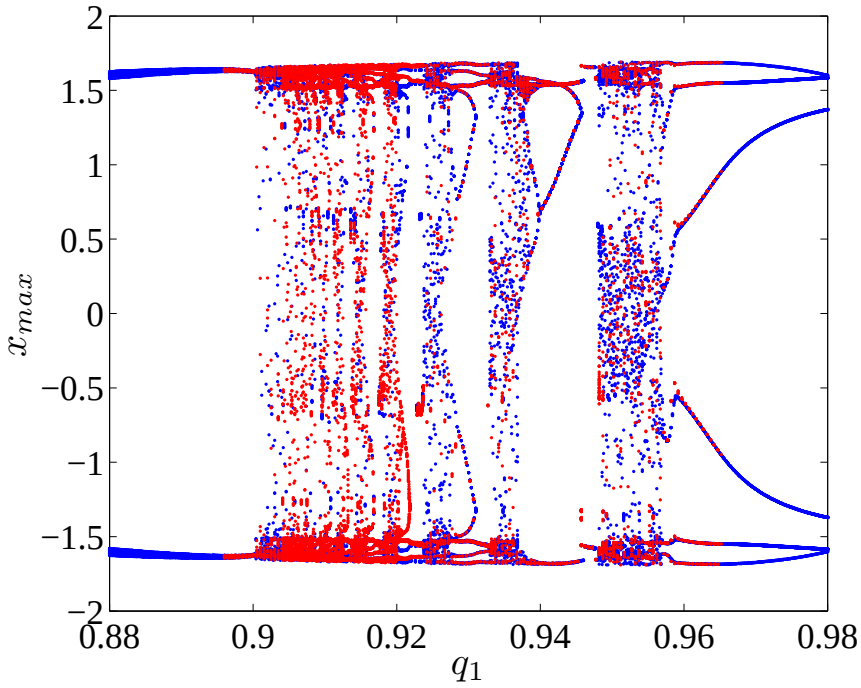

(a)

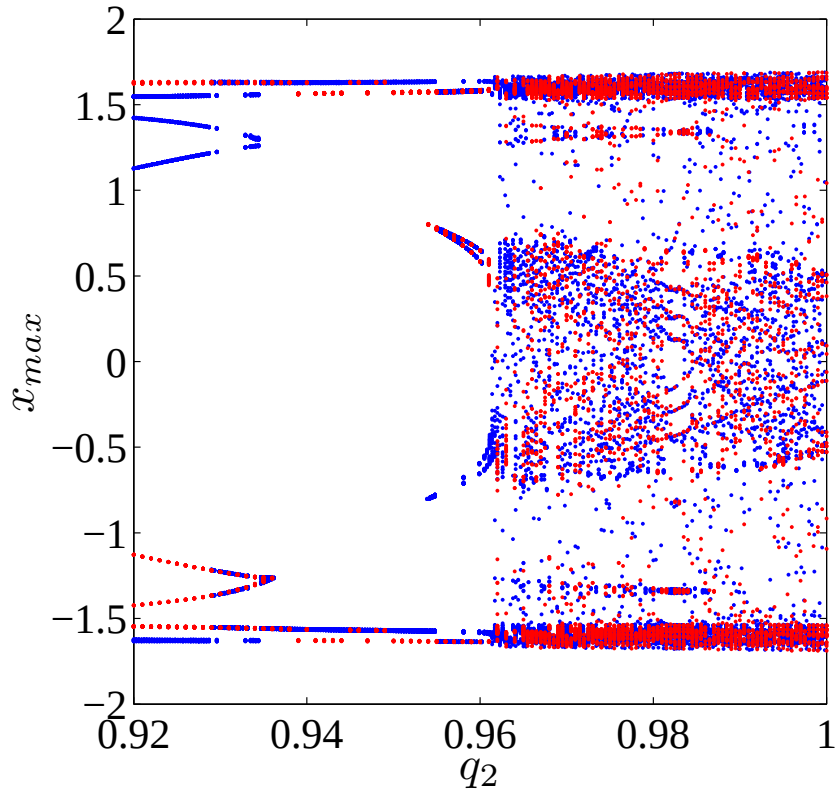

(b)

Figure 3.39: Bifurcation diagram system (2) for (a) $q_1 \in (0.88, 0.98), q_2 = 1$, (b) $q_1 = 1, q_2 \in (0.92, 1)$ with two set of initial conditions: $(x_0, y_0) = (0, 1)$ for blue plot and $(x_0, y_0) = (1, 2)$ for red plot.

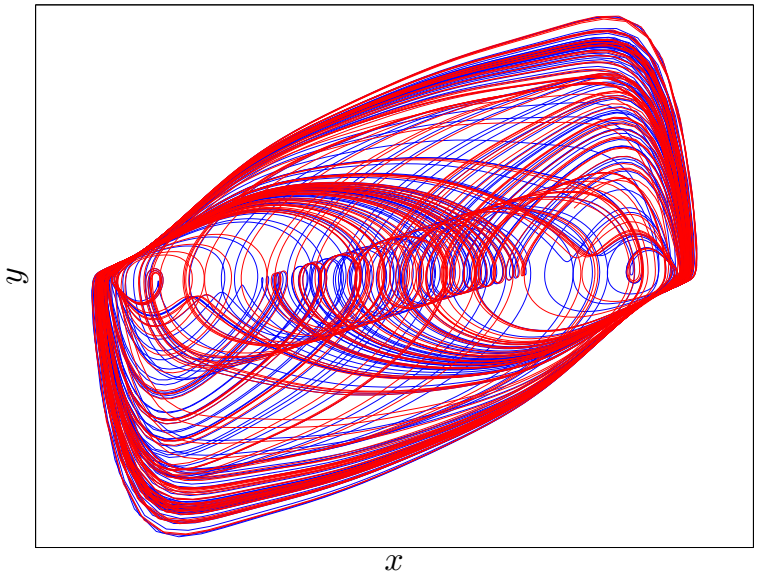

(a)

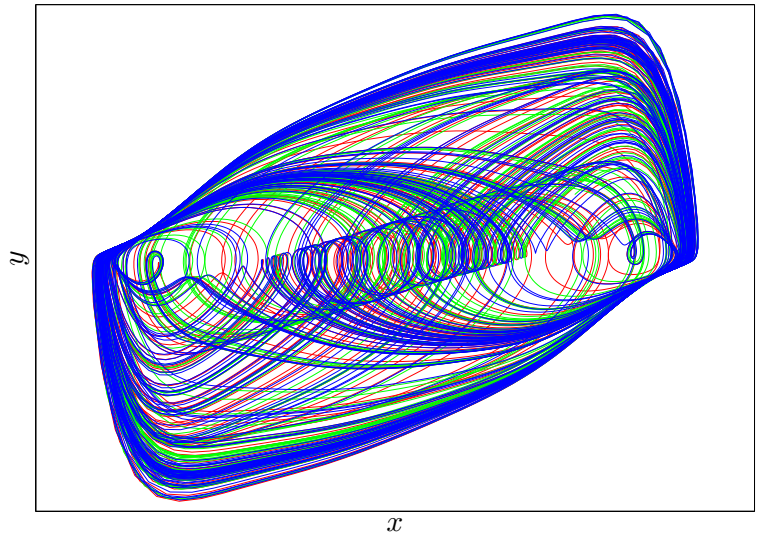

(b)

Figure 3.40: (a) Coexisting two attractors for $[q_1, q_2] = [0.95, 0.97]$ with initial values $(x_0, y_0) = (0, 1)$ for blue plot and $(x_0, y_0) = (1, 2)$ for red plot. (b) Coexisting multiple attractors for $[q_1, q_2] = [0.95, 0.97]$ with initial values $(x_0, y_0) = (0, 1)$ for blue plot, $(x_0, y_0) = (1, 2)$ for red plot and $(x_0, y_0) = (0.5, 1)$ for green plot.

of the long range memory of fractional order biological systems, the investigation has shown that the limit set of trajectories in the phase space of the fractional Van der Pol forced oscillator with incommensurate order is not unique and strongly relates with the initial conditions. This result, which might have interesting implications in the study of biological phenomena, turns out to be inaccordance with a similar result obtained by Tavazoei in the case of the fractional Van der Pol system with commensurate order.

3.4 Chaos in cancer tumour growth model with commensurate and incommensurate fractional-order derivatives

The content of this section has been published in [14, 15].

3.4.1 Introduction

In the last fifty years, great research efforts and economic resources have been directed to win the fight against cancer. In order to tackle the problem, one of the key issue is to active and control the immune system in its competition against neoplastic cells. To this purpose, the study of tumor-immune dynamics can play a role of paramount importance, given that the mathematical modelling of cancer growth is considered as one of the useful tools for the development of effectivemedical treatments. Over the years, the study of the tumor-immune dynamics has led to the discovery of remarkable phenomena, including the presence of chaos in the system dynamics. By considering integer-order dynamical systems (i.e., biological systems described by integer-order differential equations), in [137] a simple chaotic model of three competing cell populations (host, immune and tumor cells) is introduced. Topological analysis and computing observability coefficients are illustrated, with the aim to suggest new trends in understanding the interactions of some tumor cells [137].The authors of reference [138] have suggested a suitable model for the tumor growth, i.e., a discrete-time system capable of exhibiting periodic and chaotic behaviors. The model, which is validated through experimental data, can explain a number of biologically observed tumor states and dynamics [138]. Another interesting model of tumor growth is proposed in [139], based on the interactions among tumor cells, healthy tissue cells and activated immune system cells. The study, besides analyzing the stability of the system equilibria, highlights the presence of chaotic behaviors in the system dynamics [139]. Referring to biological systems, it should be noted that the behavior of most of these systems has memory or after-effects. Moreover, biological systems are usually characterized by hereditary properties and non-local distributed behaviors. As a consequence, the modeling of these systems by fractional-order differential equations has more advantages than integer-order modeling, in which such effects are neglected. This explains why fractional calculus has recently emerged as a valuable tool for describing a number of dynamic phenomena in biological systems.
Based on these considerations, this paper aims to make a contribution to the study of tumor-immune dynamics by presenting a new model of cancer growth based on fractional-order differential equations. By investigating the system dynamics, the manuscript highlights the chaotic behaviours of the proposed cancer model for both the commensurate and the incommensurate case. Moreover, some considerations regarding the biological meaning of the obtained results are reported.

3.4.2 Fractional-order cancer model and its equilibrium points

A three-dimensional integer-order cancer growth model has been studied in [139]. Its dynamic equations are described by:

$$\begin{cases} \dot{x} = ax(1-y)(1+z) - x^2 y, \\ \dot{y} = by(1-z)(1+x) - y^2 z, \\ \dot{z} = cz(1-x)(1+y) - z^2 x, \end{cases} \tag{3.4.1}$$

where $x(t)$ denotes the number of tumour cells at time t, $y(t)$ is the number of healthy host cells at time t, and $z(t)$ refers to the number of effector immune cells at time t in the single tumor-site compartment. Here, the parameters a, b and c are positive real numbers representing the growth rates of populations of $x(t), y(t)$ and $z(t)$. Specifically,

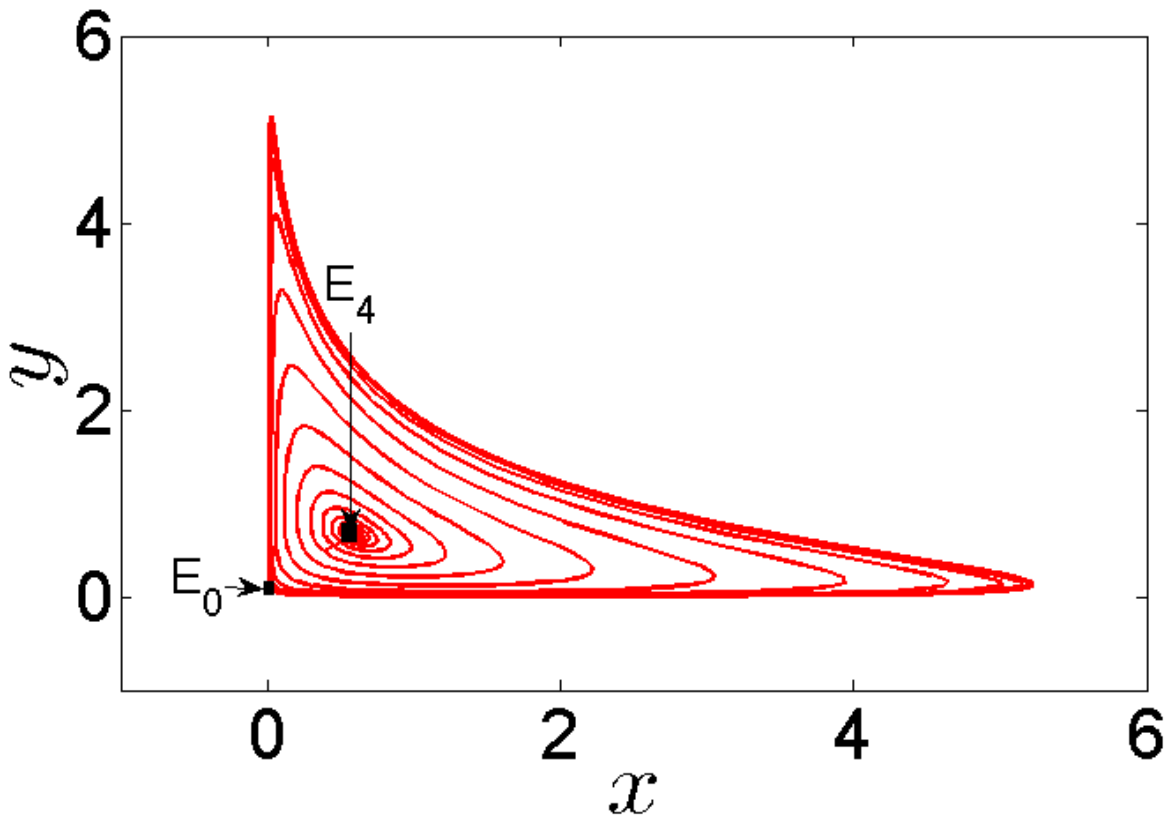

Figure 3.41: Chaotic attractor of system(3.4.1) for system parameters $a = 0.7455, b = 0.7367, c = 0.5619$ and initial conditions $(x_0, y_0, z_0) = (0.4, 0.5, 0.5)$.

the parameter a represents the growth rate of the tumour cells (measured in sec-1), the parameter b is the growth rate of the healthy host cells (measured in sec-1) whereas c represents the growth rate of the effector immune cells (measured in sec-1). Generally, the model parameters are chosen such that, the system dynamic analogies with clinical evidences reported in literatures [137, 140]. Where depending on control parameter values and initial conditions, the considered biological cancerous system should also approach different states [141]: stationary equilibrium state where any changes are damped, stable periodic process (a limit cycle) and state of instability with chaotic behavior. As shown in [6], particular values of these growth rates lead to make the behaviour of system (1)chaotic. To this purpose, the chaotic attractor of system (3.4.1) for parameters $a = 0.7455, b = 0.7367, c = 0.5619$ and initial conditions $(x_0, y_0, z_0) = (0.4, 0.5, 0.5)$ is shown in Fig. 3.41.

Herein, the fractional version of system (3.4.1) is considered. Namely, the dynamics of the proposed fractional-order cancer model (FOCM) are described by:

$$\begin{cases} D_t^{q_1} x = ax(1-y)(1+z) - x^2 y, \\ D_t^{q_2} y = by(1-z)(1+x) - y^2 z, \\ D_t^{q_3} z = cz(1-x)(1+y) - z^2 x, \end{cases} \tag{3.4.2}$$

Where D^q is q-order Caputo differential operator, $0 < q_i \leq 1$ $(i = 1, 2, 3)$ are the derivative orders of the state variables x, y and z. The fractional-order system (3.4.2) is called as commensurate if $q_1 = q_2 = q_3$ and incommensurate otherwise.

Using the definitions in section 1.4.1, Chapter1, then the numerical solution of the FOCM can be given as in (3.4.3) with parameters defined in (3.4.4) and (3.4.5) (where, $l = 1, 2, 3$ and $i = 1, 2, 3$)

$$
\begin{cases}
x_{n+1} = x_0 + \dfrac{h^{q_1}}{\Gamma(q_x+2)}[ax^p_{1+n}(1-y^p_{1+n})(1+z^p_{1+n}) - (x^p_{1+n})^2 y^p_{1+n}] \\
\qquad + \dfrac{h^{q_1}}{\Gamma(q_x+2)}\sum_{j=0}^{n}[\eta_{1,j,n+1}(ax_j(1-y_j)(1+z_j) - x_j^2 y_j)], \\
y_{n+1} = y_0 + \dfrac{h^{q_2}}{\Gamma(q_y+2)}[by^p_{1+n}(1-z^p_{1+n})(1+x^p_{1+n}) - (y^p_{1+n})^2 z^p_{1+n}] \\
\qquad + \dfrac{h^{q_2}}{\Gamma(q_y+2)}\sum_{j=0}^{n}[\eta_{2,j,n+1}(by_j(1-z_j)(1+x_j) - y_j^2 z_j)], \\
z_{n+1} = z_0 + \dfrac{h^{q_3}}{\Gamma(q_z+2)}[cz^p_{1+n}(1-x^p_{1+n})(1+y^p_{1+n}) - (z^p_{1+n})^2 x^p_{1+n}] \\
\qquad + \dfrac{h^{q_3}}{\Gamma(q_z+2)}\sum_{j=0}^{n}[\eta_{3,j,n+1}(cz_j(1-x_j)(1+y_j) - z_j^2 x_j)],
\end{cases}
\tag{3.4.3}
$$

$$
\begin{cases}
x^p_{n+1} = x_0 + \dfrac{1}{\Gamma(q_1+2)}\displaystyle\sum_{j=0}^{n}\omega_{1,j,n+1}(ax_j(1-y_j)(1+z_j) - x_j^2 y_j), \\
y^p_{n+1} = y_0 + \dfrac{1}{\Gamma(q_2+2)}\displaystyle\sum_{j=0}^{n}\omega_{2,j,n+1}(by_j(1-z_j)(1+x_j) - y_j^2 z_j), \\
z^p_{n+1} = z_0 + \dfrac{1}{\sum_{j=0}^{n}}\omega_{3,j,n+1}\Gamma(q_3+2)(cz_j(1-x_j)(1+y_j) - z_j^2 x_j),
\end{cases}
\tag{3.4.4}
$$

$$
\begin{cases}
\eta_{l,j,n+1} = \begin{cases} n^{q_i+1} - (n-q_i)(n+1)^{q_i+1}, & j = 0, \\ (n-j+2)^{q_i+1} + (n-j)^{q_i+1} - 2(n-j+1)^{q_i+1}, & 1 \le j \le n, \\ 1, & j = n+1, \end{cases} \\
\omega_{l,j,n+1} = \dfrac{h^{q_i}}{q_i}((n-j+1)^{q_i} - (n-j)^{q_i}), \qquad 0 \le l \le n.
\end{cases}
\tag{3.4.5}
$$

Note that the system (**??**) has five equilibrium points [139], four of them are obtaind analytically and can be described as follows:

- $E_0 = (0, 0, 0)$,
- $E_1 = (0, -1, \dfrac{b}{b-1})$, if $b \neq 1$
- $E_2 = (\dfrac{c}{c-1}, 0, -1)$, if $c \neq 1$
- $E_3 = (-1, \dfrac{a}{a-1}, 0)$, if $a \neq 0$

The last equilibrium E_4 corresponding to the case $(x, y, z) \neq (0, 0, 0)$,does not possess an analytical expression. It could be obtained by intersecting the three surfaces corresponding to the following equations:

$$
\begin{cases}
ax(1-y)(1+z) - x^2 y = 0, \\
by(1-z)(1+x) - y^2 z = 0, \\
cz(1-x)(1+y) - z^2 x = 0.
\end{cases}
\tag{3.4.6}
$$

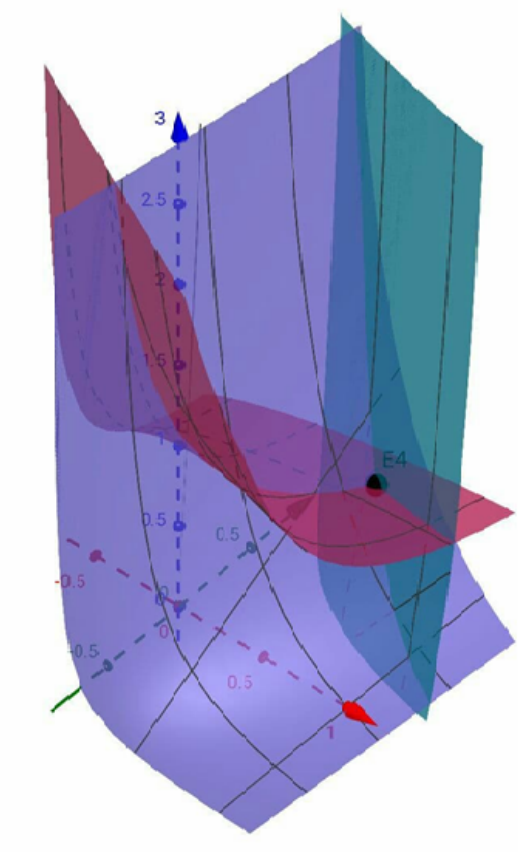

Figure 3.42: Equilibrium point E_4 obtained by intersecting the three surfaces corresponding to the Eqs. 3.4.6.

By taking the system parameters $a = 0.7455, b = 0.7367$ and $c = 0.5619$, the fixed points become $E_0 = (0,0,0)$, $E_1 = (0,-1,-2.7979)$, $E_2 = (-1.28,0,-1)$, $E_3 = (-1,-2.9293,0)$, and The fourth equilibrium point found as $E_4 = (0.5961, 0.6718, 0.6364)$. As shown in Fig. 3.42.
Note that the fixed points E_1, E_2 and E_3 have negative coordinates, indicating that the dynamics cannot take place since it is not possible to define negative populations in system (3.4.2). The fixed point E_0, which corresponds to a situation where there is no cell at all, is unstable, since its eigenvalues are given by $(0.5619, 0.7367, 0.7455)$. The fixed point E_4, which is associated with the coexistence of the three different type of cells, represents a saddle-focus equilibrium, since its eigenvalues are given by $(0.0712 \pm 1.0922i, -1.3498)$.

3.4.3 Dynamics of the commensurate fractional-order cancer model

In this Section, the dynamics of the proposed commensurate fractional-order cancer model (3.4.2) are studied by varying the fractional order q and the system parameters a, b and c. Bifurcation diagrams, Lyapuov exponents, time-behaviors and phase plots are illustrated to investigate the system dynamics in detail. Moreover, some considerations regarding the biological meaning of the obtained results are reported.

Analysis of the system dynamics by varying the fractional-order q

The study of the stability of the equilibria is important to understand the system dynamics in the proposed cancer model. Herein, analytical and numerical analyses are conducted to determine the behavior of the system trajectories when the value of the fractional order is properly varied. To this purpose, a theorem proved in reference [**?**] is now exploited.

Theorem 3.4.1. *Given the fractional system (3.4.2), a necessary condition to have a chaotic attractor around the equilibrium point E_4 is that the eigenvalues λ_i of its Jacobian matrix satisfy the condition [133]:*

$$arg(\lambda_i) > q\pi/2, \qquad 0 < q < 1,$$

By taking the fractional system (3.4.2) with parameters $a = 0.7455, b = 0.7367$ and $c = 0.5619$, the eigenvalues $\lambda_i, i = 1,2,3$ of the Jacobian matrix are evaluated at the equilibrium point E_4 are given by $(0.0712 \pm 1.0922i, -1.3498)$. By considering that the application of Theorem 3.4.1 to the equilibrium E_4 gives:

$$arg(0.0712 \pm 1.0922i) * 2/pi \approx 0.9576,$$

it follows that a necessary condition to have a chaotic attractor in the fractional system (3.4.2) is to satisfy the condition $q > 0.96$.
In order to investigate the system dynamics and numerically search for proper values of the fractional order q able to generate chaotic behaviors, the bifurcation diagram is plotted in Fig. 3.43 for $q \in (0.94, 1)$ and initial conditions $(x_0, y_0, z_0) = (0.4, 0.5, 0.5)$.
From the bifurcation diagram it can be seen that the system (3.4.2) is asymptotically stable when $q < 0.96$, whereas a number of periodic windows appear for $q \in (0.96, 0.99)$. Moreover the FOCM (3.4.2) exhibits choatic behavior for $q \in (0.99, 1)$ as confirmed by the positive values of the maximum Lyapunov exponents (see Fig. 3.44). From the biological point of view, this behaviour can be explained as follows. When $q < 1$, the system become fractional and, consequently, memory effects and hereditary properties appear in the modelling of the system dynamics. When these effects are not so strong (i.e., $0.99 < q < 1$), the system dynamics undertake chaotic behaviours. On the other hands, when these effects become stronger (i.e., $q < 0.96$), they overwhelm the system dynamics, which undertake stable behaviours.

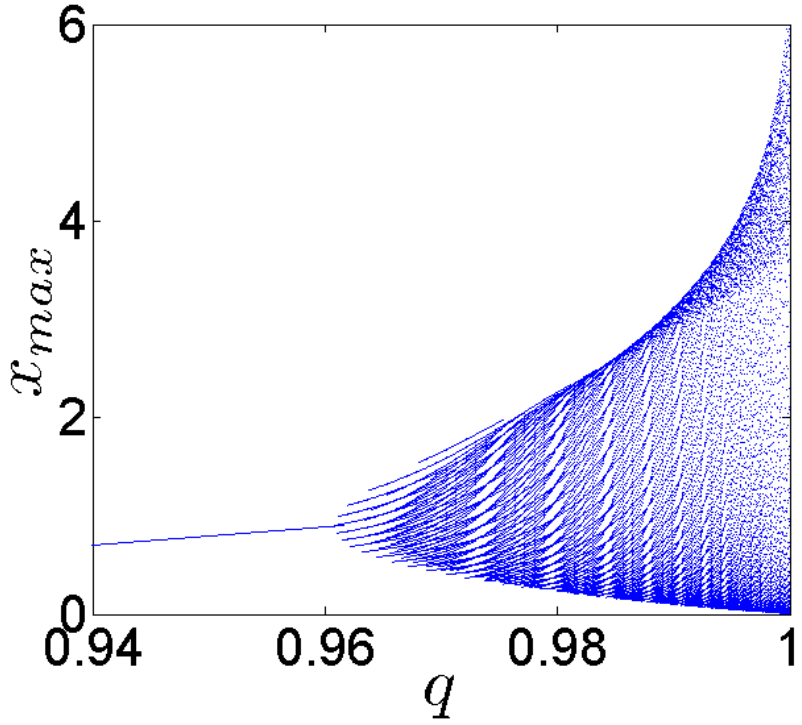

Figure 3.43: Bifurcation diagram of commensurate FOCM for $q \in (0.94, 1)$ with parameters $a = 0.7455, b = 0.7367, c = 0.5619$ and initial conditions $(x_0, y_0, z_0) = (0.4, 0.5, 0.5)$.

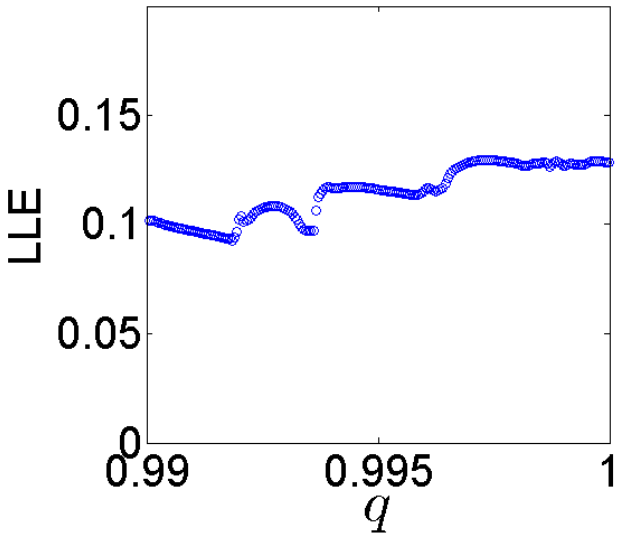

Figure 3.44: Maximum Lyapunov exponent of the commensurate FOCM (**??**) for $q \in (0.99, 1)$ with parameters $a = 0.7455, b = 0.7367, c = 0.5619$ and initial conditions $(x_0, y_0, z_0) = (0.4, 0.5, 0.5)$.

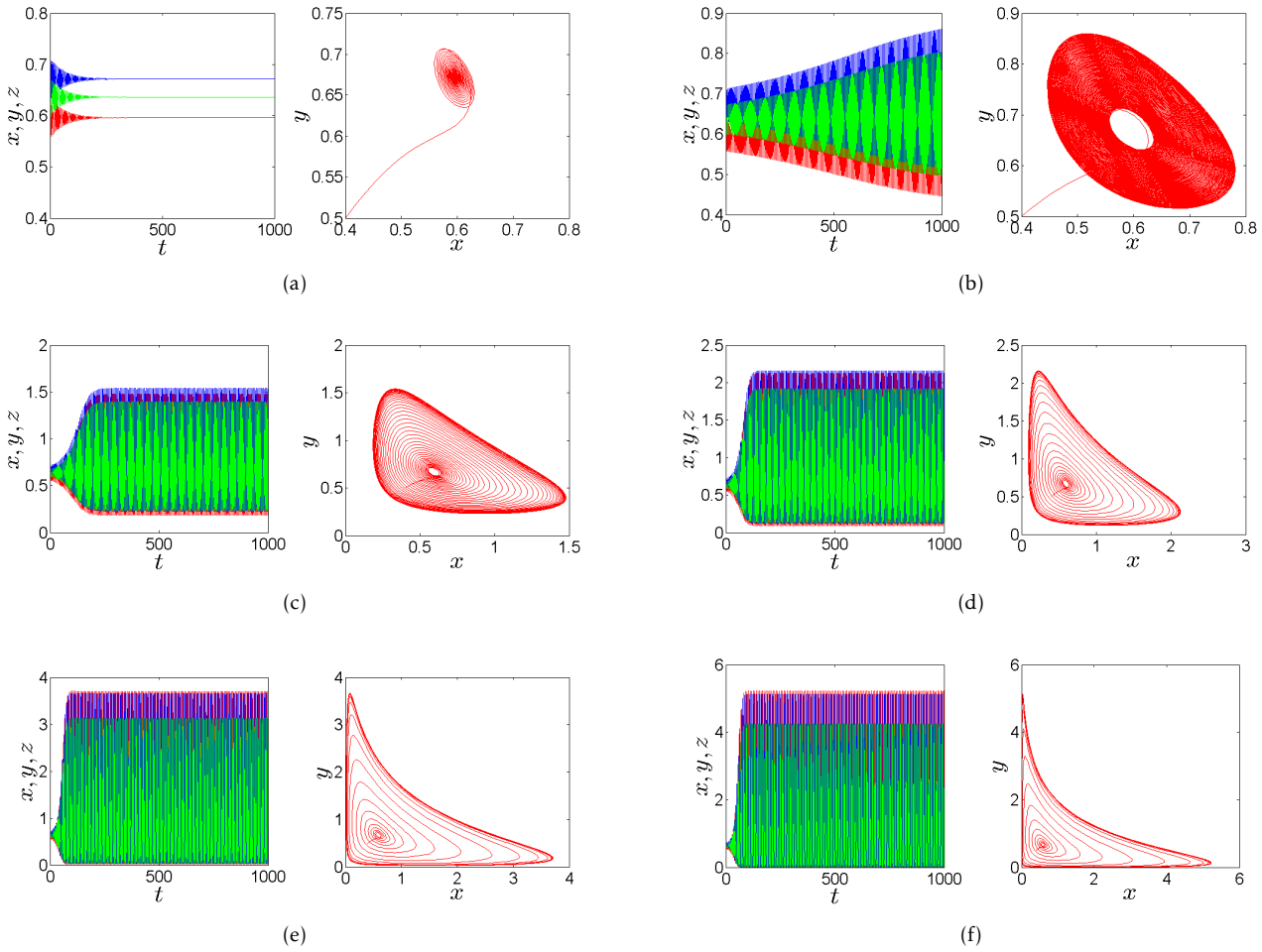

Figure 3.45: Time behaviors of the three state variables $x(t), y(t)$ and $z(t)$ (in red, blue and green color, respectively) along with the corresponding phase portraits in the x-y plan when $a = 0.7455, b = 0.7367, c = 0.5619$ and initial conditions $(x_0, y_0, z_0) = (0.4, 0.5, 0.5)$ for: (a) $q = 0.95$, (b) $q = 0.962$, (c) $q = 0.97$, (d) $q = 0.98$, (e) $q = 0.995$ and (f) $q = 1$.

By varying the value of the fractional order q, Fig. 3.45 shows the time behaviors of the three state variables: $x(t), y(t)$, and $z(t)$ (in red,blue, and green color, respectively) along with the corresponding phase portraits in the x-y plan, for the system parameters $a = 0.7455, b = 0.7367, c = 0.5619$ and initial conditions $(x_0, y_0, z_0) = (0.4, 0.5, 0.5)$. When $q = 0.95$, it can be observed that the FOCM (3.4.2) is asymptotically stable and the system trajectories converge to the equilibrium point E_4(Fig. 3.45(a)). When $q = 0.962$, the system loses its stability and a scroll begins to appear around the point E_4 (Fig. 3.45(b)). By increasing the values of q, periodic attractors appear for $q = 0.97$ and $q = 0.98$ (Fig. 3.45(c)-(d)). When $q = 0.995$, the fractional cancer model (**??**) exhibits a chaotic attractor (Fig. 3.45(e)), which is similiar to that one obtained for the integer order case (Fig. 3.45(f)).

A projection in the 3D-space of the chaotic attractor generated by the proposed fractional-order cancer model is plotted in Fig. (3.46) for $q = 0.995$. The conducted analyses clearly indicate that, in order to get chaos, the theoretical condition expressed by Theorem 3.4.1 is numerically ful filled when $q = 0.995$. From this results it can be concluded that, when the value of the fractional order decreases, the system become stable, indicating that the number of the tumor cells, of the healthy cells and of the effector cells asymptotically converge to the equilibrium point. On the other hand, when the order of the derivative increases and goes beyond the value of $q > 0.96$, the dynamics of the proposed FOCM turn to be chaotic, indicating that the number of tumor cells, of the healthy host

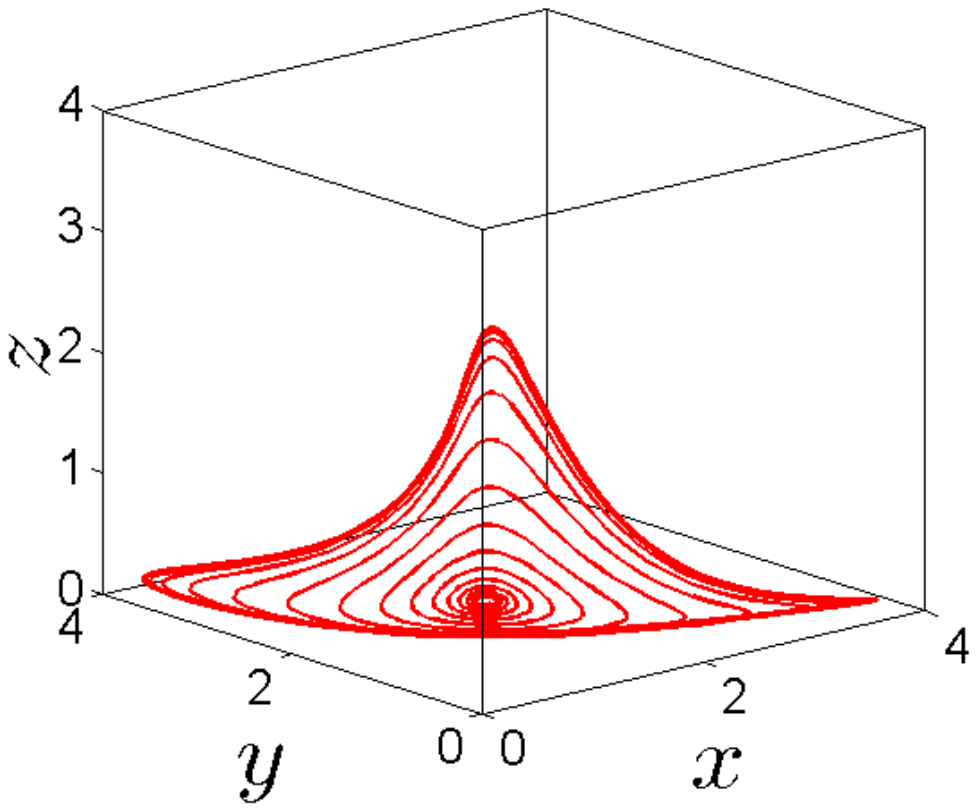

Figure 3.46: Projection in the 3D-space of the chaotic attractor of commensurate FOCM for $q = 0.995$ when $a = 0.7455, b = 0.7367, c = 0.5619$ and initial conditions $(x_0, y_0, z_0) = (0.4, 0.5, 0.5)$

cells and of the effector cells becomes unpredictable.

Analysis of the system dynamics by varying the parameters a, b and c

Herein, the analysis of the system dynamics is conducted by taking the fractional order $q = 0.99$ and the initial conditions $(x_0, y_0, z_0) = (0.4, 0.5, 0.5)$, and by varying the parameters a, b and c. At first, the parameters a and c are selected as $a = 0.7455$ and $c = 0.5619$, whereas the parameter b is varied in the interval $(0, 1)$. Note that the parameter b is related to the growth rate of host cells. Since the best strategy to face the cancer dynamics, from the biological point of view, is to act on the healthy host cells [137], herein the parameter b is varied, with the aim to investigate the behavior of the proposed cancer model. The bifurcation diagrams of the three state variables $x(t)$, $y(t)$ and $z(t)$ of the FOCM (3.4.2) are shown in Fig. 3.47, where b is the bifurcation parameter.
By varying the value of the parameter b, Fig. 3.48 shows the time behaviors of the three state variables: $x(t), y(t)$, and $z(t)$ (in red, blue and green color, respectively) along with the corresponding phase portraits in the x-y plan for the system parameters $a = 0.7455, c = 0.5619$ and initial conditions $(x_0, y_0, z_0) = (0.4, 0.5, 0.5)$. When $b = 0.28$ it can be observed that the FOCM (3.4.2) is asymptotically stable and the system trajectories converge to the equilibrium point E_4 (Fig. 3.48(a)). When the parameter b increases, a periodic route to chaos appears in the range $b \in (0.30, 0.5)$. In this range of parameter b, the system exhibits limit cycles of different periods (see Fig. 3.48(b) and Fig. 3.48(c)). Then, a chaotic attractor appears at $b = 0.53$ (see Fig. 3.48(d)) and the the system exhibits a chaotic behavior for $b \in (0.53, 1)$.
Now, the parameter b is fixed at the value $b = 0.7367$ whereas the parameter a, which represents the growth

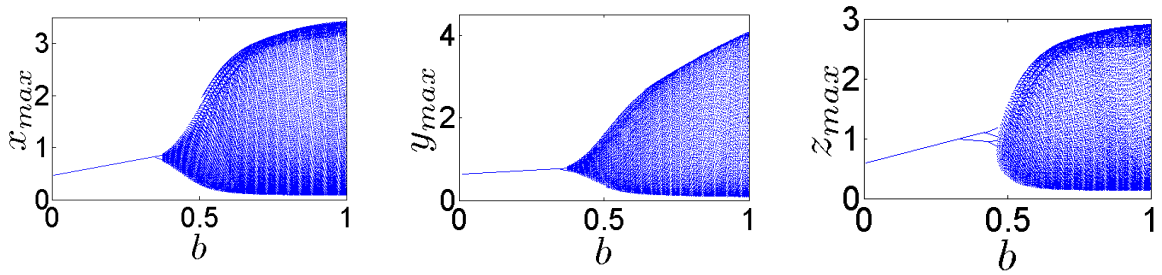

Figure 3.47: (a) Bifurcation diagrams of commensurate FOCM for $q = 0.99$, $a = 0.7455, c = 0.5619$, $(x_0, y_0, z_0) = (0.4, 0.5, 0.5)$ by varying parameter $b \in (0, 1)$ for: (a) $x(t)$ state variable, (b) $y(t)$ state variable, (c) $z(t)$ state variable.

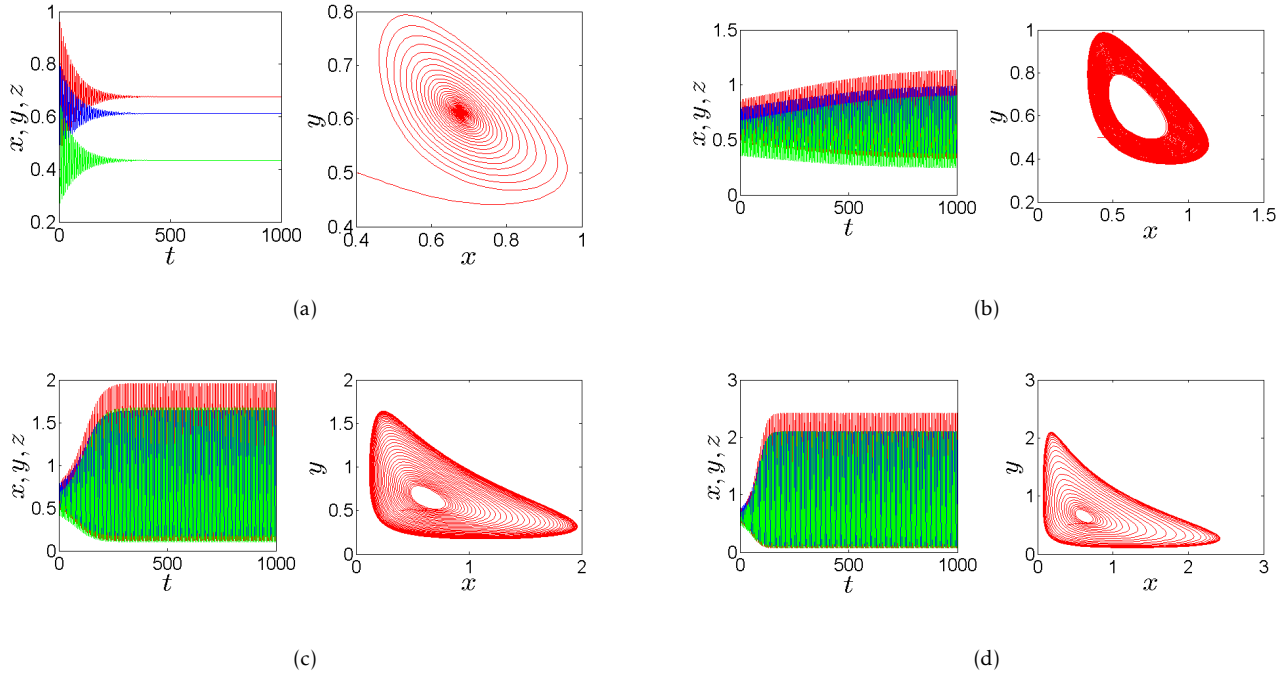

Figure 3.48: Time behaviors of the three state variables: $x(t), y(t)$ and $z(t)$ (in red, blue and green color, respectively) along with the corresponding phase portraits in the x-y plan when $q = 0.99$, $a = 0.7455, c = 0.5619$, $(x_0, y_0, z_0) = (0.4, 0.5, 0.5)$ for: (a) $b = 0.28$, (b) $b = 0.38$, (c) $b = 0.45$, (d) $b = 0.53$.

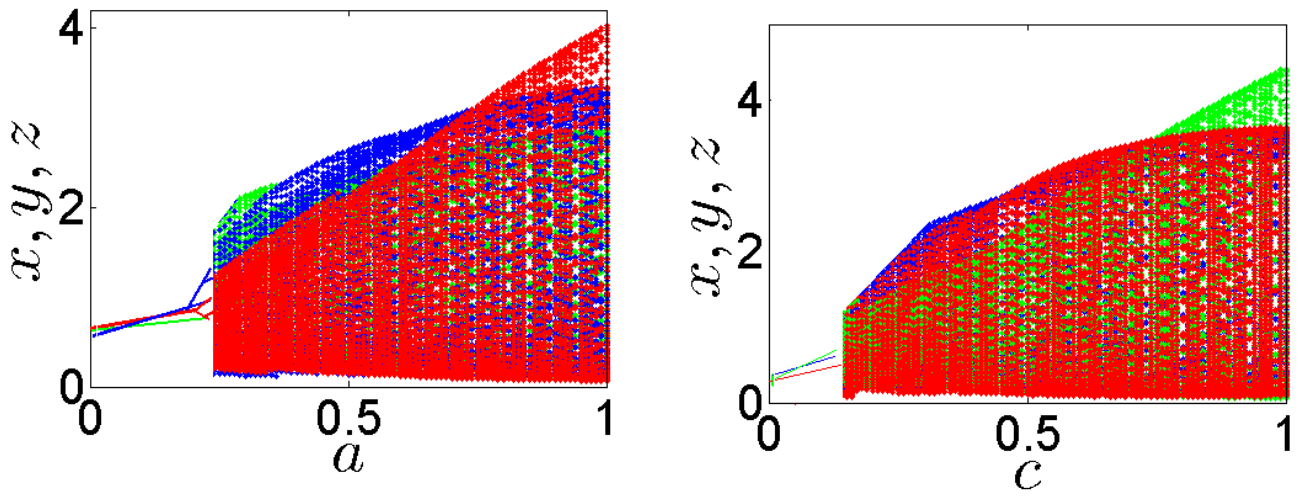

(a) (b)

Figure 3.49: Bifurcation diagrams of the variables: $x(t), y(t)$, and $z(t)$ (in red, blue and green color, respectively) of the commensurate FOCM (3.4.2) with $q = 0.99$, $b = 0.7367$, $(x_0, y_0, z_0) = (0.4, 0.5, 0.5)$ for the bifurcation parameters: (a) $a \in (0,1)$, (b) $c \in (0,1)$.

rate of the tumor cells, is varied in the interval $(0,1)$. The corresponding bifurcation diagram for the three state variables $x(t)$, $y(t)$ and $z(t)$ is plotted in Fig. 3.49(a). Similiary, by fixing the value $b = 0.7367$, the parameter c (i.e; the growth rate of the effector cells) is varied in the interval $(0,1)$. The corresponding bifurcation diagram for the three state variables $x(t)$, $y(t)$ and $z(t)$ is plotted in Fig. 3.49(b). By analysing the two bifurcation diagrams, it can be argued that the FOCM (3.4.2) loses its stability when the values of the parameters a and c are increased. Moreover, chaotic behaviors appear in the FOCM (3.4.2) when $a \in (0.5,1)$ and $c \in (0.35,1)$.
Regarding the biological meaning of these results, it should be noted that, for low values of the growth rates, the FOCM (3.4.2) has a stable equilibrium point. On the other hand, when the growth rates increase, the system loses its stability. At this stage, the tumor is ready to become invasive and even malignant [138]. With the further increase of the growth rates, the chaotic attractor of the tumor appears, being this higher tumor burden complicated by the presence of several periodic and chaotic dynamics. This is similar to what happens when parameter b increases in Fig. 3.48. On the other hand, when the growth rates decrease, the attractor corresponding to high tumor burden disappears. This is similar to what happens when a, b and c decrease in Fig. 3.47 and Fig. 3.49. These results can help the doctors for controlling the tumor burden, thus giving suggestions regarding the medical treatments.

Comparison between the dynamics of integer-order and commensurate fractional-order cancer models

Now, comparisons between the dynamics of integer-order and commensurate fractional-order cancer models are carried out. The time behaviors of the state variable $x(t)$ (representing the tumor population) are plotted in Fig. 3.50 by selecting $q = 0.90$, $q = 0.95$, $q = 0.99$, $q = 1$ and by taking different values of the system parameters a, b and c ranges. It can be observed that for smaller values of the parameter a (Fig. 3.50(a)), of the parameter b (Fig. 3.50(c)) and of the parameter c (Fig. 3.50(e)), the commensurate fractional derivatives damp the oscillation behavior. Consequently, the three states of tumor, host and effector cells approach faster the equilibrium point, indicating that the commensurate fractional derivatives enlarge the region of stability. When the values of the parameters a, b and c increase, the system is stable for small values of the fractional orders (i.e., $q = 0.90$ and

$q = 0.95$). Namely, by looking at Fig. 3.50(b), Fig. 3.50(d) and Fig. 3.50(e), it can be observed that the system trajectories tend to the equilibrium point for $q = 0.90$ and $q = 0.95$. On the other hand, chaotic oscillations with different amplitudes appear when for $q = 0.995$ and $q = 1$. Note that the amplitude of the chaotic oscillation reaches the maximum value for the integer-order case ($q = 1$).

3.4.4 Dynamics of the incommensurate fractional-order cancer model

This Section analyzes the dynamics of the incommensurate FOCM (3.4.2) by taking the parameters $a = 0.7455$, $b = 0.7367$, $c = 0.5619$, initial conditions $(x_0, y_0, z_0) = (0.4, 0.5, 0.5)$ and by selecting different values of the fractional orders q_1, q_2 and q_3. At first, the bifurcation diagrams of the variable $x(t)$ are plotted in Fig. 3.51(a) for three cases: $q_1 \in (0.6, 1)$ and $q_2 = q_3 = 1$; $q_2 \in (0.6, 1)$ and $q_1 = q_3 = 1$; $q_3 \in (0.6, 1)$ and $q_1 = q_2 = 1$. From Fig. 3.51(a) it can be seen that the equilibrium point is asymptotically stable when $q_1 < 0.75$, $q_2 < 0.74$ and $q_3 < 0.74$. When the values of q increase, periodic windows appear for $q_1 \in (0.75, 0.86)$, $q_2 \in (0.74, 0.85)$ and $q_3 \in (0.74, 0.85)$, whereas chaotic behaviors are exhibited for $q_1 \in (0.86, 1)$, $q_2 \in (0.85, 1)$ and $q_3 \in (0.85, 1)$. The existence of positive Lyapunov exponents is confirmed by the plot as a function of the fractional order q, as shown in Fig. 3.51(b). Namely, from Fig. 3.51(b) it can be seen that the fractional cancer system (3.4.2) is chaotic for $q_1 \in (0.86, 1)$, $q_2 \in (0.85, 1)$ and $q_3 \in (0.85, 1)$. Note that the maximum value of the variable $x(t)$ is obtained by varying q_3 (see Fig. 3.51(a)).

Fig. 3.52 shows the time behaviors of the three state variables $x(t)$, $y(t)$, and $z(t)$ (in red, blue and green color, respectively) along with the corresponding phase portraits in the x-y plan, for the system parameters $a = 0.7455, b = 0.7367, c = 0.5619$ and initial conditions $(x_0, y_0, z_0) = (0.4, 0.5, 0.5)$. By taking different values of the fractional order q_1, q_2 and q_3 in the incommensurate FOCM (3.4.2), some chaotic attractors appear. For example, Fig. 3.52(a) plots the chaotic attractor obtained for $q_1 = 0.999$ and $q_2 = q_3 = 1$, whereas Fig. 3.52(b) and Fig. 3.52(c) illustrate the chaotic attractors obtained for $q_2 = 0.999$ $q_1 = q_3 = 1$ and for $q_3 = 0.999$, $q_1 = q_2 = 1$, respectively. By looking at the time behaviors of the state variables, it can be noticed that the maximum amplitudes of the trajectories change from one plot to the other when the incommensurate orders are varied. Specifically, the population of the healthy host cells (i.e., the state variable $y(t)$) is the largest when $q_1 = 0.999$ (see Fig. 3.52(a)), the population of the effector immune cells (i.e., the state variable $z(t)$) is the largest when $q_2 = 0.999$ (see Fig. 3.52(b)), whereas the population of the tumor cells (i.e., the state variable $x(t)$) is the largest when $q_3 = 0.999$ (see Fig. 3.52(c)).

Now, by fixing the system parameters $a = 0.7455$ and $c = 0.5619$, the bifurcation diagrams for the variable $x(t)$ as a function of the parameter b are derived for three cases: $q_1 = 0.999$, $q_2 = q_3 = 1$; $q_2 = 0.999$, $q_1 = q_3 = 1$ and $q_3 = 0.999, q_1 = q_2 = 1$ (see Fig. 3.53). It can be noticed that the incommensurate system (**??**) exhibits chaos in all the three cases when $b \in (0.38, 1)$.

Fig. 3.54 presents the chaotic attractors of the incommensurate FOCM (3.4.2) in 3D projection by taking the parameter $b = 0.38$ for: (a) $q_1 = 0.999$, $q_2 = q_3 = 1$; (b) $q_2 = 0.999$, $q_1 = q_3 = 1$; (c) $q_3 = 0.999$, $q_1 = q_2 = 1$. By comparing this chaotic range with the range that has been obtained in Section 3.4.3 (see Fig. 3.47 and Fig. 3.48), it can be observed that the incommensurate fractional derivatives enlarge the chaotic range of the solution. From the biological point of view, it can be deduced that, when the growth rate decreases, the attractor corresponding to the high tumor burden disappears. This is in accordance with the results in Fig. 3.53, since when b decreases the system dynamics go towards stable behaviors.

Now, comparison between the dynamics of integer-order and incommensurate fractional-order cancer models are carried out. The time behaviors of the state variable $x(t)$ (representing the tumor population) are plotted in Fig. 3.55 by selecting different values of the fractional orders q_1, q_2 and q_3 when the parameter b assumes the two values $b = 0.1$ (corresponding to the stable range) and $b = 0.5$ (corresponding to the chaotic range). It can be observed that for $b = 0.1$ (see Fig. 3.55(a), Fig. 3.55(c) and Fig. 3.55(e)), the incommensurate fractional derivatives

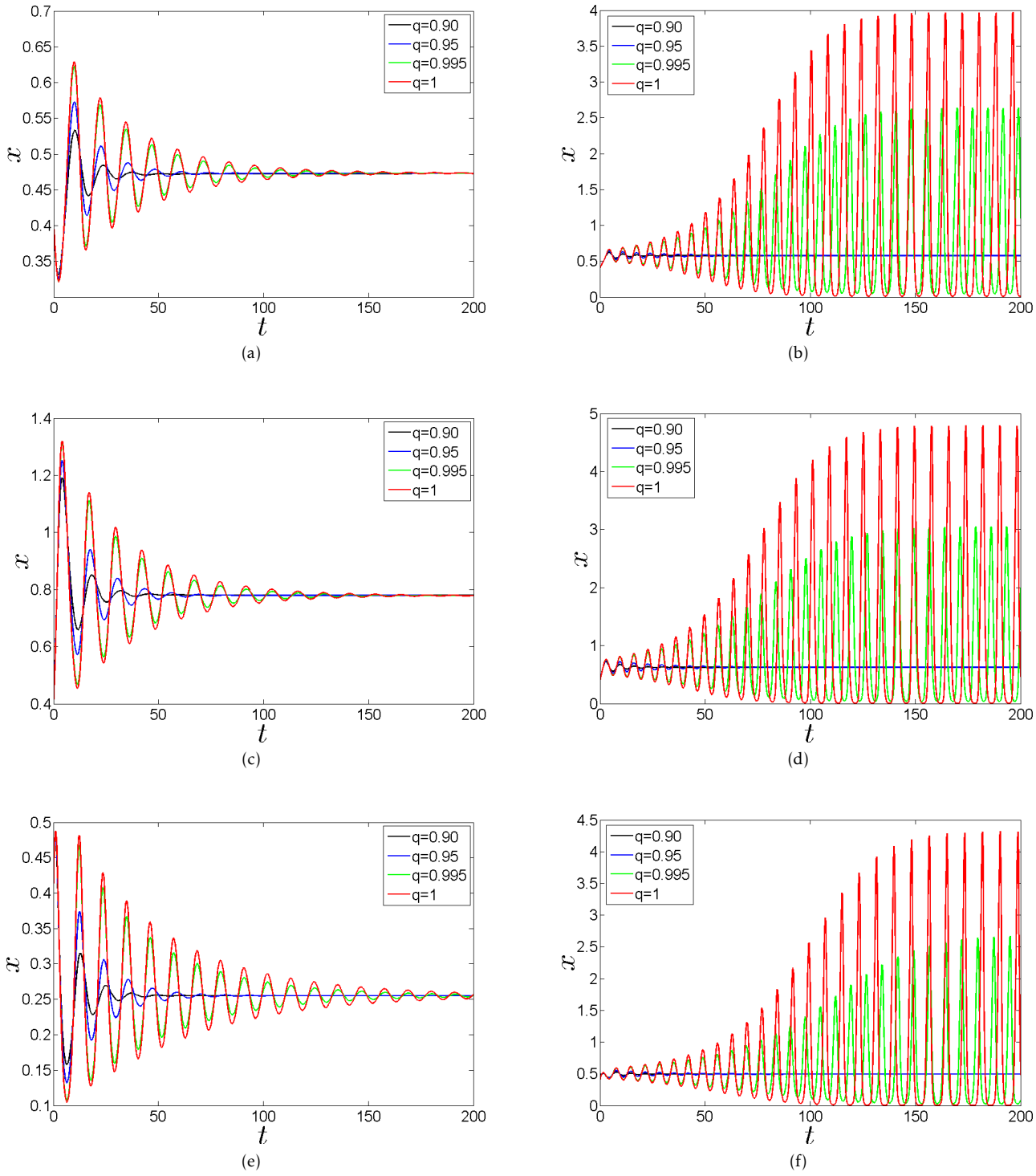

Figure 3.50: Time behaviors of state variable $x(t)$ of commensurate FOCM (**??**) for different fractional orders and system parameters: (a) $a = 0.1$, (b) $a = 0.50$, (c) $b = 0.1$, (d) $b = 0.53$, (e) $c = 0.1$ and (f) $c = 0.35$.

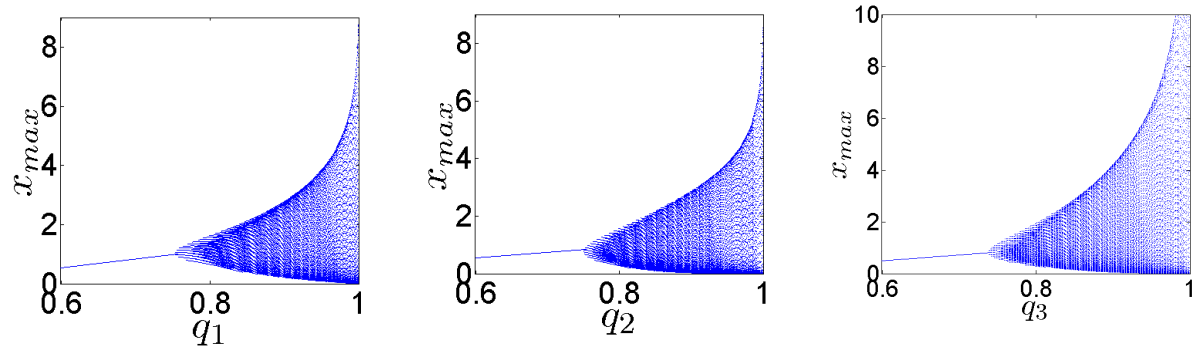

(a)

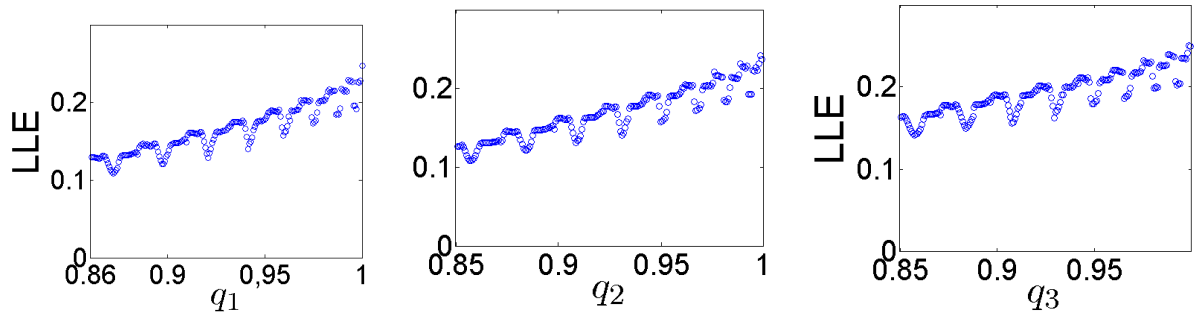

(b)

Figure 3.51: Incommensurate FOCM (**??**) for $a = 0.7455, b = 0.7367, c = 0.5619$, $(x_0, y_0, z_0) = (0.4, 0.5, 0.5)$. (a) Bifurcation diagrams for $q_1 \in (0.6, 1), q_2 = q_3 = 1$; $q_2 \in (0.6, 1), q_1 = q_3 = 1$ and $q_3 \in (0.6, 1), q_1 = q_2 = 1$, (b) LLEs for $q_1 \in (0.86, 1)$, and $q_2, q_3 \in (0.85, 1)$.

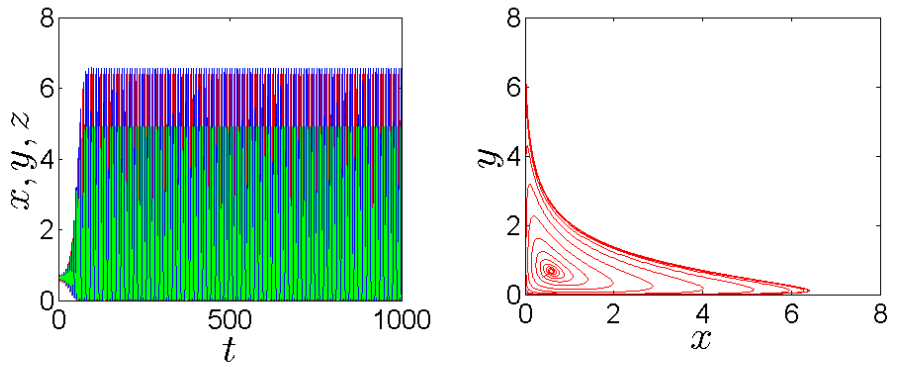

(a)

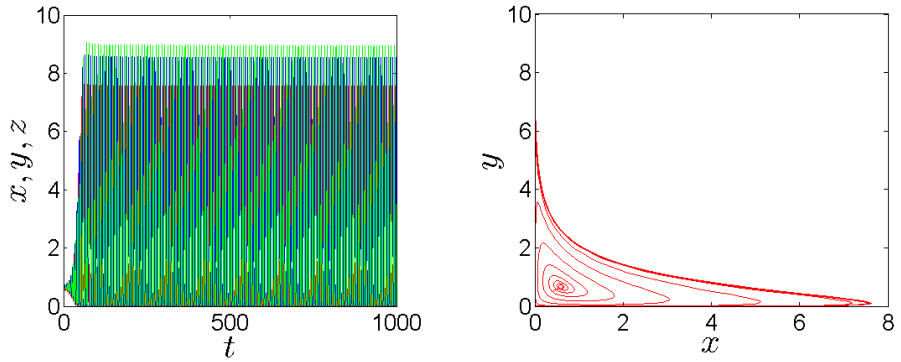

(b)

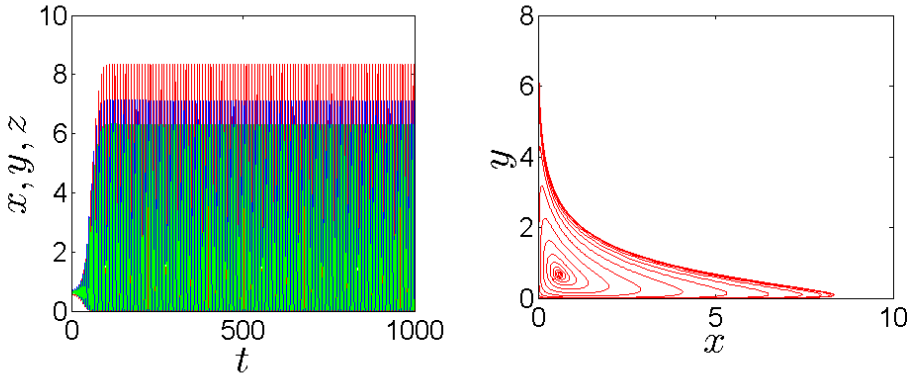

(c)

Figure 3.52: Time behaviors of of the state variables: $x(t), y(t)$ and $z(t)$ (in red,blue and green color, respectively) of the incommensurate FOCM along with the corresponding phase portraits in x-y plan when $a = 0.7455, b = 0.7367, c = 0.5619$ and $(x_0, y_0, z_0) = (0.4, 0.5, 0.5)$ for: (a) $q_1 = 0.999, q_2 = q_3 = 1$, (b) $q_2 = 0.999, q_1 = q_3 = 1$, (c) $q_3 = 0.999, q_1 = q_2 = 1$.

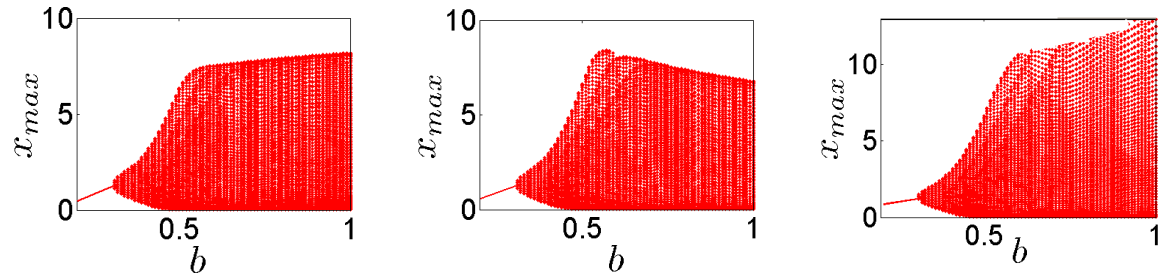

Figure 3.53: Bifurcation diagrams of the incommensurate FOCM (**??**) with $a = 0.7455$, $c = 0.5619$, $(x_0, y_0, z_0) = (0.4, 0.5, 0.5)$ by varying parameter $b \in (0.2, 1)$ for: (a) $q_1 = 0.999, q_2 = q_3 = 1$, (b) $q_2 = 0.999, q_1 = q_3 = 1$, (c) $q_3 = 0.999, q_1 = q_2 = 1$.

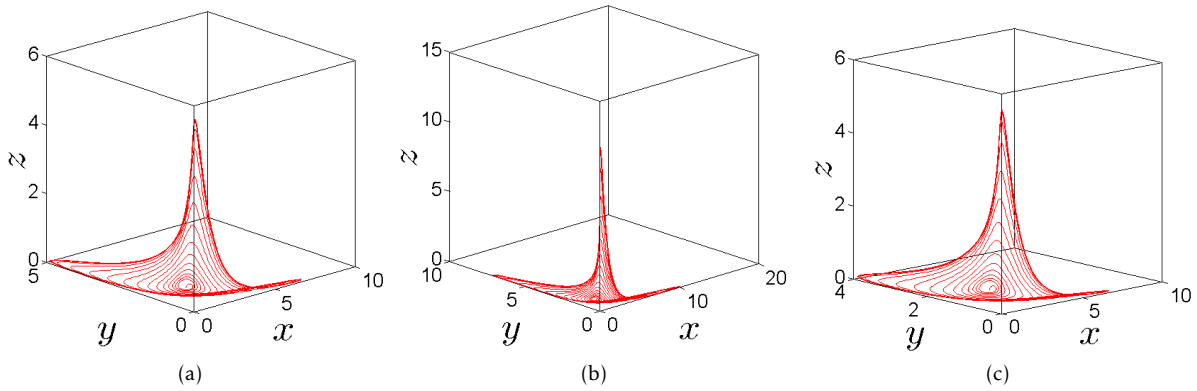

Figure 3.54: Chaotic attractors of incommensurate FOCM in 3D projection with taking initial conditions $(x_0, y_0, z_0) = (0.4, 0.5, 0.5)$, fixing parameters $a = 0.7455, c = 0.5619$ and parameter $b = 0.38$ for: (a) $q_1 = 0.999, q_2 = q_3 = 1$, (b) $q_2 = 0.999, q_1 = q_3 = 1$, (c) $q_3 = 0.999, q_1 = q_2 = 1$.

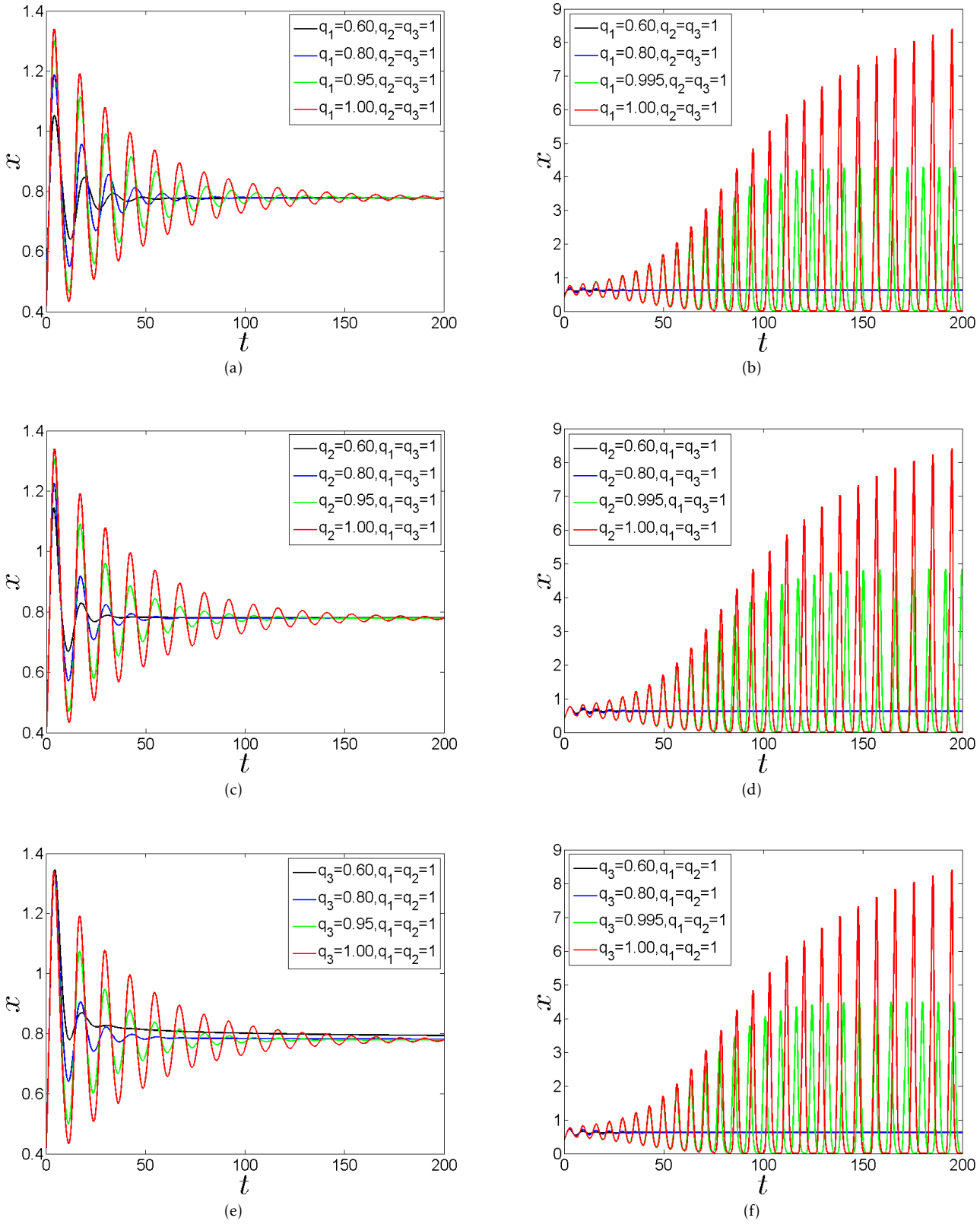

Figure 3.55: Time behaviors of the state variable $x(t)$ of incommensurate FOCM (**??**) for different fractional-orders and system parameters: (a) $b = 0.1$, (b) $b = 0.50$, (c) $b = 0.1$, (d) $b = 0.5$, (e) $b = 0.1$ and (f) $b = 0.50$.

damp the oscillation behavior. Consequently, the three states of tumor, host and effector cells approach faster the equilibrium point, indicating that the incommensurate fractional derivatives enlarge the region of stability. When the parameter b assumes the value $b = 0.5$, the system is stable for small values of the fractional orders (i.e., q_1, q_2, $q_3 = 0.60$, q_1, q_2, $q_3 = 0.80$). Namely, by looking at Fig. 3.55(b), Fig. 3.55(d) and Fig. 3.55(e), it can be observed that the system trajectories tend to the equilibrium point for q_1, q_2, $q_3 = 0.60$ and q_1, q_2, $q_3 = 0.80$. On the other hand, chaotic oscillations with different amplitudes appear when q_1, q_2, $q_3 = 0.995$ and q_1, q_2, $q_3 = 1$. Note that the amplitude of the chaotic oscillation reaches the maximum value for the integer-order case (q_1, q_2, $q_3 = 1$). The motivation of the manuscript is to provide a complete study of tumor-immune dynamics by presenting a new model of cancer growth. In order to explain the physical meaning of introducing the fractional-order into the model, it is worth noting that biological systems are characterized by memory or after-effects, hereditary properties and non-local distributed behaviors [**?**]. Since these features are neglected in integer-order modeling, this has motivated the use of fractional calculus as a tool for accurately describing dynamic phenomena in tumor-immune systems. The main advantage of the results in this paper, compared with others published in the literature, is that our approach represents an exhaustive study of tumor-immune dynamics, since it includes bifurcation diagrams, Lyapunov exponents and phases plots for both the commensurate and the incommensurate case.

3.4.5 conclusion

This study has made a contribution to the study of tumor-immune dynamics by presenting a new model of cancer growth based on fractional-order differential equations. By investigating the system dynamics, the manuscript has highlighted the chaotic behaviours of the proposed cancer model for both the commensurate and the incommensurate case. In particular, by using bifurcation diagrams, Lyapunov exponents, phase plots and a necessary condition to get chaos, the paper has shown that, when the order of the derivative goes beyond the threshold value $q > 0.96$, different chaotic behaviors are found, indicating that the number of the tumor cells, of the healthy host cells and the effector cells becomes unpredictable. Finally, simulation results reported through the manuscript have highlighted that the proposed approach can explain many biologically observed tumor states, including stable, periodic and chaotic behaviors. Regarding open research problems, an important issue is related to the development of control techniques for suppressing chaos in fractional-order biological systems. Our future plan is to work on this issue, since we believe that controlling chaos in fractional tumor-immune systems might help biologists in the fight again cancer.

CHAPTER 4

CHAOS IN FRACTIONAL-ORDER PHYSICAL SYSTEMS

In this part, we study the chaotic behaviors in three physical models by including commensurate and incommensurate fractional-orders at this models.

4.1 Chaos in fractional system with extreme events

The content of this section has been published in [16].

4.1.1 Introduction

The famous Japanese paint The Great Wave off Kanagawa illustrates an example of "extreme event". The sudden appearance of the large wave threatening fishing boats relates to rogue waves. Extreme events are characterized by extreme observed values or statistical measurements. It is noted that there are numerous definitions of extreme event in different disciplines, however, researchers have attempted to introduce a systems-based definition of extreme event. Extreme events occur in a wide range of fields from nature, economics, society to engineering. Extreme events in nature were often reported as tsunamis, earthquakes, tornadoes, hurricanes, droughts, floods. Natural extreme events launch natural hazards causing damage on people. Market crashes, credit risk are examples of extreme events in economics. In engineering, power blackouts, machine failures can be considered as extreme events. The rapid increase of new coronavirus infections in northern Italy in February 2020 can be considered to be an extreme event. Monitoring and predicting extreme events likes heart attack and epilepsy is the main aim of ubiquitous health-care systems. Extreme event may be a tipping point in changing the global dynamics and inference of extreme event should be discovered further. Kingston et al. introduced a Li´enard-type oscillator including forcing $Asin(\omega t)$ [142]. Authors observed extremely large amplitude oscillations in one of the system state variables when changing amplitude and the frequency of the forced signal. Extreme and critical transition events were found in Li´enard system with memristor [143]. Extreme events and spatiotemporal chaos were measured in a microcavity laser[144]. In the recent work [145], authors proposed a networks of Josephson junctions and obtained extreme events in a sub-population. Dynamical and statistical characteristics were studied indicating routes to extreme events [146]. Although extreme event has been an attractive object of various researches on integer order systems, there are few studies investigated extreme events in fractional order systems. Investigating extreme events in fractional order systems contributes to a deeper understanding of extreme events. A fractional-order system is studied in this work.

4.1.2 Fractional oscillator

We consider fractional-order oscillator (4.1.1):

$$\begin{aligned} D^{q_1}x &= y, \\ D^{q_2}y &= -axy + bx - cx^3 + dsin(\omega t), \end{aligned} \tag{4.1.1}$$

where a is the nonlinear damping, c is the strength of nonlinearity, and b relates to the internal frequency of the system. Parameters d and ω are amplitude and forcing frequency of the external sinusoidal signal. Here D^q is q-order Caputo differential operator [1], $0 < q_i \leq 1$ $(i = 1, 2)$ are the derivative orders of the state variables x, y. Oscillator (4.1.1) is a Liénard-type oscillator. Liénard–type oscillator is attractive because it is simple but displays multistability. In addition, Liénard-type oscillator presents a wide class of systems which have broad applications [142]. The fractional-order system (4.1.1) is called as commensurate if $q_1 = q_2$ and incommensurate otherwise. In this work, the Adams-Bashforth-Moulton predictor-corrector method is used for the numerical simulations.
System (4.1.1) has three equilibria: $E_1(0,0), E_2(-1,0)$ and $E_3(1,0)$. The Jacobian matrix of fractional-order system (4.1.1) is given by:

$$J = \begin{bmatrix} 0 & 1 \\ -ay + b - 3cx^2 & -ax \end{bmatrix}$$

To study the stability of commensurate order system (4.1.1) for parameters $a = 0.45, b = 0.5, c = 0.5, d = 0.2$, and forcing frequency $\omega = 0.7315$, the eigenvalues λ_i, $i = 1, 2$ of the Jacobian matrix J are evaluated at each equilibrium point E_i and mentioned in Table **??**.

Theorem 4.1.1. *If the eigenvalues for the equilibria E_i, $i = 1, 2, 3$ of the Jacobian matrix J, satisfy the following condition:*

$$arg(\lambda_i) > q\pi/2, \qquad 0 < q < 1.$$

The fractional-order forced system (4.1.1) is asymptotically stable, where the derivative orders $q_1 = q_2 = q$.

For the equilibrium E_2, it is obtained

$$arg(0.2250 + 0.9744i) \times 2/\pi \approx 0.86,$$

that means from the Theorem 4.1.1, the commensurate order system (4.1.1) is stable for $q < 0.86$ and we can conclude that fractional system (4.1.1) exhibits chaotic dynamics when $q > 0.86$ for E_2.
In order to verify this result numerically, the bifurcation diagram, Lyapunov exponents and phase portraits are plotted in Fig. 4.1 for $q \in (0.98, 1)$ and initial conditions $(x_0, y_0) = (1, -0.5)$. From the bifurcation diagram we can see that the commensurate order system (4.1.1) does not remain chaotic behavior for $q < 0.988$. When $0.988 \leq q < 0.997$ the system (4.1.1) displays transtion from periodic to chaotic states. route to chaos. The system exhibits complex chaotic attractor over most of the range $q \in (0.997, 1)$. The existence of a positive Lyapunov exponent confirms that the fractional-order system shows chaotic behavior. From the plot of Lyapunov exponents we observe that the fractional system (4.1.1) is chaotic for $q > 0.997$. The phase portraits in the $x - y$ plane illustrate the periodic orbits with different periods for $q = 0.98$, $q = 0.99$, $q = 0.996$ and complex chaotic attractor for $q = 0.999$.
The choice of initial conditions is related with the basin of attraction of fractional-order system (4.1.1) which is shown in Fig. 4.2 for the commensurate order $q = 0.996$. Like the integer case, the fractional-order system (4.1.1) has two basin of attractions: BAC and BAD these mean the basin of attraction of the conservative and dissipative system respectively, HO (blue line in Fig. 4.2) means the homoclinic orbit which is located inside the BAD. Fig. 4.3 shows different dynamics of fractional system (4.1.1) for different sets of initial conditions from the region of BAD.

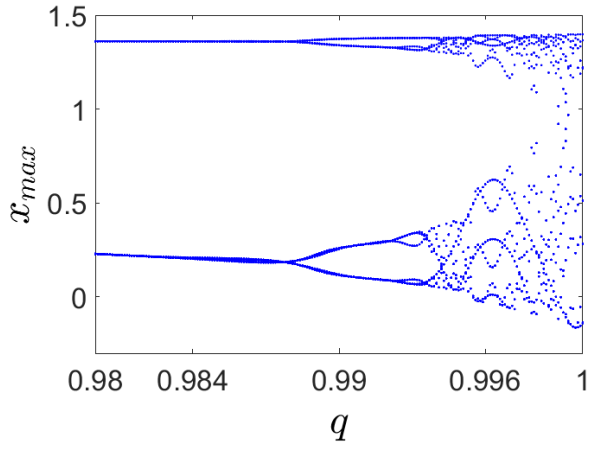

(a)

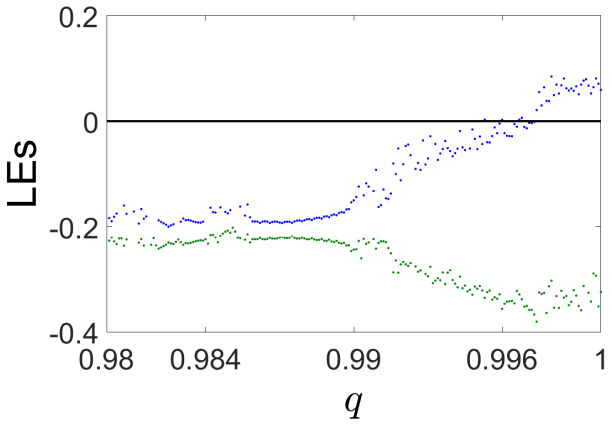

(b)

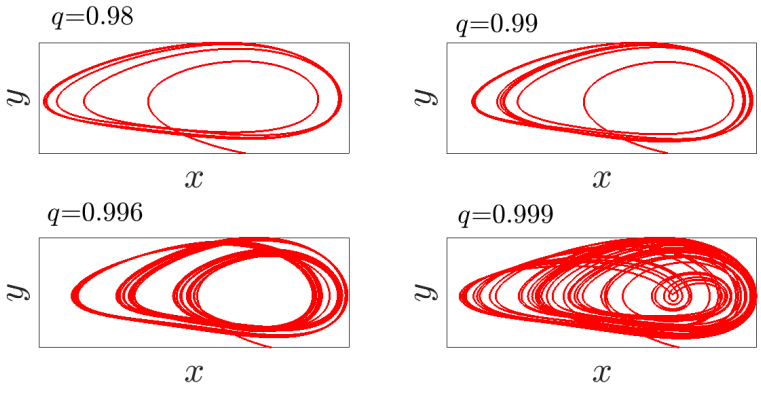

(c)

Figure 4.1: (a) Bifurcation diagram, (b) Lyapunov exponents, (c) Phase portraits of commensurate order system (4.1.1) for $q \in (0.98, 1), a = 0.45, b = 0.50, c = 0.50, d = 0.20, \omega = 0.7315$, and initial conditions $(x_0, y_0) = (1, -0.5)$.

Table 4.1: Eigenvalues and equilibria of system (4.1.1).

Equilibria(x_0, y_0)	Eigenvalues λ_i
$E_1(0,0)$	$0.7071, -0.7071$
$E_2(-1,0)$	$0.2250 \pm 0.9744i$
$E_3(1,0)$	$-0.2250 \pm 0.9744i$

When we choose initial conditions in the region inside the homoclinic orbit, the system (4.1.1) exhibits a bounded chaotic attractor for $\omega = 0.7315$ and $q = 0.999$, as well as a chaotic attractor with occasional large amplitude oscillations for $\omega = 0.65$ and $q = 0.993$. When we choose other initial conditions outside the homoclinic orbit, the system exhibits a quasiperiodic trajectories for $\omega = 0.65$, and $q = 0.993$. So, for $q = 0.993$, $\omega = 0.65$ and with two choices of initial conditions: inside and outside the HO; the fractional forced Liénard system (4.1.1) can exhibit a coexistence of chaotic attractor with large trajectories and quasiperiodic attractor which are shown in Fig. 4.4 (red and green trajectories respectively). As a notice here, the orbits of chaotic attractor are always limited by the coexisting quasiperiodic trajectories.

From the previous results, it can be remarked that the system exhibits a bounded attractor but under some values of system parameters, we noticed that the appearance of large amplitude oscillations from the bounded chaotic motion. These large oscillations are vital signatures of the existence of extreme events in the fractional-order system (4.1.1) which will be discussed further in the next section.

4.1.3 Extreme events in fractional oscillator

In this section, we discuss the effect of fractional-order derivative on the extreme events in system (4.1.1) by varying parameters of the commensurate and incommensurate fractional-order systems. Bifurcation diagrams, Lyapunov exponents, extreme event qualifier H_s, and numerical probability distribution function (PDF) are used to distinguish different cases of the system dynamics: bounded chaos, extreme events via intermittency route, extreme events via an interior crisis, and coexistence of multiple large amplitude oscillations.

Extreme events with respect to commensurate order q

Let set $a = 0.45, c = 0.50, b = 0.50, d = 0.20$, the frequency $\omega = 0.65$ and the initial conditions here are chosen inside the HO. We analyze system (4.1.1) by varying the commensurate order q. The bifurcation diagram and Lyapunov exponents for this case is plotted in Fig. 4.5. By observing the bifurcation diagram, it can be seen when $q < 0.993$, the system (4.1.1) exhibits a periodic oscillation but when $q = 0.993$ (arrow L), sudden changes occur in the amplitude of the oscillation which bifurcates to chaotic trajectory with large size. When $0.9933 \leq q < 0.9555$, the system comes back to display periodic oscillation in small ranges at this domain and then bifurcates again to chaos with large size. These large chaotic trajectories continue to appear with increasing commensurate order q from 0.9955 to 1. The same results about the existence of chaos are founded from the plot of Lyapunov exponents that presents the transition between positive values and negative values when $0.993 \leq q < 0.9955$. Positive values continue to exist when $q > 0.9955$. From Fig. 4.5(c), It can be seen different phase portraits of fractional system (4.1.1) for different values of fractional order q. The system exhibits periodic orbits or chaotic attractor with large size when $0.9933 \leq q < 0.9555$ which confirm the pervious results. Also, a chaotic attractor with large size is shown for $q = 0.9970$. Therefore, the fractional-order system (4.1.1) exhibits a periodic orbit that bifurcates to chaos with sudden expansion in the trajectories at the critical point L ($q = 0.9930$) through an intermittency route. The emergence of sudden expansion near critical fractional-order is a signature of extreme events. To

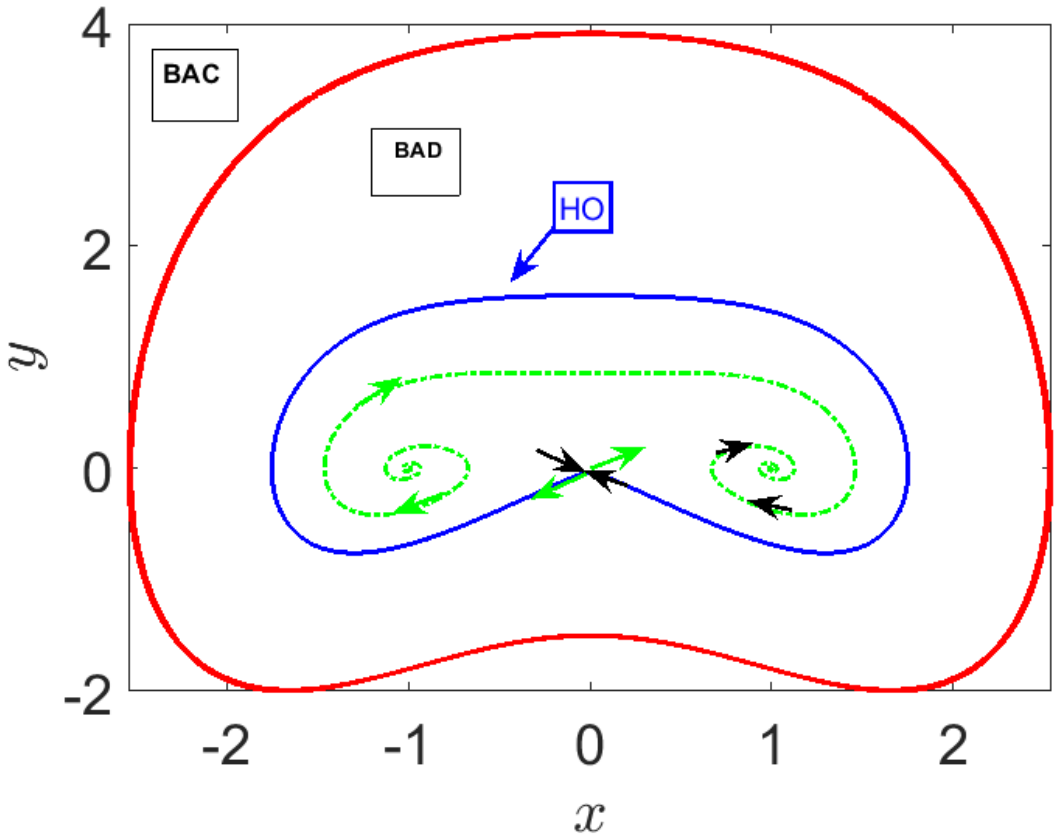

Figure 4.2: Two basin of attractions of fractional-order system (4.1.1) for $q = 0.996$: the BAC outer the red orbit and the BAD inside the red orbit with the HO in blue line. The equilibrium points in dashed spiral; E_1 at $(0,0)$; E_2 (green arrows) at $(-1,0)$, E_3 (black arrows) at $(1,0)$.

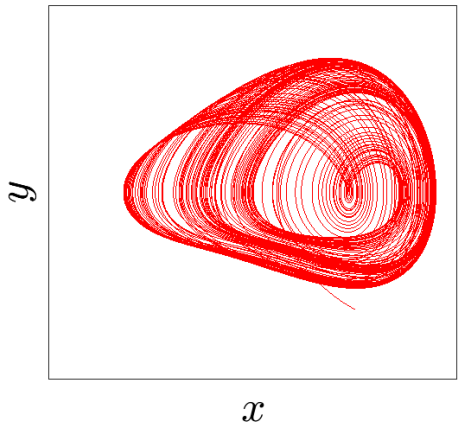

(a)

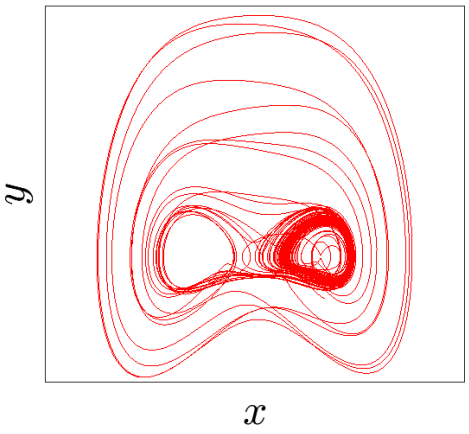

(b)

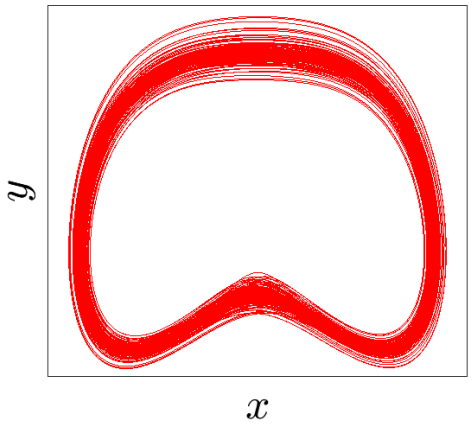

(c)

Figure 4.3: (a) Bounded chaotic attractor for $\omega = 0.7315, q = 0.999$ and $(x_0, y_0) = (1, -0.5)$, (b) Chaotic attractor with large trajectory for $\omega = 0.65, q = 0.993$ and $(x_0, y_0) = (1, -0.5)$, (c) Quasiperiodic trajectories for $\omega = 0.65, q = 0.993$ and $(x_0, y_0) = (1.5, 1.93)$.

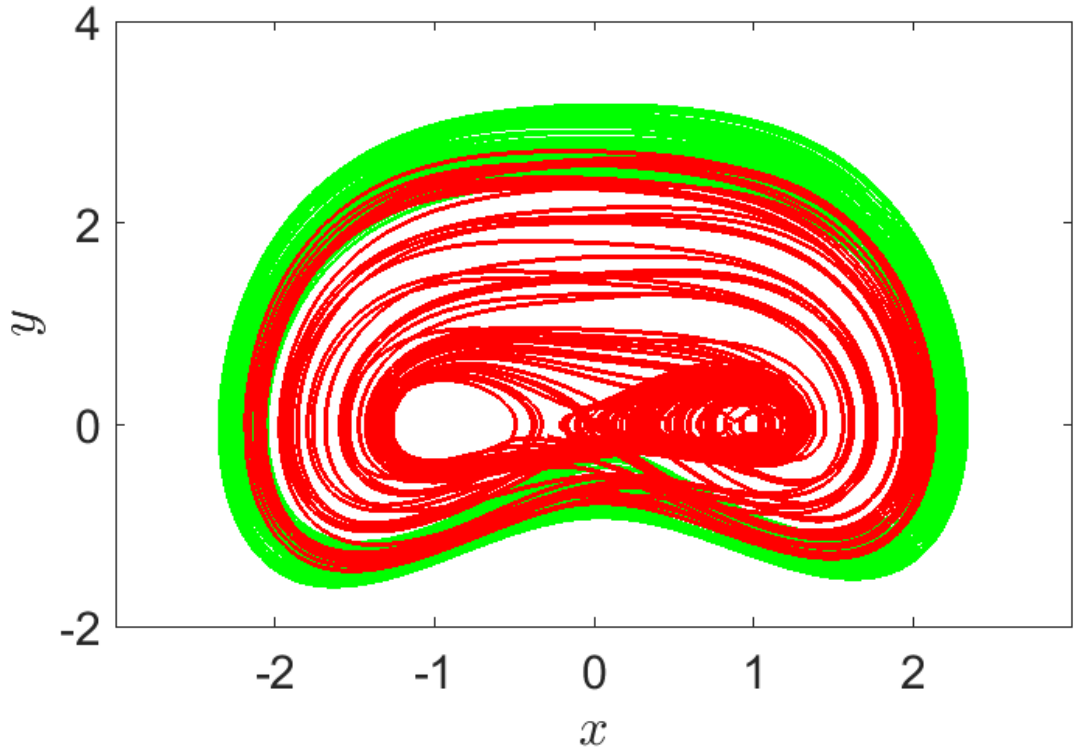

Figure 4.4: Trajectories of the commensurate order system (4.1.1) for $q = 0.9930$,$\omega = 0.65$ and two choice of initial conditions; coexisting of chaotic attractor with large trajectories in red color at $(x_0, y_0) = (1, -0.5)$(inside the HO) and quasiperiodic attractor in green color at $(x_0, y_0) = (1.5, 1.93)$ (outside the HO).

characterize this sudden expansion as an extreme event we estimate numerically the extreme event qualifier, H_S. For the estimation of H_S, we take the following steps:

- Calculate the $y(t)$ state variable by taking long temporal data as possible.
- Measure the peak values $y(t)$.i.e. P_n.
- Estimate the mean of the peaks $< P_n >$ and standard deviation σ.
- Calculate the threshold H_s: $H_s =< p_n > +8\sigma$.
- Plot the time series of $y(t)$ as function of t in short runs for better visualization and replot the H_s lines.

Especially, if the large amplitude peaks of the state variable of the system exceed H_s they can be defined as extreme events. The time series of commensurate order system (4.1.1) is plotted in Fig. 4.6 for three cases. A bounded chaos is shown in Fig. 4.6 (a) for $q = 0.9929$ (arrow C in Fig. 4.5). Extreme events is shown in Fig. 4.6 (b) for $q = 0.9930$ (arrow L in Fig. 4.5) near the intermittency regime. Here, the large excursions of the amplitude of $y(t)$ fluctuates intermittently between two phases: laminar phase which always remains bounded and turbulent phase. In the turbulent phase, the system exhibits large amplitude oscillations which is also exceed the threshold H_s (red line in Fig. 4.6(b)). Figure 4.6 (c) shows the third case for $q = 0.9960$ (a value between $q = 0.9955$ and $q = 1$ in Fig. 4.5). This case does not qualify as an extreme event because the system exhibits multiple large events with a high average value and therefore the threshold H_s becomes larger above the largest peaks.
The fractional-order system (4.1.1) can be presented also into 3D-space spanned by x, y, and t. Coexisting attractors of the system (4.1.1) are plotted in Fig. 4.7 on 3D-space for two initial conditions inside and outside the HO (see Fig. 4.4); quasiperiodic attractor in green line and chaotic attractor in red line. The 3D chaotic trajectories of system (4.1.1) are shown in Figs. 4.7(a)-4.7(c) that match to their time series in Figs. 4.6(a)-4.6(c) respectively. The plots show the different dynamics of the system for different commensurate order values: a bounded chaos for $q = 0.9929$ in Fig. 4.7(a), extreme events for $q = 0.9930$ in Fig. 4.7(b) and multiple large amplitude events for $q = 0.9960$ in Fig. 4.7(c). It can be remarked in Figs. 4.7 that the red trajectories stay always inside the green trajectories for all the three cases and this confirms the results obtained in section 4.1.2 concerning that chaotic and extreme events are confined within the boundaries of quasiperiodic attractor.

Extreme events with respect to incommensurate orders q_1, q_2

In this subsection, we assume the incommensurate order $q_1 \neq q_2$ and we study if the change of the fractional-order from commensurate case to the incommensurate case has an effect or not on the dynamics of extreme events.
Let set $a = 0.45, c = 0.50, b = 0.20, \omega = 0.68$ and the incommensurate orders are chosen as varying $q_1 \in (0.96, 1), q_2 = 1$ and varying $q_2 \in (0.96, 1), q_1 = 1$. Bifurcation diagrams, Lyapunov exponents, phase portraits and time series are plotted in Figs. 4.8-4.11 for initial conditions $(x_0, y_0) = (1, -0.5)$ inside the HO. As can be seen from the bifurcation diagrams, when the fractional-orders q_1, q_2 increase from 0.965 to 1, the system exhibits a period-doubling route to chaos with small amplitude but a very small change at the values of orders from arrow C to arrow L occurs suddenly a transition from small to very large amplitude chaotic oscillations through interior crisis. The expanded attractor continues to appear for $q_1 \in (0.97780, 1)$ (see Fig. 4.8(a)), $q_2 \in (0.9775, 1)$ (see Fig. 4.10(a)). The existence of chaotic behavior in the system is observed also in the plot of Lyapunov exponents in the same interval as above. The periodic orbits, bounded chaotic attractors and chaotic trajectories with large size are shown in Fig. 4.8(c) and Fig. 4.10(c) for different values of incommensurate orders q_1 and q_2 Here, an other scenario of extreme events is founded which is: extreme events via an interior crisis. From the plot of time series,

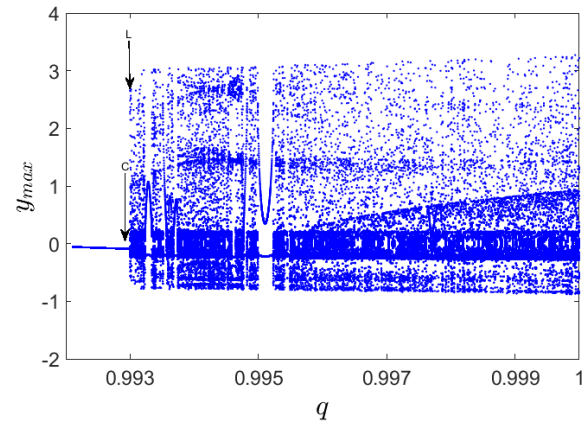

(a)

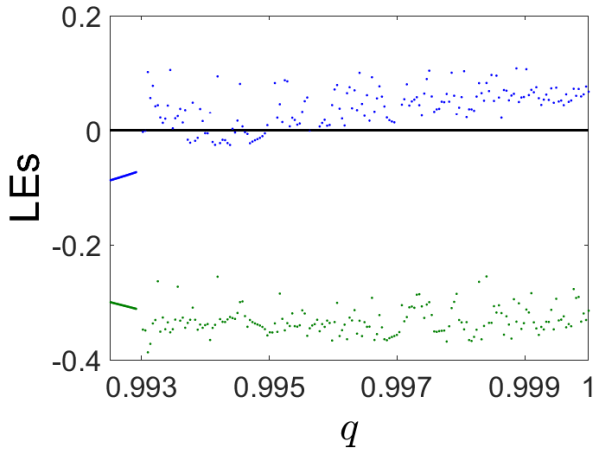

(b)

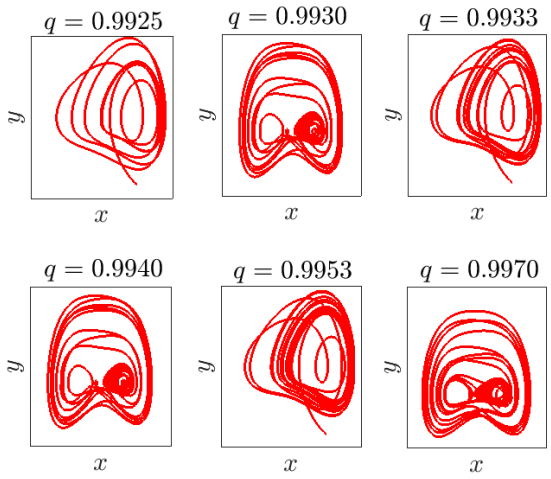

(c)

Figure 4.5: (a) Bifurcation diagram, (b) Lyapunov exponents and (c) Phase portraits of commensurate order system (4.1.1) for $a = 0.45, c = 0.50, b = 0.50, d = 0.20, \omega = 0.65$ at $(x_0, y_0) = (1, -0.5)$ with varying $q \in (0.992, 1)$.

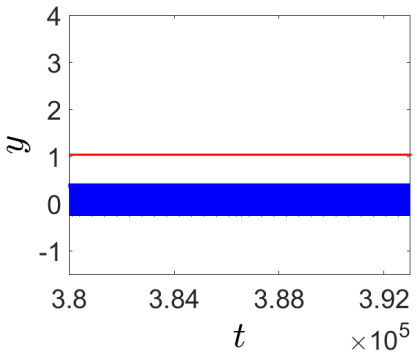

(a)

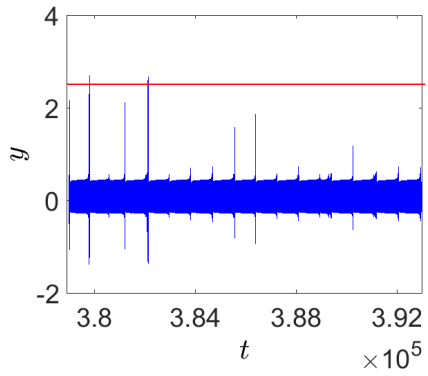

(b)

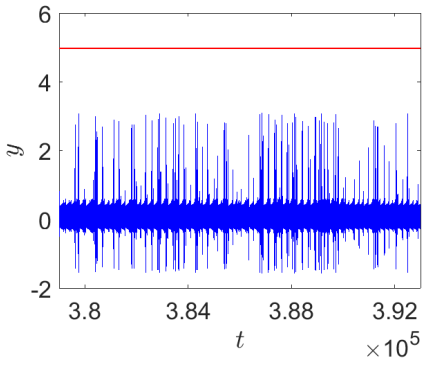

(c)

Figure 4.6: Time series of commensurate order system (4.1.1) for $a = 0.45, c = 0.50, b = 0.50, d = 0.20, w = 0.65$ at $(x_0, y_0) = (1, -0.5)$ with varying q. (a) bounded chaos for $q = 0.9929$, (b) extreme event for $q = 0.9930$, (c) multiple large amplitude events for $q = 0.9960$. The horizontal red lines indicate the threshold H_S.

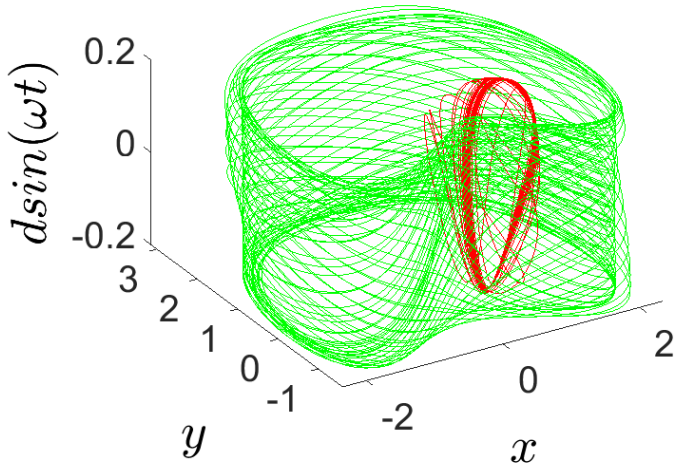

(a)

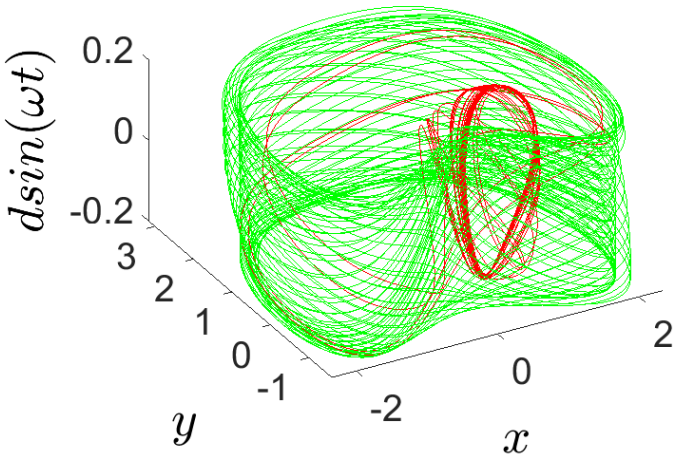

(b)

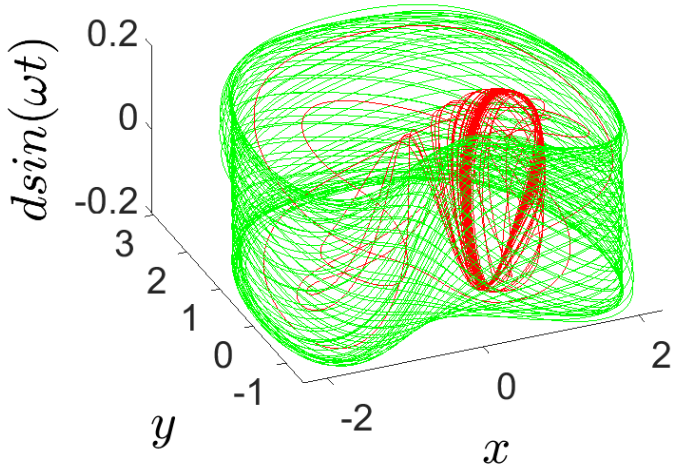

(c)

Figure 4.7: Coexisting of chaotic attractor and extreme events in red lines at $(x_0, y_0) = (1, -0.5)$ (inside the HO) with the quasiperiodic attractors in green lines at $(x_0, y_0) = (1.5, 1.93)$ (outside the HO) in 3D-spaces; (a) bounded chaos for $q = 0.9929$, (b) extreme event for $q = 0.9930$, (c) multiple large amplitude events for $q = 0.9960$.

Table 4.2: Three considered dynamic cases.

Dynamic cases	$[q_1, q_2]$	$[q_1, q_2]$
Bounded chaos (arrow C)	$[0.9770, 1]$	$[1, 0.9774]$
Extreme event (arrow L)	$[0.9780, 1]$	$[1, 0.9775]$
Multiple large amplitude events	$[0.9850, 1]$	$[1, 0.9850]$

we can see the different cases of extreme events which are mentioned in Table 4.2. When $q_1 = 0.9780, q_2 = 1$ and $q_2 = 0.9775, q_1 = 1$ (arrow L in bifurcation diagrams), the system occurs randomly chaotic oscillations with large peaks exceed the threshold H_s, these large events distinguish as an extreme events.
Now, we discuss the statistical properties of the dynamics during this scenario, leading to the emergence of extreme events. When $q_1 = 0.9780, q_2 = 1$ and $q_2 = 0.9775, q_1 = 1$, the numerical PDFs (probability distribution function of all the peaks p_n) are estimated for both the time series in Figs. 4.9(b) and 4.11(b). For the estimation, we take a long time series as possible of state $y(t)$, measure the peaks P_n then the PDFs have constructed and plotted in Figs. 4.12(a)-4.12(b). The vertical dashed lines in the figures indicate the threshold H_s. As a remark here, the saturation in the H_s is related with the length of temporal data. It can be seen from the figures long-tailed distributions overriding the threshold H_S. these results affirm the existence of extreme events. Figure 4.12(c) is a combination of the previous PDFs to compare between the extreme events. This combination shows that the distributions of varying q_1 have a long-tailed than the distributions of varying q_2.
As a result, the type of fractional order such as commensurate or incommensurate has an effect on the processes of occurrence of extreme events. From subsection 4.1.3, It can be remarked that the oscillation fluctuated intermittently between laminar phase and turbulent phase. So, the commensurate order system exhibits these events via an intermittency route but in subsection 4.1.3, the the oscillation appeared randomly. So, the incommensurate order system exhibits these events via an interior crisis.

Extreme events with respect to system parameters a, b, c and frequency ω

In this part, we study the effect of forcing frequency ω and system parameters a, b, c on the extreme events for commensurate and incommensurate fractional-order forced Liénard system (4.1.1).
Firstly, fixing $a = 0.45, c = 0.50, b = 0.50, d = 0.20$ and varying forcing frequency ω for the commensurate order $q = 0.996$, the bifurcation diagram is shown in Fig. 4.13. It can be seen here, the extreme events appear through two processes: intermittency and interior crisis. The intermittency route as shown when increasing ω in which a periodic oscillation bifurcates suddenly to a chaotic trajectory with large size at the critical point denoted by arrow L. The second process through interior crisis as shown when decreasing ω in which a small chaotic oscillation expands suddenly and randomly to a very large chaotic oscillation at an other critical point reached by arrow R. By comparing this results with the results founded in the integer-order system [**?**], we remark that the same processes are obtained. However, in fractional-order system an other extreme events through intermittency are occurred between the two critical points R and C which are not founded in the integer case.
For $\omega = 0.647$ (arrow L in Fig. 4.13) and $\omega = 0.7055$ (arrow R in Fig. 4.13) , the obtained time series of fractional system (4.1.1) is presented in Fig. 4.14(a) and Fig. 4.14(c) respectively for short runs and the probability density function (PDF) of all the peaks P_n is estimated with taking a long runs and it is shown in Fig. 4.14(b)(for $\omega = 0.647$) and Fig. 4.14(d) (for $\omega = 0.7055$). It can be seen a long-tailed distributions confirming the existence of larger events exceeding the height H_S (dashed vertical line). Furthermore, for the incommensurate orders the same both scenarios of extreme events are founded; an interior crisis and intermittency.

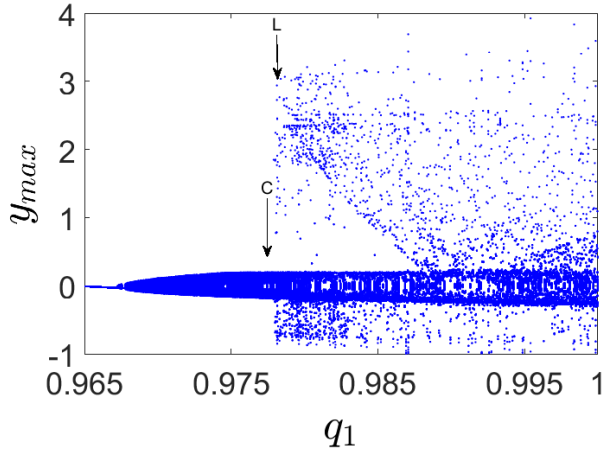

(a)

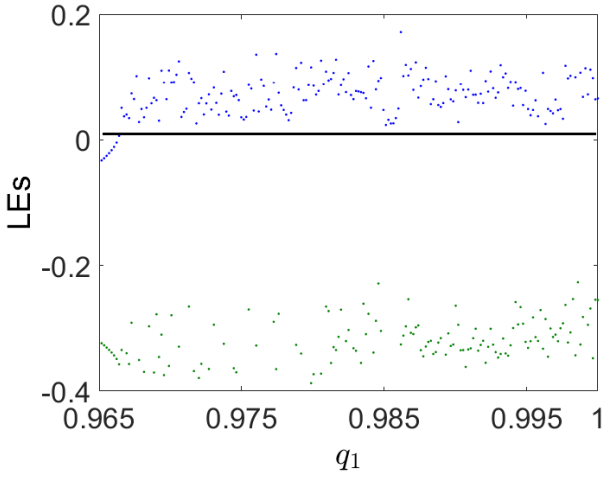

(b)

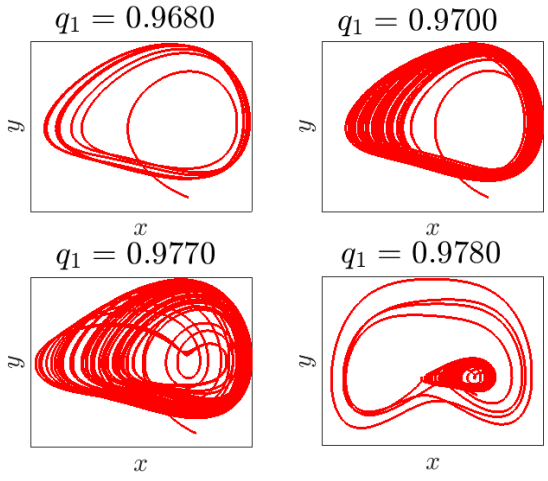

(c)

Figure 4.8: (a) Bifurcation diagram, (b) Lyapunov exponents and (c) Phase portraits of incommensurate order system (4.1.1) for $\omega = 0.68$, $q_2 = 1$, while varying q_1.

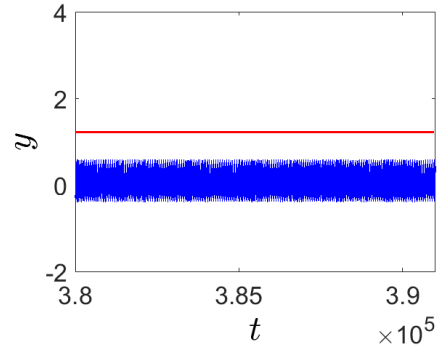

(a)

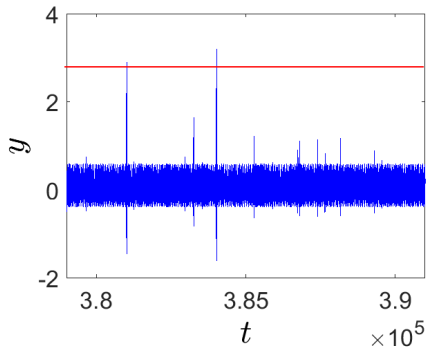

(b)

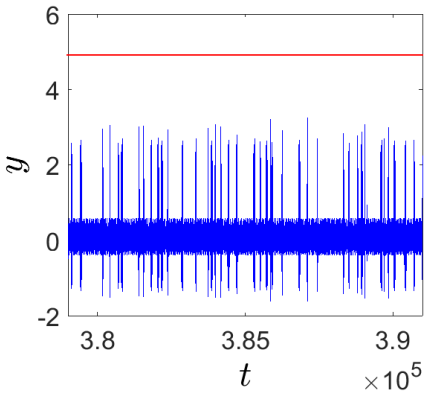

(c)

Figure 4.9: Time series of incommensurate order system (4.1.1) for $\omega = 0.68$, $q_2 = 1$, and varying q_1: (a) $q_1 = 0.9770$, (b) $q_1 = 0.9780$, (c) $q_1 = 0.9850$.

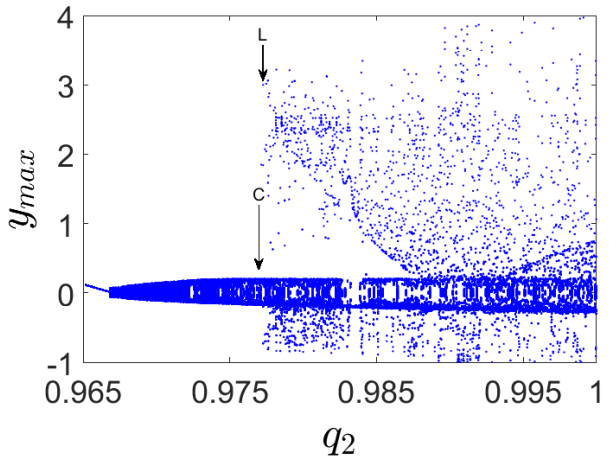

(a)

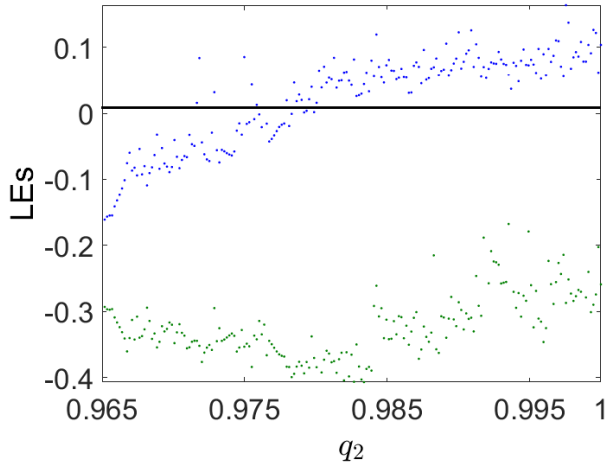

(b)

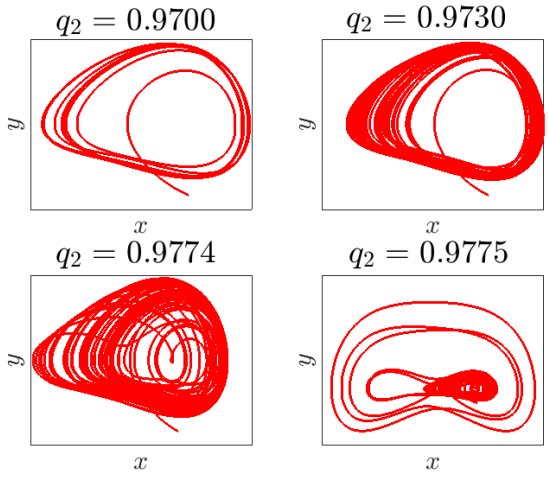

(c)

Figure 4.10: (a) Bifurcation diagram, (b) Lyapunov exponents and (c) Phase portraits of incommensurate order system (4.1.1) for $\omega = 0.68$, $q_1 = 1$, while varying q_2.

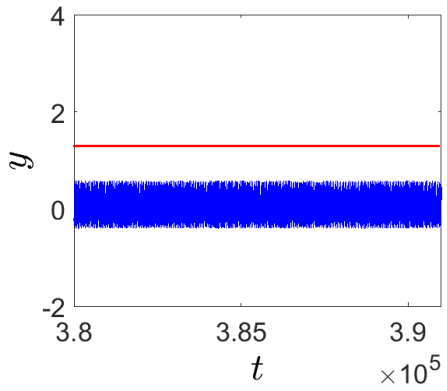

(a)

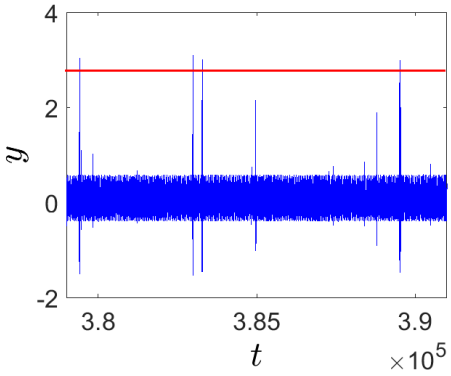

(b)

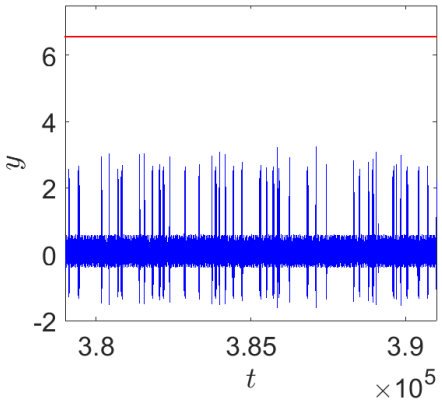

(c)

Figure 4.11: Time series of incommensurate order system (4.1.1) for $\omega = 0.68$, $q_1 = 1$, and varying q_2: (a) $q_2 = 0.9774$, (b) $q_2 = 0.9775$, (c) $q_2 = 0.9850$.

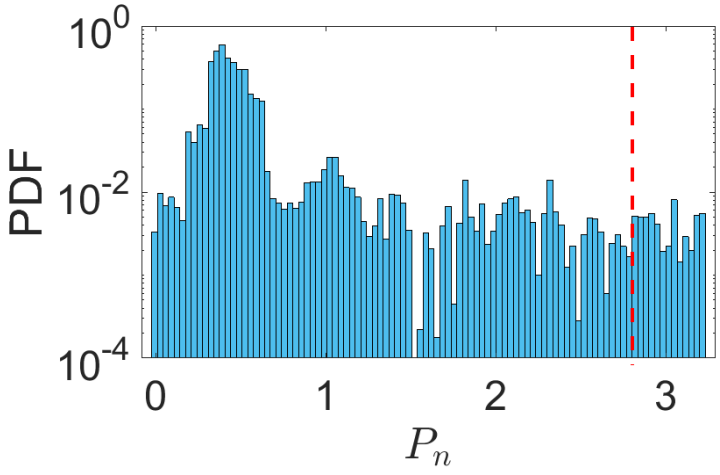

(a)

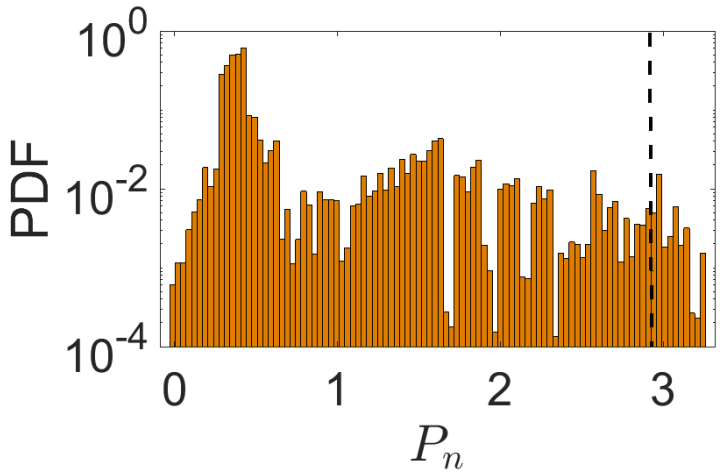

(b)

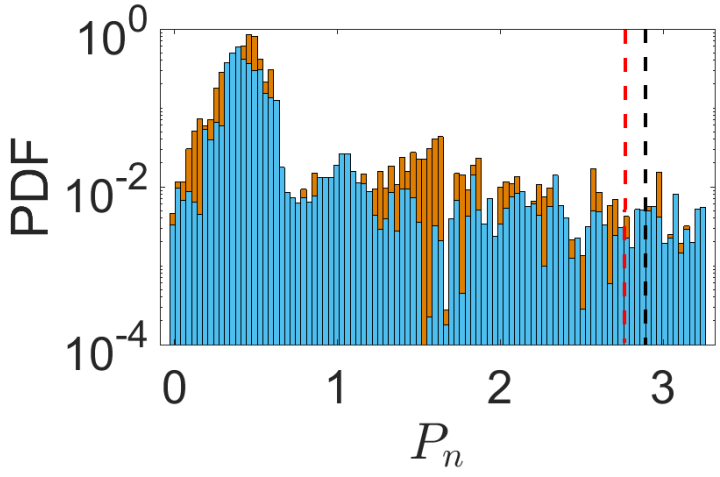

(c)

Figure 4.12: Numerical PDF of P_n for different incommensurate order values for (a) $[q_1, q_2] = [0.9780, 1]$, (b) $[q_1, q_2] = [1, 0.9775]$, (c) combination of sub-figures (a) and (b). Vertical dashed lines present the thresholds H_s.

Table 4.3: Dynamic cases with different values of a, b, and c.

Dynamic cases	Values of a	Values of b	Values of c
Bounded chaos	0.46	0.55	0.4
Extreme events	0.459	0.50	0.5
Multiple large-amplitude events	0.30	0.35	0.55

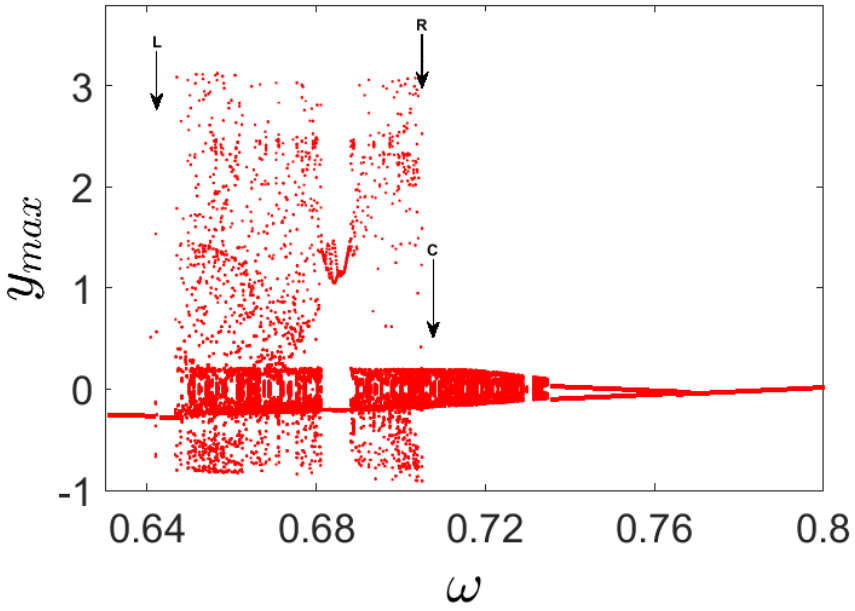

Figure 4.13: Bifurcation diagram for commensurate order $q = 0.996$ and varying $\omega \in (0.63, 0.8)$.

Now, for the commensurate order $q = 0.996$, fixing $d = 0.20, w = 0.65$ and varying system parameters a, b, c, the bifurcation diagrams and time series of fractional system (4.1.1) are reported in Figs. 4.15-4.17. Here, a transition from small to large amplitude chaotic oscillations is clearly observed through interior crisis with decreasing parameters a, b and with increasing parameter c . Thus, in this case extreme events occur via an interior crisis. Also, the thresholds H_S (the horizontal red lines in Figs. 4.15, 4.16, 4.17) are estimated numerically using the $y(t)$ state variable to distinguish extreme events for all different cases which are mentioned in Table 4.3.
The PDF of all the peaks P_n and the H_S are estimated and illustrated in Fig. 4.18 for: $a = 0.459$, $b = 0.50$, and $c = 0.50$. From Fig. 4.18, it can be seen long-tailed distributions confirming the existence of larger events exceeding the height H_S (dashed vertical line). As a remark for the incommensurate system, the same results are founded when varying q_1 and q_2.

Coexisting multiple extreme events

Recently, coexistence of attractors are found in fractional-order systems [148]. Coexistence of attractors appears when the system exhibits more than attractor for the same set of system parameters and taking different set of initial conditions. So, it is depending by the basin of attraction of the system.
In section 4.1.2, the fractional system (4.1.1) appeared existence of multistability too, but with coexisting of chaotic and quasiperiodic attractors. It interests if it is possible the proposed fractional-order forced Liénard

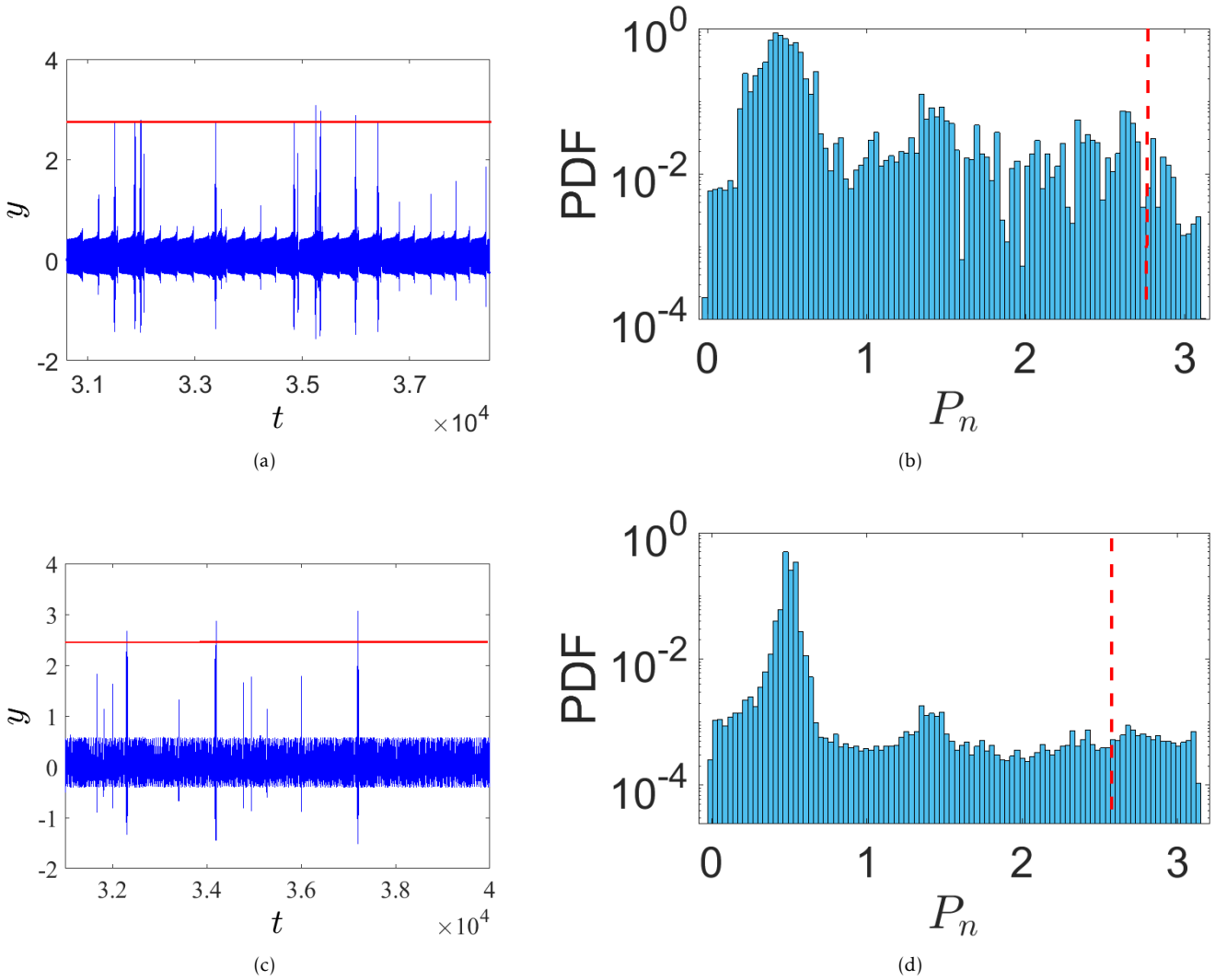

Figure 4.14: Time series and numerical PDF of P_n with commensurate order $q = 0.996$ for (a)-(b) $\omega = 0.647$ (arrow L in Fig.4.13) and (c)-(d) $\omega = 0.7055$ (arrow R in Fig.4.13) . The red line indicates threshold H_s.

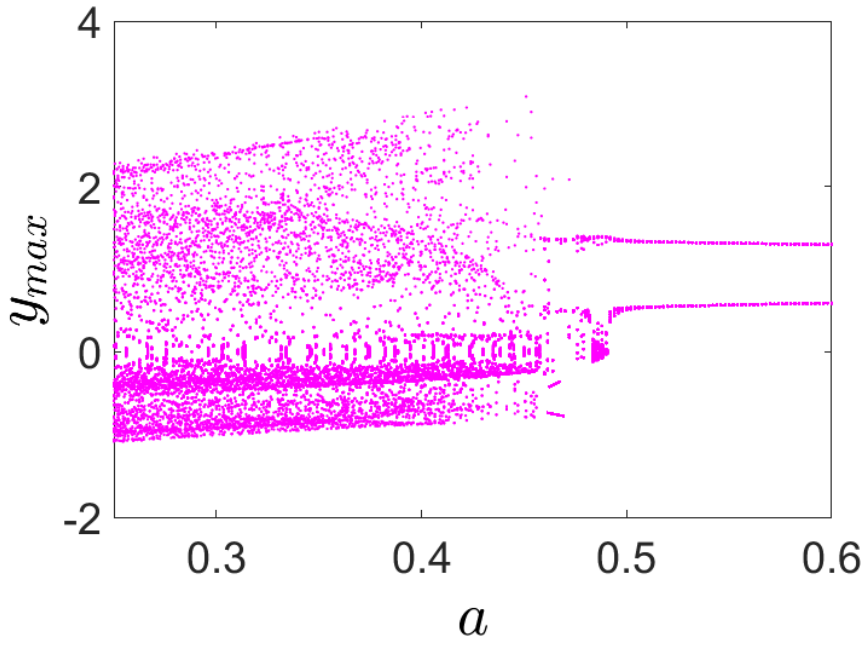

(a)

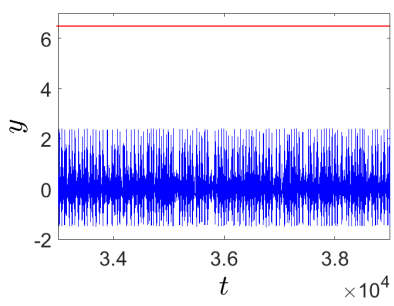

(b)

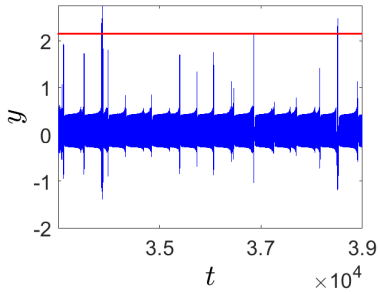

(c)

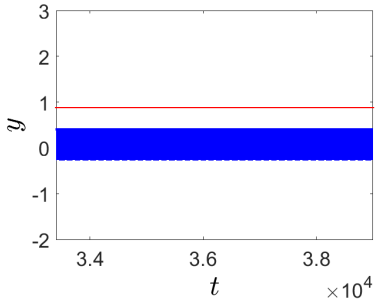

(d)

Figure 4.15: (a) Bifurcation diagram and time series for commensurate order $q = 0.996, \omega = 0.65$ and varying parameter a: (b) multiple large extreme events for $a = 0.30$, (c) extreme events for $a = 0.459$, (d) bounded chaos for $a = 0.46$.

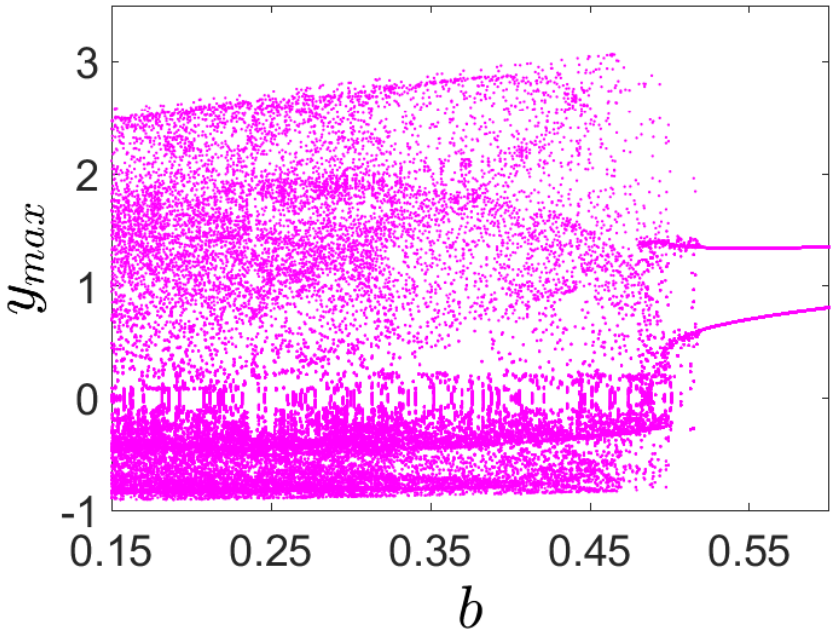

(a)

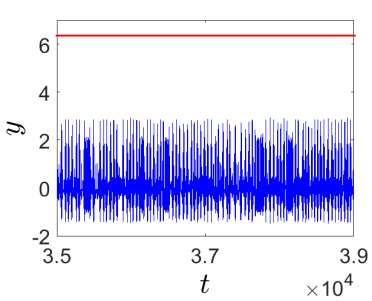

(b)

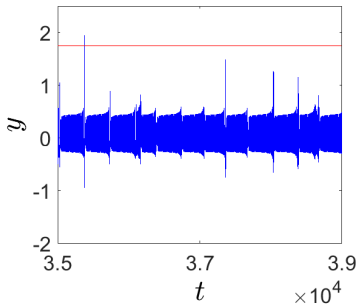

(c)

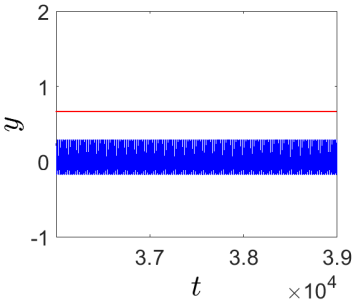

(d)

Figure 4.16: (a) Bifurcation diagram and time series for commensurate order $q = 0.996, \omega = 0.65$ and varying parameter b: (b) multiple large extreme events for $b = 0.35$, (c) extreme events for $b = 0.50$, (d) bounded chaos for $b = 0.55$.

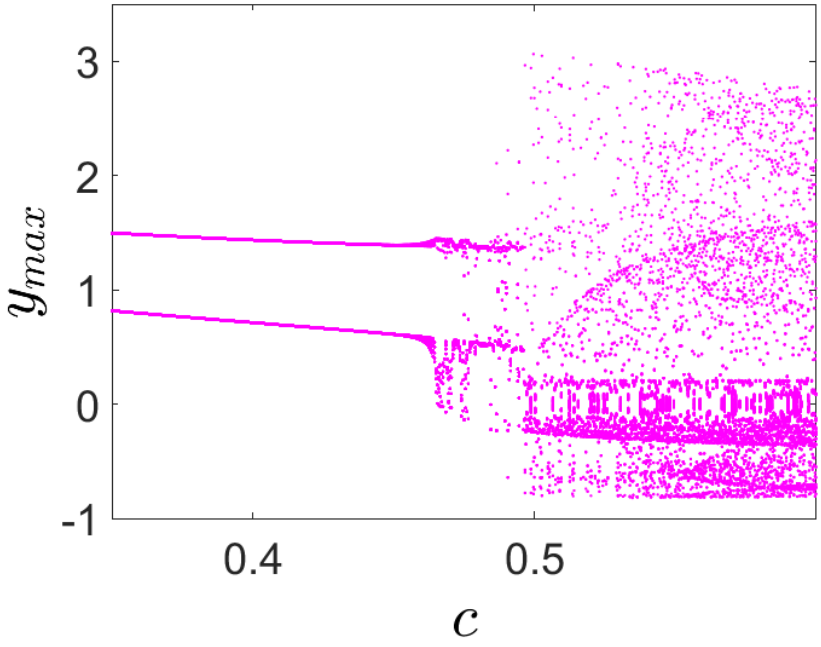

(a)

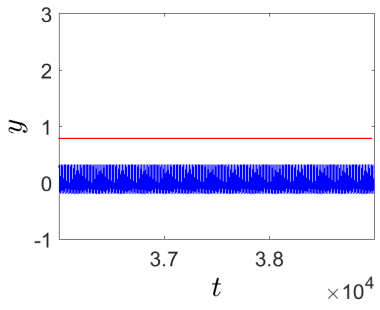

(b)

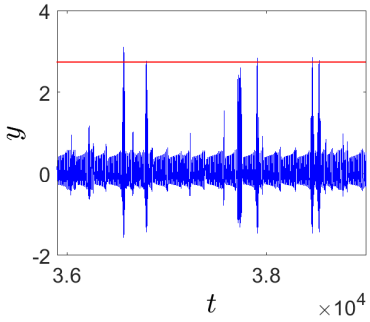

(c)

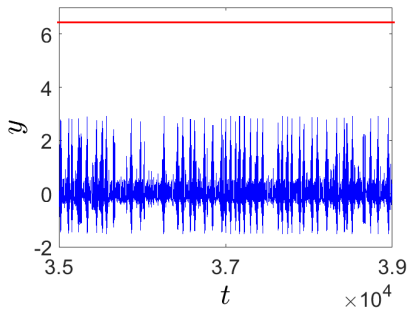

(d)

Figure 4.17: (a) Bifurcation diagram and time series for commensurate order $q = 0.996, \omega = 0.65$ and varying parameter c: (b) bounded chaos for $c = 0.40$, (c) extreme events for $c = 0.50$, (d) multiple large extreme events for $c = 0.55$.

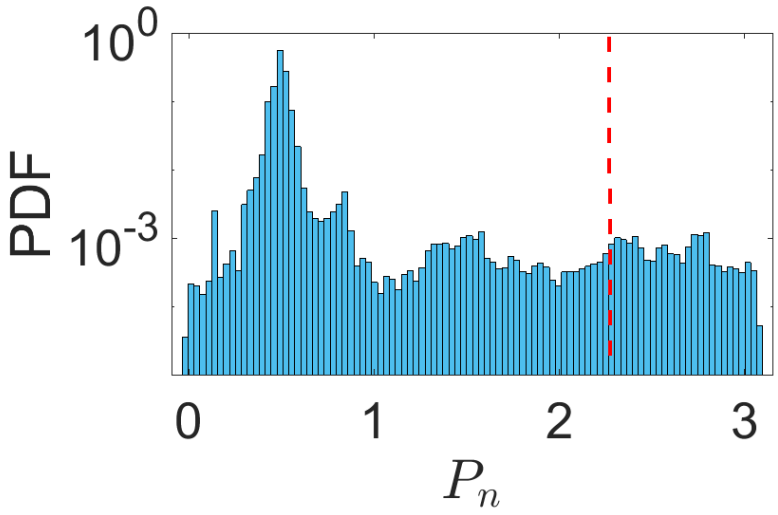

(a)

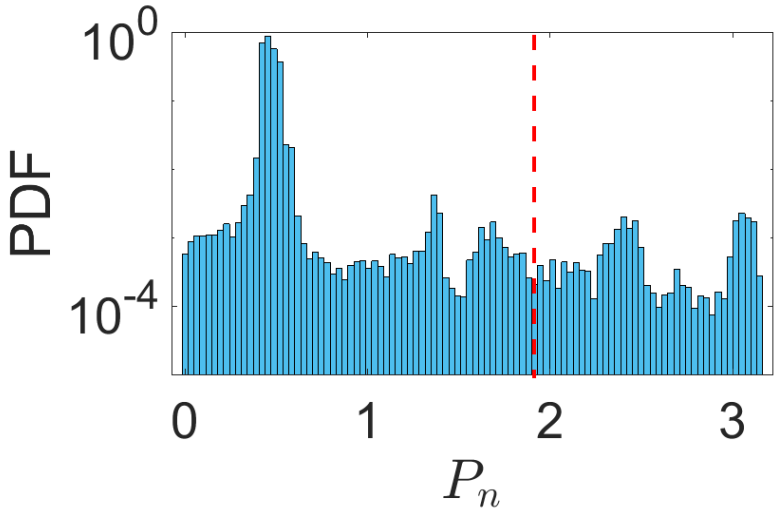

(b)

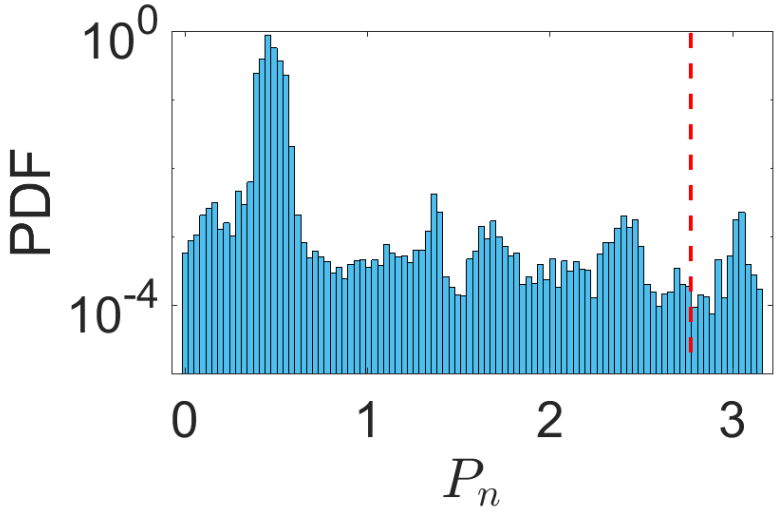

(c)

Figure 4.18: Numerical PDF of P_n for: (a) $a = 0.459$, (b) $b = 0.50$ and (c) $c = 0.50$. Long tail distribution exceeding the significant height H_S in vertical red dashed lines.

system can exhibits a multiple of coexisting attractors and therefore a multiple of extreme events. For this reason, we choose parameter set of initial conditions from the dissipative basin of attraction (BAD) of the forced Liénard system which is shown in Fig. 4.2. Space trajectories on $x-y$ plane and time series are plotted in Fig. 4.19 for three initial conditions: $(1,-0.5);(0,-0.5);(2;-0.5)$. It is founded here that the fractional system (4.1.1) exhibits multistability and coexistence of multiple extreme events.

4.1.4 Conclusion

We introduce a fractional system derived from a Liénard-type oscillator. Dynamics of the fractional system are studied. The system exhibits chaos, multistability, and extreme events. By varying parameters of the commensurate and incommensurate fractional-order cases, we have reported the effect of fractional-order derivative on the extreme events. Different tools such as bifurcation diagrams, Lyapunov exponents, extreme event qualifier H_s, and numerical PDFs have been applied. Interestingly, we have observed multistability and coexistence of multiple extreme events in such a fractional system exhibits. We believe that extreme events should be discovered further in fractional systems.

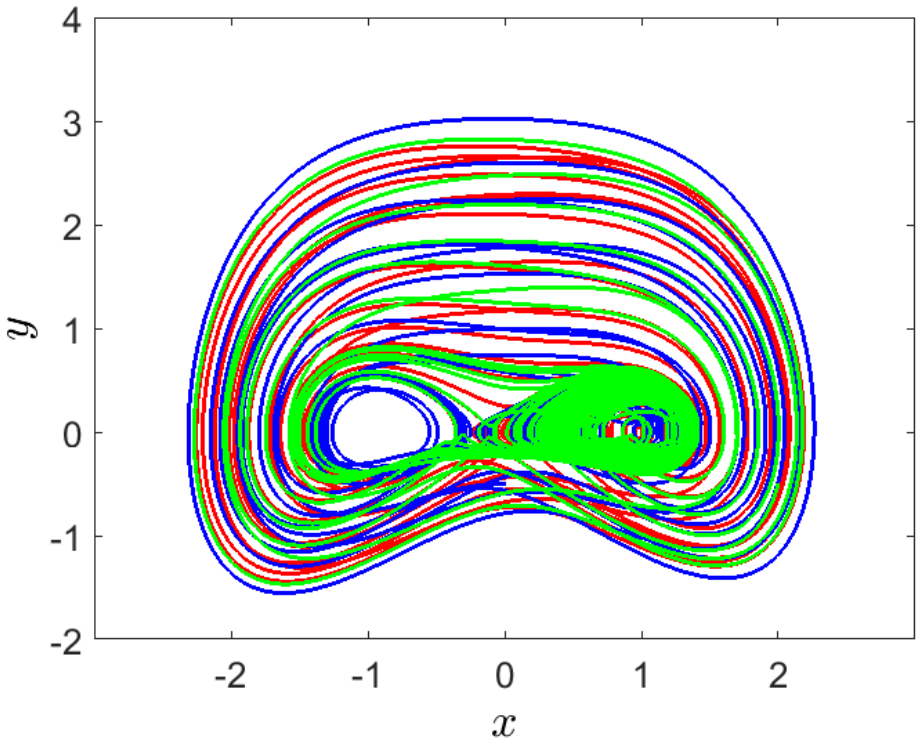

(a)

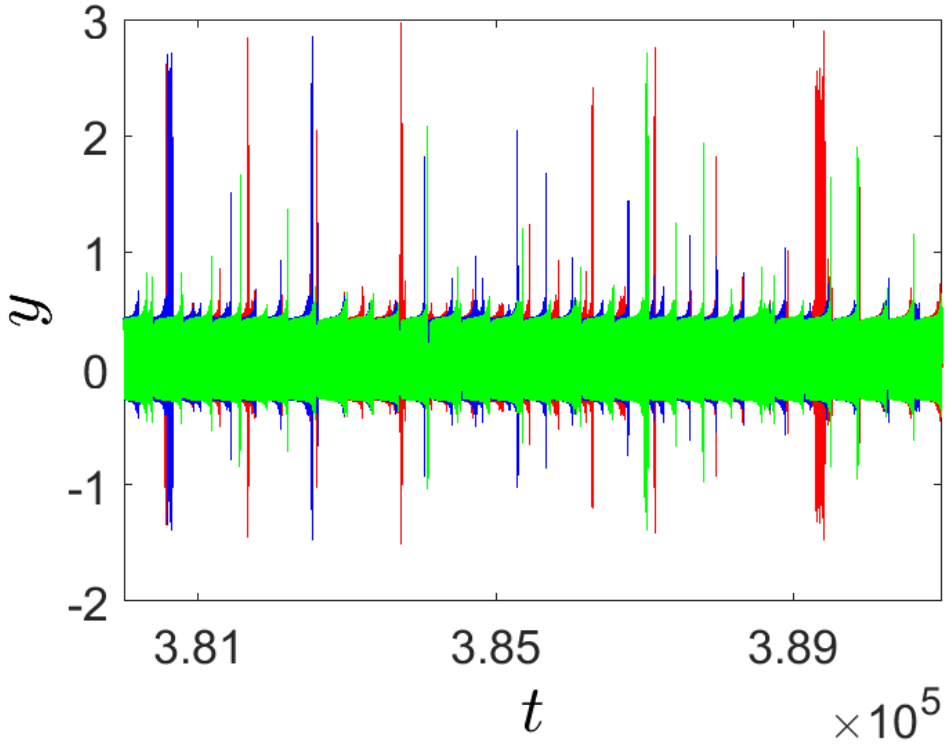

(b)

Figure 4.19: Coexisting multiple extreme events for $q = 0.993, \omega = 0.65$ and different initial conditions: blue plot for $(1, -0.5)$, red plot for $(0, -0.5)$ and green plot for $(2, -0.5)$. (a) Coexisting multiple attractors with occasional large excursion of the trajectories in $x - y$ plane, (b) Time series of fractional system (4.1.1) reveal the coexisting of multiple extreme events.

4.2 Chaotic Behavior Analysis of a New Incommensurate Fractional-Order Hopfield Neural Network System

The content of this section has been published in [17].

4.2.1 Introduction

The artificial neural networks, which is deemed one of the deepest learning technologies that included under the rubric of the so-called artificial intelligence, have recently received a considerable amount of interest by many researchers whose practical work associates with the human brain [149]. In order to make an effective progress with the development of modern engineering and electronics, it is necessarily to continuously attempt to improve this intelligent scheme. In 1943, Mcculloch and Pitts are the first ones who studied the artificial neural networks. In conformity with their investigation, numerous benign engineering and electronic applications have been employed in several applied fields. For instance, switching in electronic circuits, the oscillation of systems in accordance with the impact of an earthquake, image and signal processing, impacting machines, power circuits, and dry friction are some of such applications. In 1982, with the aim of dealing with some optimization and computational issues, and to conquer some specific problems associated with the hardwares' execution, a novel memory neural network was established by Hopfield called later on the Hopfield Neural Network (HNN). At the current time, this type of networks has begun taking its place in different industrial sectors, motivating a lot of investigators to further explore the dynamical properties for its states, and moreover deduce other ones.
Due to the key role of using the fractional calculus in formulating many phenomena rather than that of using the classical calculus, the HNNs were fractionalized to be later on called the Fractional-order Hopfield Neural Networks (FoHNNs). The basic idea of the FoHNNs' birth may be returned to Boroomand and Menhaj who carried out a replacement of the fractance instead of the ordinary capacitor within the classical HNN model. The key benefit of such replacement refers to the truth that the derivatives of fractional-order can describe the HNN more efficiency due to the infinite memory and some other hereditary properties that can be generated from its various processes [150]. From a different point of view, the inclusion process of a memory term into the HNN model by incorporating the fractional-order derivatives/integrals can provide a super calculation capability, which might be needed in, e.g., the stimulus anticipation and the information processing as well as other calculations associated with the oscillatory neuronal firing. For these reasons and more, the analysis of FoHNNs is recently considered one of the main promising topics that benefits future researchers in different applied science fields. Several significant numerical findings related to the presence of the chaotic behavior and the limit cycles for the dynamics of the FoNN are discussed in literature. For instance, the stability of the FoHNN was fully investigated through energy-like function analysis in [**?**]. Whereas a theoretical approach, based on the harmonic balance theory, was used to investigate the existence of chaos for a cellular neural networks model in [151]. A chaos neuron model was proposed and examined as novel artificial neuron model in [152]. Whereas in [22] a fractional-order cellular neural networks model was introduced by replacing the traditional first-order cell by fractional-order one. The chaotic synchronization of such networks was also discussed in several other papers. We find, for example, certain chaotic behaviors in the time-delayed FoNN system were studied well in [153]. While, the chaos feedback control and synchronization systems were constructed for a neuron network system by Zhou et al. in [154]. One year after, Zhou et al. came once again to illustrate the chaotic synchronization system for a FoNN system in [155]. In [156], the Laplace transform and the generalized Gronwall inequality were employed to examine the FoHNN models in terms of its finite-time stability, whereas various dynamic features, like constructing bifurcation diagrams, chaos, stability and multi-stability of the FoNNs were studied in [150]. In [157], an α-synchronization

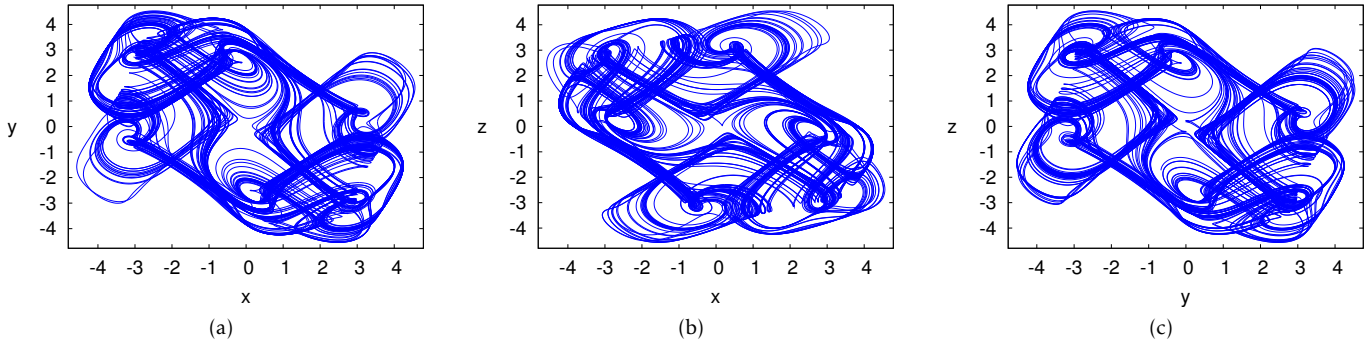

(a) (b) (c)

Figure 4.20: Chaotic attractor of system (4.2.1) when $q = 1$ according to the system parameters $a = 1$, $b = -9$ and the IC $(x_0, y_0, z_0) = (-1, 1, 1)$ on: (a) xy-plan, (b) xz-plan and (c) yz-plan.

and an α-stability were determined and explored for the FoNN models, whereas a uniform stability of such models was described and analyzed with time-delay in [134] with the help of using an efficient kind of error norm. In light of the several applications of the FoHNN models in different applied science fields and in order to go forward in further exploring more properties of the FoHNNs dynamics, this paper attempts to study different chaotic dynamics of such networks with incommensurate-order. Besides, it intends to analyze the stability of the proposed system numerically by continuous varying the fractional-order derivative values as well as the values of system's parameters. Such analysis will be carried out by performing several numerical simulations, like constructing the diagrams of bifurcation, computing Lyapunov exponents, calculating Lyapunov dimensions, and sketching the phase portraits in 2D- and 3D-projections.

4.2.2 Mathematical model

In [150], a mathematical model of FoHNN with ring structure was established, and its stability analysis was discussed in view of some feature parameters. Such model was formulated by the following three-dimensional system:

$$\begin{cases} D^q x(t) = -x(t) + 2sin(x(t)) + asin(y(t)) + bsin(z(t)), \\ D^q y(t) = -y(t) + bsin(x(t)) + 2sin(y(t)) + asin(z(t)), \\ D^q z(t) = -z(t) + asin(x(t)) + bsin(y(t)) + 2sin(z(t)), \end{cases} \tag{4.2.1}$$

where a and b are the system's parameters, D^q is the Caputo differential operator of order q, and x, y, z are the states of the system. As a matter of fact, Kaslik et al. studied and analyzed in [150] the stability of the above system by taking its fractional-order derivatives in commensurate-order case. To illustrate the neural network system, Fig. 4.20 appears the phase portraits in different planes of the choatic integer system (4.2.2) when $q = 1$. The basin of attarction of the integer system is shown in Fig. 4.21 where the initial conditions (ICs) in yellow region lead to the limit cycles in blue region lead to chaotic attractor.

In this work, we assert that if we change these derivatives to be in its incommensurate-order case, then such system will exhibit more rich complex dynamics and more chaotic patterns comparing to the previous model reported in [150]. Thus, the new incommensurate fractional-order version of the previous HNN model, which will be considered from now on, can be formulated as follows:

$$\begin{cases} D^{q_1} x(t) = -x(t) + 2sin(x(t)) + asin(y(t)) + bsin(z(t)), \\ D^{q_2} y(t) = -y(t) + bsin(x(t)) + 2sin(y(t)) + asin(z(t)), \\ D^{q_3} z(t) = -z(t) + asin(x(t)) + bsin(y(t)) + 2sin(z(t)), \end{cases} \tag{4.2.2}$$

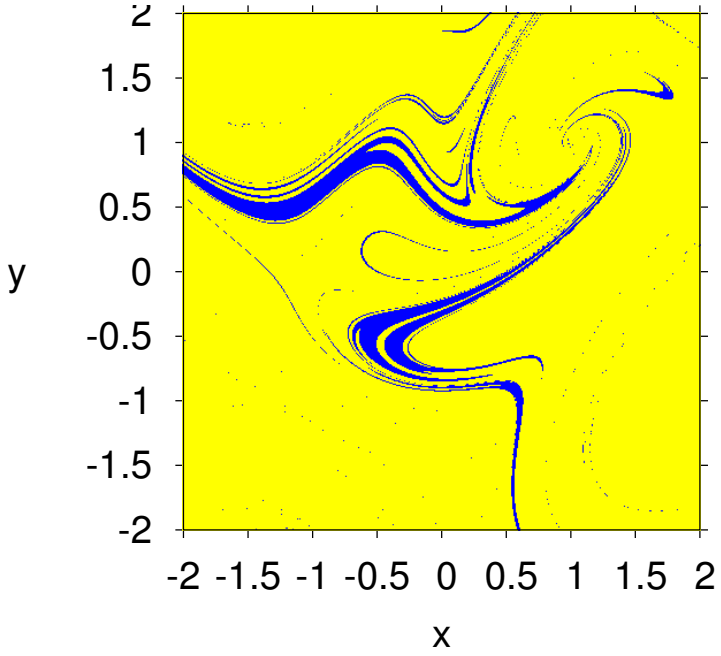

Figure 4.21: Basin of attraction of system (4.2.1) when $q = 1$ according to the system parameters $a = 1$, $b = -9$ and to the initial condition of the third state variable z = 0.

where a, b, x, y and z are defined above, while D^{q_i} is the Caputo differential operator of order q_i such that $0 < q_i \leq 1$ and $i = 1, 2, 3$. Actually, in order to solve the above system, one can implement the predictor-corrector method which was proposed by Diethelm et al. in [158]. Although this method can provide an accurate solution of a given nonlinear fractional-order system numerically, an enhanced approach called Adams-Bashforth-Moulton scheme was established in.

4.2.3 Dynamics of incommensurate fractional-order model

In this section, different complex dynamics of the incommensurate FoHNN model (4.2.2) will be numerically studied and analyzed; including discussion the stability analysis versus taking different values of incommensurate fractional-order derivatives and also of system's parameters, and presenting some special phenomena that could be generated from the proposed model such as presenting the so-called symmetry and coexisting attractors. For this purpose, several numerical tools will be used for performing some required simulations; including constructing bifurcation diagrams, sketching the phase portraits of the system dynamics in 2D- and 3D-projections, also, plotting the basin of attractions and computing Lyapunov exponents/dimensions.

Stability vs. different incommensurate fractional-order derivatives

Here, we will take the two parameters of the system as $a = 1$ and $b = -9$ as well as we will consider the Initial Condition (IC) of the states of system (4.2.2) as $(x_0, y_0, z_0) = (-1, 1, 1)$. In this part, we intend to study the stability of model (4.2.2) according to the following three cases: The first one is carried out by fixing $q_2 = q_3 = 1$ and continuous varying the value of q_1, while the second one by fixing $q_1 = q_2 = 1$ and continuous varying the value of q_2, and finally the third one which is implemented by fixing $q_1 = q_2 = 1$ and continuous varying the value of q_3. Accordingly, the bifurcation diagrams, Lyapunov exponents for such three cases are plotted in Fig. 4.22, Fig. 4.25 and Fig. 4.28, respectively. Based on these figures, one can observed the existence of positive Lyapunov exponents, confirming that the FoHNN system (4.2.2) shows chaotic behavior. In addition, one might notice, from

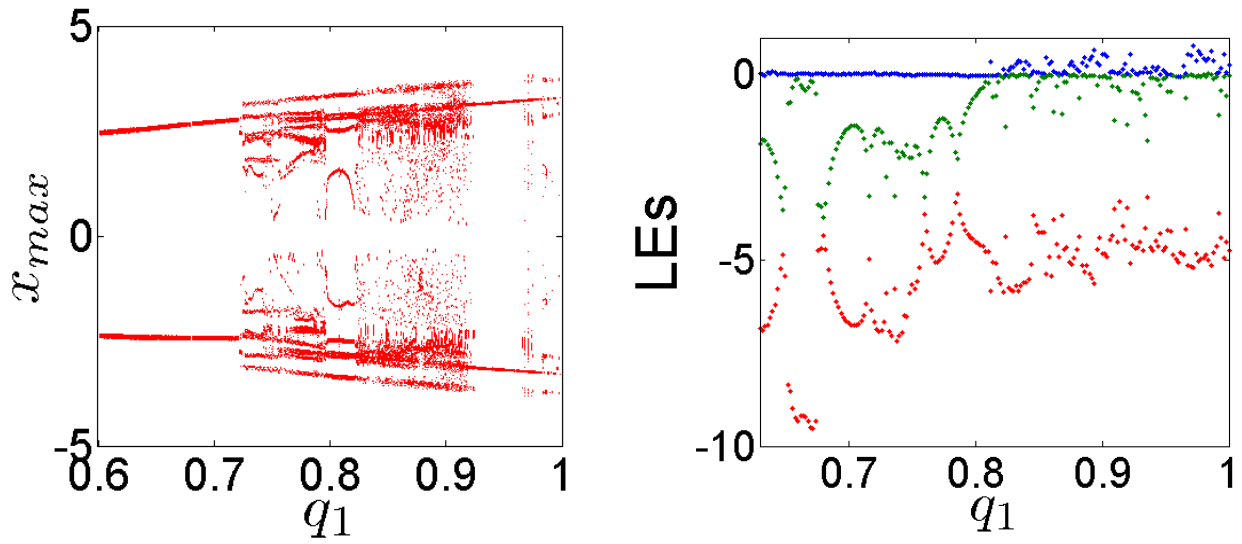

(a) (b)

Figure 4.22: (a) The diagram of bifurcation, (b) Lyapunov exponents of system (4.2.2) when $q_1 \in (0.6, 1)$ and $q_2 = q_3 = 1$ according to the system parameters $a = 1$, $b = -9$ and the IC $(x_0, y_0, z_0) = (-1, 1, 1)$.

such figures again, that system (4.2.2) is asymptotically stable to a limit cycles when $q_1, q_2, q_3 \in (0.6, 0.73)$, while it begins losing its stability and begins behaving in a chaotic mode when $q_1 \in (0.82, 1)$, $q_2 \in (0.83, 1)$ and $q_3 \in (0.84, 1)$. It might be further noticed that once the values of the incommensurate fractional-order derivatives are increased, different periodic windows will be shown. For instance, to deal with the aforesaid three cases, we may take the values of the fractional-order derivatives as $q_1 = 0.89$ and $q_2 = q_3 = 1$, which, directly, implies the three Lyapunov exponents: $LE_1 = 0.26$, $LE_2 = 0$ and $LE_3 = -4.39$ with noting that $|0.26| < |-4.398|$. On the other hand, if one takes $q_2 = 0.90$ and $q_1 = q_3 = 1$, then the following three Lyapunov exponents will be yielded: $LE_1 = 0.51$, $LE_2 = 0$ and $LE_3 = -2.63$ with noting that $|0.51| < |-2.63|$. Finally, taking $q_3 = 0.87$ and $q_1 = q_2 = 1$ gives the following three Lyapunov exponents: $LE_1 = 0.31$, $LE_2 = 0$ and $LE_3 = -5.06$ with noting that $|0.31| < |-5.06|$. Consequently, the corresponding Lyapunov dimension, which is considered an estimation of the complexity of generated attractor from the system, can be calculated according to the previous three cases by considering the following formula:

$$D_{KY} = j + \frac{1}{|LE_{j+1}|} \sum_{i=1}^{j} LE_i,$$

where j is the greatest integer number that satisfies $\sum_{i=1}^{j} LE_i \geq 0$ and $\sum_{i=1}^{j+1} LE_i < 0$. In other words, the calculated Lyapunov dimensions of system (4.2.2) according to the previous values of incommensurate fractional-order derivatives are $D_{KY} = 2.09 > 2$, $D_{KY} = 2.19 > 2$ and $D_{KY} = 2.06 > 2$, respectively. This, consequently, leads us to deduce that there is a chaotic attractor of system (4.2.2). To see this, Fig. 4.23, Fig. 4.26 and Fig. 4.29 present complex chaotic attractor of system (4.2.2) on different 2D-projections according to the three considered cases: ($q_1 = 0.89$ and $q_2 = q_3 = 1$), ($q_2 = 0.90$ and $q_1 = q_3 = 1$) and ($q_3 = 0.87$ and $q_1 = q_2 = 1$), respectively. In addition, Fig. 4.24, Fig. 4.27 and Fig. 4.30 exhibit the corresponding 3D-projections of the chaotic attractors that generated by system (4.2.2).

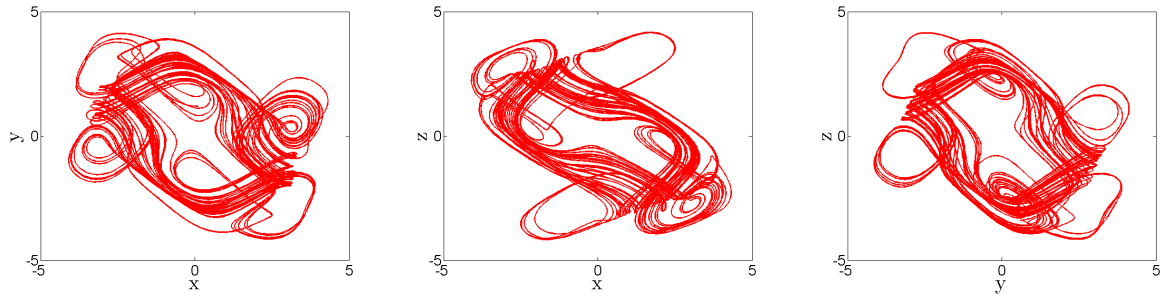

Figure 4.23: Chaotic attractor of system (**??**) when $q_1 = 0.89$ and $q_2 = q_3 = 1$ according to the system parameters $a = 1$, $b = -9$ and the IC $(x_0, y_0, z_0) = (-1, 1, 1)$ on: (a) xy-plan, (b) xz-plan and (c) yz-plan.

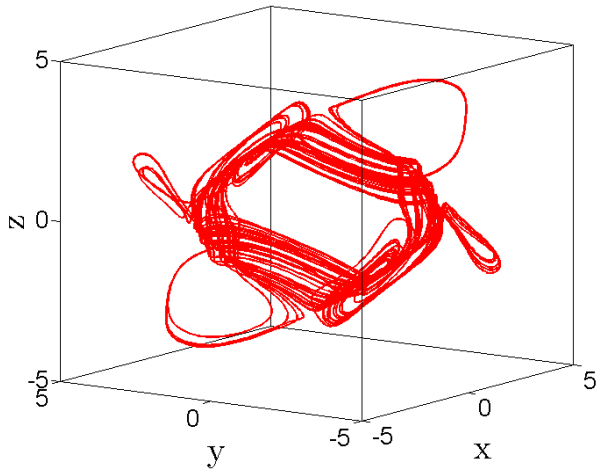

Figure 4.24: Chaotic attractor of system (4.2.2) on 3D-projections when $q_1 = 0.89$ and $q_2 = q_3 = 1$ according to the system parameters $a = 1$, $b = -9$ and the IC $(x_0, y_0, z_0) = (-1, 1, 1)$

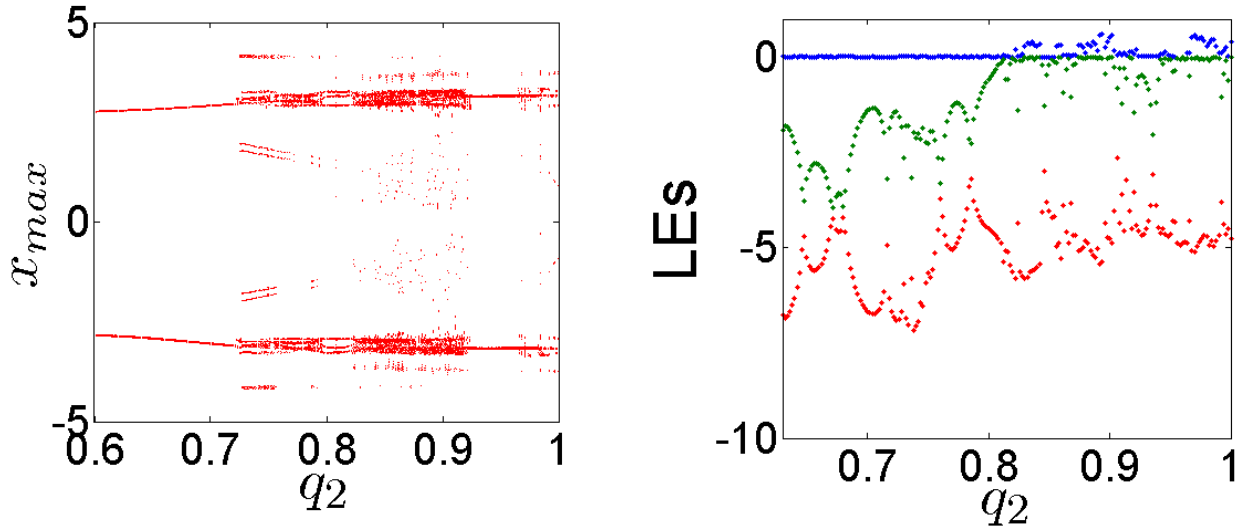

Figure 4.25: (a) The diagram of bifurcation, (b) Lyapunov exponents of system (4.2.2) when $q_2 \in (0.6, 1)$and $q_1 = q_3 = 1$ according to the system parameters $a = 1$, $b = -9$ and the IC $(x_0, y_0, z_0) = (-1, 1, 1)$.

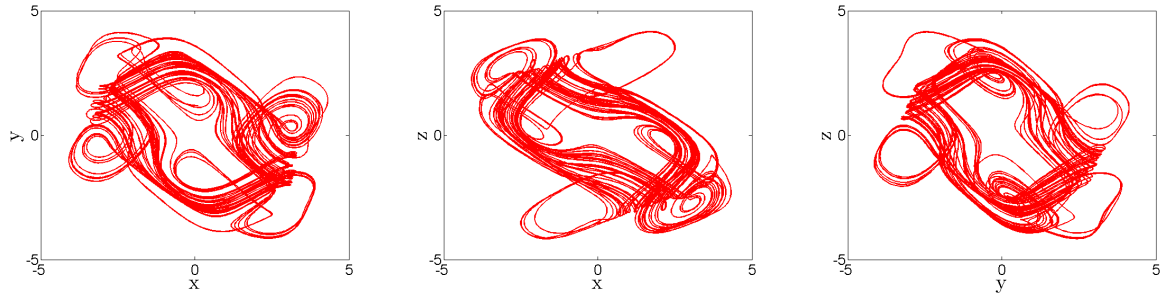

Figure 4.26: Chaotic attractor of system (4.2.2) when $q_2 = 0.90$ and $q_1 = q_3 = 1$ according to the system parameters $a = 1$, $b = -9$ and the IC $(x_0, y_0, z_0) = (-1, 1, 1)$ on: (a) xy-plan, (b) xz-plan and (c) yz-plan.

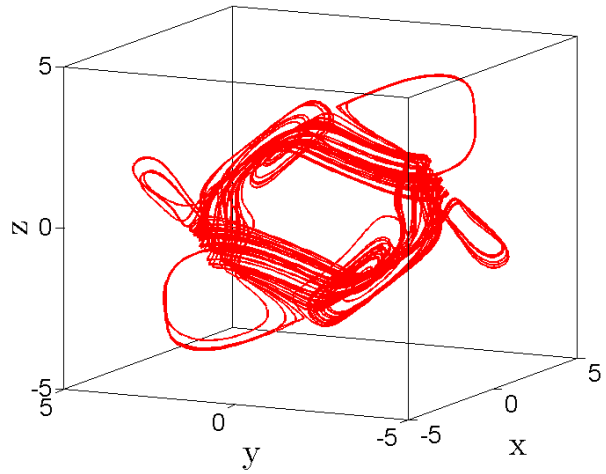

Figure 4.27: Chaotic attractor of system (4.2.2) on 3D-projections when $q_2 = 0.90$ and $q_1 = q_3 = 1$ according to the system parameters $a = 1$, $b = -9$ and the IC $(x_0, y_0, z_0) = (-1, 1, 1)$.

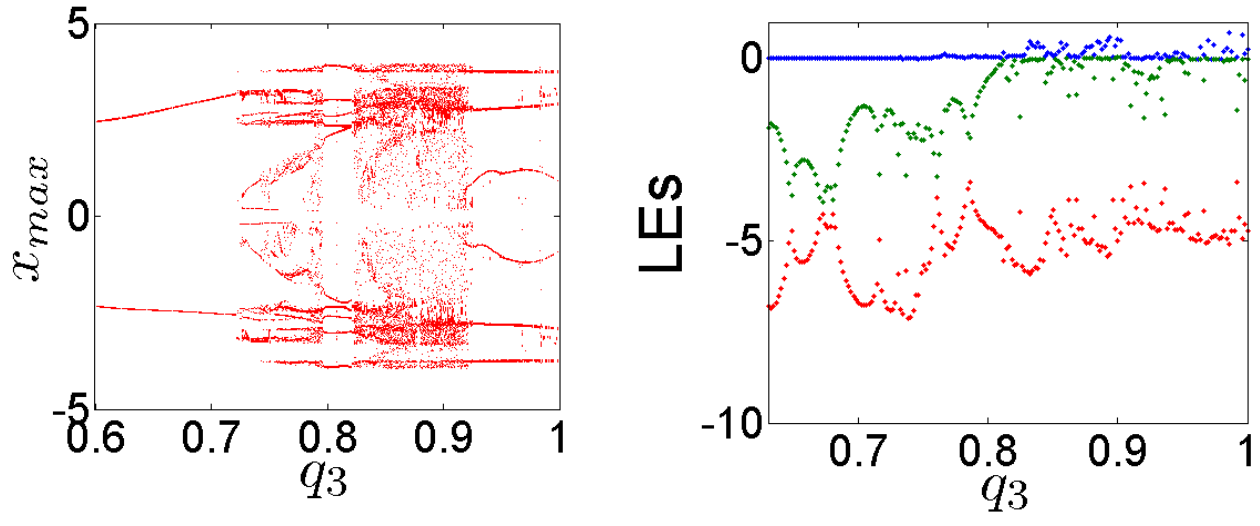

Figure 4.28: (a) The diagram of bifurcation, (b) Lyapunov exponents of system (4.2.2) when $q_1 \in (0.6, 1)$and $q_2 = q_3 = 1$ according to the system parameters $a = 1$, $b = -9$ and the IC $(x_0, y_0, z_0) = (-1, 1, 1)$.

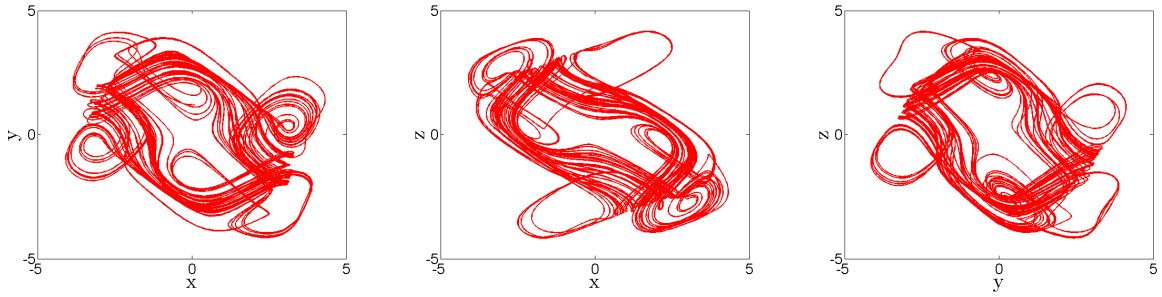

Figure 4.29: Chaotic attractor of system (4.2.2) when $q_3 = 0.87$ and $q_1 = q_2 = 1$ according to the system parameters $a = 1$, $b = -9$ and the IC $(x_0, y_0, z_0) = (-1, 1, 1)$ on: (a) xy-plan, (b) xz-plan and (c) yz-plan.

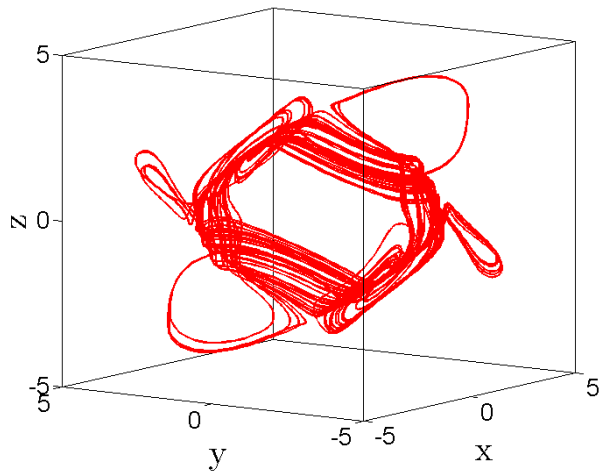

Figure 4.30: Chaotic attractor of system (4.2.2) on 3D-projections when $q_3 = 0.87$ and $q_1 = q_2 = 1$ according to the system parameters $a = 1$, $b = -9$ and the IC $(x_0, y_0, z_0) = (-1, 1, 1)$.

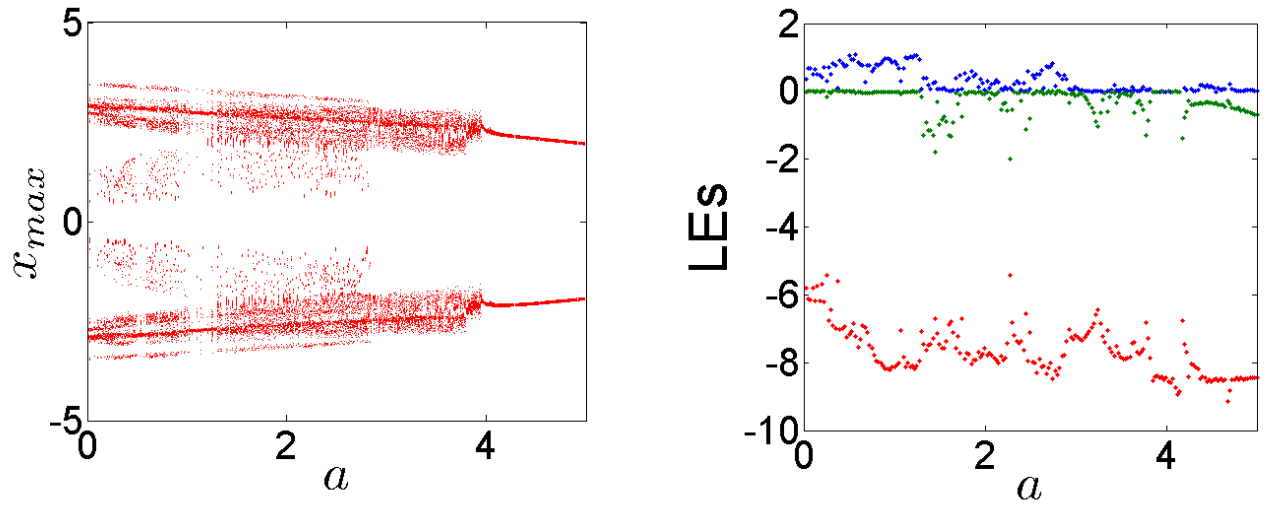

(a) (b)

Figure 4.31: (a) The diagram of bifurcation, (b) Lyapunov exponents of system (4.2.2) when $a \in (0,5)$ according to the other system parameter $b = -9$, the incommensurate fractional-order $[q_1, q_2, q_3] = [0.8, 0.90, 0.91]$ and the IC $(x_0, y_0, z_0) = (-1, 1, 1)$.

Stability vs. different values of the system parameters

This subsection will explore the stability of system (4.2.2) by continuous varying the values of the system parameters a and b and by fixing the incommensurate fractional-order derivative values at $[q_1, q_2, q_3] = [0.8, 0.90, 0.91]$ as well as fixing the IC at $(x_0, y_0, z_0) = (-1, 1, 1)$. Immediately, Fig. 4.31 and Fig. 4.32 represent the bifurcation diagrams togather with the Lyapunov exponents of system (4.2.2) when $a \in (0,5)$ and $b \in (-20, 0)$, respectively. One might observe based on such plots that when the values of the system parameters are decreased, system (4.2.2) will be asymptotically stable, and then it will exhibit periodic oscillations to chaos. Moreover, the chaotic ranges with periodic windows will be as $a \in (0, 2.9)$ and $b \in (-20, -7.5)$. Obviously, there exist certain positive Lyapunov exponents within these ranges, confirming the chaotic behavior of system (4.2.2).

Symmetry, bistability and coexisting chaotic attractors

A symmetric dynamical systems are typically obtained when they often exhibit a symmetric pair of coexisting attractors. This property has attracted considerable interest in the field of nonlinear dynamic systems. To obtain a complete overview about such property, the reader may refer to the reference [135]. In regard to our study, we will assume that the system's parameters are $a = 1$, $b = -9$, and we will select two ICs as $(x_0, y_0, z_0) = (1, 1, 1)$ for a red trajectory and $(x_0, y_0, z_0) = (-1, -1, -1)$ for a blue trajectory. In light of these values, we observe that system (4.2.2) will, e.g., generate a symmetric pair of coexisting limit cycles when $[q_1, q_2, q_3] = [0.70, 1, 1]$ (see Fig. 4.33(a)), while it will generate a symmetric pair of coexisting periodic attractors when $[q_1, q_2, q_3] = [0.80, 1, 1]$ (see Fig. 4.33(b)), and moreover it will generate a symmetric pair of coexisting chaotic attractors when for $[q_1, q_2, q_3] = [0.89, 1, 1]$ (see Fig. 4.33(c)).

On the other hand, the bistability property, which is deemed one of the most recent dynamic phenomena of a system, has lured many researchers in recent years. For more clarification about this property, the reader may refer to the reference [**?**]. However, in order to show the bistability within system (4.2.2), we plot the bifurcation diagrams in Fig. 4.34(a) when $[q_1, q_2, q_3] = [0.8, 0.90, 0.91]$ and $a = 1$, $b = -9$. It is worth noting that two sets of

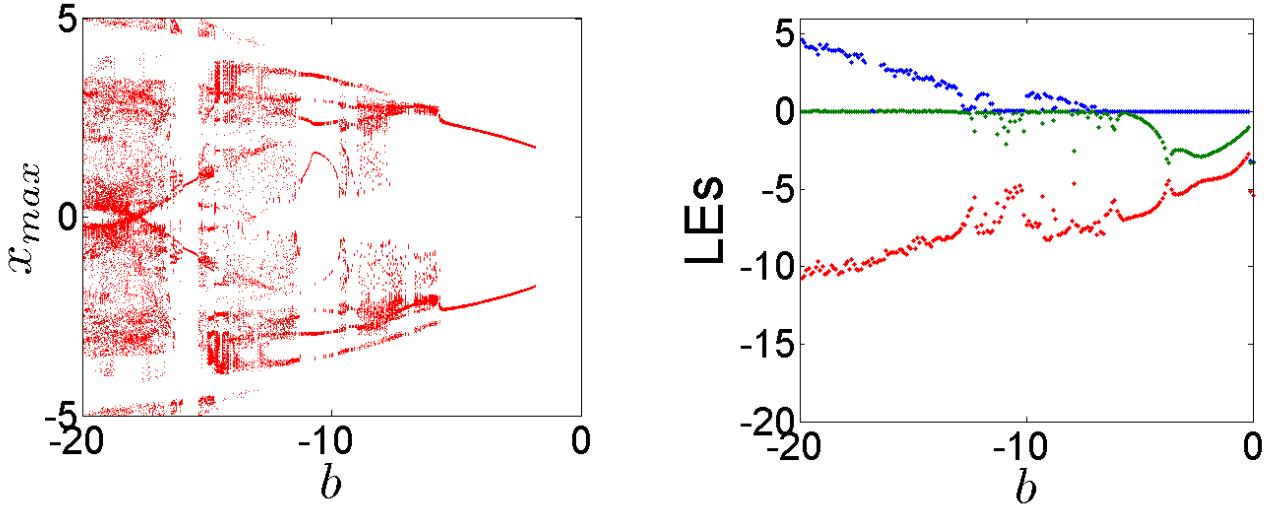

(a) (b)

Figure 4.32: (a) The diagram of bifurcation, (b) Lyapunov exponents of system (4.2.2) when $b \in (-20, 0)$ according to the other system parameter $a = 1$, the incommensurate fractional-order $[q_1, q_2, q_3] = [0.8, 0.90, 0.91]$ and the IC $(x_0, y_0, z_0) = (-1, 1, 1)$.

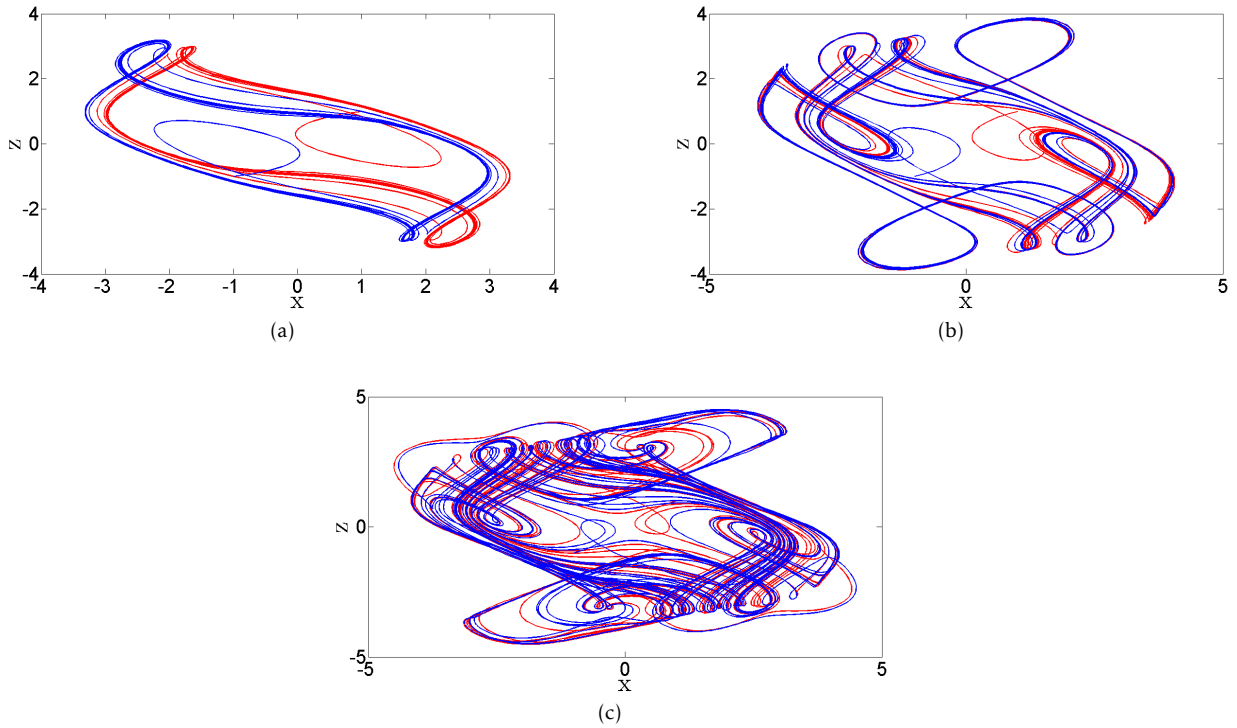

(a) (b) (c)

Figure 4.33: Phase portraits of coexisting symmetric attractors according to the system's parameters $a = 1$, $b = -9$, the IC $(x_0, y_0, z_0) = (1, 1, 1)$ for the red line and the IC $(x_0, y_0, z_0) = (-1, -1, -1)$ for the blue line by continuous varying q_i as: (a) $[q_1, q_2, q_3] = [0.70, 1, 1]$, (b) $[q_1, q_2, q_3] = [0.80, 1, 1]$ and (c) $[q_1, q_2, q_3] = [0.89, 1, 1]$.

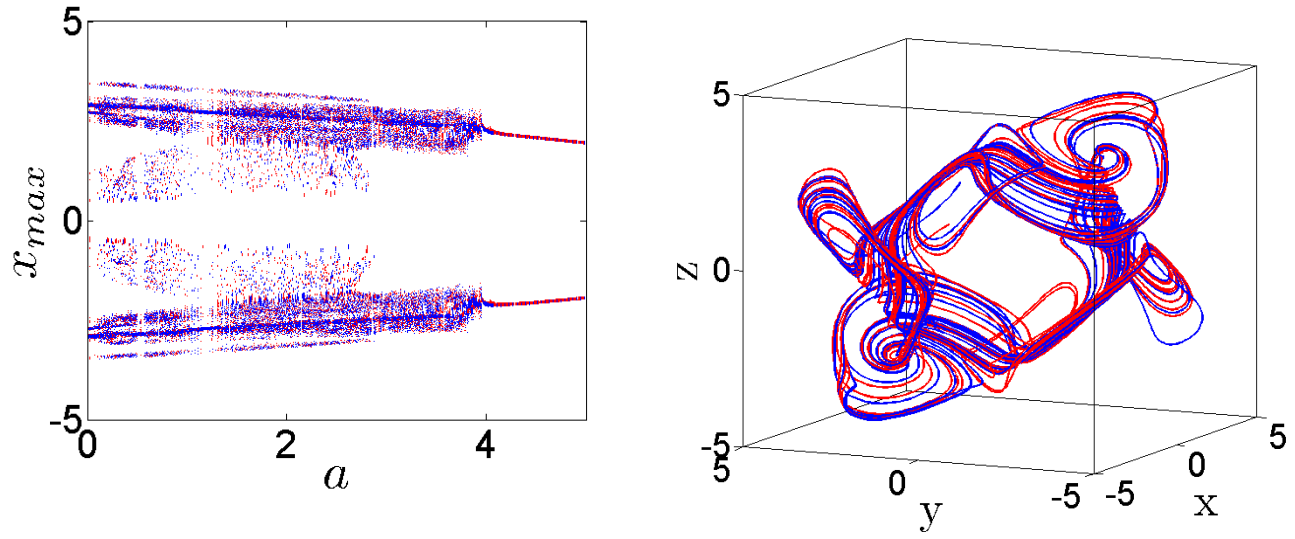

(a) (b)

Figure 4.34: (a) The diagram of bifurcation of system (4.2.2) for continuous varying $a \in (0,5)$, (b) coexisting chaotic attractors for $a = 1$, $b = -9$ and $[q_1, q_2, q_3] = [0.80, 0.90, 0.91]$ subject to the ICs: $(x_0, y_0, z_0) = (-1, 1, 1)$ for the red plot and $(x_0, y_0, z_0) = (0.1, 1.2, 2)$ for the blue plot.

ICs are considered to perform the simulation of such figure. The first one is $(x_0, y_0, z_0) = (-1, 1, 1)$ which was for the red plot, while the second one is $(x_0, y_0, z_0) = (0.1, 1.2, 2)$ which was for the blue plot. These two plots show certainly that system (4.2.2) will exhibit bistability phenomenon if the incommensurate fractional-order value is increased. For $a = 1$, $b = -9$ and $[q_1, q_2, q_3] = [0.80, 0.90, 0.91]$, both coexisting attractors of such system are drawn in Fig. 4.34(b) according to the two ICs: $(x_0, y_0, z_0) = (-1, 1, 1)$ for the red plot and $(x_0, y_0, z_0) = (0.1, 1.2, 2)$ for the blue plot. Furthemore, The basin of attarction of the system (4.2.2) is shown in Fig. 4.35 correspondig to Figs. 4.34(a) and 4.34(b) where the initial conditions (ICs) in yellow region lead to the two region of limit cycles in blue and red colors lead to the two chaotic attractors.

4.2.4 Variable-boostable attractors of incommensurate fractional-order model

With the aim of accomplishing the complete range of the signal's linear transformations, the offset boosting might be jointed with amplitude control. It was reported in [135] that an inserted of anew developed boosting controller may destroy the symmetry of the variable-boostable model. From this perspective, we will add to the system's states x, y, and z three additional controlled scalers m, n, and k respectively. In view of this addition, system (4.2.2) will be turned into the following form:

$$\begin{cases} D^{q_1}x(t) = -(x(t)+m) + 2sin(x(t)+m) + asin(y(t)+n) + bsin(z(t)+k), \\ D^{q_2}y(t) = -(y(t)+n) + bsin(x(t)+m) + 2sin(y(t)+n) + asin(z(t)+k), \\ D^{q_3}z(t) = -(z(t)+k) + asin(x(t)+m) + bsin(y(t)+n) + 2sin(z(t)+k). \end{cases} \tag{4.2.3}$$

In the next subsections, we intend to address system (4.2.3) in light of three different cases for the system's parameters $a = 1$ and $b = -9$. Besides, we will select the incommensurate fractional -order values as $[q_1, q_2, q_3] = [0.80, 0.90, 0.91]$. AS a remark about the choice of initial conditions, When the system has unbounded solutions, the variable boosting should be accompanied with a modification of the initial conditions, while the initial conditions can be ignored in the systems with global attraction.

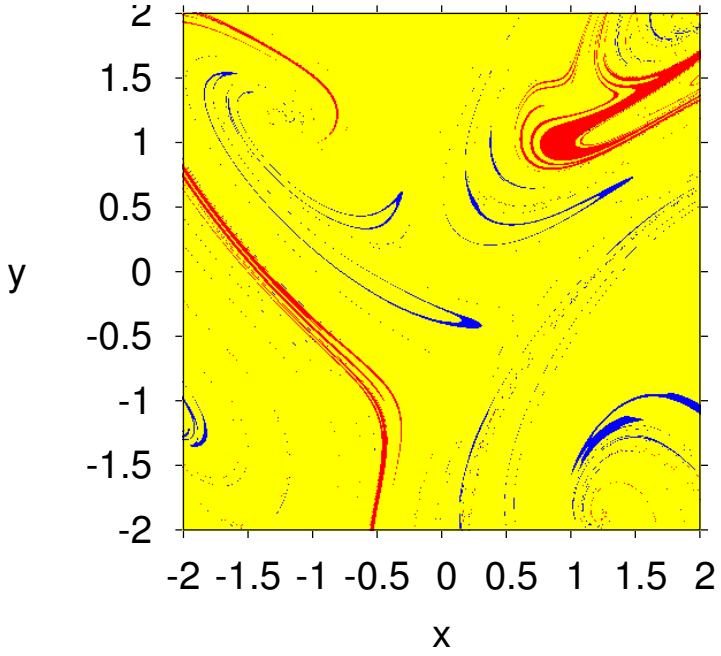

Figure 4.35: Basin of attraction of system (4.2.2) when $[q_1, q_2, q_3] = [0.80, 0.90, 0.91]$ according to the system parameters $a = 1$, $b = -9$ and to the initial condition of the third state variable z = 0.

A line of variable attractors

A variable chaotic attractor can be scattered along 1D-line, if we carried out a certain control so that the offset boosting parameters take the following cases:

- Whenever the parameter m is frequently varied and the rest two parameters be as $n = k = 0$, then we will gain variable chaotic attractors scattered on the x-axis as exhibited in Fig. 4.36(a).
- Whenever the parameter n is frequently varied and the rest two parameters be as $m = k = 0$, then we will gain variable chaotic attractors scattered on the y-axis as exhibited in Fig. 4.36(b).
- Whenever the parameter k is frequently varied and the rest two parameters be as $m = n = 0$, then we will gain variable chaotic attractors scattered on the z-axis as exhibited in Fig. 4.36(c).

A lattice of variable attractors

Herein, two controlled parameters will be simultaneously adjusted and the rest parameter will be kept at zero. This would yield a 2D-lattice of variable chaotic and periodic attractors. In particular, one might consider the following three cases:

- Whenever the two parameters m and n are frequently varied and the third-one parameter be as $k = 0$, then we will gain variable chaotic attractors scattered on the xy-lattice as exhibited in Fig. 4.37(a).
- Whenever the two parameters m and k are frequently varied and the third-one parameter be as $n = 0$, then we will gain variable chaotic attractors scattered on the xz-lattice as exhibited in Fig. 4.37(b).
- Whenever the two parameters n and k are frequently varied and the third-one parameter be as $m = 0$, then we will gain variable chaotic attractors scattered on the yz-lattice as exhibited in Fig. 4.37(c).

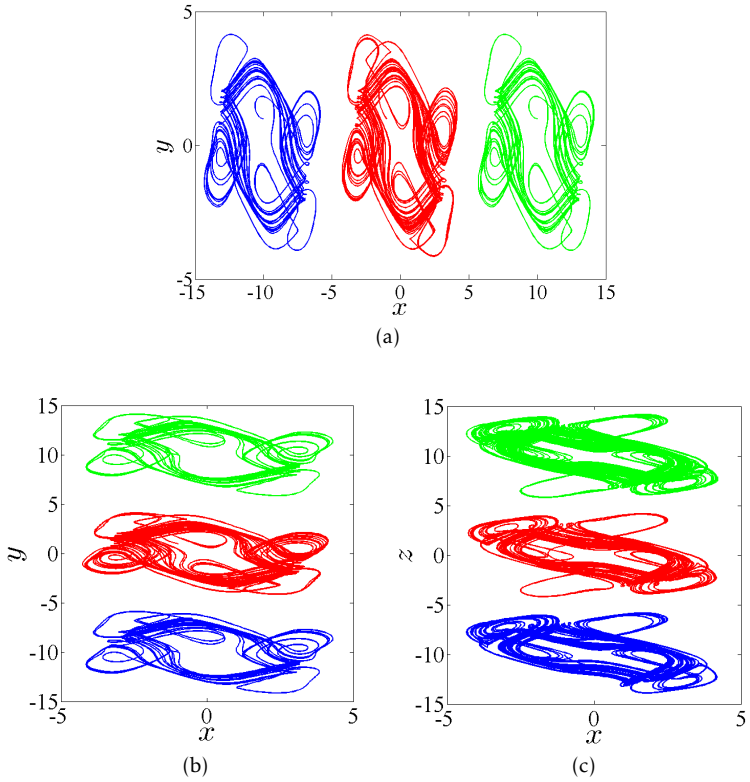

Figure 4.36: Scattering of the variable chaotic attractor on a 1D-line for $a = 1$, $b = -9$ and $[q_1, q_2, q_3] = [0.80, 0.90, 0.91]$. (a) x-line when $m = \pm 10$ and $m = 0$, (b) y-line when $n = \pm 10$ and $n = 0$, (c) z-line when $k = \pm 10$ and $k = 0$.

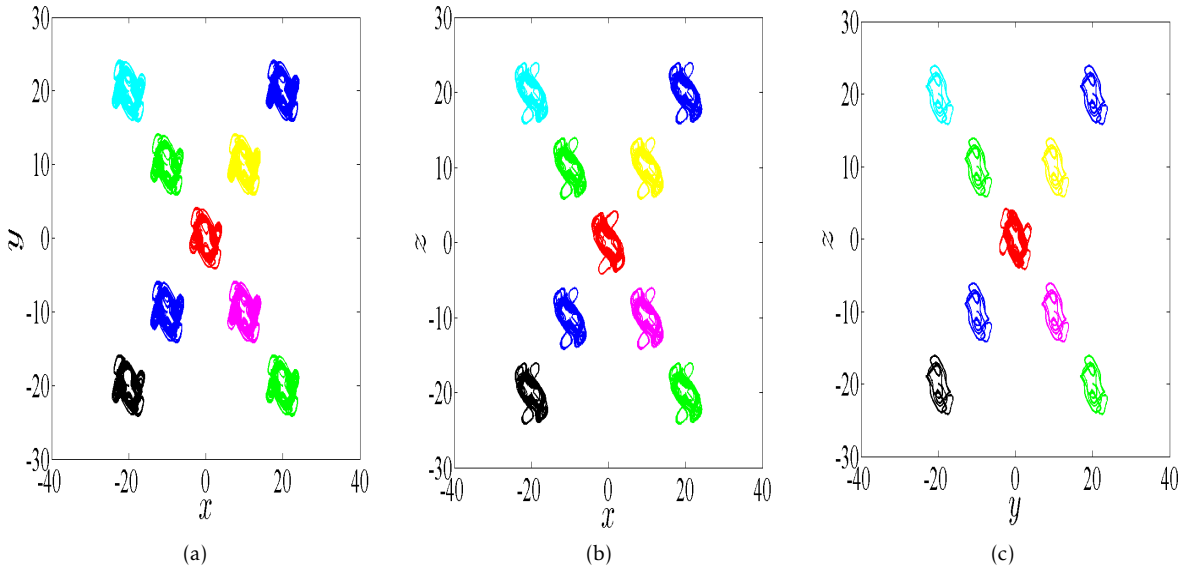

Figure 4.37: A 2D-lattice of a variable attractor for incommensurate fractional-order $[q_1, q_2, q_3] = [0.80, 0.90, 0.91]$ with $a = 1$, $b = -9$. (a) xy-lattice for $(m,n) = (0,0)$, $(10,10)$, $(10,-10)$, $(-10,10)$, $(-10,-10)$, $(20,20)$, $(20,-20)$, $(-20,20)$, $(-20,-20)$; (b) xz-lattice for $(m,k) = (1,1)$, $(10,10)$, $(10,-10)$, $(-10,10)$, $(-10,-10)$, $(20,20)$, $(20,-20)$, $(-20,20)$, $(-20,-20)$ and (c) yz-lattice for $(n,k) = (1,1)$, $(10,10)$, $(10,-10)$, $(-10,10)$, $(-10,-10)$, $(20,20)$, $(20,-20)$, $(-20,20)$, $(-20,-20)$.

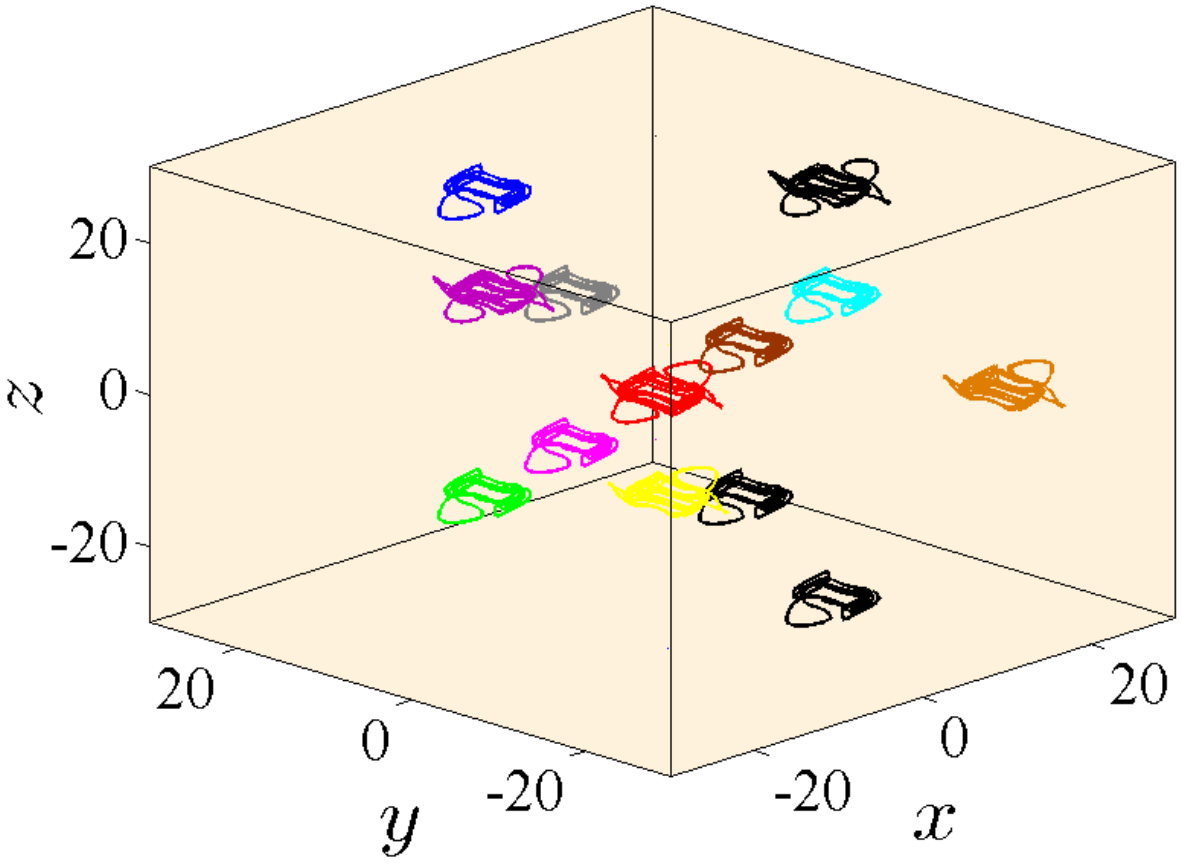

Figure 4.38: A 3D-grid of a variable periodic and chaotic attractors when $[q_1, q_2, q_3] = [0.80, 0.90, 0.91]$ with $a = 1$, $b = -9$ for $(m, n, k) = (0, 0, 0)$, $(0, 10, 10)$, $(0, 10, -10)$, $(0, -10, 10)$, $(0, -10, -10)$, $(0, 20, 20)$, $(0, 20, -20)$, $(0, -20, 20)$, $(20, 20, -20)$, $(-20, 0, -20)$, $(20, 0, -20)$, $(20, 20, 0)$, $(-20, 20, 0)$.

A 3D-grid of variable attractors

In this subsection, certain values of the three controlled parameters m, n and k will be simultaneously adapted. This would yield, after taking the fractional-order values as, e.g., $[q_1, q_2, q_3] = [0.80, 0.90, 0.91]$, a 3D-grid of variable chaotic and periodic attractors as illustrated in Fig. 4.38. Furthemore, The basin of attarction of the system (4.2.2) is shown in Fig. 4.39 correspondig to Fig 4.38 where the initial conditions (ICs) in yellow region lead to the region of limit cycles in different colors lead to the two chaotic attractors.

4.2.5 Conclusion

This work has formulated a novel version of Hopfield neural network models with incommensurate fractional-order using the Caputo differential operator. Through continuous varying of the values of the system's parameters as well as the fractional-order derivative values, the stability of the proposed model has been analyzed numerically, and many rich complex dynamics, including symmetry, bistabilty and coexisting chaotic attractors, have been generated. It has been turned out, through adapting certain additional controlled constants, that the proposed model possesses the offset boosting of three variables. In addition, it has been shown that the resultant periodic and chaotic attractors generated from such model can be distributed in several forms, including 1D-line, 2D-lattice, 3D-grid, and even in an arbitrary location of the phase space.

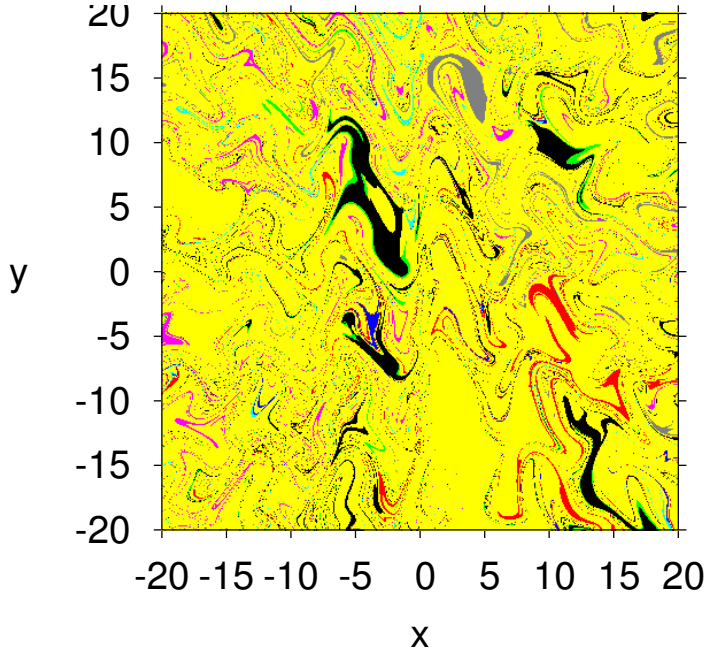

Figure 4.39: Basin of attraction of system (4.2.2) when $[q_1, q_2, q_3] = [0.80, 0.90, 0.91]$ according to the system parameters $a = 1$, $b = -9$ and to the initial condition of the third state variable z = 0. The colors in this figure associate with the colors of the attractors given in Fig. **??**

4.3 Secure Multiple-Input Multiple-Output Communications Based on F-M Synchronization of FOCS with Non-Identical Dimensions and Orders

The content of this section has been published in [18].

4.3.1 Introduction

Synchronization is the process of controlling the output of a chaotic dynamical slave system in order to force its variables to match those of a corresponding master system in time [159, 160]. The subject of synchronization has been around for about 30 years. Over the course of this period, the subject has attracted the interest of researchers from a variety of fields including but not limited to engineering, natural sciences, social sciences, physics, chemistry, and many more [161, 162, 163, 164, 165, 166].

Although the amount of literature related to chaotic dynamical systems is vast, an exact definition of such systems is not easy to find. The general consensus, however, is that a chaotic system is one with an extremely high sensitivity to small variations in the initial conditions. The trajectory of the solutions is seemingly random and difficult to pretend. However, if the initial conditions are known, the trajectory can be exactly reproduced. Chaotic systems and their synchronization are of particular interest in the field of secure communications due to the many similarities between chaos and the encryption of data being transmitted. Synchronization in general requires some form of control strategy. Various kinds of control schemes can be found in the literature aimed at synchronizing integer-order chaotic systems [167, 168, 169]. However, most of the existing studies consider only the simple case where both systems have exact same order and the same dimensions. Attempts have been dedicated to synchronize systems with different dimensions such as those shown in Table 1. The importance of different dimensional dynamic system synchronization stems from its wide range of applications as well as its enrichment of control

Table 4.4: Synchronization schemes for integer-order systems with different dimensions.

Synchronization Schemes
Inverse full state hybrid projective synchronization [170, 171, 172, 173, 174, 175]
Matrix projective synchronization [176].
Generalized synchronization [177, 178, 179, 180].
Inverse generalized synchronization [181, 182].
Hybrid synchronization [183].
F-Q synchronization [184].
Q-S synchronization [185, 186].
Reduced order synchronization [187].
Increased order generalized synchronization [188].

theory.

In addition to integer-order systems, the research community has also been looking at fractional-order ones due to the added flexibility chaotic nature which they add to the mix [189]. The same progress made with integer-order systems has been attempted here. Some studies have examined the synchronization of fractional-order systems with identical dimensions [190] and others considered the more general case of arbitrary dimensions [191]. This study presents a novel contribution to the topic. We investigate F-M synchronization, which combines generalized synchronization based on a functional relationship F with inverse matrix projective synchronization based on a matrix M with synchronization index d, which basically represents the dimension of the synchronization error. By exploiting the fractional Laplace transform along with the stability theory related to linear systems with integer orders, the F-M synchronization of fractional-order systems is proven for the case $d = m$ showing that the zero solution of the error system is globally asymptotically stable. The case $d < m$ is also considered and the synchronization demonstrated. The proposed scheme is rather general with the only restriction on the scaling functions being that they must be differentiable. Chaos has attracted considerable attention in the field of wireless and optical communications over the last two decades. The main reason for this attraction is the many similarities between chaos and encryption, which is a necessary part of any modern communications system [192, 193, 194, 195, 196, 197, 198, 199]. Traditionally, encryption was performed at higher layers within the Open Systems Interconnection (OSI) communications model. With chaos, security concerns have shifted to the physical layer where the carriers of information, which were always sine and cosine waves, are replaced with chaotic or hyperchaotic signals. The amount of literature concerning the use of chaos in communications is vast [200]. However, they may be generally classified into five main categories: masking schemes, modulations schemes, multiple access schemes, multicarrier schemes, and secret/public key encryption schemes. In this section, we employ the proposed F-M synchronization strategy to form a multiple input multiple output (MIMO) secure communications system based on message masking. The developed system is tested through numerical simulations to verify its validity.

4.3.2 Problem Formulation

We start with the definitions of some properties which used in this study. As defined in [1], the Laplace transform of the Riemann?Liouville operator (1) is given by:

$$\mathbf{L}\{I^q f(t)\} = s^{-q}F(s), \quad (q > 0). \tag{4.3.1}$$

Similarly, according to [201], the Laplace transform of Caputo fractional derivative is defined as:

$$\mathbf{L}\{D_t^p f(t)\} = s^p F(s) - \sum_{k=0}^{n-1} s^{\alpha-k-1} f^{(k)}(0), \tag{4.3.2}$$

for $p > 0$ and$n-1 < p \leq n$. Obviously, if $p \in (0,1]$, then Label (4.3.2) simplifies to:

$$\mathbf{L}\{D_t^p f(t)\} = s^p F(s) - s^{p-1} f^{(k)}(0). \tag{4.3.3}$$

With these definitions in mind, let us now consider as master-slave pair the general chaotic systems

$$\begin{cases} D_t^p X(t) = f(X(t)), \\ D_t^q Y(t) = BY(t) + g(Y(t)) + U, \end{cases} \tag{4.3.4}$$

where $X(t) \in \mathbb{R}^n$ and $Y(t) \in \mathbb{R}^m$ are the master and slave state vectors, respectively, $0 < p < 1$, $f : \mathbb{R}^n \to \mathbb{R}^n, U = (u_i)_{1\leq i\leq m}$ is a vector controller, and $B \in \mathbb{R}^{m\times m}$ and $g :: \mathbb{R}^m \to \mathbb{R}^m$ are the linear and nonlinear parts of the slave system, respectively. In this paper, we are concerned with the rather general F-M synchronization, which encompasses multiple types of synchronization as will be explained in the following definition and the remark thereafter.

Definition 4.3.1. The maste-slave pair (4.3.4) is said to be F-M synchronized with dimension d if there exists a controller $U = (u_i)_{1\leq i\leq m'}$, a differentiable function $\mathbf{F} : \mathbb{R}^m \to \mathbb{R}^d$, and a function matrix $\mathbf{M}(t) = (\mathbf{M}(t)_i)_{d\times n}$ such that

$$\lim_{t\to+\infty} \|e(t) = \mathbf{F}(Y(t)) - \mathbf{M}(t)X(t)\| = 0. \tag{4.3.5}$$

Remark 4.3.1. Depending on the pair $(\mathbf{F}(.), \mathbf{M})$, different synchronization types may arise:

- Complete synchronization for $(\mathbf{F}(.), \mathbf{M}) = (I, X(t))$.
- Anti-synchronization for $(\mathbf{F}(.), \mathbf{M}) = (I, -X(t))$.
- Matrix projective synchronization for $(\mathbf{F}(.), \mathbf{M}) = (I, \mathbf{M}(t))$.
- Inverse generalized synchronization for $(\mathbf{F}(.), \mathbf{M}) = (\mathbf{F}(Y(t)), I)$.

4.3.3 F-M Synchronization

Establishing the control laws of the proposed F-M will be tackled in two main steps. First, we look at the simpler case where the dimension d is equal to the dimension of the slave. Then, we move to prove the existence of a control law guaranteeing synchronization for cases where $d < m$.

Case1: $d = m$

Let us start by defining the error system between the master and slave systems in Label (4.3.4) for the F-M synchronization of dimension m as:

$$e(t) = \mathbf{F}(Y(t)) - \mathbf{M}(t)X(t). \tag{4.3.6}$$

By defining the matrix:

$$\mathbf{DF}(Y(t)) = \begin{pmatrix} \frac{\partial \mathbf{F}_1}{\partial y_1} & \frac{\partial \mathbf{F}_1}{\partial y_2} & \cdots & \frac{\partial \mathbf{F}_1}{\partial y_m} \\ \frac{\partial \mathbf{F}_2}{\partial y_1} & \frac{\partial \mathbf{F}_2}{\partial y_2} & \cdots & \frac{\partial \mathbf{F}_2}{\partial y_m} \\ \cdots & \cdots & \ddots & \cdots \\ \frac{\partial \mathbf{F}_m}{\partial y_1} & \frac{\partial \mathbf{F}_m}{\partial y_2} & \cdots & \frac{\partial \mathbf{F}_m}{\partial y_m} \end{pmatrix}$$

we may reformulate (4.3.6) as:

$$\dot{e}(t) = \mathbf{DF}(Y(t))\dot{Y}(t) - \dot{\mathbf{M}}(t)X(t) - \mathbf{M}(t)\dot{X}(t). \tag{4.3.7}$$

It was shown in [202] that the fractional derivative of the product M(t)-X (t), for instance, results in an infinite sum containing integer and fractional order derivatives. Hence, we may not use Label (4.3.7) directly. Instead, let us rewrite it in the more convenient form:

$$\dot{e}(t) = (B - C)e(t) + \mathbf{DF}(Y(t))\dot{Y}(t) + R, \tag{4.3.8}$$

with $C \in \mathbb{R}^{m\times m}$ being our new constant control matrix to be selected later and

$$R = (C - B)e(t) - \dot{\mathbf{M}}(t)X(t) - \mathbf{M}(t)\dot{X}(t). \tag{4.3.9}$$

To achieve synchronization between the systems in Label (4.3.4), we assume that $\mathbf{DF}(Y(t))$ is an invertible matrix with its inverse denoted by $\mathbf{D}^{-1}$. This leads us to the following theorem.

Theorem 4.3.1. *There exists a suitable feedback gain matrix $C \in \mathbb{R}^{m\times m}$ such that*

$$U = -BY(t) - g(Y(t)) + J^{1-q}(-\boldsymbol{D}^{-}1 \times R), \tag{4.3.10}$$

whereby m-dimensional F-M synchronization is realized for the master-slave pair (4.3.4).

Proof. See [18] □

Case2: $d < m$

Let us now assume that the synchronization dimension $d < m$. We define the vectors $\dot{Y}_1(t) = (\dot{y}_1(t), ..., \dot{y}_d(t))^T$ and $\dot{Y}_2(t) = (\dot{y}_{d+1}(t), ..., \dot{y}_m(t))^T$ along with matrices

$$\mathbf{D}_1 = \begin{pmatrix} \frac{\partial \mathbf{F}_1}{\partial y_1} & \frac{\partial \mathbf{F}_1}{\partial y_2} & \cdots & \frac{\partial \mathbf{F}_1}{\partial y_d} \\ \frac{\partial \mathbf{F}_2}{\partial y_1} & \frac{\partial \mathbf{F}_2}{\partial y_2} & \cdots & \frac{\partial \mathbf{F}_2}{\partial y_d} \\ \cdots & \cdots & \ddots & \cdots \\ \frac{\partial \mathbf{F}_d}{\partial y_1} & \frac{\partial \mathbf{F}_d}{\partial y_2} & \cdots & \frac{\partial \mathbf{F}_d}{\partial y_d} \end{pmatrix},$$

$$\mathbf{D}_2 = \begin{pmatrix} \frac{\partial \mathbf{F}_1}{\partial y_{d+1}} & \frac{\partial \mathbf{F}_1}{\partial y_{d+2}} & \cdots & \frac{\partial \mathbf{F}_1}{\partial y_m} \\ \frac{\partial \mathbf{F}_{d+2}}{\partial y_{d+1}} & \frac{\partial \mathbf{F}_{d+2}}{\partial y_{d+2}} & \cdots & \frac{\partial \mathbf{F}_{d+2}}{\partial y_m} \\ \cdots & \cdots & \ddots & \cdots \\ \frac{\partial \mathbf{F}_d}{\partial y_{d+1}} & \frac{\partial \mathbf{F}_d}{\partial y_{d+2}} & \cdots & \frac{\partial \mathbf{F}_d}{\partial y_m} \end{pmatrix},$$

and

$$T = diag(c_1, c_2, ..., c_d)e(t) - \dot{\mathbf{M}}X(t) - \mathbf{M}(t)\dot{X}(t), \tag{4.3.11}$$

The error system (4.3.6) may be rearranged to the form

$$\dot{e}(t) = -diag(c_1, c_2, ..., c_d)e(t) + \mathbf{D}_1\dot{Y}_1(t) + \mathbf{D}_2\dot{Y}_2(t) + T, \tag{4.3.12}$$

where c_i are positive control constants for $1 \leq i \leq$d. We assume that matrix $\mathbf{D}_1$ is invertible and we denote its inverse by $\mathbf{D}_1^{-1}$. The following theorem states the control laws for the F-M synchronization criterion.

Theorem 4.3.2. *Given the four matrices $B_1 = (b_{ij})_{d\times m'}, B_2 = (b_{ij})_{(m-d)\times m'}, G_1 = (g_i)_{1\leq i\leq d'}$, the master-slave pair (4.3.4) is globally F-M synchronized with dimension d subject to*

$$(u_1, u_2, ..., u_d)^T = -B_1 - G_1 - J^{1-q}(\boldsymbol{D}_1^{-1} \times T), \tag{4.3.13}$$

$$(u_{d+1}, u_{d+2}, ..., u_m)^T = -B_2 - G_2. \tag{4.3.14}$$

Proof. See [18]. □

4.3.4 Numerical Example

In this section, we present some numerical simulations that verify and illustrate the effectiveness of the theoretical analysis in Section 3. It is noted that the Adams-Bashforth-Moulton method with the step size 0.001. We consider as master the fractional order permanent magnet synchronous motor (PMSM) model presented in [203]. A PMSM is a type of alternating current (AC) synchronous motor that uses permanent magnets to produce torque even at zero speed and can have a higher torque density compared to other types of motors. In terms of its mathematical model, it is considered a nonlinear coupling system with multiple variables. Traditionally, the PMSM was modeled as an integer-order dynamical system, which only takes into consideration the local knowledge of the states and inputs. The basic idea behind the fractional model in [203] is that, unlike integer calculus, fractional calculus involves an infinite number of terms. These terms can be employed to represent the past history of an arbitrary dynamical system. The considered model is of the form

$$D_t^p X(t) = f(X(t)), \tag{4.3.15}$$

where $X(t) = (x_1, x_2, x_3)^T$,

$$f(X(t)) = \begin{pmatrix} -x_1 + x_2x_3 \\ -x_2 - x_1x_3 + ax_3 \\ b(x_2 - x_3) \end{pmatrix},$$

$(a, b) = (100, 10)$, and $p = 0.95$.

As for the slave system, let us also consider the 4-component hyperchaotic fractional order system proposed in [204] with the addition of a control term yielding

$$D_t^q Y(t) = BY(t) + g(Y(t)) + U, \tag{4.3.16}$$

with

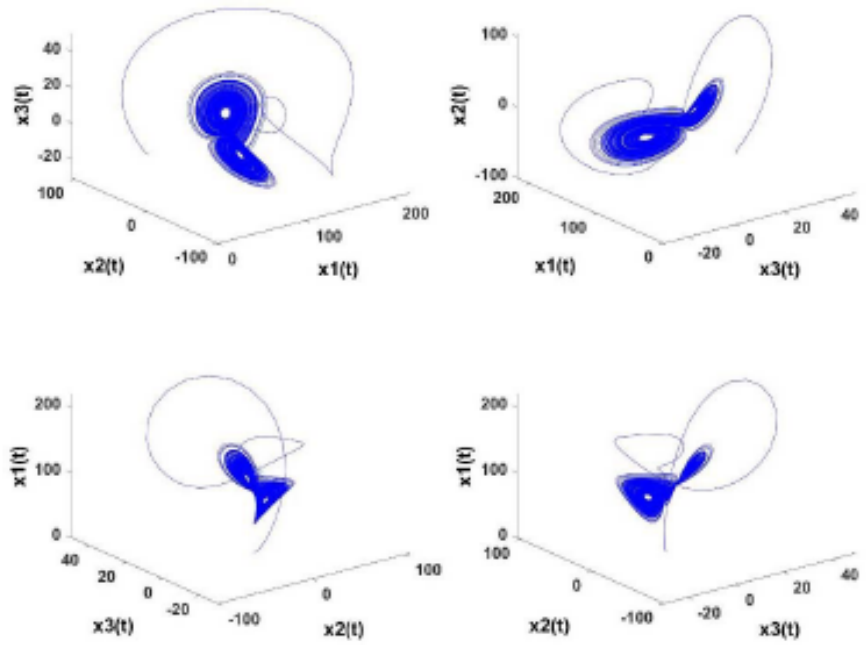

Figure 4.40: Chaotic attractors of the master system (4.3.15) when $(a,b) = (100,10)$ and $p = 0.95$.

$$B = \begin{pmatrix} -10 & 10 & 0 & 0 \\ 28 & 1 & 0 & -1 \\ 0 & 0 & -8/3 & 0 \\ 0 & 0 & 0 & 0 \end{pmatrix}, G = \begin{pmatrix} 0 \\ -y_1 y_3 \\ -y_1 y_2 \\ 0.1 y_2 y_3 \end{pmatrix}, U = \begin{pmatrix} u_1 \\ u_2 \\ u_3 \\ u_4 \end{pmatrix}.$$

The authors of [204] showed that, subject to $0.916 \leq q \leq 1$, the system always exhibits hyperchaotic behavior. Hence, we choose the arbitrary fractional order $q = 0.94$. System (4.3.16) was proposed as the fractional counterpart of the integer-order hyperchaotic system proposed in [205]. A new modified generalized projective synchronization scheme was developed for (4.3.16) and applied to a secure communication system in [204].
The chaotic attractors of the proposed master and slave systems are depicted in Figures 4.40 and 4.41, respectively. The F-M synchronization strategy aims to force the error

$$e(t) = \mathbf{F}(y_1, y_2, y_3, y_4) - \mathbf{M}(t) \times (x_1, x_2, x_3)^T \tag{4.3.17}$$

to zero as $t \to +\infty$. Recall from Remark 1 that our choice of matrix $\mathbf{M}$ and function $\mathbf{F}$ can lead to different types of conventional synchronization schemes. In the following, we present numerical results confirming the validity and convergence of the proposed control schemes for $d = m = 4$, $d = 3 < m, d = 2 < m$, respectively.

case1.

For $d = m = 4$, we may choose

$$\mathbf{F} = \begin{pmatrix} y_1 + y_3 + y_4 \\ 2y_2 + y_4 \\ 3y_3 \\ 4y_4 \end{pmatrix}, \mathbf{M}(t) = \begin{pmatrix} 1/(t+1) & 10 & 1 \\ 1 & cost & 4 \\ 1 & 2 & 0 \\ e^{-t} & 2 & 3 \end{pmatrix},$$

leading to

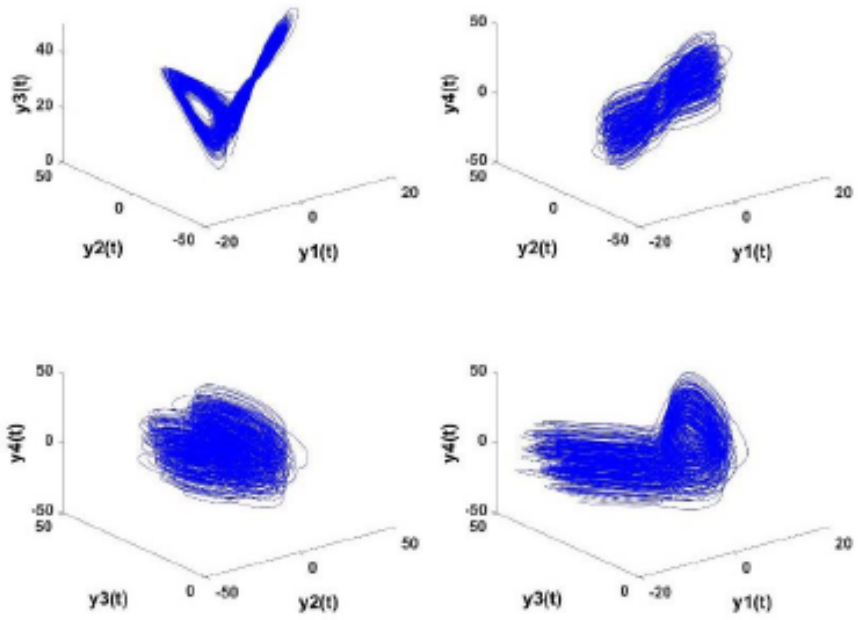

Figure 4.41: Attractors of the slave system (4.3.16) when $q = 0.94$ and $u_1 = u_2 = u_3 = u_4 = 0$.

$$\mathbf{DF}(Y(t)) = \begin{pmatrix} 1 & 0 & 1 & 1 \\ 0 & 2 & 0 & 1 \\ 0 & 0 & 3 & 0 \\ 0 & 0 & 0 & 4 \end{pmatrix}, \mathbf{D}^{-1} = \begin{pmatrix} 1 & 0 & 0 & 0 \\ 0 & 2 & 0 & 0 \\ 0 & 0 & 3 & 0 \\ 0 & 0 & 0 & 4 \end{pmatrix},$$

Our choice of control matrix C must satisfy condition (4.3.10) as stated in Theorem 4.3.1. For instance, we may consider

$$C = \begin{pmatrix} 1 & 10 & 0 & 0 \\ 28 & 2 & 0 & -1 \\ 0 & 0 & 0 & 0 \\ 0 & 0 & 0 & 1 \end{pmatrix},$$

as all the eigenvalues of $B - C$ have negative real parts. The resulting error system may be described by

$$\begin{cases} \dot{e}_1 = -10e_1, \\ \dot{e}_2 = -e_2, \\ \dot{e}_3 = -8/3e_3, \\ \dot{e}_4 = -e_4. \end{cases} \tag{4.3.18}$$

Its evolution over time is depicted in Figure 4.42 for initial conditions $(e_1(0), e_2(0), e_3(0), e_4(0))^T = (9, 7, 12, 21)^T$. Clearly, the error decays to zero given sufficient time, which means that the master and slave are synchronized.

Case2.

For $d = 3 < m$, we have

$$\mathbf{F} = \begin{pmatrix} y_1 + y_4^2 \\ y_2 + y_4 \\ y_3 + 1 \end{pmatrix}, \mathbf{M}(t) = \begin{pmatrix} 1 & sint & 0 \\ 2 & 0 & 1/(1 + ln(t+1)) \\ 0 & 1/(1+\sqrt{t}) & 3 \end{pmatrix},$$

yielding

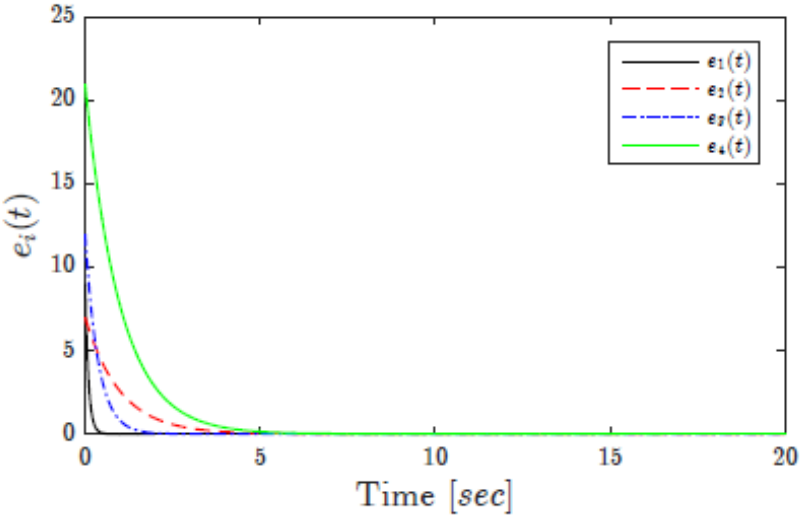

Figure 4.42: Time evolution of the synchronization error for the 4D case.

$$\mathbf{DF}(Y(t)) = \begin{pmatrix} 1 & 0 & 0 & 2y_4 \\ 0 & 2 & 0 & 1 \\ 0 & 0 & 1 & 0 \end{pmatrix}, \mathbf{D}_2 = \begin{pmatrix} 2y_4 \\ 1 \\ 0 \end{pmatrix}.$$

In order to satisfy control rule (4.3.13), we must first calculate $\mathbf{D}_1^{-1}$, which turns out to be:

$$\mathbf{DF}(Y(t)) = \begin{pmatrix} 1 & 0 & 0 \\ 0 & 1/2 & 0 \\ 0 & 0 & 1 \end{pmatrix}.$$

The control constants $(c_i)_{1\leq i\leq 3}$ can then be chosen as:

$$(c_1, c_2, c_3) = (1, 2, 3).$$

The error system is described by:

$$\begin{cases} \dot{e}_1 = -e_1, \\ \dot{e}_2 = -2e_2, \\ \dot{e}_3 = -3e_3. \end{cases} \tag{4.3.19}$$

Figure 4.43, displays the time evolution of the error with initial conditions $(e_1(0), e_2(0), e_3(0))^T = (36, 6, 3)^T$:

$$\begin{pmatrix} e_1(0) \\ e_2(0) \\ e_3(0) \end{pmatrix} = \begin{pmatrix} 36 \\ 6 \\ 3 \end{pmatrix}.$$

Case 3.

As for the two-dimensional case, we consider the matrices:

$$\mathbf{F} = \begin{pmatrix} 2y_1 + y_2 + y_3y_4 \\ y_1 + 2y_2 + y_3^2 + y_4^2 \end{pmatrix}, \mathbf{M}(t) = \begin{pmatrix} 3 & 0 & cost \\ 0 & 1 & sint \end{pmatrix}.$$

which leads to:

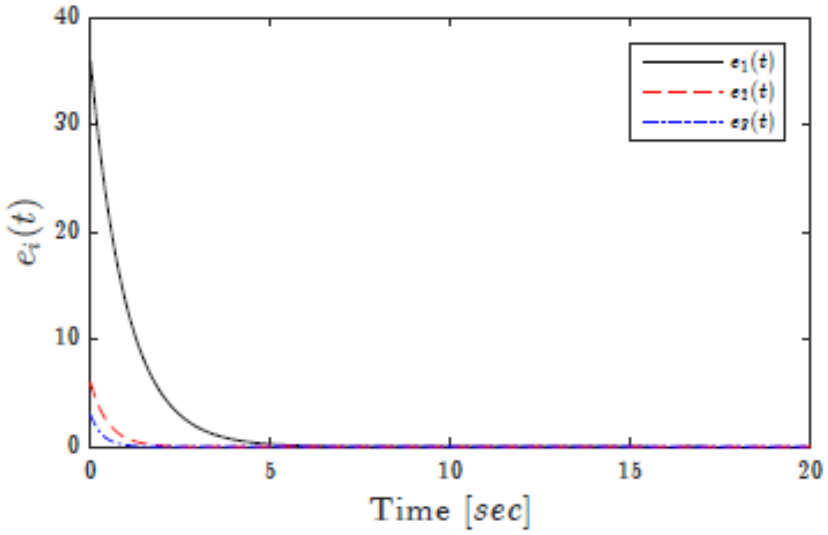

Figure 4.43: Time evolution of the synchronization error for the 3D case.

$$\mathbf{D}_1 = \begin{pmatrix} 2 & 1 & y_4 & y_3 \\ 1 & 2 & 2y_3 & 2y_4 \end{pmatrix}, \mathbf{D}_2 = \begin{pmatrix} y_4 & y_3 \\ 2y_3 & 2y_4 \end{pmatrix}, \mathbf{D}_1^{-1} = \begin{pmatrix} 1 & 0 \\ 0 & 1 \end{pmatrix},$$

In this case, the control constants can be chosen as $(c_1, c_2) = (0.1, 0.2)$ and yielding the error system:

$$\begin{cases} \dot{e}_1 = -0.1e_1, \\ \dot{e}_2 = -0.2e_2. \end{cases} \tag{4.3.20}$$

The time-evolution of the error is depicted in Figure 4.44 for $(e_1(0), e_2(0))^T = (31, 10)^T$.

Remark 4.3.2. For the application to MIMO Secure Communications, see section 5 in [18].

4.3.5 Conclusion

This study investigated the F-M synchronization with index d of fractional-order systems differential systems with non-identical dimensions. The main novelty of this piece of work is the combination of two distinct types of synchronization, namely generalized synchronization based on a functional relationship **F** and inverse matrix projective synchronization based on a matrix **M**. The developed approach exploits nonlinear controllers and the stability theory of integer-order systems in order to synchronize an m-dimensional slave with an n-dimensional master system. The approach has proved to be effective in achieving synchronized dynamics not only when the synchronization index d is equal to the slave's dimension m, but even when $d < m$. To the best of the authors' knowledge, this finding is both novel and forms a considerable contribution to the field of study. In order to confirm the findings of this study and highlight the capabilities of the developed scheme, a numerical example was considered where the master is a 3D chaotic fractional system and the slave is a 4D hyperchaotic fractional system. In addition, a MIMO communications system employing F-M synchronization was proposed and verified through computer simulations. In the proposed system, matrix **M** is used to condition the master chaotic states used to mask our messages and function **F** is used to condition the slave states. When synchronization is achieved, the two become identical and the masked messages are recovered.

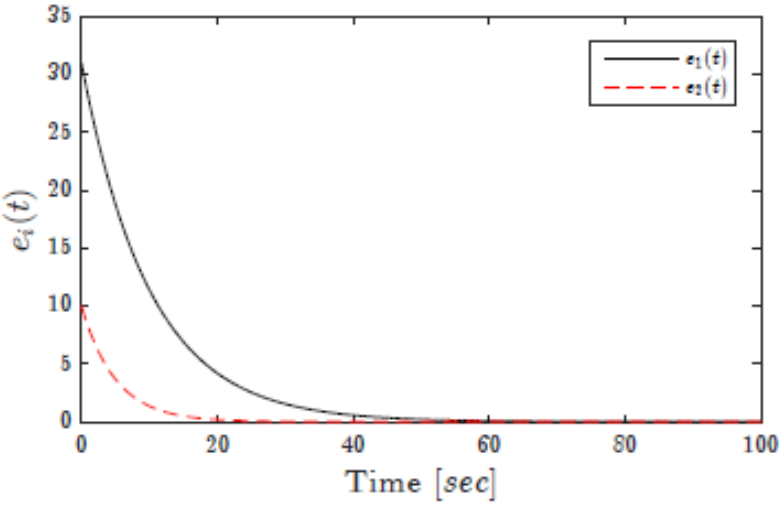

Figure 4.44: Time evolution of the synchronization error for the 2D case.

CHAPTER 5

CHAOS IN FRACTIONAL-ORDER GENERAL SYSTEMS

In this part, we study the chaotic behaviors in two general models by including commensurate and incommensurate fractional-orders at this models.

5.1 Dynamics of fractional-order chaotic and hyper-chaotic systems

The content of this section has been published in [19].

5.1.1 Introduction

Recent days, the applications of fractional-order dynamical systems play a more vital role in real life problems, for example fuzzy fractional integral sliding mode control, digital cryptography, authenticated encryption scheme. Thus, investigation of fractional-order dynamical systems is not only meaningful in the theory, but also significant in practice.

In the past, the lack of methods for solving fractional differential equations was the reason for using only integer-order models. Nowadays, a number of techniques are available for approximating fractional derivatives and integrals.

One of the importance studies is to find the minimum effective dimension in a fractional order dynamical system for which the system remains chaotic.

Furthermore, several such examples have been proposed, notably the Liu system, complex Lorenz system. The analytical conditions necessary for a system to exhibit chaotic behaviour have been presented in the literature[133]. In this paper, we propose a fractional-order chaotic and hyper-chaotic systems that were introduced on [206] and [207]. We study commensurate and incommensurate ordered systems and find lowest order at which chaos exist by numerical experiments. In case of commensurate ordered 3D system (4D system) the lowest order turns out to be 2.82(3.48), where as in incommensurate case the lowest order is 2.81(3.12).

5.1.2 Fractional-order 3D autonomous chaotic system

A three-dimensional autonomous chaotic system was proposeed by S. Dadras et al [206], which was described by the following nonlinear differential equations :

Equilibrium points	Eignvalues	Nature
O(0,0,0)	-1.6,3,9	saddle point
E_2(1.9496, 1.1354, 1.7472)	0.4217 ± 4.0806i,-8.4434	Saddle focus point
E_3(-1.9496, -1.1354, 1.7472)	0.4217 ± 4.0806i,-8.4434	Saddle focus point
E_4(1.9119, -1.7508, -2.7472)	-10.8293,1.6147 ± 4.5976i	Saddle focus point
E_5(-1.9119, +1.7508, -2.7472)	-10.8293,1.6147 ± 4.5976i	Saddle focus point

Table 5.1: Equilibrium points and corresponding eigenvalues.

$$\begin{cases} \frac{dx(t)}{dt} = y - ax + yz, \\ \frac{dy(t)}{dt} = by - xz, \\ \frac{dz(t)}{dt} = cxy - dz - hx^2, \end{cases} \tag{5.1.1}$$

where for the parameters a = 1.6, b = 3, c = 8, d=9, h=0.5 this system yields chaotic behavior.
The system (5.1.1) has five equilibrium points [206] denoted as:

$$\begin{cases} O(0,0,0), \\ E_2(\sqrt{\frac{db(1+\Delta)}{(c(-1+\Delta)-2hb)}}, \frac{-1+\sqrt{\Delta}}{2b}\sqrt{\frac{(db(1+\Delta)}{(c(-1+\Delta)-2hb)}}, \frac{-1+\sqrt{\Delta}}{2}), \\ E_3(-\sqrt{\frac{db(1+\Delta)}{(c(-1+\Delta)-2hb)}}, \frac{+1-\sqrt{\Delta}}{2b}\sqrt{\frac{(db(1+\Delta)}{(c(-1+\Delta)-2hb)}}, \frac{-1+\sqrt{\Delta}}{2}), \\ E_4(\sqrt{\frac{db(1+\Delta)}{(c(-1+\Delta)+2hb)}}, \frac{-1-\sqrt{\Delta}}{2b}\sqrt{\frac{(db(1+\Delta)}{(c(-1+\Delta)+2hb)}}, \frac{-1-\sqrt{\Delta}}{2}), \\ E_5(-\sqrt{\frac{db(1+\Delta)}{(c(-1+\Delta)+2hb)}}, \frac{1+\sqrt{\Delta}}{2b}\sqrt{\frac{(db(1+\Delta)}{(c(-1+\Delta)+2hb)}}, \frac{-1-\sqrt{\Delta}}{2}), \end{cases}$$

where $\Delta = 1 + 4ab$.
Assuming a = 1.6, b = 3, c = 8, d=9, h=0.5, one can obtain

$$\begin{cases} O(0,0,0), \\ E_2(1.9496, 1.1354, 1.7472), \\ E_3(-1.9496, -1.1354, 1.7472), \\ E_4(1.9119, -1.7508, -2.7472), \\ E_5(-1.9119, +1.7508, -2.7472), \end{cases}$$

The Jacobian matrix of the system (5.1.1) for equilibrium E* = (x*,y*, z*) is

$$J = \begin{pmatrix} -a & 1+z & y \\ -z & b & -x \\ cy - 2hx & cx & -d \end{pmatrix}$$

The real equilibrium points and the eigenvalues of the Jacobian matrix are given in Table 5.1.
All these eigenvalues satisfy the condition for the system to be chaotic.
Here, the fractional-order system is considered, where integer order derivative is replaced by a fractional one, as follows :

$$\begin{cases} D^{q_1} x(t) = y - ax + yz, \\ D^{q_2} y(t) = by - xz, \\ D^{q_3} z(t) = cxy - dz - hx^2, \end{cases} \tag{5.1.2}$$

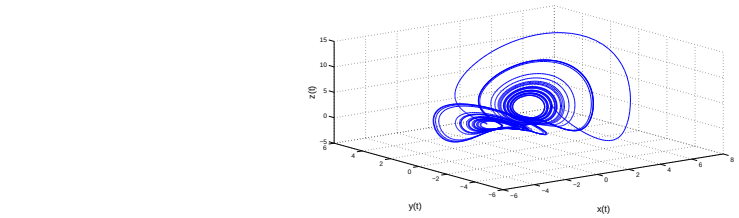

(a)

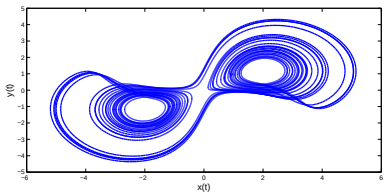

(b)

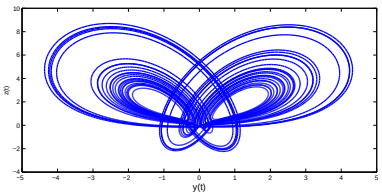

(c)

Figure 5.1: The chaotic attractors for q=0.95, a=1.6, b =3, c=8, d=9, h=0.5

where $q_i \in (0,1)$.

Numerical solution of the fractional-order 3D system (5.1.2) is realised by Grünwald-Letnikov approximation method, with step $h = 0.005s$ given as follows:

$$x(t_k) = (y(t_{k-1}) - ax(t_{k-1}) + y(t_{k-1})z(t_{k-1}))h^{q_1} - \sum_{j=v}^{k} c_j^{(q_1)} x(t_{k-j}),$$

$$y(t_k) = (by(t_{k-1}) - x(k)z(t_{k-1})h^{q_2} - \sum_{j=v}^{k} c_j^{(q_2)} y(t_{k-j}),$$

$$z(t_k) = (cx(t_k)y(t_k) - dz(t_{k-1}) - gx(t_k)^2)h^{q_3} - \sum_{j=v}^{k} c_j^{(q_3)} z(t_{k-j}),$$

where T_{sim} is the simulation time, $k = 1,2,3,...,N$, for $N = [T_{sim}/h]$ and $(x(0),y(0),z(0))$is the start point(initial conditions). The binomial coefficients $c_j^{(q_i)}, \forall i$ are calculated according to the relation (1.4.6) in section (1.4.2).

Commensurate ordered system

In the case of commensurate-order system, where $q_1 = q_2 = q_3 = q$ we can determine a minimal order to satisfy a necessary condition for chaotic behavior. For the equilibria E_2 and E_3 it is $q > 0.94$ and for the equilibria E_4 and E_5 it is $q > 0.79$.

where initial conditions $(x(0),y(0),z(0) = (-1,1,0.5))$ and derivative order$q_1 = q_2 = q_3 = 0.95$ yield chaotic trajectories (Figure 5.1):

We use the Benettin-Wolf algorithm to determine all Lyapunov exponents for a class of fractional-order systems [81](see also [208]).

The corresponding Lyapunov exponents diagram as function of t

for t $\in (0,100)$ is shown in Figure (5.3(b)). The three Lyapunov exponents are:

$$LE_1 = 0.4886, LE_2 = -0.0321, LE_3 = -9.8583.$$

and the Lyapunov dimension is 2.0463.

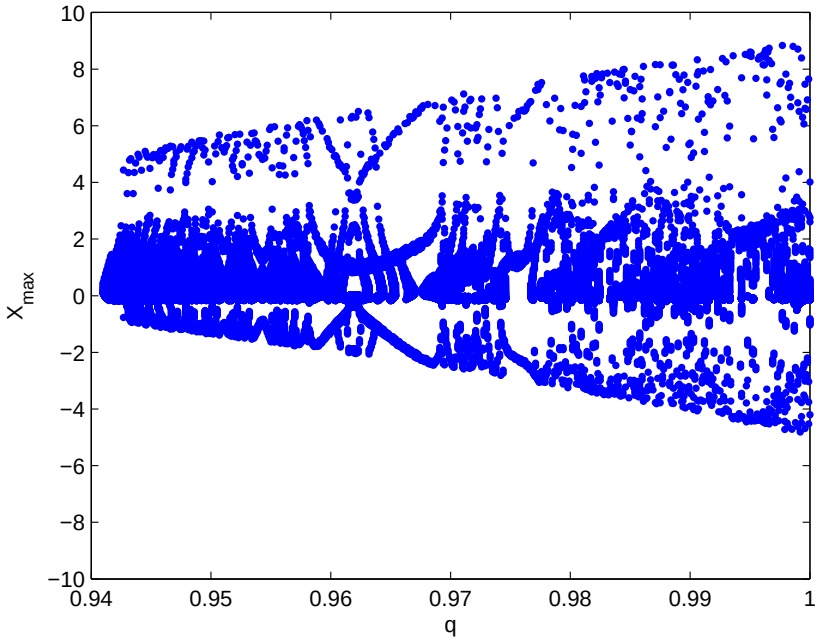

Figure 5.2: Bifurcation diagram of the system (5.1.2) versus the fractional order q$\in [0.94, 1]$

The Lyapunov exponents diagram as function of q for q $\in (0.94, 1)$ is shown in Figure (5.3(a)).
The Lyapunov exponents have been calculated indicating the system is chaotic with the aforementioned set of parameters.

The bifurcation diagram of system (5.1.2) is shown in Figure (5.2). When q>0.94 the system (5.1.1) exhibits a chaotic behavior which sopport the pervious results.

Incommensurate ordered system

In this subsection we only consider several groups of typical differential order values.The bifurcations versus different derivative orders are obtained by numerical simulations. Here, we have chosen the same system parametrs as above.
First, fixing $q_2 = q_3 = 1$ and $X(0) = (-1, 1, 0.5)$, dynamic behaviors with fractional derivative order $q_1 \in [0.8, 1]$ is shown in Figure(5.4(a)). From the bifurcation diagram, it is shown that the fractional-order system is chaotic over most of the scope $q_1 \in [0.81, 1]$. Now, Fixing $q_1 = q_3 = 1$ and $q_1 = q_2 = 1$ and $X(0) = (1, 1, 0.5)$ dynamic behaviors with fractional derivative order $q_2 \in [0.92, 1]$ and $q_3 \in [0.75, 1]$ is shown in Figure (5.4(b)-5.4(c)) respectively. From the bifurcation diagrams,we can see that the system exhibits period-1, period-2, and period-4 for different orders, the fractional-order system is chaotic over most of the scope $q_2 \in [0.95, 1]$and $q_3 \in [0.84, 1]$.The chaotic attractor for $q_2 = 0.95$, $q_1 = q_3 = 1$ and initial conditions $X(0) = (1, 1, 0.5)$ is shown in Figure(5.4(d)).

5.1.3 Fractional-order 4D autonomous chaotic system

A 4D autonomous chaotic system was proposeed by S. Dadras et al[207], which was described by the following nonlinear differential equations :

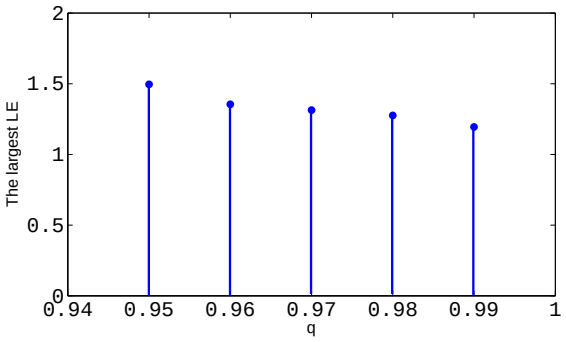

(a)

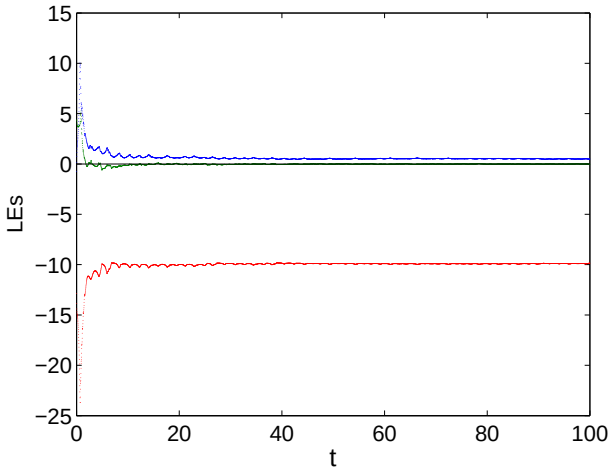

(b)

Figure 5.3: The Lyapunov exponents

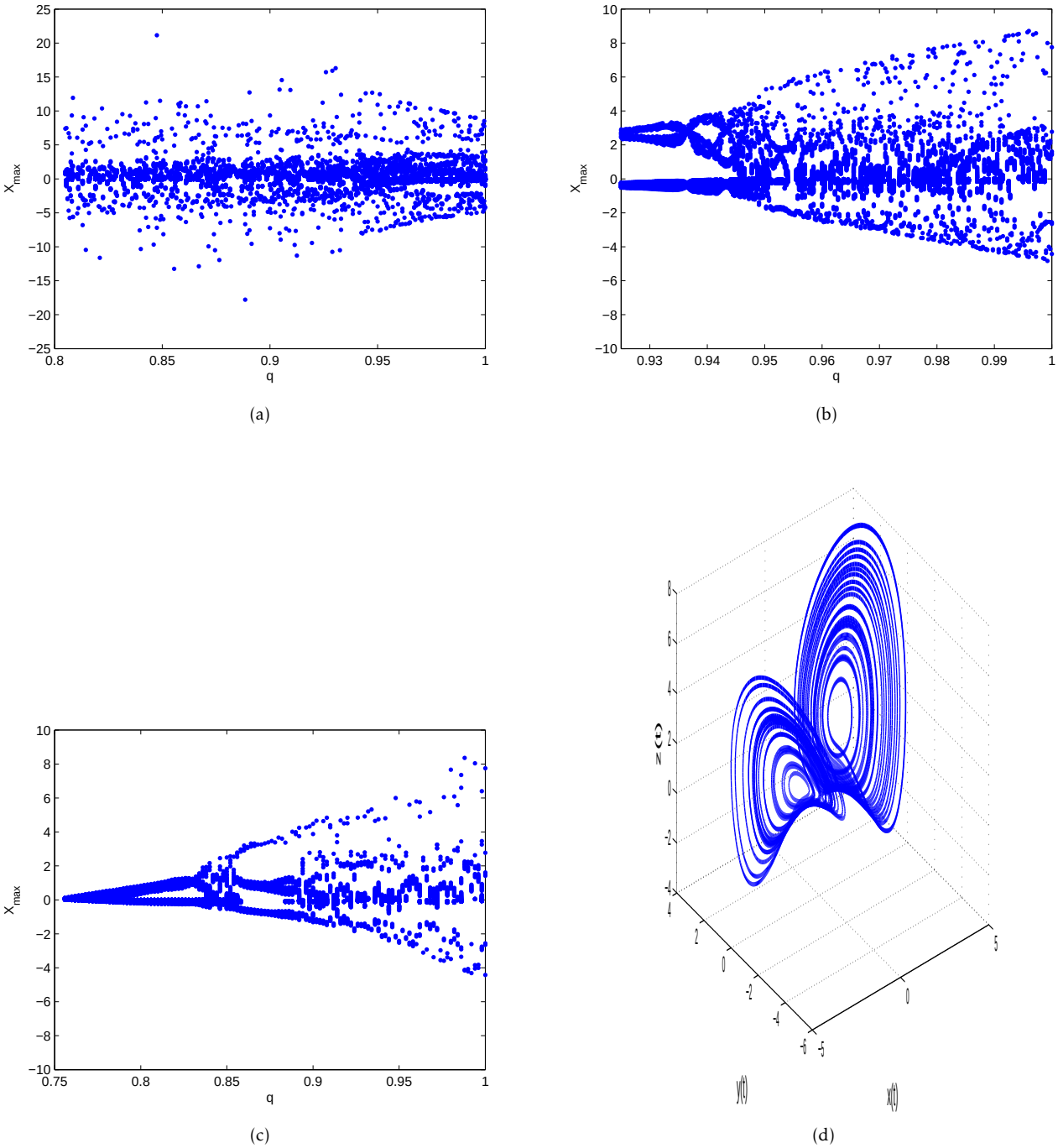

Figure 5.4: Dynamics of incommensurate ordered system (5.1.2)

Equilibrium points	Eignvalues	Nature
O(0,0,0)	8.0,0.05,-40.0,-14.0	saddle point
E_2(-5.0452,2.2563,-17.8885,9.02527)	-39.3984 , -3.3214±15.4351i , 0.0912	Saddle focus point
E_3(5.0452,2.2563,17.8885,9.0252)	-39.3984 , -3.3214±15.4351i , 0.0912	Saddle focus point
E_4(5.0452,-2.2563,-17.8885,-9.0252)	-39.3984 , -3.3214±15.4351i , 0.0912	Saddle focus point
E_5(-5.0452,-2.2563,17.8885,-9.0252)	-39.3984 , -3.3214±15.4351i , 0.0912	Saddle focus point

Table 5.2: Equilibrium points and corresponding eigenvalues.

$$\begin{cases} \frac{dx(t)}{dt} = ax - yz, \\ \frac{dy(t)}{dt} = xz - by, \\ \frac{dz(t)}{dt} = cxy - dz + gxw, \\ \frac{dw(t)}{dt} = kw - hy, \end{cases} \tag{5.1.3}$$

where for the parameters $a = 8, b = 40, c = 2, d = 14, g = 5, h = 0.2, k = 0.05$, this system yields chaotic behavior.
The system (5.1.3) has five equilibrium points [207] denoted as:

$$\begin{cases} O(0,0,0), \\ E_2(-\sqrt{\frac{b\Delta}{a}}, \sqrt{\Delta}, -\sqrt{ab}, \frac{h\sqrt{\Delta}}{k}), \\ E_3(\sqrt{\frac{b\Delta}{a}}, \sqrt{\Delta}, \sqrt{ab}, \frac{h\sqrt{\Delta}}{k}), \\ E_4(\sqrt{\frac{b\Delta}{a}}, -\sqrt{\Delta}, -\sqrt{ab}, -\frac{h\sqrt{\Delta}}{k}), \\ E_5(-\sqrt{\frac{b\Delta}{a}}, -\sqrt{\Delta}, \sqrt{ab}, -\frac{h\sqrt{\Delta}}{k}), \end{cases}$$

where $\Delta = \frac{adk}{ck + gh}$.
Assuming $a = 8, b = 40, c = 2, d = 14, g = 5, h = 0.2, k = 0.05$, one can obtain

$$\begin{cases} O(0,0,0), \\ E_2(-5.0452, 2.2563, -17.8885, 9.0252), \\ E_3(5.0452, 2.2563, 17.8885, 9.0252), \\ E_4(5.0452, -2.2563, -17.8885, -9.0252), \\ E_5(-5.0452, -2.2563, 17.8885, -9.0252), \end{cases}$$

The Jacobian matrix of the system (5.1.3) for equilibrium E* = (x*,y*, z*,w*) is

$$J = \begin{pmatrix} a & -z & -y & 0 \\ z & -b & x & 0 \\ cy + gw & cx & -d & gx \\ 0 & -h & 0 & k \end{pmatrix}$$

The real equilibrium points and the eigenvalues of the Jacobian matrix are given in Table 5.2.
All these eigenvalues satisfy the condition for the system (5.1.3) to be chaotic.
Here, the fractional-order system is considered, where integer order derivative is replaced by a fractional one, as follows :

$$\begin{cases} D^{q_1}x(t) = ax - yz, \\ D^{q_2}y(t) = xz - by, \\ D^{q_3}z(t) = cxy - dz + gxw, \\ D^{q_4}w(t) = kw - hy, \end{cases} \tag{5.1.4}$$

where $q_i \in (0,2)$.

Numerical solution of the fractional-order 4D system (5.1.4) is realised by Grünwald-Letnikov approximation method, with step $h = 0.005s$ given as follows:

$$x(t_k) = (ax(t_{k-1}) - y(t_{k-1})z(t_{k-1}))h^{q_1} - \sum_{j=v}^{k} c_j^{(q_1)} x(t_{k-j}),$$

$$y(t_k) = (x(k)z(t_{k-1}) - (by(t_{k-1}))h^{q_2} - \sum_{j=v}^{k} c_j^{(q_2)} y(t_{k-j}),$$

$$z(t_k) = (cx(k)y(k) - dz(t_{k-1}) + gx(t_k)w(t_{k-1}))h^{q_3} - \sum_{j=v}^{k} c_j^{(q_3)} z(t_{k-j}),$$

$$w(t_k) = (kw(t_{k-1}) - hy(k))h^{q_4} - \sum_{j=v}^{k} c_j^{(q_4)} w(t_{k-j}),$$

where T_{sim} is the simulation time, $k = 1, 2, 3, ..., N$, for $N = [T_{sim}/h]$ and $(x(0), y(0), z(0), w(0))$is the start point(initial conditions).The binomial coefficients $c_j^{(q_i)}, \forall i$ are calculated according to the relation (1.4.6) in section 1.4.2.

Commensurate ordered system

In the case of commensurate-order system, where $q_1 = q_2 = q_3 = q_4 = q$ we can determine a minimal order to satisfy a necessary condition for chaotic behavior.For the equilibria E_2, E_3, E_4 and E_5 it is $q > 0.87$.
where $a = 8, b = 40, c = 2, d = 14, g = 5, h = 0.2, k = 0.05$ and initial conditions $(x(0), y(0), z(0), w(0)) = (-0.5, 0.5, -0.5, -0.5))$ and derivative order:
when $q_1 = q_2 = q_3 = q_4 = 0.885$ yield chaotic trajectories (see Figure 5.5),

We use the Benettin-Wolf algorithm to determine all Lyapunov exponents for a class of fractional-order systems [79](see also [208]).
The corresponding Lyapunov exponents diagram as function of t∈(0,100) is shown in Figure (5.6(a)). The four Lyapunov exponents are:

$$LE1 = 2.1168, LE2 = 0.5353, LE3 = -0.7644, LE4 = -65.4406.$$

and the Lyapunov dimension is 3.0288.
The Lyapunov exponents diagram as function of q for q ∈ (0.87, 0.99) is shown in Table 5.3.
The Lyapunov exponents have been calculated indicating the system (5.1.4) is hyperchaotic with the aforementioned set of parameters.

The bifurcation diagram as a function of q∈(0.83,1.1) is shown in Figure (5.6(b)). On this figure we can see that when $0.87 < q \leq 1.1$ the system (5.1.4) exhibits a chaotic behavior, which is in agreement with the theoretical results. Note that here when varying the fractional order the system can display a four scroll chaotic attractor. Furthermore when $1 \leq q \leq 1.1$ the system candisplay a new chaotic attractor not observed in the integer order case(see Figure 5.7).

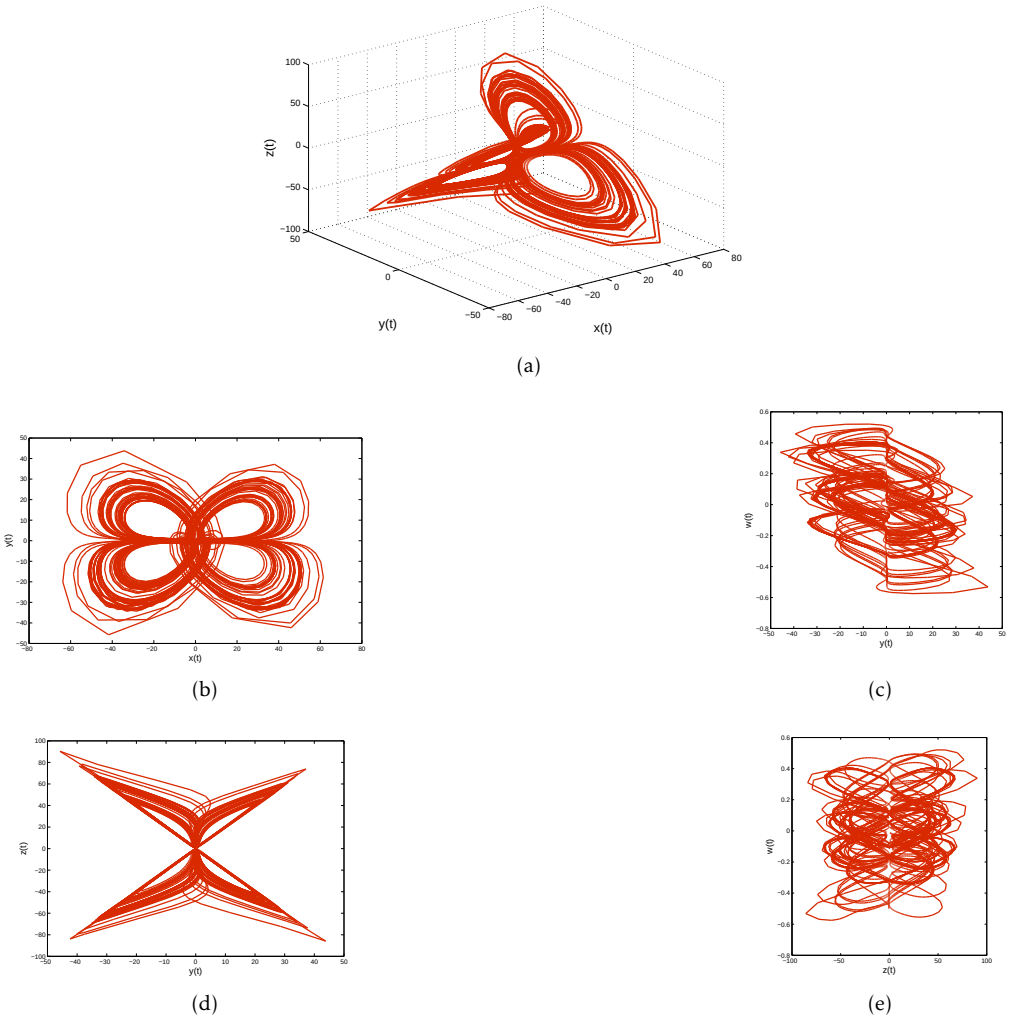

Figure 5.5: The chaotic attractors for q=0.885, and a=8 , b=40, c=2, d=14, g=5, h=0.2, k=0.05.

Order q	λ_1	λ_2
0.87	2.5741	0.6275
0.89	2.4991	0.5818
0.91	2.0134	0.6354
0.92	2.1295	0.5952
0.94	1.5560	0.3376
0.96	1.7829	0.5819
0.97	1.9888	0.4572
0.99	1.8446	0.4278

Table 5.3: The largest Lyapunov exponent λ_{max}.

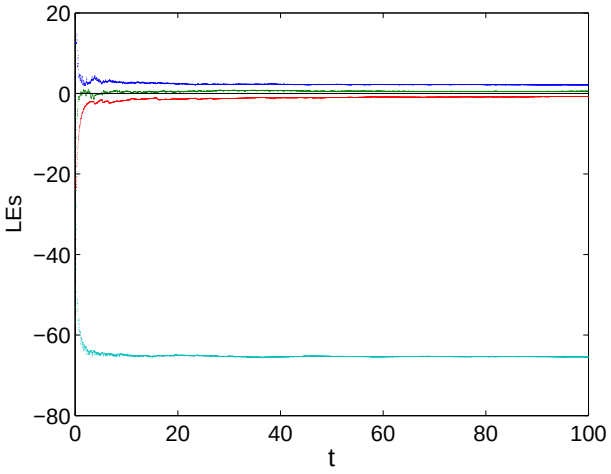

(a)

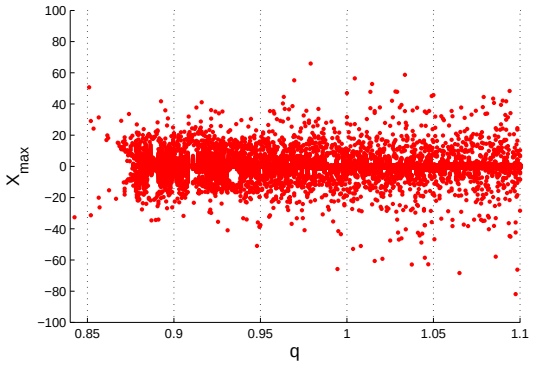

(b)

Figure 5.6: Dynamics of system (9)

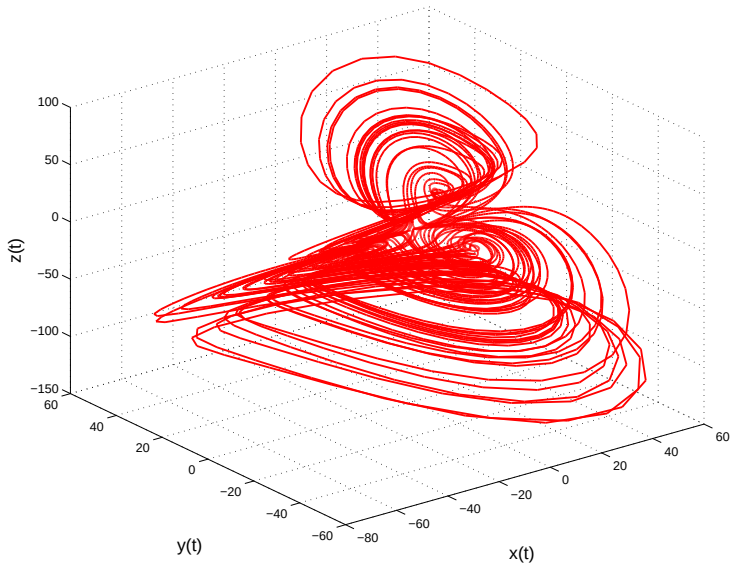

Figure 5.7: A new chaotic attractor for q=1.1

Incommensurate ordered system

In this case, the system parameters and the initial conditions are chosen is the same as above and the values of four derivative orders for system (5.1.4) are non-identical.
First, fixing $q_2 = q_3 = q_4 = 1$ and $q_1 = q_3 = q_4 = 1$ and vary derivative order q_1 and q_2 from 0.6 to 1.35 and from 0.9 to 1.2, the bifurcation diagrams are shown in Figure (5.8(a)-5.8(b)) resp. The system approaches chaos by doubling periodic bifurcation along the increasing of q_1 from 0.64 and q_2 from 0.9 resp.

Now, fixing $q_1 = q_2 = q_4 = 1$ and $q_3 \in (0.4, 1.43)$, From the bifurcation diagram (see Figure (4d)), it is shown that the fractional-order system is chaotic over most of the scope $q_1 \in [0.5, 1.42]$.But we remark that the system (see Figure (5.8(c)-5.8(d))) here exihibits an attractor with four scrolls from $q_3 = 0.8$to 1.42.

Finally, about q_4 and $q_1 = q_2 = q_3 = 1$ we found an important result because the smallest value where the system appraoches chaos is 0.12 to 1.34.(see Figure 5.8(d)).

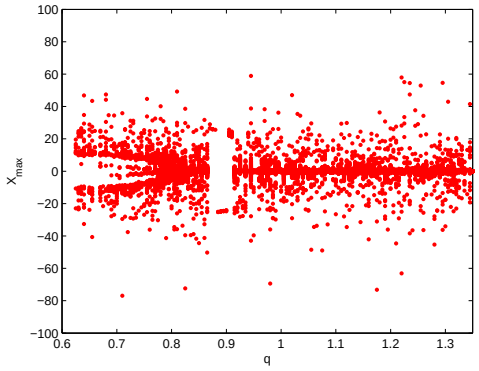

(a)

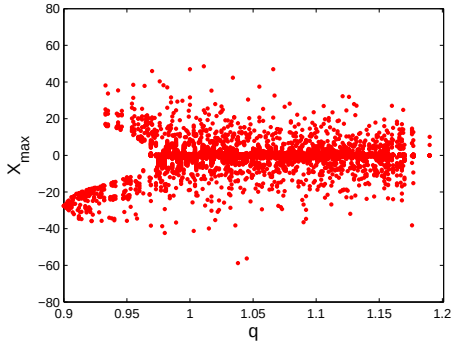

(b)

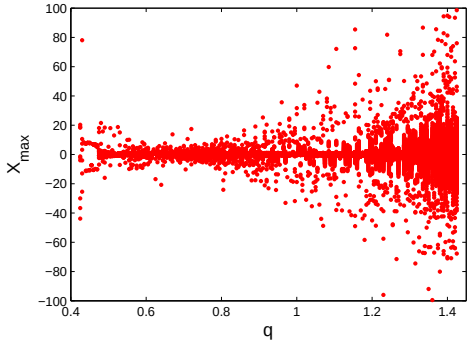

(c)

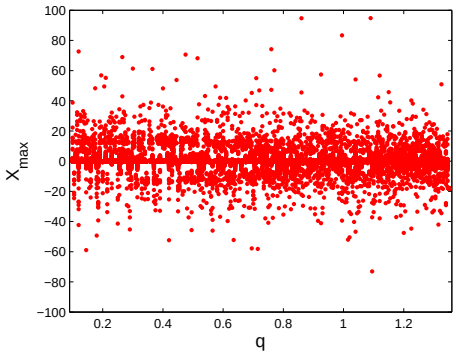

(d)

Figure 5.8: Dynamics of incommensurate ordered system (9)

5.2 Generating multidirectional variable hidden attractors via newly commensurate and incommensurate non equilibrium fractional-order chaotic systems

The content of this section has been published in [20].

5.2.1 Introduction

The dynamical system of fractional-order is certainly deemed as a generalization structure of the Integer-order System (IoS). Such system in its fractional-order case has been employed in a broad spectrum of applied sciences such as materials engineering, general mechanics, electrical circuit, physics. It turned out recently that the differential equations of fractional-order can be much better than the Ordinary Differential Equations (ODEs) in describing lots of physical phenomena. For this reason, lots of scholars have been progressively motivated to deeply explore the Fractional-order Systems (FoSs) in their chaotic modes. Till date, several chaotic FoSs have been broadly analyzed, in particular regarding the Lorenz system of fractional-order, the Chua system of fractional-order, and also the Chen system of fractional-order.

More recently, lots of efforts have been devoted to the FoSs that have no equilibrium points, generating complex chaotic behaviors for their modes. In particular, these systems can exhibit special attractors named the hidden attractors. As a matter of fact, there are two classes of chaotic attractors: The so-called self-excited attractors and the hidden ones. It turns out that any unstable equilibrium point does not have any limited neighborhood in which it connects with any attraction basins of such attractors. This is absolutely different than the second class in which an unstable equilibria can excite it. In general, the nonlinear system that has either a stable-, or a line-equilibrium points, or even with non of them, can exhibit such hidden attractors. Due to the absence of any equilibrium, it is extremely complicated to numerically place the attractors of the FoSs through employing the Standard Computational Procedure (SCP), in contrast with a self-excited attractor which could be identified via the SCP itself. The hidden attractors could be considered an exceedingly critical problem, especially in some engineering applied subjects. This, however, returns to their abilities in generating some disastrous perturbations and some other unexpected responses to, e.g, an infrastructure of a bridge, or even a body of an aircraft wing.

In other respects, as a consequence of the resultant chaotic signals from the chaotic system with variable attractors that can be designed with any polarity, such system is deemed as a appropriate solution for lots of chaos-based applied studies in which it can diminish plenty of electronic component parts needed for signal conditioning. In other words, the position of the chaotic attractor will definitely be variable in the phase space, and it could be arbitrarily selected in accordance with the parameters of the offset control. In recent years, a wide diversity of literature have addressed lots of chaotic FoSs with one- and two-boostable variables [210]. Only a few works have addressed these systems with three-boostable variables [211].

In [212], Zhang et al. have established a novel non-equilibrium chaotic IoS of three dimensions. This system is considered the most uncomplicated system in comparison with the other proposed non-equilibrium chaotic systems; since it has a constant, a non-quadratic signum function, and a straightforward linear algebraic construction. Besides, this system hold three inconstant variables, and the hidden attractor has been diffused along each line x, y, z; inside each xz-, yz-, xz-lattice; and within xyz-grid by inserting another three additional controlled constants. In addition, through using some traditional nonlinear analysis schemes, some rich and complex hidden dynamic modes, like the transient transition mode and the chaotic bursting mode have been exposed and investigated numerically.

In view of the aforementioned considerations, this work intends to construct a new FoS based on a chaotic IoS

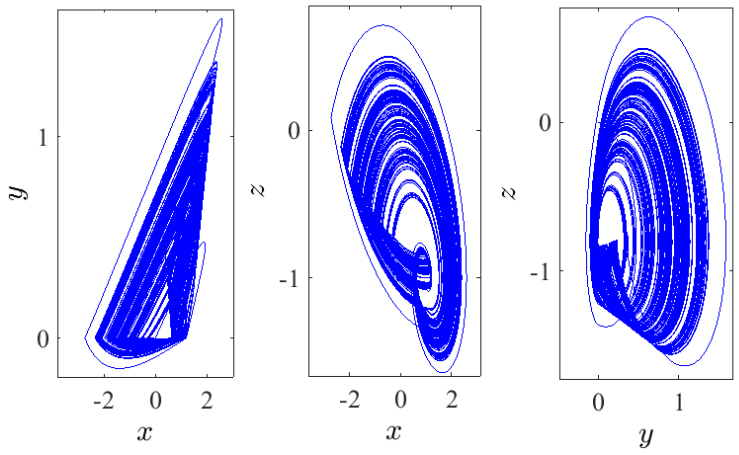

Figure 5.9: System (5.2.1) with its chaotic hidden attractors exhibited in distinct planes according to the IC $(0,0,0)$ when $\alpha = 2.8$, $\beta = 2.8$, $\gamma = 1$ and $\lambda = 0.8$.

that has been recently proposed by Zhang et al. in [212]. Besides, it intends to examine the impact of the incommensurate and commensurate fractional-order derivative on the FoS numerically. Different complex dynamical behaviors of the proposed commensurate and incommensurate FoS is discussed through performing several numerical simulations. Such results are reported with the help of phase portraits in 2D projections, Lyapunov Exponents (LEs), and bifurcation diagrams. The proposed FoS can exhibit different striking phenomena including inversion property, hidden bursting oscillation, coexisting multiple attractors. This system can also degenerate into a 1D-line, 2D-lattice and 3D-grid of variable hidden attractors by including offset boosting parameters for the fractional-order in its both cases; commensurate and incommensurate cases.

5.2.2 A non-equilibrium FoS

A new 3D chaotic IoS has been recently studied in [212]. This system can be expressed by three nonlinear DEs reported below:

$$\begin{cases} \dot{x} = \alpha sgn(y) + \beta z, \\ \dot{y} = \lambda + z, \\ \dot{z} = -\gamma x - z, \end{cases} \tag{5.2.1}$$

where α, β, and λ are nonnegative parameters, $\gamma \neq 0$ is constant, whereas $sgn(y)$ represents the signum function that can be outlined as:

$$sgn(y) = \begin{cases} 1, & y > 0 \\ 0, & y = 0 \\ -1, & y < 0. \end{cases} \tag{5.2.2}$$

In view of some selections of appropriate values for the system's parameters together with the function $sgn(y)$ as it has been addressed in [212], system (5.2.1) will have no equilibria, and a chaotic hidden attractor will be exhibited according to the Initial Condition (IC) $(0,0,0)$ for $\alpha = 2.8$, $\beta = 2.8$, $\gamma = 1$, $\lambda = 0.8$, as it can be seen in Fig. 5.9. However, next we state certain key preliminaries in regard with the non-integer calculus [1]:

Definition 5.2.1. The integral operator of fractional-order q in the sense of Riemann-Liouville of the function

$g \in C^m(0,T]$ is outlined as:

$$I^q g(t) = \frac{1}{\Gamma(q)} \int_0^t \frac{g(s)}{(t-s)^{(1-q)}} ds, \tag{5.2.3}$$

where $q > 0$, $m \in \mathbb{N}$ and $T > 0$.

Definition 5.2.2. The differential operator of fractional-order q in the sense of Caputo of the function $g \in C^m(0,T]$ is outlined as:

$$D^q g(t) = \begin{cases} \dfrac{1}{\Gamma(m-q)} \displaystyle\int_0^t (t-s)^{m-q-1} g^{(m)}(s) ds, & q \in (m-1, m), \\ g^{(m)}(t), & q = m, \end{cases} \tag{5.2.4}$$

where $q \in [m-1, m]$, $m \in \mathbb{N}$ and $T > 0$.

From now on, we intend to generalize the IoS reported in (5.2.1) by considering the following FoD:

$$\begin{cases} D^{q_1} x = \alpha sgn(y) + \beta z, \\ D^{q_2} y = \lambda + z, \\ D^{q_3} z = -\gamma x - z, \end{cases} \tag{5.2.5}$$

where D^{q_j} is the Caputo's operator of order $0 < q_j \leq 1$, $j = 1, 2, 3$, whereas x, y, z are the system's variables. Observe that this system will be a system of commensurate order if $q_1 = q_2 = q_3$, otherwise it will be called an incommensurate system. In this work, although the same parameter values of system (5.2.5) are taken like in [212], this system has no equilibrium point. For all performed numerical simulations, the so-called Adams-Bashforth-Moulton Predictor-Corrector (ABMPC) method [**?**, **?**] is extensively employed to study all resultant behaviors.

5.2.3 The commensurate FoS

In this part, we intend to investigate different dynamics features of the commensurate FoS given in (5.2.5), including the dynamic states analysis of such system versus slight changes in the fractional-order values as well as some other slight changes in the values of system's parameters, inversion property, bursting of hidden attractor, coexisting hidden attractors.

Chaos vs. the variety in the fractional-order values

The dynamic states analysis of system (5.2.5) in its commensurate order case is studied in this subsection through varying the fractional-order value q, and fixing the IC $(0, 0, 0)$ together with the system's parameters $\alpha = 2.8$, $\beta = 2.8$, $\gamma = 1$, and $\lambda = 0.8$. In particular, one can see the bifurcation diagram when $q \in (0.90, 1)$ in Fig. 5.10(a). Based on such figure, different dynamic states of system (5.2.5) are presented in table (5.4). One can observe that system (5.2.5) start from period-1, then develops period-2, period-4 next changes into quasiperiodic state, and finally drops into chaos when commensurate order $q = 0.9747$. The chaos exists when $q \in [0.9747, 0.988) \cup [0.995, 1]$.
At the same time, estimating the LEs is considered another numerical method employed for indicating chaos in the FoS given in (5.2.5), in which the existence of a chaotic behavior for such system can be indicated by the existence of positive LEs. Here Lyapunov exponents are denoted by $LE_i, i = 1, 2, 3$ with $LE_1 > LE_2 > LE_3$. Obviously, the proposed system is chaotic according to the values of the exponents bounded as $LE_1 > 0$, $LE_2 = 0$ and $LE_3 < 0$ with $|LE_1| < |LE_2|$. In [84], the so-called Benettin-Wolf Algorithm (BWA) is presented to identify all LEs for a category of FoSs established using the Caputo's operator. Actually, this method can not be implemented

Table 5.4: Dynamic states of system (5.2.5)

q	Dynamic state
$q \in [0.9000, 0.9300)$	period-1
$q \in [0.9300, 0.9640)$	period-2
$q \in [0.9640, 0.9720)$	period-4
$q \in [0.9720, 0.9747)$	quasiperiodic
$q \in [0.9747, 0.9880)$	chaos
$q \in [0.9880, 0.9950)$	periodic-route
$q \in [0.9950, 1.0000]$	chaos

here as system (5.2.5) is classified as nonsmooth. Therefore, to calculate the LEs, we will first use the same scheme presented in [213], with considering the following substitution [214]:

$$sgn(y) \rightarrow tanh(\rho y),$$

where ρ is constant. In fact, this smooth approximation of the signum function allows to estimate the LEs using the BWA. Indeed, using this algorithm has helped us to calculate all LEs of system (5.2.5) which can be seen in Fig. 5.10(b) for $\rho = 15$. For the fractional order $q = 0.9747$, the three Lyapunov exponents are $LE_1 = 0.08, LE_2 = 0, LE_3 = -1.29$ and $|0.08| < |-1.29|$. The fractional dimension, which presents the complexity of attractor, is defined by

$$D_{KY} = j + \frac{1}{LE_{j+1}} \sum_{i=1}^{j} LE_i,$$

where j is the largest integer satisfying $\sum_{i=1}^{j} LE_i \geq 0$ and $\sum_{i=1}^{j+1} LE_i < 0$. The calculated dimension of system (5.2.5) when $q = 0.9747$ is $D_{KY} = 2.0620 > 2$. In consequence, a chaotic attractor is detectable in the system (See Fig. 5.11). Besides, as a result of system (5.2.5) has no equilibria, the dectecting chaotic attracor is hidden with one scroll, as it can be shown in Fig. 5.11 on different planes for $q = 0.9747$, the IC $(0, 0, 0)$, and the system's parameters $\alpha = 2.8$, $\beta = 2.8$, $\gamma = 1$, $\lambda = 0.8$. Fig. 5.12 presents the basin of attraction of system (5.2.5) for $q = 0.98$. Initial conditions in the yellow region lead to unbounded orbits and those in the blue region lead to chaotic attractor. There is no fixed point in the system for the selected parameters; therefore the chaotic attractor is hidden.

Chaos vs. the variety in the values of system's parameters

In this part, a bifurcation analysis of system (5.2.5) with its commensurate order $q = 0.98$ is discussed by varying the system's parameters α, β, λ, and fixing the parameter $\gamma = 1$. In accordance with the IC $(0, 0, 0)$, several diagrams of bifurcation of system (5.2.5) are demonstrated in Fig. 5.13. In particular, for $\alpha \in (2.3, 3.2)$, the diagram of the bifurcation can be shown in Fig. 5.13(a). Based on such figure, it can be observed that as α reduces, system (5.2.5) displays a periodic route of period-2, period-4. Besides, such system is then turned from a quasiperiodic state to a chaos when $\alpha = 2.85$. In general, this chaotic behavior still exists till $\alpha = 2.75$. After this value, the system appears again a periodic state, while it appears a chaotic state from $\alpha = 2.58$ to $\alpha = 2.68$. In addition, this chaotic behavior disappears after $\alpha = 2.58$.

On the other hand, Fig. 5.13(b) demonstrates the diagram of bifurcation for $\beta \in (2, 3.2)$. Observe that once the parameter β increases, system (5.2.5) appears a periodic route of period 1-2-4, and then it will turn from a quasiperiodic state to a chaos state when $\beta = 2.79$. This chaotic behavior still exists till $\beta = 2.85$. After this

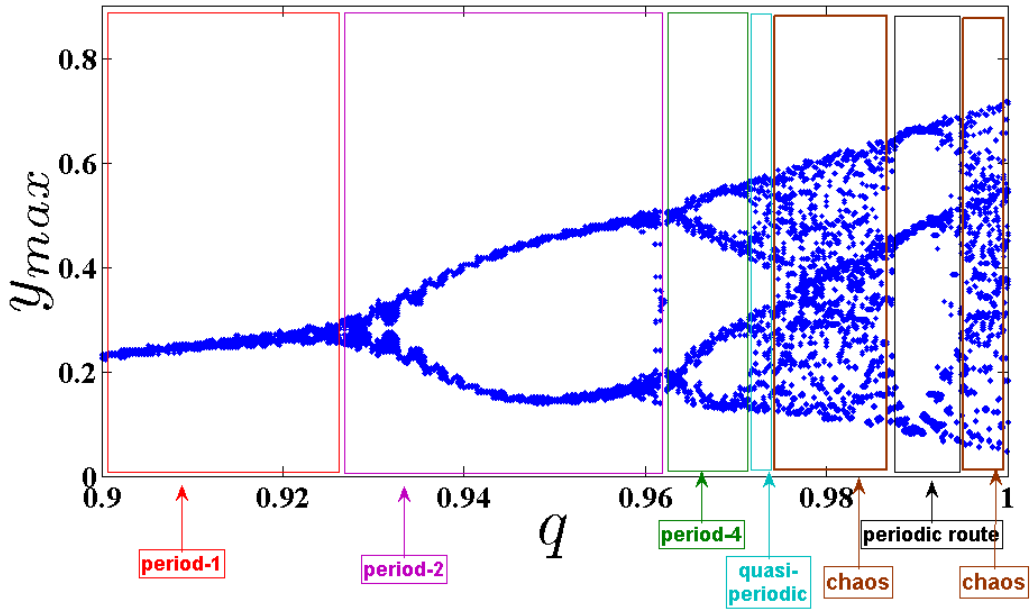

(a)

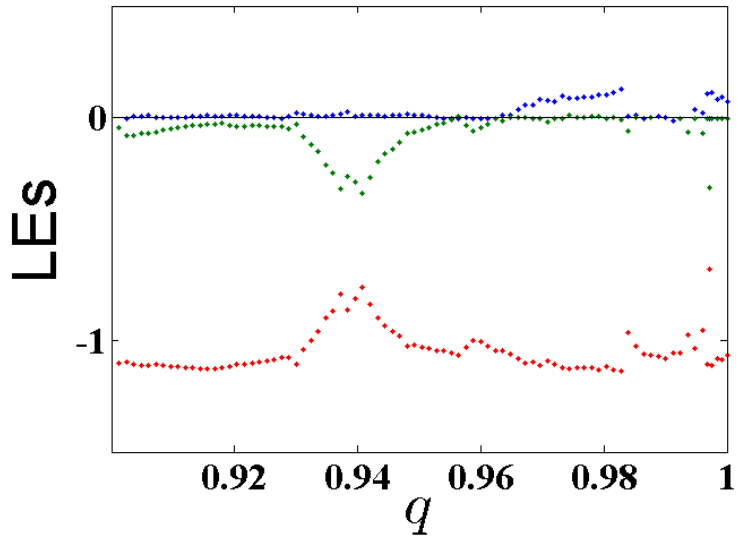

(b)

Figure 5.10: (a) The diagram of bifurcation , (b) LEs, of system (5.2.5) with commensurate order by varing $q \in (0.90, 1)$ according to the IC $(0, 0, 0)$, and the system's parameters $\alpha = 2.8$, $\beta = 2.8$, $\gamma = 1$, $\lambda = 0.8$.

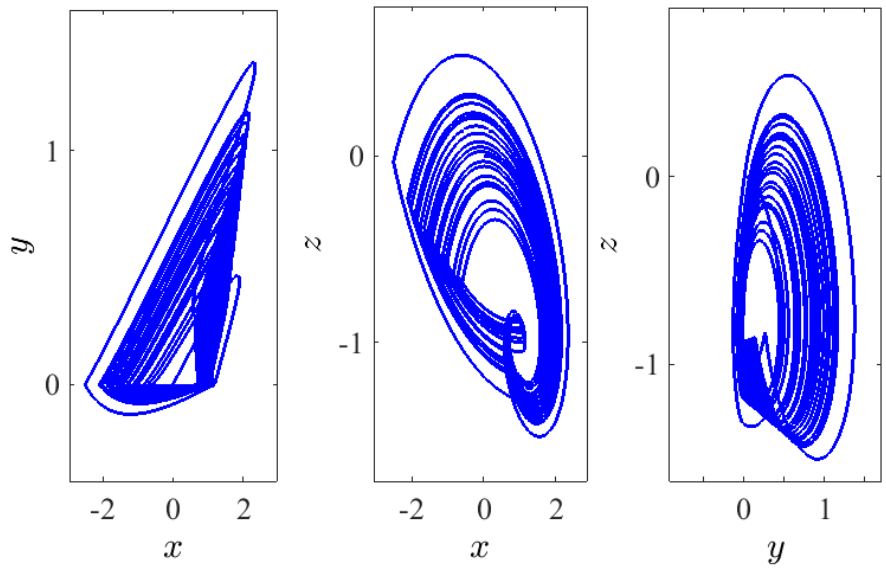

Figure 5.11: Chaotic hidden attractor of system (5.2.5) with commensurate order $q = 0.9747$, shown on different planes according to the IC $(0, 0, 0)$, and the system's parameters $\alpha = 2.8$, $\beta = 2.8$, $\gamma = 1$, $\lambda = 0.8$.

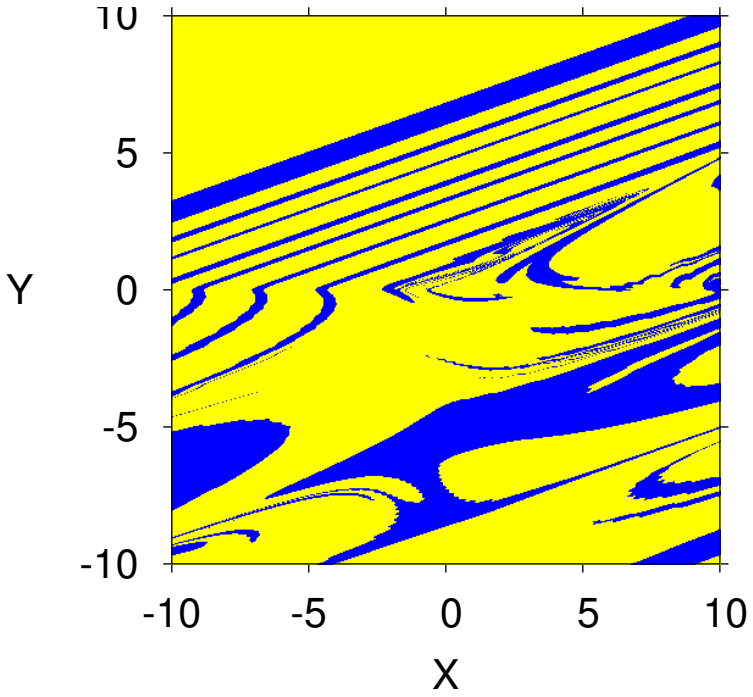

Figure 5.12: Basin of attraction section $x - y$ of attractor shown in Fig.(5.11), for $q = 0.98$, and an initial condition in the third state variable z = 0.

value, a periodic state will be again appeared for this system, and then a chaotic state form $\beta = 2.91$ to $\beta = 3.04$. Afterward, at $\beta = 3.04$, the chaotic behavior of this system will be disappeared.
Finally, Fig. 5.13(c) shows the bifurcation diagram for $\lambda \in (0.1, 1)$. It can be noted that system (5.2.5) will turn from a periodic route to a chaos state when $\lambda = 0.79$. Such chaotic behavior will still exist as $\lambda \in (0.79,\ 0.81) \cup (0.83,\ 0.87)$, and the overall of the chaos state will disappear after this range.

Inversion property

In [212], Zhang et al. have reported that for all signals (x, y, and z) of the IoS given in (5.2.1), the parameter λ possesses an inversion control. This means that the polarity of these signals will be altered when the polarity of the parameter λ is changed. In this subsection, we find that it is interesting to explore whether this property still exists or not for the proposed FoS. For this reason, and according to the IC $(0, 0, 0)$, we take $q = 0.98$, $\alpha = 2.8$, $\beta = 2.8$, and $\gamma = 1$, we plot the phase portraits on different projections as well as the time series graph of system (5.2.5) for two opposite values of parameter $\lambda = \pm 0.8$, as demonstrated respectively in Fig. 5.14 and Fig. 5.15. In view of these two figures, it can be pointed out that when the polarity of term λ is changed, the polarity of all signals x, y and z will be changed too. In other words, the inversion property still exists in the FoS.

Hidden bursting oscillation

The bursting is a particular complex nonlinear practical application which can be witnessed as a significant communication operation in, e.g., endocrine cells and biological neurons [215]. In general, the bursting arises due to the trajectory that subdues several transitions between the fast subsystem's attractors. These transitions can be adapted by the sluggish variable once it periodically crosses through the fast subsystem's bifurcation points [216]. Actually, this exciting application has been extensively handled in several nonlinear FoSs [217]. However, the time series of the state-space variable x together with the phase portraits of system (5.2.5) are plotted in Fig. 5.16 by taking $\alpha = 2.8$, $\beta = 3.4$, $\gamma = 1$, $\lambda = 0.8$, $q = 0.985$, and by assuming the IC $(0, 0, 0)$. For instance, the time series in Fig. 5.16(a) can show a periodic bursting oscillations, whereas the two other figures, Fig. 5.16(b) and Fig. 5.16(c), show the phase portraits which exhibit the chaotic bursting pattern. In particular, when one chooses $q = 0.985$, $\alpha = 2.8$, $\beta = 3.2$, $\gamma = 1$, $\lambda = 0.8$ and the IC as $(1,\ 1,\ -1)$, a new kind of behavior associated with passing transition of system (5.2.5) will be noticed clearly. For more insight, Fig. 5.17(a) shows the time-domain waveform of the state-space variable x, while Fig. 5.17(b) shows its corresponding phase portrait in 3D projection. It can be remarked from these two figures that the trajectories of the FoS given in (5.2.5) incur, with the evolution of time, a transition that ends at a steady chaotic bursting oscillation after it begins at an unstable sink, resulting happening of a complex behavior of the state transition.

Coexisting hidden attractors

The coexisting attractors of the FoS is deemed as an extraordinary phenomenon. It has recently attracted much attention by a number of research groups. Actually, the coexisting attractors of a dynamical system relates to its ICs. For the purpose of showing the coexisting attractors of system (5.2.5), we plot the bifurcation diagram for $q \in (0.9, 1)$ and with $\alpha = 2.8$, $\beta = 2.8$, $\gamma = 1$, $\lambda = 0.8$ as exhibited in Fig. 5.18(a). Two sets of ICs have been considered: The first one is $(0, 0, 0)$ for blue plot and the second one is $(0.5,\ 1,\ -0.2)$ for red plot. The corresponding two plots for the two ICs show that the system will exhibit periodic routes to chaos if the commensurate order q is increased. For instance, the two coexisting hidden attractors of system (5.2.5) are plotted in Fig. 5.18(b) when $q = 0.98$ (arrow L in Fig. 5.18(a)) together with the IC $(0, 0, 0)$ for blue plot, and together with the IC $(0.5, 1, -0.2)$ for red plot. Two periodic and chaotic hidden attractors coexist when $q = 0.9882$ (arrow R in Fig. 5.18(a)) together

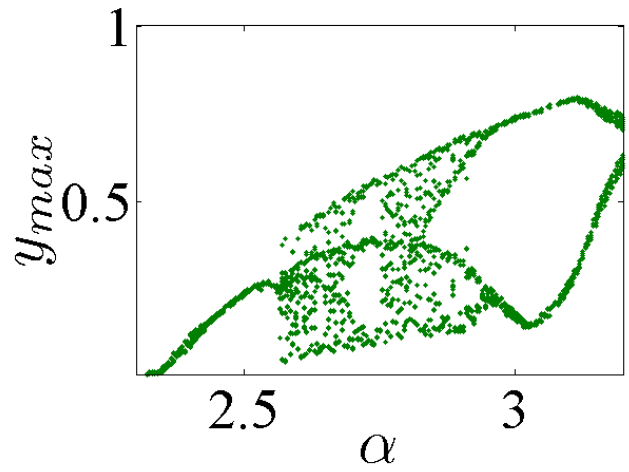

(a)

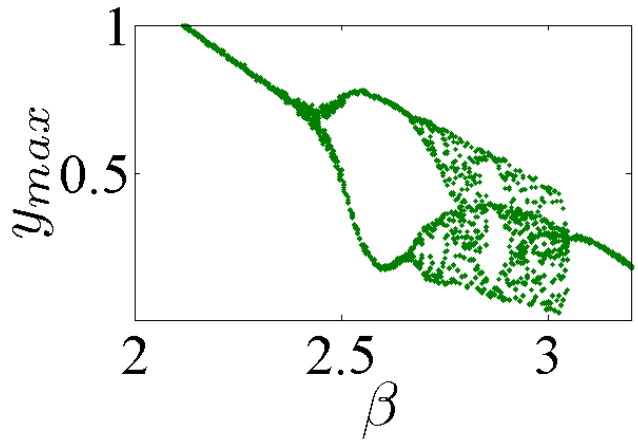

(b)

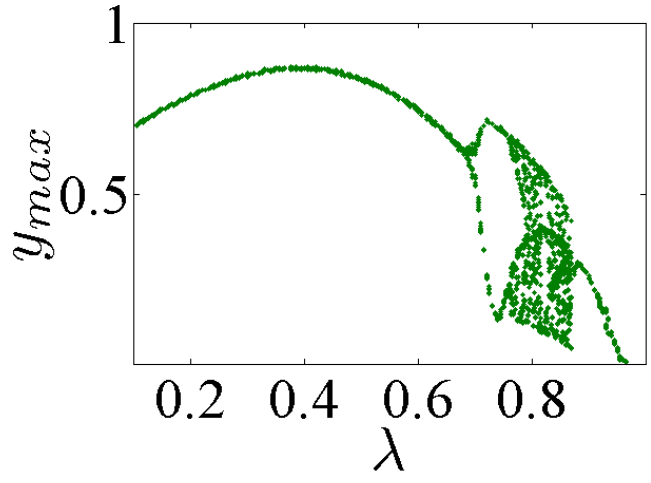

(c)

Figure 5.13: Bifurcation diagrams of system (5.2.5) with commensurate $q = 0.98$ through fixing $\gamma = 1$ and varying the parameters: (a) $\alpha \in (2.3,\ 3.2)$, (b) $\beta \in (2,\ 3.2)$, (c) $\lambda \in (0.1,\ 1)$ according to the IC $(0, 0, 0)$.

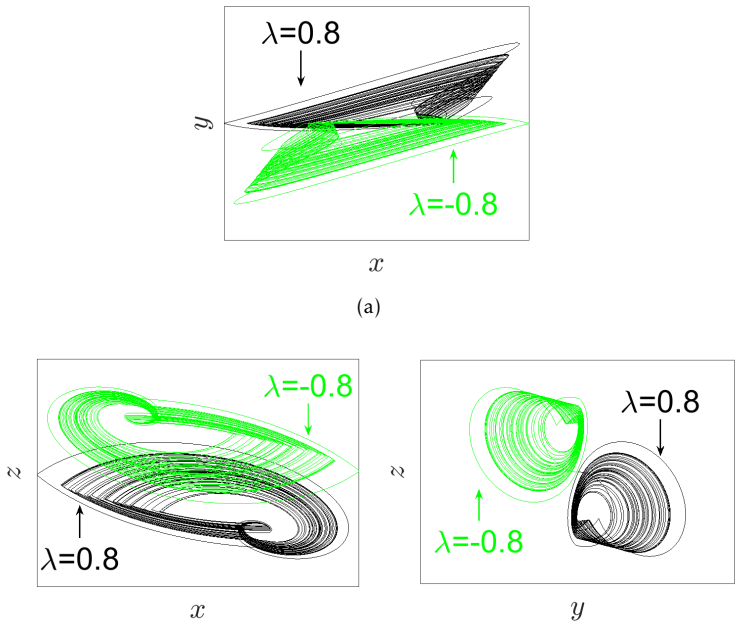

Figure 5.14: The phase portraits of system (5.2.5) with its commensurate order $q = 0.98$ according to IC $(0, 0, 0)$, and the parameters' values $\alpha = 2.8$, $\beta = 2.8$, $\gamma = 1$, $\lambda = \pm 0.8$ on different projections (black plot for $\lambda = 0.8$, green plot for $\lambda = -0.8$). (a) xy-plane, (b) xz-plane, (c) yz-plane.

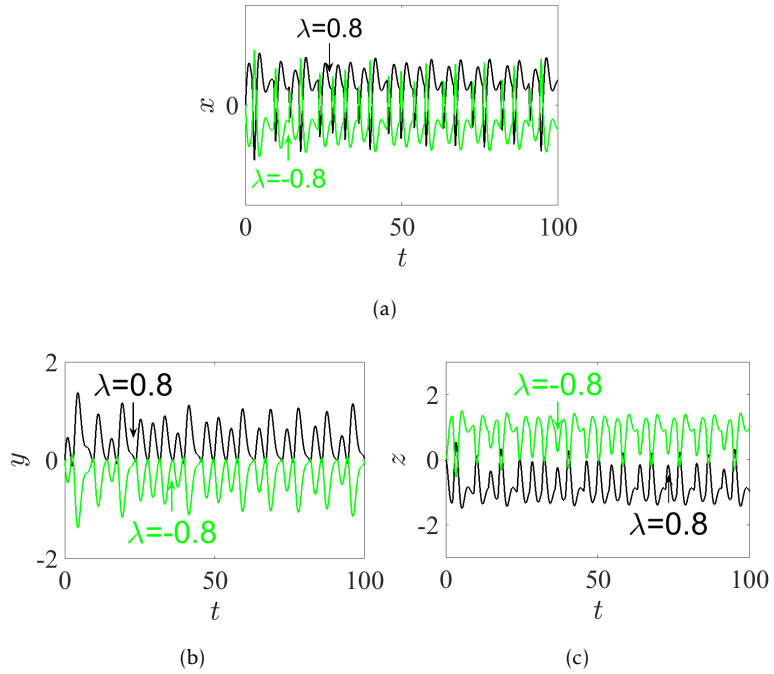

Figure 5.15: The time series of system (5.2.5) with its commensurate order $q = 0.98$, corresponding to its IC $(0, 0, 0)$ and its parameters $\alpha = 2.8$, $\beta = 2.8$, $\gamma = 1$, and $\lambda = \pm 0.8$ (black plot for $\lambda = 0.8$, green plot for $\lambda = -0.8$). (a) The state-space variable x, (b) The state-space variable y, (c) The state-space variable z.

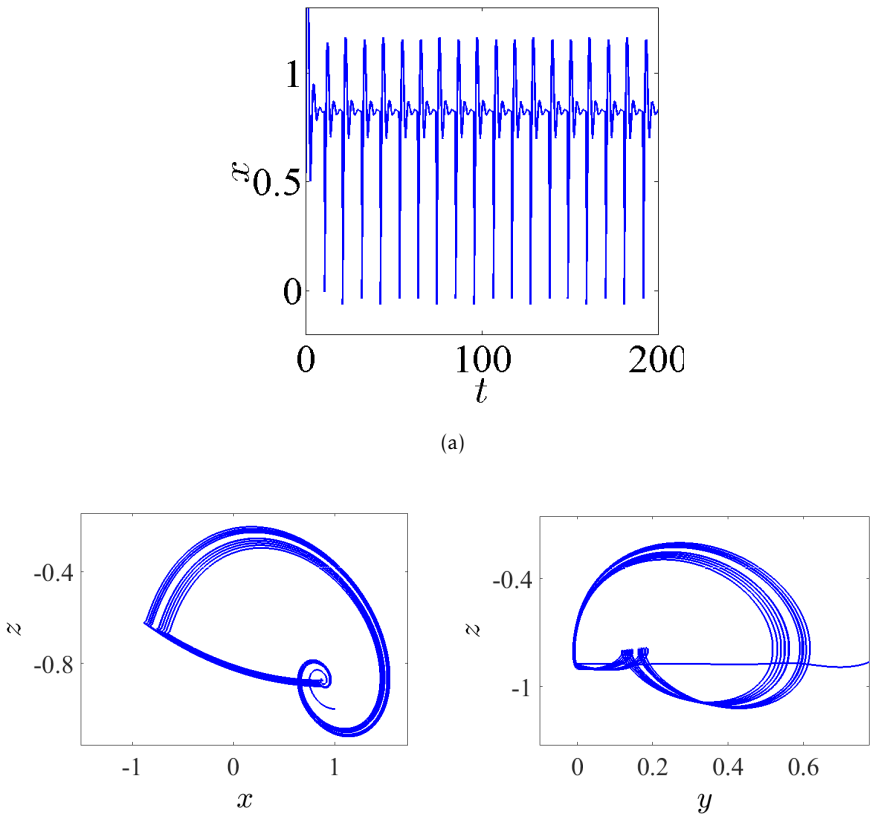

Figure 5.16: The chaotic bursting oscillation according to the IC $(0,0,0)$, with $q = 0.985$, $\alpha = 2.8$, $\beta = 3.4$, $\gamma = 1$, $\lambda = 0.8$, (a) The time series of the state-space variable x. (b) The phase portrait in xz-plane, (c) The phase portrait in yz-plane.

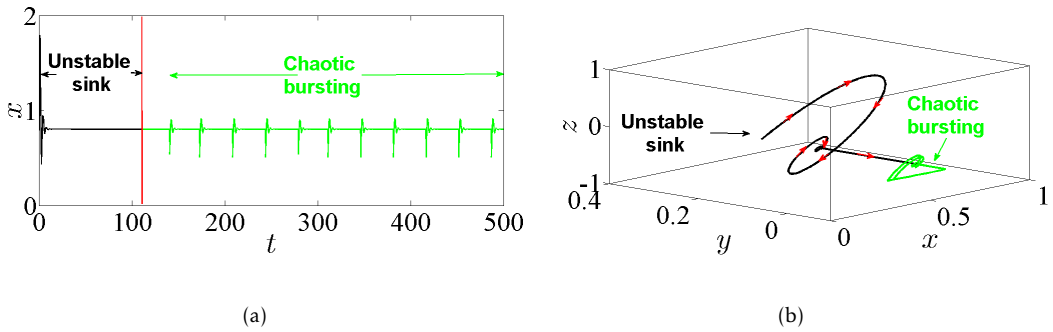

Figure 5.17: Passing transition behavior according to the IC $(1,\ 1,\ -1)$, with $q = 0.985$, $\alpha = 2.8$, $\beta = 3.2$, $\gamma = 1$, $\lambda = 0.8$, (a) The corresponding time series of the state-space variable x, (b) The phase portrait in 3D projection.

with the IC $(0,0,0)$ for blue plot, and together with the IC $(0.5,1,-0.2)$ for red plot. It is noticed that the type of hidden attractors not only depend on the value of q but also on the initial condition. The basin of attractions in Fig. 5.18(c) supports this results whereas initial conditions in yellow region leads to unbounded orbits and those in the two regions red and blue lead to chaotic attractors. Besides, the system can offer numerous coexisting hidden attractors as shown in Fig. 5.19(a), with three ICs: $(0,0,0)$, $(0.5,\ 1,\ -0.2)$ and $(0.2,\ -0.2,\ 0.2)$, the corresponding basin of attractions is shown in Fig. 5.19(b).

5.2.4 Incommensurate FoS

This part studies the same dynamics features, which have been discussed in the previous section, of the FoS given in (5.2.5), but this time for incommensurate order. First of all, we intend to study the dynamic states of this system by varying its incommensurate orders q_1, q_2 and q_3, fixing its parameters $\alpha = 2.8$, $\beta = 2.8$, $\gamma = 1$, $\lambda = 0.8$, and also fixing its IC as $(0,0,0)$. The diagrams of bifurcation and the LEs of this system (5.2.5) with its incommensurate order given above are exhibited in Fig. 5.20, Fig. 5.21 and Fig. 5.22, respectively. Actually, these figures display the ranges that illustrate where the system appears periodic states, quasiperiodic states, and also chaos states.
With the aim of demonstrating the impact of changing the nature of the fractional-order value on the system's dynamics, we intend to perform a comparison between the two system's dynamical states gained from both cases, commensurate and incommensurate cases, in accordance with varying the system's parameter γ. For this reason, the Lyapunov exponents are calculated and plotted in Fig. 5.23 as function of parameter γ by selecting the commensurate order as $q = 0.98$ (see Fig. **??**(a)) and the incommensurate orders as $[q_1,q_2,q_3] = [0.97,1,1]$, $[q_1,q_2,q_3] = [1,0.97,1]$ and $[q_1,q_2,q_3] = [1,1,0.99]$, see Fig. **??**(b), Fig.5.23(c), Fig. 5.23(d), respectively. It can be seen from these figures that the ranges in which system (5.2.5) exhibits chaos are different. As parameter c increases, arrow C in Figs. 5.23 represents the maximum value as possible of c where the system generates chaos. In particular, the largest range in which the chaos exists is the range that appears when taking the commensurate order $q = 0.98$ as exhibited in Fig. 5.23(a). Besides, the closest range to the chaotic one, which is exhibited from the IoS given in (5.2.1), is occurred when the incommensurate order $[q_1,q_2,q_3] = [1,0.97,1]$ are taken (see Fig. 5.23(c) and Fig. [212]). In general, all these results confirm that the nature of fractional-order value has a key role in effecting on the dynamics of the FoS.
For the purpose of exhibiting the inversion property of system (5.2.5) with its incommensurate orders, such orders are selected as $[q_1,q_2,q_3] = [0.97,1,1]$, the system's parameters are picked to be as $\alpha = 2.8$, $\beta = 2.8$, $\gamma = 1$, and the IC is set to be as $(0,0,0)$. It turns out that this system has the phase portraits plotted in Fig. 5.24 on distinct projections according to two opposite values of parameter $\lambda = \pm 0.8$. In view of such numerical findings, one could conclude that when the polarity of λ is changed, all system's signals x, y and z will be consequently changed. This implies that the inversion property will still exist if the FoS has incommensurate orders.
From another point of view, letting the incommensurate orders to be as $[q_1,q_2,q_3] = [0.97,1,1]$, the parameters as $\alpha = 2.8$, $\beta = 3.2$, $\gamma = 1$, $\lambda = 0.8$, and the IC to be as $(1,\ 1,\ -1)$ yield Fig. 5.25 that exhibits the time-domain waveform of the state-space variable x (see Fig. 5.25(a)) and its corresponding phase portrait in 3D projection (see Fig. 5.25(b)). It can be remarked from these figures that the trajectories of system (5.2.5) incur a transition, with the evolution of time, which ends at a steady chaotic bursting oscillation after it begins at an unstable sink. Therefore, a bursting hidden attractor is indeed exhibited for system (5.2.5) with its incommensurate orders.
In accordance with different incommensurate fractional orders and three ICs: $(0,0,0)$, $(0.5,\ 1,\ -0.2)$ and $(0.2,\ -0.2,\ 0.2)$, system (5.2.5) can also exhibit multiple coexisting hidden attractors for for $[q_1,q_2,q_3] = [0.97,1,1]$as shown in Fig.**??**.

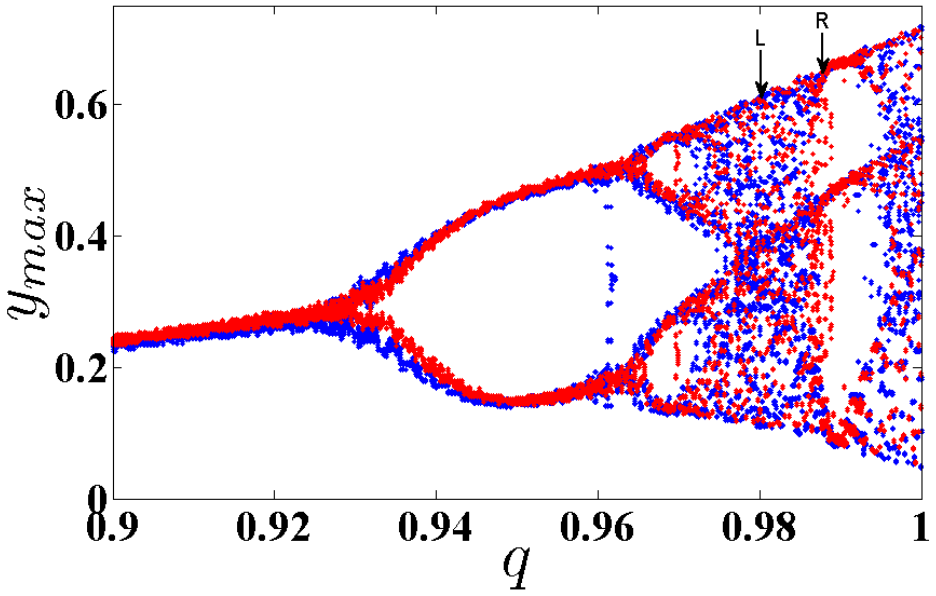

(a)

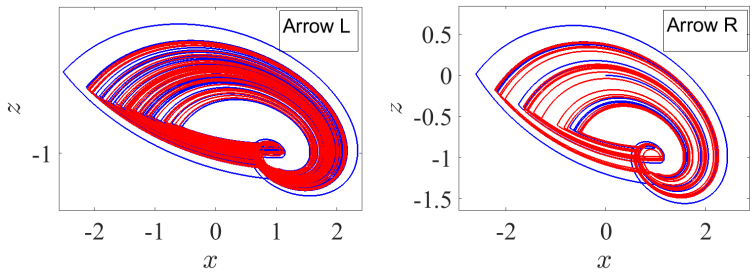

(b)

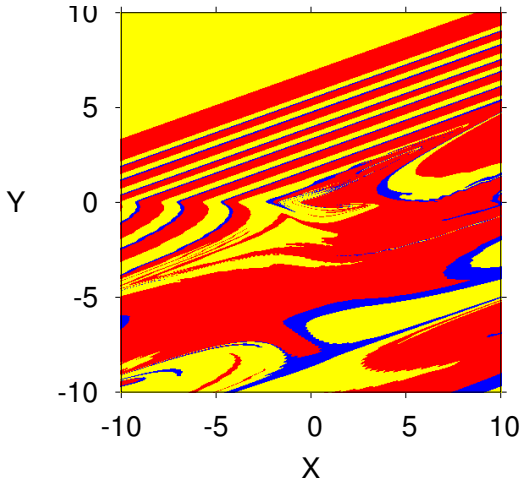

(c)

Figure 5.18: (a) The diagram of bifurcation of the FoS given in (5.2.5) for $q \in (0.9, 1)$ with two set of ICs: $(0, 0, 0)$ (blue plot) and $(0.5,\ 1,\ -0.2)$ (red plot), (b) Two coexisting hidden attractors for $q = 0.98$ (arrow L in Fig. 5.18(a)) and for $q = 0.9882$ (arrow R in Fig. 5.18(a)) corresponding to two set of ICs: $(0, 0, 0)$ (blue plot) and $(0.5,\ 1,\ -0.2)$ (red plot). (c)Basin of attraction section $x - y$ of attractors shown in Fig. 5.18(b)(arrow L), for $q = 0.98$, and an initial condition in the third state variable $z = 0$. The colors in the figure, are related to the colors in the attractors from Fig. 5.18(b)(arrow L).

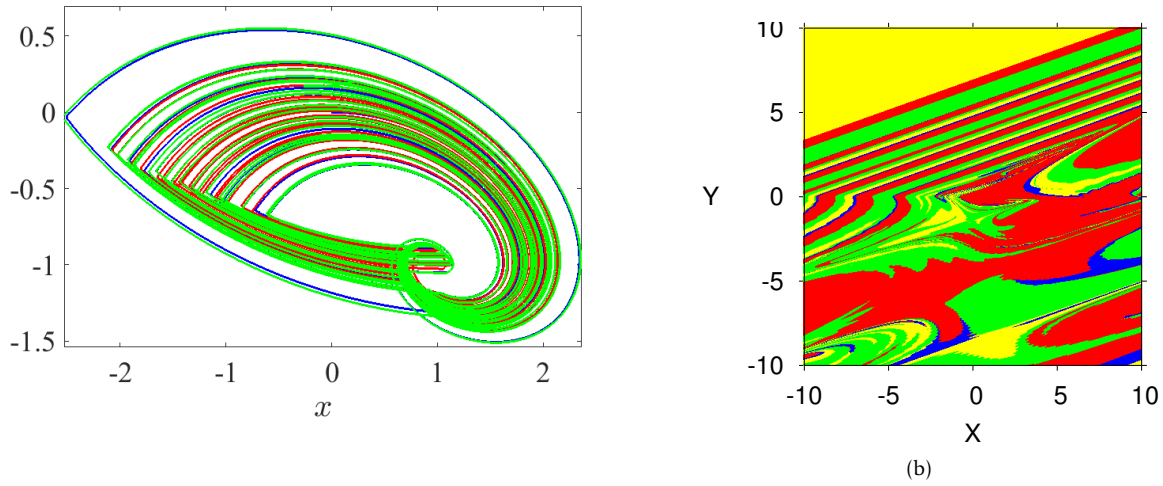

(b)

(b)

Figure 5.19: (a)Multiple coexisting hidden attractors for three ICs: $(0, 0, 0)$, $(0.5,\ 1,\ -0.2)$ and $(0.2,\ -0.2,\ 0.2)$. (b) Basin of attraction section $x - y$ of attractors shown in Fig. 5.19(a), for $q = 0.98$, and an initial condition in the third state variable $z = 0$. The colors in the figure, are related to the colors in the attractors from Fig. 5.19(a) .

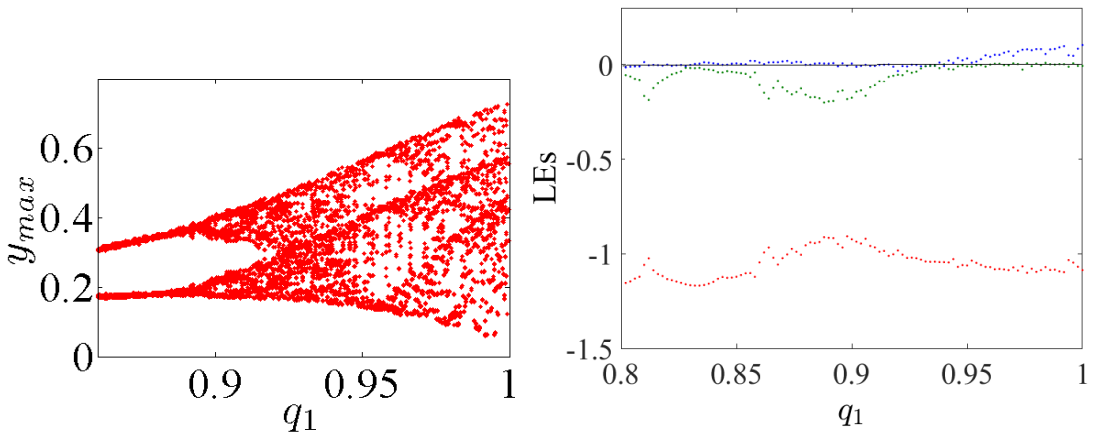

(a) (b)

Figure 5.20: (a) The diagram of bifurcation, (b) The LEs of system (5.2.5) with incommensurate order by varying $q_1 \in (0.80,\ 1)$, and fixing $q_2 = 1$, $q_3 = 1$ with $\alpha = 2.8$, $\beta = 2.8$, $\gamma = 1$, $\lambda = 0.8$ and with the IC $(0, 0, 0)$.

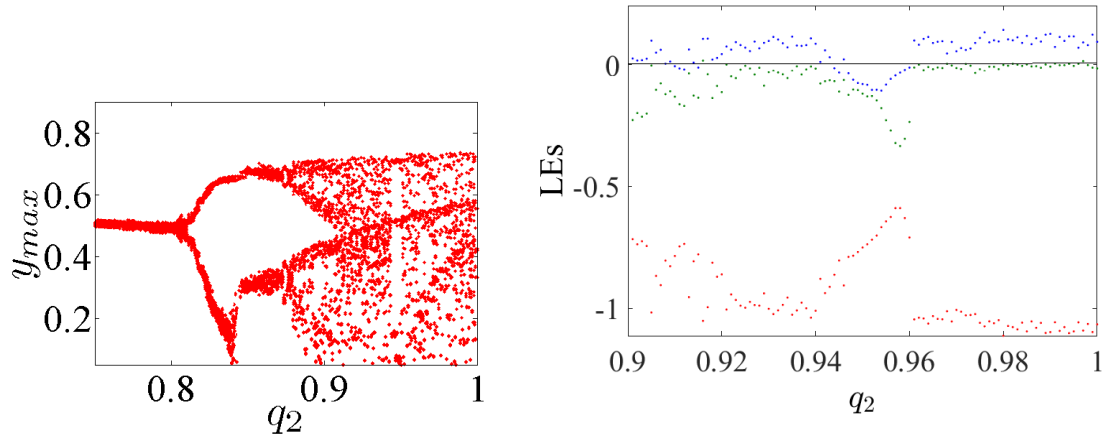

(a) (b)

Figure 5.21: (a) The diagram of bifurcation, (b) The LEs of system (5.2.5) with incommensurate order by varying $q_2 \in (0.75,\ 1)$, and fixing $q_1 = 1$, $q_3 = 1$ with $\alpha = 2.8$, $\beta = 2.8$, $\gamma = 1$, $\lambda = 0.8$ and with the IC $(0, 0, 0)$.

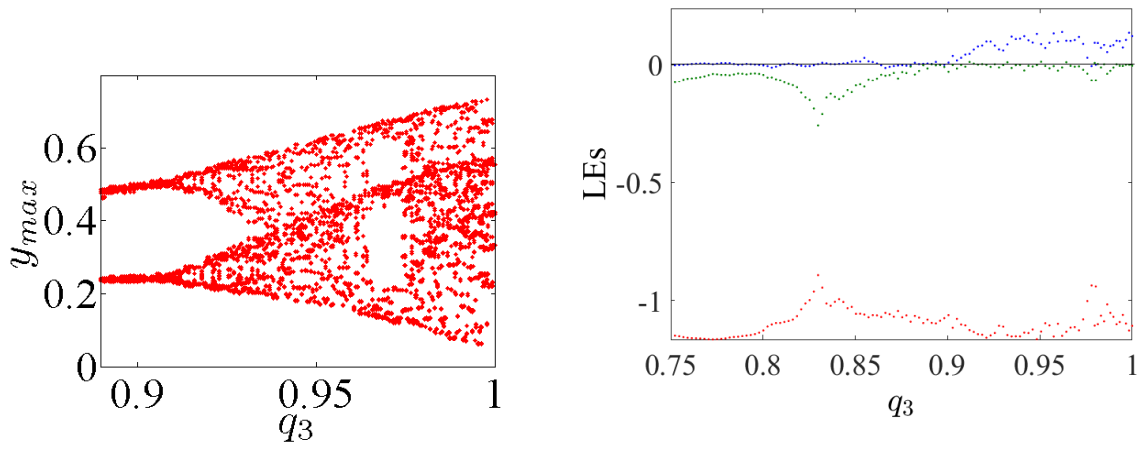

(a) (b)

Figure 5.22: (a) The diagram of bifurcation, (b) The LEs of system (5.2.5) with incommensurate order by varying $q_3 \in (0.75,\ 1)$, and fixing $q_1 = 1$, $q_2 = 1$ with $\alpha = 2.8$, $\beta = 2.8$, $\gamma = 1$, $\lambda = 0.8$ and with the IC $(0, 0, 0)$.

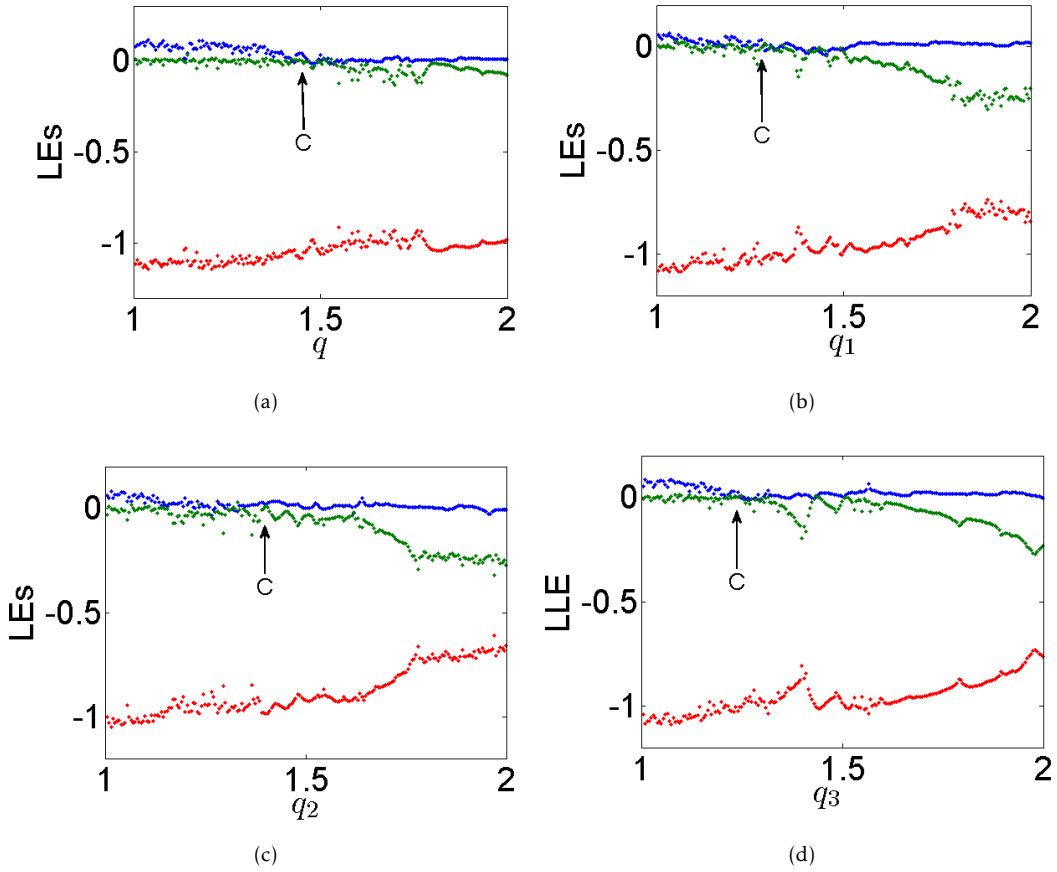

Figure 5.23: The diagrams of LEs of incommensurate system (5.2.5) as function of γ for: (a) commensurate order $q = 0.98$ and incommensurate orders: (b) $[q_1, q_2, q_3] = [0.97, 1, 1]$, (c) $[q_1, q_2, q_3] = [1, 0.97, 1]$, (d) $[q_1, q_2, q_3] = [1, 1, 0.99]$.

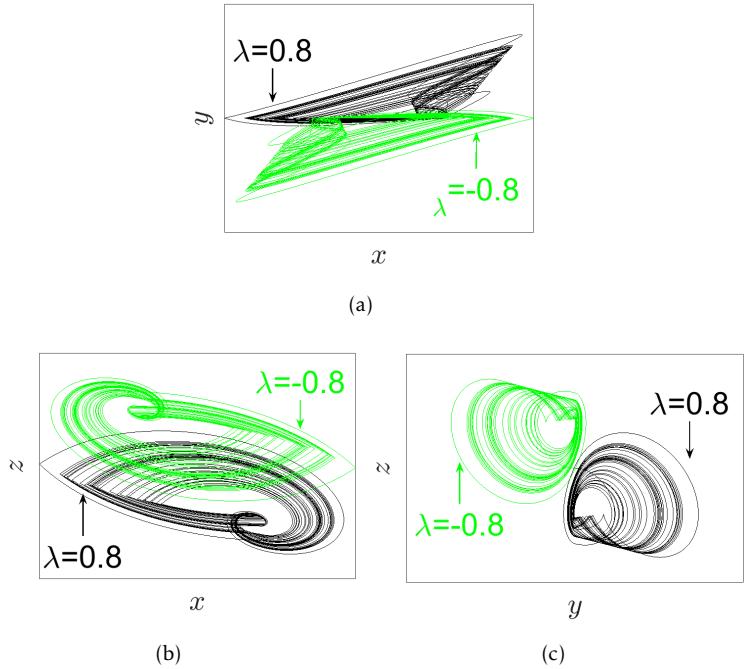

Figure 5.24: The phase portraits of system (5.2.5) with the incommensurate orders $[q_1, q_2, q_3] = [0.97, 1, 1]$, and with $\alpha = 2.8$, $\beta = 2.8$, $\gamma = 1$, in accordance with the IC $(0, 0, 0)$ and with the parameter $\lambda = \pm 0.8$ on distinct projections (black plot for $\lambda = 0.8$, green plot for $\lambda = -0.8$). (a) xy-plane, (b) xz-plane, (c) yz-plane.

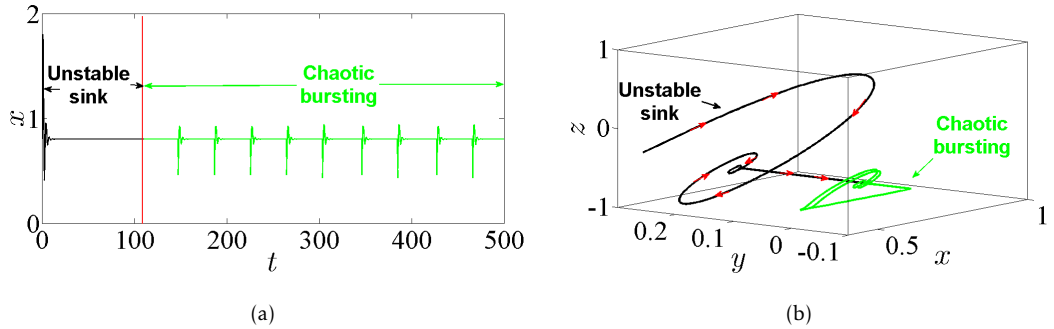

Figure 5.25: Passing transition behavior by taking the orders $[q_1, q_2, q_3] = [0.97, 1, 1]$, the parameters $\alpha = 2.8$, $\beta = 3.2$, $\gamma = 1$, $\lambda = 0.8$, and the IC $(1,\ 1,\ -1)$. (a) The corresponding time series of the state-space variable x and (b) The phase portrait in 3D projection.

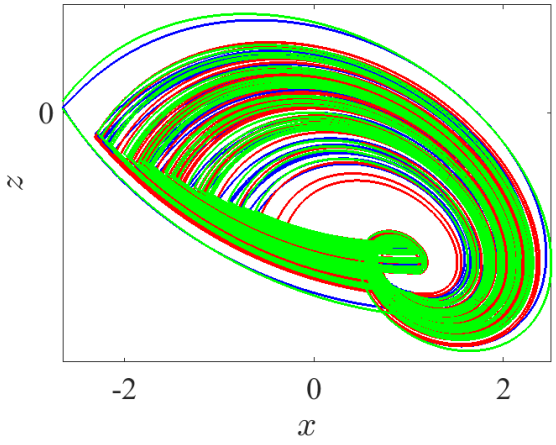

Figure 5.26: Multiple coexisting hidden attractors according to three ICs: $(0,0,0)$, $(0.5,1,-0.2)$ and $(0.2,-0.2,0.2)$ for $[q_1,q_2,q_3]=[0.97,1,1]$.

5.2.5 Variable-boostable hidden attractors of commensurate and incommensurate FoS

In order to attain the complete range of the signal's linear transformations, the offset boosting can be set together with the so-called amplitude control. It appeared that a novel boosting controller, which was introduced in [135], has an ability of destroying the symmetry of the variable-boostable system. In this part, we intend to introduce three additional controlled constants η, ω, and ℓ in accordance with the variables x, y, and z, respectively. The FoS given in (5.2.5) will then be as:

$$\begin{cases} D^{q_1}x=\alpha sgn(y+\omega)+\beta(z+\ell),\\ D^{q_2}y=\lambda+(z+\ell),\\ D^{q_3}z=-\gamma(x+\eta)-(z+\ell). \end{cases} \tag{5.2.6}$$

Next, in accordance with $\alpha=2.8$, $\beta=2.8$, $\gamma=1$, $\lambda=0.8$ together with the IC $(0,0,0)$, three numerical cases will be examined for dealing with the variable-boostable hidden attractors of system (5.2.6). Besides, we will further select the commensurate and incommensurate fractional-order values as $q=0.98$ and $[q_1,q_2,q_3]=[0.98,1,1]$, respectively. It should be noted here that all the attractors of system (5.2.6) are hidden because it has no equilibria irrespective of the system's parameters, the additional controlled values, and even the initial values.

State 1: A line of variable hidden attractors

Through controlling each parameter of the offset boosting, a variable hidden attractor can be distributively ordered on a line. That is;

* Once $\omega=\ell=0$ and η varies, the variable hidden attractor will be diffused on the x-axis as evidenced in Fig. **??**(a) for commensurate system, and Fig. 5.28(a) for incommensurate system.

* Once $\eta=\ell=0$ and ω varies, the variable hidden attractor will be diffused on the y-axis as evidenced in Fig. **??**(b) for commensurate system, and Fig. 5.28(b) for incommensurate system.

* Once $\eta=\omega=0$ and ℓ varies, the variable hidden attractor will be diffused on the z-axis as evidenced in Fig. **??**(c) for commensurate system, and Fig. 5.28(c) for incommensurate system.

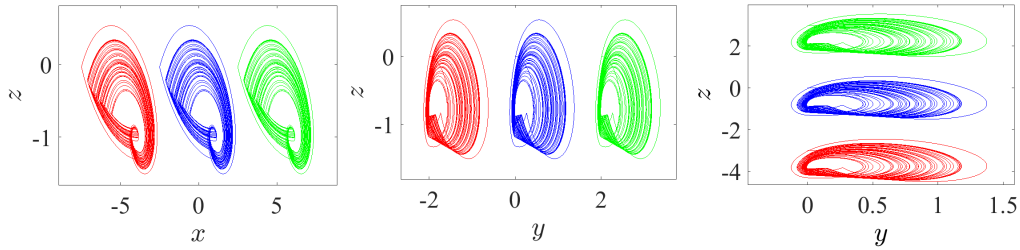

Figure 5.27: Propagating of the variable one-scroll chaotic hidden attractor on a line corresponding to the IC $(0,0,0)$, and according to $\gamma = 1$, $\lambda = 0.8$, $\alpha = 2.8$, $\beta = 2.8$ and $q = 0.98$. (a) x-line when $\eta = 0$ and $\eta = \pm 5$, (b) y-line when $\omega = 0$ and $\omega = \pm 2$, (c) z-line when $\ell = 0$ and $\ell = \pm 3$.

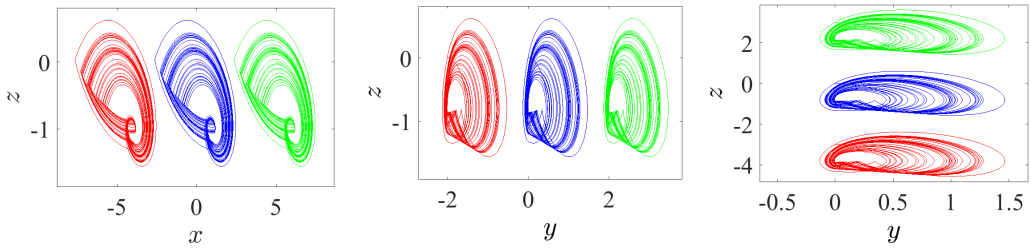

Figure 5.28: Propagating of the variable one-scroll chaotic hidden attractor on a line corresponding to the IC $(0,0,0)$, and according to $\gamma = 1$, $\lambda = 0.8$, $\alpha = 2.8$, $\beta = 2.8$, and $[q_1, q_2, q_3] = [0.98, 1, 1]$. (a) x-line when $\eta = 0$ and $\eta = \pm 5$, (b) y-line when $\omega = 0$ and $\omega = \pm 2$, (c) z-line when $\ell = 0$ and $\ell = \pm 3$.

State 2: A lattice of variable hidden attractors

To gain a lattice dynamics consisting of variable hidden attractors, one of the controlled parameters should be kept at zero, while the other two ones should be simultaneously adjusted. However, one can track the following manner for appropriate selection of such combination:

* Once $\omega = 0$ and each of η and ℓ vary, the variable hidden attractors will be diffused on the xz-lattice as demonstrated in both figures; Fig. 5.29(a) for commensurate system, and Fig. 5.30(a) for incommensurate system.

* Once $\eta = 0$ and each of ω and ℓ vary, the variable hidden attractors will be diffused on the yz-lattice as demonstrated in both figures; Fig. 5.29(b) for commensurate system, and Fig. 5.30(b) for incommensurate system.

* Once $\ell = 0$ and each of η and ω vary, the variable hidden attractors will be diffused on the xy-lattice as demonstrated in both figures; Fig. 5.29(c) for commensurate system, and Fig. 5.30(c) for incommensurate system.

State 3: A 3D grid of variable hidden attractors

In this state, all three control parameters η, ω and ℓ are simultaneously changed to meet suitable values. However, the variable hidden attractors are plotted in two figures; Fig. 5.31 for commensurate system, and Fig. **??** for incommensurate system. These attractors are clearly distributively ordered on the xyz-grid. Fig. 5.33 present basin

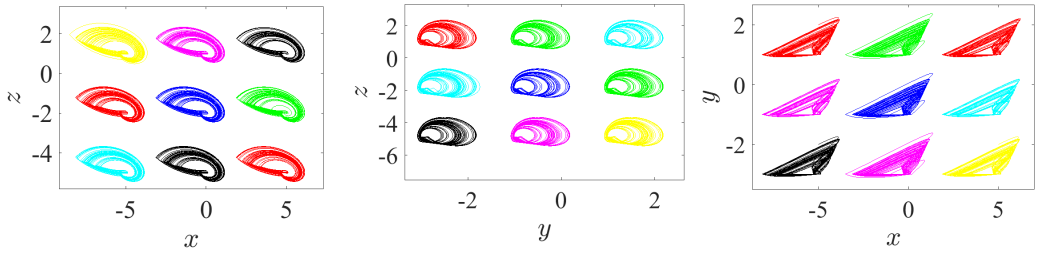

Figure 5.29: Propagating of the variable one-scroll chaotic hidden attractor on a lattice corresponding to the IC $(0,0,0)$, and according to $\gamma = 1$, $\lambda = 0.8$, $\alpha = 2.8$, $\beta = 2.8$ and $q = 0.98$. (a) xz-lattice when $(\eta,\ell) = (-4,4)$, $(-4,-2)$, $(-4,1)$, $(6,-2)$, $(6,1)$, $(6,4)$, $(1,-2)$, $(1,4)$, $(1,1)$; (b) yz-lattice when $(\omega,\ell) = (3,-2)$, $(3,4)$, $(-1,4)$, $(-1,-2)$, $(-1,1)$, $(1,4)$, $(1,-2)$, $(3,1)$, $(1,1)$; (c) xy-lattice when $(\eta,\omega) = (6,-1)$, $(6,3)$, $(6,1)$, $(-4,3)$, $(-4,-1)$, $(-4,1)$, $(1,3)$, $(1,-1)$, $(1,1)$.

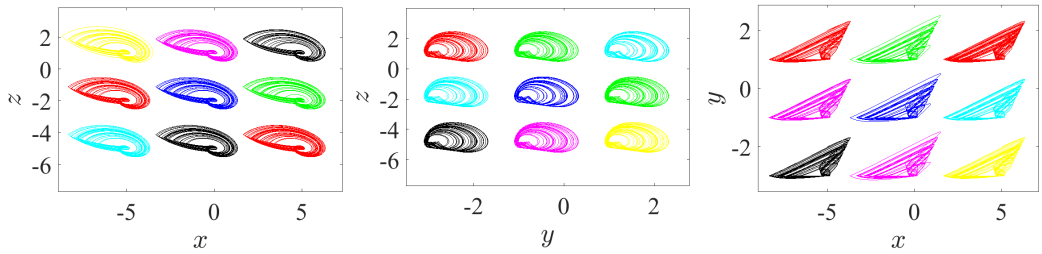

Figure 5.30: Propagating of the variable one-scroll chaotic hidden attractor on a lattice corresponding to the IC $(0,0,0)$, and according to $\gamma = 1$, $\lambda = 0.8$, $\alpha = 2.8$, $\beta = 2.8$ and $[q_1,q_2,q_3] = [0.98,1,1]$. (a) xz-lattice when $(\eta,\ell) = (-4,4)$, $(-4,-2)$, $(-4,1)$, $(6,-2)$, $(6,4)$, $(6,1)$, $(1,-2)$, $(1,4)$, $(1,1)$; (b) yz-lattice when $(\omega,\ell) =(3,-2)$, $(3,4)$, $(3,1)$, $(-1,4)$, $(-1,-2)$, $(-1,1)$, $(1,4)$, $(1,-2)$, $(1,1)$; (c) xy-lattice when $(\eta,\omega) = (6,-1)$, $(6,3)$, $(6,1)$, $(-4,3)$, $(-4,-1)$, $(-4,1)$, $(1,3)$, $(1,-1)$, $(1,1)$.

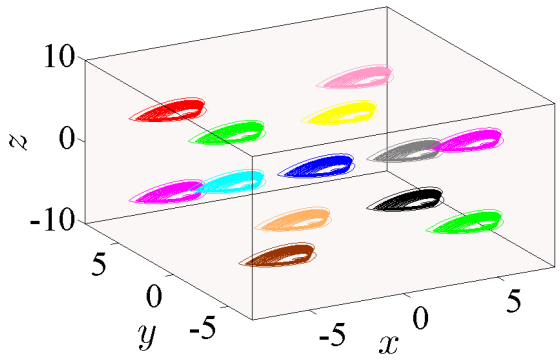

Figure 5.31: Propagating of the variable one-scroll chaotic hidden attractor on a 3D xyz-grid corresponding to the IC $(0,0,0)$, and according to $\gamma = 1$, $\lambda = 0.8$, $\alpha = 2.8$, $\beta = 2.8$ and $q = 0.98$, for $(\eta,\omega,\ell) = (0,0,0)$, $(-3,-3,-3)$, $(?3,3,?3)$, $(?3,3,3)$, $(3,-3,3)$, $(3,?3,-3)$, $(3,3,3)$, $(-5,-5,-5)$, $(-5,5,-5)$, $(-5,5,5)$, $(5,-5,5)$, $(5,-5,-5)$, $(5,5,5)$.

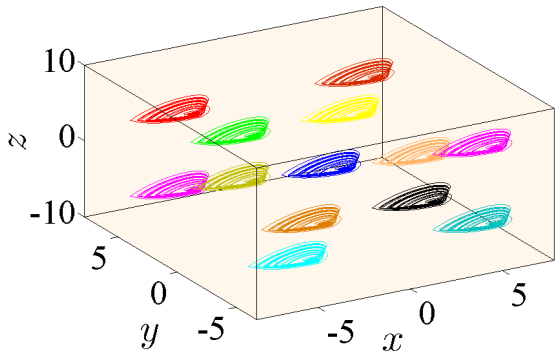

Figure 5.32: Propagating of the variable one-scroll chaotic hidden attractor on a 3D xyz-grid corresponding to the IC $(0,0,0)$, and according to $\gamma = 1$, $\lambda = 0.8$, $\alpha = 2.8$, $\beta = 2.8$ and $[q_1,q_2,q_3] = [0.98,1,1]$, for $(\eta,\omega,\ell) = (0,0,0)$, $(-3,-3,-3)$, $(?3,3,?3)$, $(?3,3,3)$, $(3,-3,3)$, $(3,?3,-3)$, $(3,3,3)$, $(-5,-5,-5)$, $(-5,5,-5)$, $(-5,5,5)$, $(5,-5,5)$, $(5,-5,-5)$, $(5,5,5)$.

of attractions of many attractors shown in Fig. 5.32 (seven attractors from the grid), for $[q_1,q_2,q_3] = [0.98,1,1]$. Initial conditions in gray color lead to unbounded orbits and those in the different colors lead to strange attractors. There is no fixed points in the system for the selected parameters; therefore the chaotic attractor is hidden.

5.2.6 Conclusion

A newly three dimensional version of non-equilibrium chaotic system of fractional-order has been established, and numerically explored its properties and scaling behaviors. Various dynamical behaviors have also been revealed for this system, such as examining its dynamic states in accordance with commensurate and incommensurate fractional-order of its derivatives, investigating its dynamic states in accordance with its parameters, knowing whether if it possesses the inversion property, exploring its hidden chaotic bursting, and also its coexistng multiple hidden attractors. It has been turned out that there are three changeable variables are possessed by this fractional-order system. Besides, the hidden attractors of such system in its two cases, the commensurate and incommensurate ones, can be diffused on a1D-line, 2D-lattice and also on 3D-grid, through inserting three additional controlled constants to the system itself.

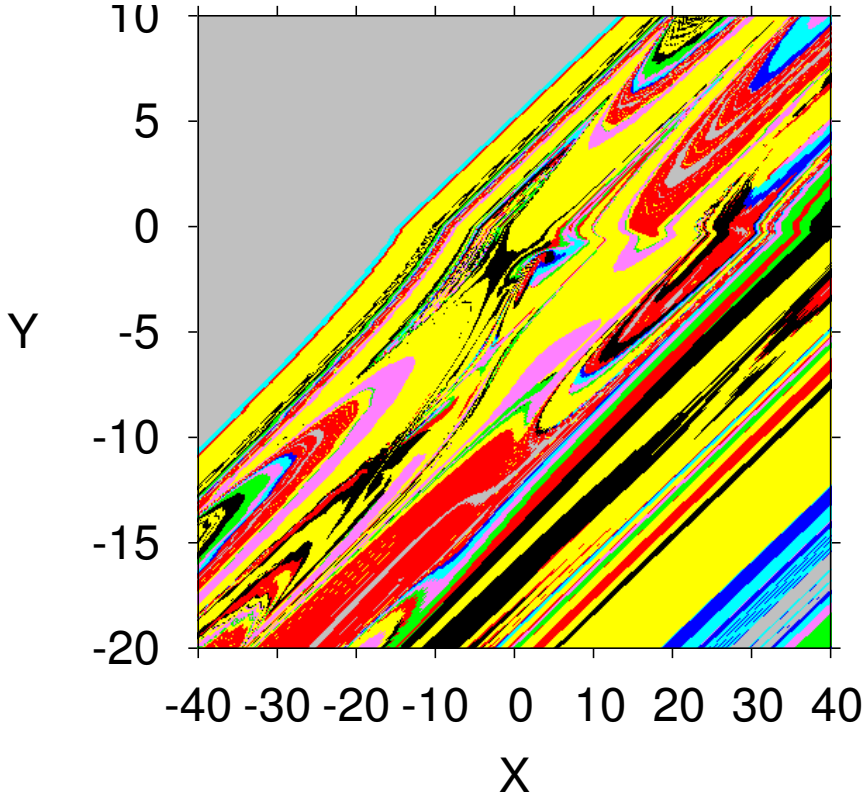

Figure 5.33: Basin of attraction section x-y of many attractors shown in Fig. **??**, for $[q_1, q_2, q_3] = [0.98, 1, 1]$, and an initial condition in the third state variable $z = 0$. The colors in the figure, are related to the colors in the attractors from Fig. **??**.

GENERAL CONCLUSION

In this work, we presented a study of some fractional-order chaotic systems, to achieve the objective of this study we have divided our thesis into five chapters. The first two chapters contain some basic concepts, mathematic tools and numerical methods which are eventually used in study of chaotic fractional-order systems. The last three chapters contain our studies of the applications of fractional-order chaotic systems where ten articles are presented in three domains. In the first domain, we have studied the chaotic behaviors in some biological systems including a novel COVID-19 pandemic model, a biological system, a glucose-insulin regulatory system, and a Cancer model. In the second domain, we have studied the chaotic behaviors in some physical systems including a chaotic system with extreme events, a Hopfield Neural Network System and a secure multiple-input multiple-output communications Based on F-M synchronization of FOCS with non-identical dimensions and orders. A chaotic behaviors in some general systems have been studied in the last domain including a chaotic and hyperchatioc systems and a generating multidirectional variable hidden attractors via newly commensurate and incommensurate non-equilibrium fractional-order chaotic system.

Various dynamical behaviors have been revealed for this systems, such as examining its dynamic states in accordance with commensurate and incommensurate fractional-order of its derivatives, investigating its dynamic states in accordance with its parameters. Moreover, during our studies, a special phenomena have been founded like, existing of hidden attractors, bistability, coexisting of symmetric attractors, multistability, coexisting of multiple attractors, inversion property, exploring hidden chaotic bursting, existing of extreme events, hyperchaos, variable boostable attractors, hidden attractors of some systems can be diffused on a 1D-line, 2D-lattice and also on 3D-grid in its two cases, the commensurate and incommensurate ones.

GLOSSARY

Fractional calculus is a branch of mathematical analysis that studies the possibility of differentiation and integration of arbitrary real or complex orders of the differential operator.
Differintegral in fractional calculus is a combined differentiation/integration operator.
Short memory principle means taking into account the behavior of function only in the "recent past".
Singlevalued function is a function that, for each point in the domain, has a unique value in the range.
Multivalued function is a function that assumes two or more distinct values in its range for at least one point in its domain.
State space is the set of all possible states of a dynamical system, where each state of the system corresponds to a unique point in the state space.
Equilibrium point, sometimes called fixed point is a solution of the autonomous system of ordinary differential equations that does not change with time.
Jacobian matrix is the matrix of all first-order partial derivatives of a vectorvalued function. It describes the orientation of a tangent plane to the function at a given point. The behavior of the system near a stationary point is related to the eigenvalues of the Jacobian at the equilibrium point.
Saddle point is when all eigenvalues are real and at least one of them is positive and at least one is negative. Saddles are always unstable.
Node point is when all eigenvalues are real and have the same sign. The node is stable (unstable) when the eigenvalues are negative (positive).
Focus point, called also spiral point, is when eigenvalues are complex-conjugate. The focus is stable when the eigenvalues have negative real part and unstable when they have positive real part.
Focus-Node point is when it has one real eigenvalue and a pair of complexconjugate eigenvalues, and all eigenvalues have real parts of the same sign. This equilibrium is stable (unstable) when the sign is negative (positive).
Saddle-Focus point is when it has one real eigenvalue with the sign opposite to the sign of the real part of a pair of complex-conjugate eigenvalues. This type of equilibrium is always unstable.
Center equilibrium occurs when a system has only two eigenvalues on the imaginary axis, namely, one pair of pure-imaginary eigenvalues.
Instability measure for equilibrium points of the fractional-order nonlinear system is mathematically equivalent to difference between the angle of stability border given by necessary stability condition and minimal angle of all roots obtained from characteristic equation of the system.
Lyapunov exponent of a dynamical system is a quantity that characterizes the rate of separation of infinitesimally close trajectories.

BIBLIOGRAPHY

[1] I. Podlubny, Fractional Differential Equations. Academic Press, New York, 1999.

[2] Ernesto Zambrano Serrano, "Fractional Order Chaotic Systems and Their Electronic Design", doctotal thesis, San Luis Potosí, S.L.P., Julio 2017.

[3] S. G. Samko, A. A. Kilbas, and O. I. Marichev. Fractional Integrals and Derivatives. Gordon and Breach Science Publishers, Amsterdam, 1993.

[4] Miller K. S. and Ross B., An Introduction to the Fractional Calculus and Fractional Differential Equations, John Wiley & Sons. Inc., New York, 1993.

[5] E. Capelas de Oliveira and J. A. Tenreiro-Machado. A review of definitions for fractional derivatives and integral. Mathematical Problems in Engineering, 2014:1?6, 2014.

[6] Y. Zhou. Basic Theory of Fractional Differential Equations. World Scientific Publishing, Hackensack, NJ, USA, 2014.

[7] K. B. Oldham and J. Spanier. The Fractional Calculus, Theory and Applications of Differentiation and Integration to Arbitrary Order. Dover Publications, Inc., 2002.

[8] K. Diethelm. The Analysis of Fractional Differential Equations: An Application- Oriented Exposition Using Differential Operators of Caputo Type, volume 2004 of Lecture Notes in Mathematics. Springer Berlin Heidelberg, Germany, 2010.

[9] Podlubny I., *Geometric and physical interpretation of fractional integration and fractional differentiation*, Fractional Calculus and Applied Analysis, 5, 367-386 , 2002.

[10] Mohammed-Salah Abdelouahab, "Les systèmes chaotiques à la dérivées fractionnaires", Doctoral thesis, university of constantine 1, 2013.

[11] N. Debbouche, A. Ouannas, Iqbal M. Batiha and G. Grassi, *Chaotic dynamics in a novel COVID-19 pandemic model described by commensurate and incommensurate fractional-order derivatives* ,Nonlinear Dyn, https://doi.org/10.1007/s11071-021-06867-5, 2021.

[12] N. Debbouche, A. Othman Almatroud, A. Ouannas and Iqbal M. Batiha, *Chaos and coexisting attractors in glucose-insulin regulatory system with incommensurate fractional-order derivatives*, Chaos, Solitons and Fractals 143, 110575,https://doi.org/10.1016/j.chaos.2020.110575, 2021.

[13] N. Debbouche, A. Ouannas, S. Momani, D. Cafagna, and V. T. Pham, *Fractional-order biological system: chaos, multistability and coexisting attractors*, Eur. Phys. J. Spec. Top., https://doi.org/10.1140/epjs/s11734-021-00308-5, 2021.

[14] N. Debbouche and A. Ouannas, *On New Fractional-Order Cancer Model: Bifurcations and Chaos*, 2021 International Conference on Recent Advances in Mathematics and Informatics (ICRAMI), 2021, pp. 1-6, doi: 10.1109/ICRAMI52622.2021.9585954.

[15] N. Debbouche, A. Ouannas , G. Grassi, A. A. Al-Hussein, F. R. Tahir, K. M. Saad, H. Jahanshahi and A. A. Aly, *Chaos in Cancer Tumor Growth Model with Commensurate and Incommensurate Fractional-Order Derivatives*, Hindawi, Computational and Mathematical Methods in Medicine Volume 2022, Article ID 5227503, 13 pages, https://doi.org/10.1155/2022/5227503.

[16] A. Ouannas, N. Debbouche, V.T. Pham, S. . Kingston, and T. Kapitaniak, *Chaos in fractional system with extreme events*, Eur. Phys. J. Spec. Top., https://doi.org/10.1140/epjs/s11734-021-00135-8, 2021.

[17] N. Debbouche, A. Ouannas, I. M. Batiha, G. Grassi, M. K. A. Kaabar, H. Jahanshahi, A. A. Aly and A. M. Aljuaid, *Chaotic Behavior Analysis of a New Incommensurate Fractional-Order Hopfield Neural Network System* , Hindawi Complexity Volume 2021, Article ID 3394666, 11 pages, https://doi.org/10.1155/2021/3394666, 2021.

[18] A. Ouannas, N. Debbouche, X. Wang, V. T. Pham and O. Zehrour, *Secure Multiple-Input Multiple-Output Communications Based on F-M Synchronization of Fractional-Order Chaotic Systems with Non-Identical Dimensions and Orders*, Appl. Sci., 8, 1746; https://doi.org/10.3390/app8101746, 2018.

[19] Debbouche N., Zehrour O., and Zetili S., *Dynamics of fractional-order chaotic and hyper-chaotic systems*, NONLINEAR STUDIES, Vol. 26, No. 2, pp. 401-413, 2019.

[20] Debbouche N.; Momani, S.; Ouannas, A.; Shatnawi, M.T.; Grassi,G.; Dibi, Z.; Batiha, I.M. *Generating Multidirectional Variable Hidden Attractors via Newly Commensurate and Incommensurate Non- Equilibrium Fractional-Order Chaotic Systems.* Entropy 2021, 23, 261. http://doi.org/10.3390/e23030261, 2021.

[21] Oldham K. B. and Spanier J., The Fractional Calculus, Academic Press, New York, 1974.

[22] Ivo Petráš, Fractional-Order Nonlinear Systems Modeling, Analysis and Simulation,Nonlinear Physical Science, 2011.

[23] D. Matignon, *Stability result on fractional differential equations with applications to control processing*, In IMACS-SMC Proceedings, Lille-France, pages 963-968, July 1996.

[24] A. Oustaloup, J. Sabatier, P. Lanusse, R. Malti, P. Melchior, X. Moreau, and M. Moze, *An overview of the crone approach in system analysis, modelling and identification, observation and control*, In Proc. of the 17th World Congress IFAC, Soul, Korea, pages 14254-14265, July 6-11 2008.

[25] W. Deng, C. Li, and J. Lü, *Stability analysis of linear fractional differential system with multiple time delays*, Nonlinear Dyn, 48:409-416, 2007.

[26] M.S. Tavazoei and M. Haeri,*Chaotic attractors in incommensurate fractional order systems*, Physica D 237, 2628-2637, 2008.

[27] W. Deng and C. Li and J. Lu, *Stability analysis of linear fractional differential system with multiple time delays*, Nonlinear Dynam 48, 409-416, 2007.

[28] Varsha Daftardar-Gejji and Sachin Bhalekar, *Chaos in fractional ordered Liu system*, Computers and Mathematics with Applications 59, 1117-1127, 2010.

[29] D. Baleanu, K. Diethelm, E. Scalas and J. Trujillo, *Fractional calculus models and numerical methods*, World Scientific Publishing Company, 2012.

[30] https://www.mathworks.com/matlabcentral/mlc-downloads/... downloads/submissions/32918/versions/5/previews/fde12.m/index.html

[31] Garrappa R.: Numerical Solution of Fractional Differential Equations: a Survey and a Software Tutorial, Mathematics 2018,6(2),16. doi: https://doi.org/10.3390/math6020016

[32] Dorčák L.,*Numerical Models for the Simulation of the Fractional-Order Control Systems*,.UEF-04-94, The Academy of Sciences, Inst. of Experimental Physic,Košice, Slovakia,1994.

[33] Vinagre B. M., Chen Y. Q. and Petráš I., *Two direct Tustin discretization methods for fractional -order differentiator/integrator*,J. Franklin Inst., 340, 349-362,2003.

[34] P. Maneville, Systèmes dynamiques et chaos, Ecole polytechnique, Palaiseau. 1999.

[35] Adel Ouannas, "Sur La Synchronisation Des Systèmes Chaotiques Discrets", Doctoral thesis, University of Frères Mentouri, Constantine, 2015.

[36] AA Khennaoui, A Ouannas, S Bendoukha, X Wang, VT Pham, "On chaos in the fractional-order discrete-time unified system and its control synchronization", Entropy 20 (7), 530.

[37] A Ouannas, X Wang, AA Khennaoui, S Bendoukha, VT Pham, FE Alsaadi, "Fractional form of a chaotic map without fixed points: Chaos, entropy and control", Entropy 20 (10), 720.

[38] X Wang, A Ouannas, VT Pham, HR Abdolmohammadi, "A fractional-order form of a system with stable equilibria and its synchronization", Advances in Difference Equations 2018 (1), 1-13.

[39] R. M. May, *Simple mathematical models with very complicated dynamics*, Nature 261, , 459-467, 1976.

[40] A Ouannas, AA Khennaoui, S Bendoukha, TP Vo, VT Pham, VV Huynh, "The fractional form of the Tinkerbell map is chaotic", Applied Sciences 8 (12), 2640.

[41] AA Khennaoui, A Ouannas, S Bendoukha, G Grassi, RP Lozi, VT Pham, "On fractional?order discrete?time systems: Chaos, stabilization and synchronization Chaos," Solitons & Fractals 119, 150-162.

[42] VV Huynh, A Ouannas, X Wang, VT Pham, XQ Nguyen, FE Alsaadi, "Chaotic map with no fixed points: entropy, implementation and control", Entropy 21 (3), 279.

[43] A Ouannas, AA Khennaoui, S Bendoukha, G Grassi, "On the dynamics and control of a fractional form of the discrete double scroll", International Journal of Bifurcation and Chaos 29 (06), 1950078 24 2019.

[44] A Ouannas, AA Khennaoui, Z Odibat, VT Pham, G Grassi , "On the dynamics, control and synchronization of fractional-order Ikeda map Chaos," Solitons & Fractals 123, 108-115.

[45] A Ouannas, AA Khennaoui, G Grassi, S Bendoukha,"On chaos in the fractional-order Grassi?Miller map and its control, Journal of Computational and Applied Mathematics 358, 293-305

[46] L Jouini, A Ouannas, AA Khennaoui, X Wang, G Grassi, VT Pham, "The fractional form of a new three-dimensional generalized Hénon map", Advances in Difference Equations 2019 (1), 1-12 33 2019.

[47] AA Khennaoui, A Ouannas, S Bendoukha, G Grassi, X Wang, VT Pham, "Chaos, control, and synchronization in some fractional-order difference equations", Advances in Difference Equations 2019 (1), 1-23.

[48] A Ouannas, AA Khennaoui, S Momani, G Grassi, VT Pham, "Chaos and control of a three-dimensional fractional order discrete-time system with no equilibrium and its synchronization", AIP Advances 10 (4), 045310 27 2020.

[49] AA Khennaoui, A Ouannas, S Boulaaras, VT Pham, A Taher Azar, "A fractional map with hidden attractors: chaos and control", The European Physical Journal Special Topics 229 (6), 1083-1093.

[50] AA Khennaoui, AO Almatroud, A Ouannas, MM Al-sawalha, G Grassi, "The effect of caputo fractional difference operator on a novel game theory model", Discrete & Continuous Dynamical Systems-B 26 (8), 4549 3 2021.

[51] Hannachi Fareh, "Attracteurs Etranges et chaos", Doctoral thesis, University of Larbi Ben M'hidi, Oum El Bouaghi, 2018.

[52] E.N. Lorenz, *Deterministic nonperiodic flow*, J. Atmos. Sci. 20, 130, 1963.

[53] K.T. Alligood, T.D. Sauer and J. A. Yorke, Chaos: An Introduction to Dynamical Systems, Springer, New York, 2008.

[54] S. Bowong and F. M. Kakmeni, *Synchronization of uncertain chaotic systems via backstepping approach*, Chaos Solitons Fractals 21, 999-1011, 2004.

[55] V. Daftardar-Gejji and S. Bhalekar, *Chaos in fractional ordered Liu system*, Comput. Math. Appl. 59, 1117?1127, 2010.

[56] W. H. Deng and C. P. Li, *Chaos synchronization of the fractional L'u system*, Physica A 353, 61-72, 2005.

[57] AA Khennaoui, A Ouannas, Z Odibat, VT Pham, G Grassi, "On the three-dimensional fractional-order Hénon map with Lorenz-like attractors", International Journal of Bifurcation and Chaos 30 (11), 2050217 9 2020.

[58] A Ouannas, AA Khennaoui, X Wang, VT Pham, S Boulaaras, S Momani, "Bifurcation and chaos in the fractional form of Hénon-Lozi type map", The European Physical Journal Special Topics 229 (12), 2261-2273.

[59] F Hadjabi, A Ouannas, N Shawagfeh, AA Khennaoui, G Grassi, "On two-dimensional fractional chaotic maps with symmetries", Symmetry 12 (5), 756 16 2020.

[60] A Ouannas, AA Khennaoui, S Momani, VT Pham, R El-Khazali, "Hidden attractors in a new fractional?order discrete system: chaos, complexity, entropy, and control", Chinese Physics B 29 (5), 050504 27 2020.

[61] A Ouannas, AA Khennaoui, S Momani, G Grassi, VT Pham, R El-Khazali, "A quadratic fractional map without equilibria: Bifurcation, 0?1 test, complexity, entropy, and control", Electronics 9 (5), 748.

[62] A Ouannas, AA Khennaoui, S Bendoukha, Z Wang, VT Pham, "The dynamics and control of the fractional forms of some rational chaotic maps", Journal of Systems Science and Complexity 33 (3), 584-603 9 2020.

[63] VP Thoai, MS Kahkeshi, VV Huynh, A Ouannas, VT Pham, "A nonlinear five-term system: Symmetry, chaos, and prediction" , Symmetry 12 (6), 879 7 2020 .

[64] AA Khennaoui, AO Almatroud, A Ouannas, MM Al-sawalha, G Grassi, "An unprecedented 2-dimensional discrete-time fractional-order system and its hidden chaotic attractors", Mathematical Problems in Engineering 2021.

[65] AO Almatroud, AA Khennaoui, A Ouannas, VT Pham, " Infinite line of equilibriums in a novel fractional map with coexisting infinitely many attractors and initial offset boosting", International Journal of Nonlinear Sciences and Numerical Simulation.

[66] A Abbes, A Ouannas, N Shawagfeh, AA Khennaoui, "Incommensurate Fractional Discrete Neural Network: chaos and complexity", The European Physical Journal Plus 137 (2), 1-15 1 2022.

[67] Haiping Ye and Yongsheng Ding, *Nonl inear Dynamics and Chaos in a Fractional-Order HIV Model*, Hindawi Publishing Corporation, Mathematical Problems in Engineering, Volume 2009, Article ID 378614, 2009.

[68] Marius-F. Danca, *Coexisting Hidden and Self-Excited Attractors in an Economic Model of Integer or Fractional Order*, International Journal of Bifurcation and Chaos, Vol. 31, No. 4, 2150062, 2021.

[69] Vallis G., *El Niño: A chaotic dynamical system?*, Science 232, 243-245, 1986.

[70] Vallis G., *Conceptual models of El Niño and the Southern oscillation*, J. Geophys. Res. 93, 13979-13991, 1988.

[71] Krishchenko A. and Starkov K., *Localization of compact invariant compact sets of nonlinear timevarying,systems*, Int. J. Bifurcation and Chaos 18, 1599–1604, 2008.

[72] Euzebio R. and Llibre J., *Periodic solutions of El Niño model through the Vallis differential system*, Discr. Contin. Dyn. Syst. 34, 3455–3469, 2014.

[73] Alkahtani B. and Atangana A., *Chaos on the Vallis model for El Niño with fractional operators*, Entropy 18, 100, 2016.

[74] Amey Deshpande and Varsha Daftardar-Gejji, *Chaotic Dynamics Of Fractional Vallis System For El-Niño*, Fract. Calc. Appl. Anal., Vol. 22, No 3, pp. 825?842, 2019.

[75] Mira C., Gardini L., Bugola A. and Cathala J-C, Chaotic dynamics in two-dimensional noninvertible maps World Scieniific, 1996.

[76] Alligood K.T., Sauer T.D. and Yorke J.A. Chaos : an Introduction to Dynamical Systems, Springer-Verlag édition, 1996.

[77] Tidjani Menacer, " Synchronization des systèmes dynamiques chaotiques à dérivées fractionnaires", doctoral thesis, university of constantine 1, 2014.

[78] Rosenstein M., Collins J. and Deluca C. , *A practical method for calculating largest Lyapunov exponents for small data sets*, Physica, Vol. 65, pp. 117-134, 1993.

[79] Wolf A., Swift J., Swinney H. and Vastano J. , *Determining Lyapunov exponents from a time series*, Physica, Vol. 16, pp. 285-317, 1985.

[80] Parker T.S. and Chua L.O. Pratical Numerical Algorithms For Chaotic Systems. Edition Springer-Verlay, 1989.

[81] G. Benettin, L. Galgani, A. Giorgilli, and J-M. Strelcyn, *Lyapunov characteristic exponents for smooth dynamical systems and for hamiltonian systems; a method for computing all of them*, part 1: theory. Meccanica, 15:9–20, 1980.

[82] R. Brown, P. Bryant, and H. D. Abarbanel,*Computing the lyapunov spectrum of a dynamical system from an observed time series*, Phys. Rev. A, 43:2787–2806, 1991.

[83] J. Holzfuss and W. Lauterborn,*Lyapunov exponents from a time series of acoustic chaos*, Phys. Rev. A, 39:2146–2152, 1989.

[84] Danca M.-F. and Kuznetsov N., *Matlab code for Lyapunov exponents of fractional-order systems*, Int. J. Bifurcation and Chaos 28, 1850067-1-14, 2018.

[85] Marius-F. Danca, *Matlab Code for Lyapunov Exponents of Fractional-Order Systems*, *Part II: The Noncommensurate Case*, Int. J. Bifurcation and Chaos 31, 2150187-12-14, 2021.

[86] Li T-Y., York J.A. , *Period three implies chaos*, Amer. Math. Mon., Vol. 82, pp.985-992, 1975.

[87] Kaplan J., Yorke J., *Functional Differential Equations and Approximations of Fixed Points*, *Chaotic behavior of multidimensional difference equations*, Springer. pp. 204?227, 1979.

[88] Grebogi C., OTT E., Pelikan S. and Yorke J.A. , *Strange attractors that are not chaotic*, Physica D, Vol. 13, pp. 261-268, 1984.

[89] Ruelle, David; Takens, Floris, *On the nature of turbulence*, Communications in Mathematical Physics. 20 (3): 167-192, 1971.

[90] Dudkowski D, Jafari S, Kapitaniak T, et al., *Hidden attractors in dynamical systems*, Phys Rep, 637:1-50, 2016.

[91] Leonov GA, Kuznetsov NV, Vagaitsev VI, *Localization of hidden Chua?s attractors*, Phys Lett A, 375(23):2230-2233, 2011.

[92] Leonov GA, Kuznetsov NV, Vagaitsev VI, *Hidden attractor in smooth Chua systems*, Phys D, 241(18):1482-1486, 2012.

[93] Wuhan Municipal Health and Health Commission Report on the current pneumonia epidemic situation in our city. Wuhan Municipal Health Commission, 2019. Available at http://wjw.wuhan.gov.cn/front/web/showDetail/2019123108989

[94] Mangiarotti, S., Peyre, M., Zhang, Y., Huc, M., Roger, F., Kerr, Y., *Chaos theory applied to the outbreak of COVID- 19: an ancillary approach to decision making in pandemic context.* Epidemiol. Infect. 148, 1-29 (2020). https://doi. org/10.1017/S0950268820000990

[95] Postavaru, O., Anton, S.R., Toma, A.,*COVID-19 pandemic and chaos theory.* Math Comput. Simul. 181, 138-149 (2021). https://doi.org/10.1016/j.matcom.2020.09.029

[96] Wang, J., Liu, S., Zheng, B., Takeuchi, Y., *Qualitative and bifurcation analysis using an SIR model with a saturated treatment function.* Math. Comput. Model. 55(3-4), 710-722 (2012). https://doi.org/10.1016/j.mcm.2011.08.045

[97] Zhou, X., Cui, J., *Analysis of stability and bifurcation for an SEIR epidemic model with saturated recovery rate.* Commun. Nonlinear Sci. Numer. Simul. 16(11), 4438-4450 (2011). https://doi.org/10.1016/j.cnsns.2011.03.026

[98] National Health Commission of the People's Republic of China (2020) Available at http://www.nhc.gov.cn/yjb/ pzhgli/new_list.shtml (Accessed 21 March 2020)

[99] Johns Hudson University (2020). Available at https:// github.com/CSSEGISandData/COVID_19/tree/master/csse_covid_19_data (Accessed 21 March 2020)

[100] Li, H.-L., Zhang, L., Hu, C., Jiang, Y.-L., Teng, Z., *Dynamical analysis of a fractional-order predator-prey model incorporating a prey refuge.* J. Appl.Math. Comput. 54, 435-449 (2017).

[101] Khan, H., Ibrahim, M., Abdel-Aty, A.-H., Khash, M.M., Khan, F.A., Khane, A., *A fractional order Covid-19 epidemic model with Mittag-Leffler. Kernel*, Chaos, Solitons Fract. 148, 111030 (2021).

[102] Chatterjee, A.N., Ahmad, B., *A fractional-order differential equation model of COVID-19 infection of epithelial cells.* Chaos, Solitons Fract. 147, 110952 (2021).

[103] Higazy, M., *Novel fractional order SIDARTHE mathematical model of COVID-19 pandemic.* Chaos, Solitons Fract. 138, 110007 (2020).

[104] Algehyne, E.A., Ibrahim, M., *Fractal-fractional order mathematical vaccine model of COVID-19 under non-singular kernel.* Chaos, Solitons Fract. 150, 111150 (2021).

[105] Jahanshahi,H., Munoz-Pacheco, J.M., Bekiros, S., Alotaibi, N.D., *A fractional-order SIRD model with time-dependent memory indexes for encompassing the multi-fractional characteristics of the COVID-19.* Chaos, Solitons Fract. 143, 110632 (2021).

[106] Rajagopal, K., Hasanzadeh,N., Parastesh, F., Hamarash, I.I., Jafari, S., Hussain, I., *A fractional-ordermodel for the novel coronavirus (COVID-19) outbreak.* Nonlin. Dyn. 101, 711-718 (2020).

[107] Boudaoui, A., El hadj Moussa, Y., Hammouch, Z., Ullah, S., *A fractional-order model describing the dynamics of the novel coronavirus (COVID-19) with nonsingular kernel.* Chaos, Solitons Fract (2021).

[108] Xu, C., Yu, Y., Chen, Y., Lu, Z., *Forecast analysis of the epidemics trend of COVID-19 in the USA by a generalized fractional-order SEIR model.* Nonlin. Dyn. 101, 1621-1634 (2020).

[109] Yadav, R.P.,Verma, R., *A numerical simulation of fractional order mathematical modeling of COVID-19 disease in case of Wuhan China.* Chaos, Solitons Fract. (2020).

[110] Lu, Z.,Yu,Y., Chen,Y.Q., Ren, G.,Xu, C.,Wang, S.,Yin, Z., *A fractional-order SEIHDRmodel forCOVID-19 with intercity networked coupling effects.* Nonlin. Dyn. 101, 1717-1730 (2020).

[111] Ackerman, E., Rosevear, J. W. and McGuckin, W. F. *A mathematical model of the glucose- tolerance test*, Physics in Medicine & Biology 9, 203, 1964.

[112] Almeida, R., *A Caputo fractional derivative of a function with respect to another function*, Commun. Nonlinear Sci. Numer. Simul. 44, 460?481, 2017.

[113] Scherer, R., Kalla, S.L., Tang, Y. and Huang, J., *The Grünwald?Letnikov method for fractional differential equations*, Comput. Math. Appl. 62(3), 902?917, 2011.

[114] A. Rocco and B. J. West, *Fractional calculus and the evolution of fractal phenomena*, Physica A, vol. 265, no. 3, pp. 535?546, 1999.

[115] Cho, Y., Kim, I. and Sheen, D., A fractional-order model for minmod millennium Math. Biosci. 262, 36-45, 2015.

[116] Lekdee, N., Sirisubtawee, S. and Koonprasert, S., *Exact solutions and numerical comparison of methods for solving fractional-order differential systems*, In: IMECS 2018. Lecture Notes in Engineering and Computer Science, vol. 2, pp. 459-466, 2018.

[117] Sakulrang, S., Moore, E.J., Sungnul, S., and Gaetano, A., *A fractional differential equation model for continuous glucose monitoring data* Adv. Differ. Equ. 2017(1), 150, 2017.

[118] Lekdee N, Sirisubtawee S and Koonprasert S., *Bifurcations in a delayed fractional model of glucose-insulin interaction with incommensurate orders*, Adv Differ Equations 2019,1?22, 2019.

[119] MuhammadWaleed Khan, Muhammad Abid and Abdul Qayyum Khan. *Fractional Order Bergman.s Minimal Model-A Better Representation Of Blood Glucose-Insulin System*, 978-1-7281-2353-0/19 2019 IEEE.

[120] Karthikeyan RAJAGOPAL, Atiyeh BAYANI, Sajad JAFARI,AnithaKARTHIKEYAN and Iqtadar HUSSAIN, *Chaotic dynamics of a fractional order glucose-insulin regulatory system*, Frontiers of Information Technology & Electronic Engineering. ISSN 2095-9230, 2019.

[121] Payam Sadeghi Shabestari, Shirin Panahi a, Boshra Hatef, Sajad Jafari and Julien C. Sprott, *A new chaotic model for glucose-insulin regulatory system*, Chaos, Solitons and Fractals 112, 44–510, 2018.

[122] Elsadany A-EA , et al. *Chaos and bifurcation of a nonlinear discrete prey-predator system*, Comput Ecol Software, 2(3):169, 2012.

[123] Letellier C , Denis F and Aguirre LA . *What can be learned from a chaotic cancer model?* J Theor Biol, 322:7–16, 2013.

[124] Viet-Thanh Pham ,Sundarapandian Vaidyanathan,Christos Volos and Tomasz Kapitaniak. Nonlinear Dynamical Systems with Self-Excited andHidden Attractors. https://doi.org/10.1007/978-3-319-71243-7 (2018).

[125] Z. Hammouch, T. Mekkaoui, Nonauton. Dyn. Syst. **1**, (2014), 61-71.

[126] H.G. EnjieuKadji, J.B. ChabiOrou, R. Yamapi, P. Woafo, Chaos, Solitons and Fractals **32**, (2007), 862–882.

[127] F. Kaiser, *Specific Effects in Externally Driven Self-sustained Oscillating Biophysical Model Systems, in Fröhlich H., Kremer F. (eds.) Coherent Excitations in Biological Systems, Proceedings in Life Sciences*, (Springer, Berlin, Heidelberg, 1983).

[128] B. Van der Pol, Radio Review (later Wireless World) **1**,(1920), 701–710.

[129] R. FitzHugh, Biophysics J **1**, (1961), 445–466.

[130] J. Nagumo, S.Arimoto, and S. Yoshizawa, Proc. IRE **50**, (1962), 2061–2070.

[131] A. Venkatesan, M. Lakshmanan, *Bifurcation and chaos in the double-well Duffing–Van der Pol oscillator: numerical and analytical studies*, (Physical Review E, 56 (6), 6321, 1997).

[132] R.S. Barbosa, J.A. Tenreiro Machado, B.M. Vinagre, A.J. Calderón, Journal of Vibration and Control **13 (9-10)**, (2007), 1291-1301.

[133] M.S. Tavazoei, M. Haeri, M.Attari, S.Bolouki and M.Siami, Journal of Vibration and Control **15 (6)**, (2009),803-819.

[134] J. Chen, Y. Shen, X.H. Li, S. Yang, S. Wen, *Bifurcation and stability analysis of commensurate fractional-order van der Pol oscillator with time-delayed feedback*, (Indian Journalof Physics, 2019).

[135] C. Li, J.C.Sprott, H. Xing, Nonlinear Dyn. **87**, (2017), 1351-1358.

[136] C. Li, W. Hu, J.C. Sprott, and X. Wang, Eur. Phys. J. Special Topics 224, (2015), 1493-1506.

[137] C. Letellier, F. Denis and L.A. Aguirre," What can be learned from a chaotic cancer model?". Journal of Theoretical Biology 322, pp. 7-16, 2013.

[138] M. Moghtadaei, M. R. A. Golpayegani and R. Malekzadeh, "Periodic and chaotic dynamics in a map-based model of tumor-immune interaction". Journal of Theoretical Biology 334, pp. 130-140, 2013.

[139] Ravi Kiran Maddali, Divya Ahluwalia, Adwitiya Chaudhuri, Sk. Sarif Hassan, " Dynamics of a Three Dimensional Chaotic Cancer Model", International Journal of Mathematics Trends and Technology (IJMTT) - Volume 53 Number 5 January 2018.

[140] F. Denis and C. Letellier, "Radiotherapy and chaos theory: the tit bird and the butterfly.," Cancer Radiother. J. la Soc. Fr. Radiother. Oncol., vol. 16, no. 5-6, pp. 404-409, 2012.

[141] L. Dzyubak, O. Dzyubak, and J. Awrejcewicz, "Controlling and stabilizing unpredictable behavior of metabolic reactions and carcinogenesis in biological systems," Nonlinear Dyn., vol. 97, no. 3, pp. 1853-1866, 2019.

[142] S.L. Kingston, K. Thamilmaran, P. Pal, U. Feudel, S.K.ana, Phys. Rev. E 96, 052204 (2017)

[143] S.L. Kingston, K. Suresh, K. Thamilmaran, T. Kapitaniak,Eur. Phys. J. Spec. Top. 96(229), 1033 (2020)

[144] S. Coulibaly, M.G. Clerc, F. Selmi, S. Barbay, Phys.Rev. A 95, 023816 (2017)

[145] A. Ray, A. Mishra, D. Ghosh, T. Kapitaniak, S.K. Dana, C. Hens, Phys. Rev. E 101, 032209 (2020)

[146] A. Mishra, S.L. Kingston, C. Hens, T. Kapitaniak, U. Feudel, S.K. Dana, Chaos 30, 063114 (2020)

[147] C.A. Monje, Y.Q. Chen, B.M. Vinagre, D. Xue, V. Feliu, Fractional Differential Equations (Academic Press, New York, 1999)

[148] C. Zhou, Z. Li,Y. Zeng, S. Zhang, Int. J. Bifurcat.Chaos 29(01), 1950004 (2019)

[149] J. Fleck, "Development and establishment in artificial intelligence", The Question of Artificial Intelligence. 16 (2018) 106-164.

[150] E. Kaslik, S. Sivasundaram, "Nonlinear dynamics and chaos in fractional-order neural networks", Neural Network 32 (2012) 245-256.

[151] P. Arena, L. Fortuna, D. Porto, "Chaotic behavior in nonintegerorder cellular neural networks", Physical Review E 61(1) (2000) 776-781.

[152] T. Matsuzaki, M. Nakagawa, "A chaos neuron model with fractional differential equation", Journal of the Physical Society of Japan 72(10) (2003) 2678-2684.

[153] H. Zhu, S. Zhou, W. Zhang, Chaos and synchronization of time delayed fractional neuron network system, 2008 The 9th International Conference for Young Computer Scientists, Hunan, China, 2008, pp. 2937-2941.

[154] S. Zhou, H. Li, Z. Zhu, "Chaos control and synchronization in a fractional neuron network system", Chaos, Solitons and Fractals 36(4) (2008) 973-984.

[155] S. Zhou, P. Hu, H. Li, Chaotic synchronization of a fractional neuron network system with time-varying delays, 2009 International Conference on Communications, Circuits and Systems, Milpitas, CA, USA, 2009, pp. 863-867.

[156] R. Wu, X. Hei, L. Chen, "Finite-time stability of fractional-order neural networks with delay", Commun. Theor. Phys. (Beijing) 60 (2013) 189-193.

[157] J. Yu, C. Hu, H. Jiang," α-stability and α-synchronization for fractional-order neural networks", Neural Netw. 5 (2012) 82-87.

[158] K. Diethelm, N.J. Ford, A.D. Freed, "A Predictor-Corrector Approach for the Numerical Solution of Fractional Differential Equations", Nonlinear Dynamics 29 (2002) 3-22.

[159] Luo, A.C. "A theory for synchronization of dynamical systems". Commun. Nonlinear Sci. Numer. Simul. 2009, 14, 1901-1951.

[160] A Ouannas, Z Odibat, T Hayat, "Fractional analysis of co-existence of some types of chaos synchronization", Chaos, Solitons & Fractals 105, 215-223.

[161] A Ouannas, M Abdelli, Z Odibat, X Wang, VT Pham, G Grassi, A Alsaedi, "Synchronization control in reaction-diffusion systems: Application to Lengyel-Epstein system", Complexity 2019.

[162] A Ouannas, X Wang, VT Pham, G Grassi, VV Huynh, "Synchronization results for a class of fractional-order spatiotemporal partial differential systems based on fractional Lyapunov approach", Boundary Value Problems 2019 (1), 1-12.

[163] F Mesdoui, A Ouannas, N Shawagfeh, G Grassi, VT Pham, "Synchronization methods for the Degn-Harrison reaction-diffusion systems", IEEE Access 8, 91829-91836.

[164] A Ouannas, F Mesdoui, S Momani, I Batiha, G Grassi, "Synchronization of FitzHugh-Nagumo reaction-diffusion systems via one-dimensional linear control law", Archives of Control Sciences 31.

[165] F Mesdoui, N Shawagfeh, A Ouannas, "Global synchronization of fractional?order and integer?order N component reaction diffusion systems: Application to biochemical models", Mathematical Methods in the Applied Sciences 44 (1), 1003-1012

[166] A Ouannas, IM Batiha, S Bekiros, J Liu, H Jahanshahi, AA Aly, "Synchronization of the glycolysis reaction-diffusion model via linear control law", Entropy 23 (11), 1516.

[167] Martinez-Guerra, R.; Pérez-Pinacho, C.A.; Gómez-Cortés, G.C. Synchronization of Integral and Fractional Order Chaotic Systems; Springer: Cham, Switzerland, 2015.

[168] A Ouannas, AA Khennaoui, G Grassi, S Bendoukha, "On the?Chaos Synchronization of Fractional-Order Discrete-Time Systems: General Method and Examples", Discrete Dynamics in Nature and Society 2018.

[169] A Ouannas, AA Khennaoui, O Zehrour, S Bendoukha, G Grassi, VT Pham, "Synchronisation of integer-order and fractional-order discrete-time chaotic systems", Pramana 92 (4), 1-9.

[170] Ouannas, A.; Grassi, G. "Inverse full state hybrid projective synchronization for chaotic maps with different dimensions". Chinese Phys. B 2016, 25, 090503.

[171] A Ouannas, AT Azar, S Vaidyanathan, "A new fractional hybrid chaos synchronisation ", International Journal of Modelling, Identification and Control 27 (4), 314-322.

[172] A Ouannas, S Bendoukha, A Karouma, S Abdelmalek, "A general method to study the co-existence of different hybrid synchronizations in fractional-order chaotic systems", International Journal of Nonlinear Sciences and Numerical Simulation 20 (3-4 ? 5 2019).

[173] A Ouannas, AT Azar, T Ziar, "Fractional inverse full state hybrid projective synchronisation", International Journal of Advanced Intelligence Paradigms 17 (3-4), 279-298.

[174] B Wang, A Ouannas, Y Karaca, WF Xia, H Jahanshahi, AF Alkhateeb,, "A HYBRID APPROACH FOR SYNCHRONIZING BETWEEN TWO REACTION?DIFFUSION SYSTEMS OF INTEGER-AND FRACTIONAL-ORDER APPLIED ON CERTAIN CHEMICAL MODELS", Fractals, 2240145.

[175] A Ouannas, G Grassi, X Wang, T Ziar, VT Pham, "Function-based hybrid synchronization types and their coexistence in non-identical fractional-order chaotic systems," Advances in Difference Equations 2018 (1), 1-12 5 2018.

[176] Ouannas, A.; Abu-Saris, R. "On matrix projective synchronization and inverse matrix projective synchronization for different and identical dimensional discrete-time chaotic systems". J. Chaos 2015, 2016, 4912520.

[177] Ouannas, A.; Odibat, Z. "Generalized synchronization of different dimensional chaotic dynamical systems in discrete-time". Int. J. Nonlinear Dyn. Chaos Eng. Sys. 2015, 81, 765-771.

[178] A Ouannas, AT Azar, S Vaidyanathan, "A robust method for new fractional hybrid chaos synchronization", Mathematical Methods in the Applied Sciences 40 (5), 1804-1812.

[179] Z Chougui, A Ouannas, "A new generalized synchronization scheme to control fractional chaotic dynamical systems with different dimensions and orders," Nonlinear Studies 27 (3).

[180] A Ouannas, X Wang, VT Pham, T Ziar, " ? ? ? generalized synchronization: application to fractional hyperchaotic systems with arbitrary dimensions and orders," Automatika 61 (4), 554-563.

[181] Ouannas, A.; Odibat, Z. "On inverse generalized synchronization of continuous chaotic dynamical systems." Int. J. Appl. Comput. Math. 2016, 2, 1-11.

[182] AA Khennaoui, A Ouannas, S Bendoukha, G Grassi, X Wang, VT Pham, "Generalized and inverse generalized synchronization of fractional-order discrete-time chaotic systems with non-identical dimensions", Advances in Difference Equations 2018 (1), 1-14.

[183] Ouannas, A.; Grassi, G. "A new approach to study the coexistence of some synchronization types between chaotic maps with different dimensions". Int. J. Nonlinear Dyn. Chaos . Eng. Sys. 2016, 86, 1319-1328.

[184] Ouannas, A.; Al-Sawalha, M.M. "A new approach to synchronize different dimensional chaotic maps using two scaling matrices". Nonlinear Dyn. Sys. Theory 2015, 15, 400-408.

[185] Ouannas, A.; Abu-Saris, R. "A robust control method for Q-S synchronization between different dimensional integer-order and fractional-order chaotic systems". J. Control Sci. Eng. 2015, 2015, 703753.

[186] A Ouannas, Z Odibat, A Alsaedi, A Hobiny, T Hayat, "Investigation of QS synchronization in coupled chaotic incommensurate fractional order systems", Chinese journal of physics 56 (5), 1940-1948.

[187] Ogunjo, S. "Increased and reduced order synchronization of 2D and 3D dynamical systems". Int. J. Nonlinear Sci. 2013, 16, 105-112.

[188] Ojo, K.S.; Ogunjo, S.T.; Njah, A.N.; Fuwape, I.A. "Increased-order generalized synchronization of chaotic and hyperchaotic systems". Pramana 2014, 84, 33-45.

[189] Azar, A.T.; Vaidyanathan, S.; Ouannas, A. "Fractional Order Control and Synchronization of Chaotic Systems; Studies in Computational Intelligence;" Springer: Berlin, Germany, 2017; Volume 688, ISBN 978-3-319-50248-9.

[190] Zhang, F.; Chen, G.; Li, C.; Kurths, J. "Chaos synchronization in fractional differential systems". Philos. Trans. R. Soc. A 2013, 371, 1990.

[191] Ouannas, A.; Al-sawalha, M.M.; Ziar, T." Fractional chaos synchronization schemes for different dimensional systems with non-identical fractional-orders via two scaling matrices". Optik 2016, 127, 8410-8418.

[192] Alvarez, G.; Li, S. "Some basic cryptographic requirements for chaos based cryptosystems". Int. J. Bifurc. Chaos 2006, 16, 2129–2151.

[193] A Ouannas, G Grassi, T Ziar, Z Odibat, "On a function projective synchronization scheme for non-identical fractional-order chaotic (hyperchaotic) systems with different dimensions and orders", Optik 136, 513-523.

[194] A Ouannas, X Wang, VT Pham, T Ziar, "Dynamic analysis of complex synchronization schemes between integer order and fractional order chaotic systems with different dimensions", Complexity 2017.

[195] A Ouannas, A Karouma, "Different generalized synchronization schemes between integer-order and fractional-order chaotic systems with different dimensions", Differential Equations and Dynamical Systems 26 (1), 125-137 16 2018.

[196] A Ouannas, O Zehrour, Z Laadjal, "Nonlinear methods to control synchronization between fractional-order and integer-order chaotic systems", Nonlinear Studies 25 (1).

[197] A Ouannas, X Wang, VT Pham, G Grassi, T Ziar, "Co-existence of some synchronization types between non-identical commensurate and incommensurate fractional-order chaotic systems with different dimensions", Advances in Difference Equations 21 10 2018.

[198] S Bendoukha, A Ouannas, X Wang, AA Khennaoui, VT Pham, G Grassi, "The Co-existence of different synchronization types in fractional-order discrete-time chaotic systems with non?identical dimensions and orders", Entropy 20 (9), 710.

[199] A Ouannas, X Wang, VT Pham, G Grassi, T Ziar, "Coexistence of identical synchronization, antiphase synchronization and inverse full state hybrid projective synchronization in different dimensional fractional-order chaotic", Advances in Difference Equations 2018 (1), 1-16 12 2018.

[200] Kocarev, L.; Lian, S. Chaos-Based Cryptography: Theory, Algorithms and Applications; Springer: Berlin/Heidelberg, Germany, 2011.

[201] Samko, S.G.; Kilbas, A.A.; Marichev, O.I. Fractional Integrals and Derivatives, Theory and Applications; Gordon and Breach: Amsterdam, The Netherlands, 1993.

[202] Aguila-Camacho, N.; Duarte-Mermoud, M.A. "Comments on Fractional order Lyapunov stability theorem and its applications in synchronization of complex dynamical networks?." Commun. Nonlinear Sci. Numer. Simul. 2015, 25, 145-148.

[203] Xue, W.; Li, Y.; Cang, S.; Jia, H.; Wang, Z. "Chaotic behavior and circuit implementation of a fractional-order permanent magnet synchronous motor model". J. Frankl. Inst. 2015, 352, 2887-2898.

[204] Wu, X.; Wang, H.; Lu, H. "Modified generalized projective synchronization of a new fractional-order hyper-chaotic system and its application to secure communication". Nonlinear Anal. Real World Appl. 2012, 13, 1441-1450.

[205] Gao, T.; Chen, G.; Chen, Z.; Cang, S. "The generation and circuit implementation of a new hyper-chaos based upon Lorenz system". Phys. Lett. A 2007, 361, 78-86.

[206] Sara Dadras · Hamid Reza Momeni · Guoyuan Qi, *Analysis of a new 3D smooth autonomous system with different wing chaotic attractors and transient chaos*,Nonlinear Dyn (2010) 62: 391–405.

[207] S. Dadras, H.R. Momeni, G. Qi, Z.l. Wang. Guoyuan Qi, *Four-wing hyper-chaotic attractor generated from a new 4D system with one equilibrium and its fractionalorder form*,Nonlinear Dyn. 67 (2) (2012) 1161-1173.

[208] Shimada, I. and Nagashima, T. *A numerical approach to ergodic problem of dissipative dynamical systems* , Progress of Theoretical Physics 61, 1605-1616, 1979.

[209] S. Effati, J. Saberi-Nadjafi, H. Saberi Nik, *Optimal and adaptive control for a kind of 3D chaotic and 4D hyper-chaotic systems*,Applied Mathematical Modelling 38 (2014) 759-774.

[210] S. T. Tchinda, G. Mpame, A. N. Takougang, and V. K. Tamba, *Dynamic analysis of a snap oscillator based on a unique diode nonlinearity effect, offset boosting control and sliding mode control design for global chaos synchronization*, J. Control Autom. Electric. Syst. 30, 970-984 (2019).

[211] J. M. Munoz-Pacheco, E. Zambrano-Serrano, C. Volos,O. I. Tacha,N. Stouboulos, and V. T. Pham, ?A fractional order chaotic system with a 3D grid of variable attractors,? Chaos Solitons Fractals 113, 69-78 (2018).

[212] Sen Zhang, Xiaoping Wang, Zhigang Zeng, *A simple no-equilibrium chaotic system with only one signum function for generating multidirectional variable hidden attractors and its hardware implementation*, Chaos 30, 053129 (2020); doi: 10.1063/5.0008875.

[213] Kehui Sun, J. C. Sprott, *Periodically Forced Chaotic System With Signum Nonlinearity* , International Journal of Bifurcation and Chaos, Vol. 20, No. 5 (2010) 1499-1507.

[214] Gans, R. F., *When is cutting chaotic*, J. Sound Vibr. (1995) 188, 75-83.

[215] B. C. Bao, P. Wu, H. Bao, Q. Xu, and M. Chen, *Chaotic bursting in memristive diode bridge-coupled Sallen-Key lowpass filter*, Electron. Lett. 53, 1104-1105 (2017).

[216] X. Han, Y. Yu, C. Zhang, F. Xia, andQ. S. Bi, *Turnover of hysteresis determines novel bursting in duffing system with multiple-frequency external forcings*, Int. J. Non Linear Mech. 89, 6-74 (2017).

[217] Meng Jiao Wang, Xiao Han Liao, Yong Deng, Zhi Jun Li, Yi Ceng Zeng, Ming Lin Ma, *Bursting, Dynamics, and Circuit Implementation of a New Fractional-Order Chaotic System With Coexisting Hidden Attractors* , J. Comput. Nonlinear Dynam. Jul 2019, 14(7): 071002.

ABSTRACT

In this thesis, some problems regarding dynamic behaviors of fractional-order chaotic systems in continuous-time are studied for both commensurate and incommensurate orders. The effect of fractional-order has been shown on different models such as biological, physical, and general models. The results are proved analytically by applying the stability condition for the fractional system. Numerically by constructing bifurcation diagrams, computing Lyapunov exponents, calculating Lyapunov dimensions, the basin of attractions, and sketching the phase portraits in 2D and 3D projections.

Keywords. Fractional-order derivatives, commensurate and incommensurate orders, continuous dynamical system, Stability, Bifurcation, Lyapunov exponents, Chaos.

RÉSUMÉ

Dans cette thèse, certains problèmes concernant les comportements dynamiques des systèmes chaotiques d'ordre fractionnaire en temps continu sont étudiés pour les ordres commensurables et incommensurables. L'effet de l'ordre fractionnaire a été montré sur différents modèles tels que les modèles biologiques, physiques et généraux. Les résultats sont prouvés analytiquement en appliquant la condition de stabilité pour le système fractionnaire. Numériquement en construisant des diagrammes de bifurcation, en calculant les exposants de Lyapunov, en calculant les dimensions de Lyapunov, le bassin d'attractions, et en esquissant les portraits de phase en projections 2D et 3D.

Mots clés. Dérivées d'ordre fractionnaire, ordres commensurables et incommensurables, système dynamique continu, Stabilité, Bifurcation, Exposants de Lyapunov, Chaos.

ARABIC ABSTRACT

ملخص

في هذه الأطروحة ، تمت دراسة بعض المشكلات المتعلقة بالسلوكيات الديناميكية للأنظمة الفوضوية ذات الترتيب الكسري في الوقت المستمر لكل من الأوامر المتكافئة وغير المتكافئة. تم عرض تأثير الترتيب الجزئي على نماذج مختلفة مثل النماذج البيولوجية والفيزيائية والعامة. تم إثبات النتائج بشكل تحليلي من خلال تطبيق شرط الاستقرار للنظام الكسري. و بشكل عددي من خلال إنشاء مخططات التشعب ، وحساب أسس ليابونوف، وحساب أبعاد ليابونوف ، وحوض عوامل الجذب ، ورسم صور المرحلة في إسقاطات ثنائية وثلاثية الأبعاد.

الكلمات المفتاحية. المشتقات ذات الترتيب الجزئي ، الأوامر المتكافئة وغير المتكافئة ، النظام الديناميكي المستمر ، الاستقرار ، التشعب ، أسس ليابونوف ، الفوضى.